VOLUME 96 NUMBER 3

THE ASTROPHYSICAL JOURNAL

AN INTERNATIONAL REVIEW OF SPECTROSCOPY AND ASTRONOMICAL PHYSICS

Founded in 1895 by GEORGE E. HALE *and* JAMES E. KEELER

NOVEMBER 1942

THE UNIVERSITY OF CHICAGO PRESS
CHICAGO, ILLINOIS, U.S.A.

November 1942 Vol. 96, No. 3

THE ASTROPHYSICAL JOURNAL

AN INTERNATIONAL REVIEW OF SPECTROSCOPY AND ASTRONOMICAL PHYSICS

The Astrophysical Journal is published bimonthly by the University of Chicago at the University of Chicago Press, 5750 Ellis Avenue, Chicago, Illinois, during July, September, November, January, March, and May. ¶The subscription price is $10.00 a year; the price of single copies is $2.00. Orders for service of less than a full year will be charged at the single-copy rate. ¶Postage is prepaid by the publishers on all orders from the United States and its possessions, Argentina, Bolivia, Brazil, Chile, Colombia, Costa Rica, Cuba, Dominican Republic, Ecuador, Guatemala, Haiti, Republic of Honduras, Mexico, Morocco (Spanish Zone), Nicaragua, Panama, Paraguay, Peru, Rio de Oro, El Salvador, Spain (including Balearic Islands, Canary Islands, and the Spanish Offices in Northern Africa; Andorra), Spanish Guinea, Uruguay, and Venezuela. ¶Postage is charged extra as follows: for Canada and Newfoundland, 42 cents on annual subscriptions (total $10.42); on single copies, 7 cents (total $2.07); for all other countries in the Postal Union, 96 cents on annual subscriptions (total $10.96), on single copies 16 cents (total $2.16). ¶Patrons are requested to make all remittances payable to The University of Chicago Press, in United States currency or its equivalent by postal or express money orders or bank drafts.

The following are authorized agents:

For the British Empire, except North America, India, and Australasia: The Cambridge University Press, Bentley House, 200 Euston Road, London, N.W. 1, England. Prices of yearly subscriptions and of single copies may be had on application.

Claims for missing numbers should be made within the month following the regular month of publication. The publishers expect to supply missing numbers free only when losses have been sustained in transit, and when the reserve stock will permit.

Business correspondence should be addressed to The University of Chicago Press, Chicago, Illinois.

Communications for the editors and manuscripts should be addressed to: Otto Struve, Editor of THE ASTROPHYSICAL JOURNAL, Yerkes Observatory, Williams Bay, Wisconsin.

Line drawings and photographs should be made by the author, and all marginal notes such as co-ordinates, wave lengths, etc., should be included in the cuts. It will not be possible to set up such material in type.

One copy of the corrected galley proof should be returned as soon as possible to the editor, Yerkes Observatory, Williams Bay, Wisconsin. Authors should take notice that the manuscript will not be sent to them with the proof.

The cable address is "Observatory, Williamsbay, Wisconsin."

The articles in this journal are indexed in the *International Index to Periodicals*, New York, N.Y.

Applications for permission to quote from this journal should be addressed to The University of Chicago Press, and will be freely granted.

Entered as second-class matter, July 31, 1940, at the Post-Office at Chicago, Ill., under the act of March 3, 1879.
Acceptance for mailing at special rate of postage provided for in United States Postal Act of October 3, 1917, Section 1103, amended February 28, 1925.

[PRINTED IN U.S.A.]

THE ASTROPHYSICAL JOURNAL

AN INTERNATIONAL REVIEW OF SPECTROSCOPY AND ASTRONOMICAL PHYSICS

VOLUME 96 NOVEMBER 1942 NUMBER 3

CURVES OF GROWTH FOR THE A DWARFS, γ GEMINORUM AND SIRIUS

LAWRENCE H. ALLER[1]

ABSTRACT

Curves of growth are derived for γ Geminorum and Sirius from plates taken at the McDonald and Mount Wilson observatories. The excitation temperature of these stars turns out to be about 6000° and the ionization temperature about 8700°, as compared with an effective temperature of 10,000°. The electron pressure derived from the broadening of the hydrogen lines is about 1.2×10^2 dynes, as compared with about 7×10^2 dynes predicted by theory. If iron is half-ionized in the sun, the amount of metallic vapor above the photosphere of the sun is about twenty times the amount above the photosphere of Sirius. This result is in good agreement with that obtained by Adams and Russell in 1928. The amount of hydrogen in the A dwarfs is found to be about a thousand times the amount of iron (by weight).

The analysis and interpretation of the spectra of the A dwarfs should be one of the most straightforward and tractable of modern astrophysical problems. The lines of the metals, although faint, are visible and measurable. Many of these lines are present also in the sun, and their approximate strengths, as obtained from the curve of growth, are available. The outstanding features of A-type spectra are, of course, the hydrogen lines, which are greatly broadened by the Stark effect. The profiles of these lines have been measured by a number of investigators who have attributed the widening to the action of interatomic electrostatic fields amounting to as much as hundreds of electrostatic units.[2]

The opacity, whose estimation is difficult and uncertain for cooler stars, is probably due to continuous absorption by atomic hydrogen in the stars; and accurate theoretical calculations of this quantity may be made. Accordingly, it should be possible to calculate the properties of model atmospheres with some confidence and compare predictions based upon them with the observations.

We shall calculate such a model atmosphere and compare the predicted electron pressures with those estimated from the hydrogen lines. Also in this paper the excitation and ionization temperatures of the atmospheres of A dwarfs will be derived from the curves of growth constructed from measures of equivalent widths. We shall attempt to derive the relative numbers of atoms above the photospheres of the sun and an A dwarf and, from a comparison of the relative numbers of iron atoms above the photospheres of the sun and γ Geminorum, shall try to derive the ratio of hydrogen to iron. It will be shown

[1] Society of Fellows, Harvard University.

[2] See, e.g., E.G. Williams, *Ann. Solar Phys. Obs., Cambridge*, **2**, 25, 1932; C. T. Elvey, *Ap. J.*, **68**, 147, 1928, and **71**, 191, 1930; D. S. Evans, *M.N.*, **99**, 17, 1938; and A. Vibert Douglas and D. C. West, *M.N.*, **102**, 35, 1942.

that the abundance of hydrogen by weight is of the order of a thousand times that of iron. Although the line intensities upon which the investigation is based are provisional, it seems that we may draw certain definite conclusions from them.

Except near the Balmer limit it is easy to draw in the continuous spectrum of an A-type star. On the other hand, the lines are of low intensity, and the accidental errors in measuring them are rather high, with the result that there is a large scatter in the curves of growth.

The observational data upon which the present investigation rests are summarized in Table 1. The Mount Wilson Coudé plates of Sirius were traced there by Louis Berman

TABLE 1

OBSERVATIONAL DATA

Plate	Type	Date	Exp.	Region
	Plates of Sirius (Mt. Wilson)			
Coudé 370	15-foot grating	Nov. 2, 1930	35m	λλ 3800–4124
377		Feb. 9, 1931	90	5816–6575
445	15-foot prism	Feb. 21, 1931	102	5100–6580
635		April 12, 1933	35	4127–4960
640		April 13, 1933	92	5314–6580
859			.....	5314–6580
	Plates of Sirius (Lick)			
17123P	Mills 3-prism	Feb. 12, 1930	.....	λλ 4289–4635
17198M		March 20, 1930	.....	4289–4635
U30	Quartz slit spec.	Jan. 9, 1938	.....	3800–4000
U31		Jan. 20, 1938	.....	.....
U32		Jan. 20, 1938	.....	.....
	Plates of γ Geminorum (McDonald Observatory)			
Cd 101	Coudé	Feb. 10, 1941 5h47m G.C.T.	67m	λλ 3850–4703
Cd 105		Feb. 11, 1941 7 56	75	.....

and reduced by him and the author. I am indebted to him for permitting me to use this material in the present discussion. Plates taken at the Lick Observatory with the Mills 3-prism spectrograph attached to the 36-inch refractor supplement these data in the region λλ 4300–4600. D. M. Popper, then at the Lick Observatory, kindly obtained several plates of Sirius with the quartz ultraviolet spectrograph attached to the Crossley reflector.

Dr. Jesse Greenstein obtained two plates of γ Geminorum at the McDonald Observatory with the Coudé spectrograph. The emulsion used was Astro-Blue Sensitive, Eastman IaO. The standardizations were made with the aid of a tube photometer and a blue filter and an ultraviolet filter (18A). The observations cover the ordinary blue-violet region of the spectrum.

Reduction of the Coudé plates of Sirius showed that the earlier Mount Wilson grating plates were markedly affected by scattered light. I derived profiles of the hydrogen lines,

$H\epsilon$, $H\zeta$, and $H\eta$ from Popper's plates and compared with them profiles derived from the Coudé 370 plate. The hydrogen lines are so wide that the finite resolving-power of the instrument affects them only slightly. Generally, prism spectrographs do not scatter much light in the direction of dispersion, whereas grating instruments may do so to a substantial degree. Accordingly, I assumed that the light scattered by the prism was negligible and that the scattered light of the grating could be evaluated from the differences between the grating and the prism profiles. The scattered light in plate 370 amounted to 22 per cent. The metallic lines were so weak that they could be measured only on the high-dispersion grating plates in the region λλ 3800–4100, and their intensities had to be corrected for the effect of scattered light. The line intensities in this region of the spectrum are to be regarded as less accurate than those in the rest of the photographic region. Intensities of lines in the visual region are likewise deemed less accurate than those in the photographic region. I combined the intensities measured on the Mills plates with those obtained from the Coudé plates to obtain the final values for the photographic region.

The reduction of the McDonald plates of γ Geminorum revealed intensities generally the same as in Sirius. In Table 2 are presented the wave lengths, identifications, lower excitation potentials, and provisional intensities of the lines used in the present discussion. Many more lines than are tabulated were measured in each of these stars; some were blends, and strengths were not available for others. Whenever possible, I have taken the wave lengths from measures of Cd 105, which I made at the Yerkes Observatory. Otherwise, solar wave lengths have been used. For convenience of discussion the excitation potentials of the lower levels have also been given. The last two columns give log W/λ, where W is the equivalent width. These values are provisional. Although these values are probably adequate for the discussion at hand, improved measures are desirable. The letter *b* indicates that the line in question falls in a wing of a hydrogen line; in such a case the intensity is measured with respect to the profile of the hydrogen line.

Sirius is probably the best-known A dwarf. Its parallax, absolute brightness, and mass are accurately known, and its radius and surface gravity have been calculated from its luminosity, temperature, and mass. For this star we adopt the values given by Kuiper,[3] viz.:

$$\text{Mass} = 2.35\ , \qquad \text{Radius} = 1.8\ , \qquad \log g = 4.31\ .$$

Our information concerning the star γ Geminorum is not so complete. Dr. Carl L. Stearns of the Van Vleck Observatory has very kindly summarized for me the results of the parallax work on this star. The McCormick[4] and Yerkes observations[5] give trigonometric parallaxes of $+0''.028 \pm 0.006$ and $+0''.044 \pm 0.010$, respectively, while Stearns has derived a value of $+0''.025 \pm 0.007$. The Yale Catalogue of 1935 quotes a value, $\pi = +0''.040 \pm 0.006$. Since the apparent magnitude of the star is 1.93, the absolute magnitude is about 0.0 if we adopt the Yale Catalogue parallax and about −1.0 if we adopt Stearns's parallax. Evidently, γ Geminorum lies somewhat above the main sequence. The star is apparently a binary; Harper[6] obtained for it a period of 2175 days and a value of asini $= 1.74 \times 10^8$ km. Stearns[7] states that residuals from the parallax solution indicate the presence of oscillations in the proper motion in X and Y co-ordinates with semiamplitudes of $0''.049$ and $0''.071$, respectively, in Harper's period of 2175 days. He estimates that $a = 0''.08$ and $i = 78°$. Hence, from Harper's orbit, $a = 1.75 \times 10^8$ km. Luyten[8] has discussed the orbital motion of γ Geminorum and has derived a parallax of $0''.04$ and a mass ratio of 2.7:1. This value of the mass ratio yields a separation between primary and secondary of about 4.4 astronomical units.

[3] *Ap. J.*, **88**, 429, 1938.

[4] *Pub. McCormick Obs.*, **4**, 285.

[5] *A.J.*, **33**, 92, 1921.

[6] *J.R.A.S. Canada*, **6**, 179, 1912.

[7] *Pub. A.A.S.*, **10**, 174, 1942.

[8] *A.J.*, **43**, 109, 1933.

TABLE 2

PROVISIONAL EQUIVALENT WIDTHS OF ABSORPTION LINES IN SIRIUS AND γ GEMINORUM

λ	Iden.	Excitation Potential	−log W/λ		Note
			Sirius	γ Gem.	
3862.61	Si II	.....	0.098	.....	
3925.97	Fe I	2.896	.....	5.50	
3927.95	Fe I	0.110	5.09	4.92	
3930.31	Fe I	0.087	4.91	5.16	
3932.02	Ti II	1.126	.....	5.03	
3933.68	Ca II	0.000	.....	3.56	
3944.01	Al I	0.000	4.78	4.75	
3947.56	Fe I	2.819	.....	5.13	
3948.12	Fe I	3.227	.....	4.75	
3949.95	Fe I	2.167	.....	5.55	
3950.41	V II	0.104	.....	5.48	
3951.97	V II	1.470	.....	5.39	
3956.64	Fe I	2.681	.....	5.01	
3961.52	Al I	0.014	.....	4.78	
3962.36b	Fe I	3.252	5.18	.....	
3968.52b	Ca II	0.000	.....	4.10	
3986.79	Mg I	4.327	.....	5.27	
3997.40	Fe I	2.716	.....	5.26	
3998.03	Fe I	2.681	.....	5.47	
4001.69	Fe I	2.167	5.26	.....	
4005.26	Fe I	1.551	4.71	4.89	
4005.70	V II	1.809	5.19	5.03	
4007.21	Fe I	2.747	5.11	.....	
4009.75	Fe I	2.213	5.30	.....	
4015.52	Ni II	4.015	.....	5.28	
4016.38	Fe I	3.269	5.10	.....	
4017.17	Fe I	3.039	5.49	5.49	
4021.88	Fe I	2.747	5.19	5.19	
4024.59	Fe II	.....	.....	.....	
4025.14	Ti II	0.605	.....	4.94	
4028.35	Ti II	1.884	5.04	4.86	
4030.77	Mn I	0.000	5.01	5.10	
4033.02	Mn I	0.000	5.07	4.82	
4034.47	Mn I	0.000	.....	5.40	
4035.63	V II	1.785	5.30	4.91	
4041.35	Mn I	.....	.....	5.26	1
4044.00	Fe II	.....	.....	.....	
4045.80	Fe I	1.478	4.70	4.63	
4062.50	Fe I	2.833	5.10	5.50	
4063.61	Fe I	1.551	4.62	4.73	
4067.05	Ni II, Cr II	.....	.....	.....	
4067.99	Fe I	3.197	5.31	5.33	
4071.76	Fe I	1.601	4.59	4.90	
4073.87	Fe I	3.252	4.80	5.37	
4075.49	Si II	.....	.....	5.29	
4076.69b	Fe I	3.197	4.96	4.95	
4077.70	Sr II	0.000	4.53	4.72	
4122.64	Fe II	2.572	5.07	4.91	
4128.06	Si II	.....	.....	4.66	
4128.75	Fe II	2.572	5.08	5.18	
4130.88	Si II	.....	4.37	4.71	
4132.04	Fe I	1.601	4.72	4.88	
4132.97	Fe I	1.601	5.14	.....	
4134.67	Fe I	2.819	5.18	5.71	
4143.37	Fe I	3.034	5.25	5.28	
4143.87	Fe I	1.551	4.81	5.00	
4153.90	Fe I	3.382	5.50	.....	
4154.49	Fe I	2.819	5.77	.....	
4154.82	Fe I	3.354	5.92	.....	
4157.80	Fe I	3.402	5.83	.....	
4163.65	Ti II	2.579	4.72	4.81	
4167.27	Mg I	4.327	5.10	5.06	
4171.00	Fe I	3.004	5.47	5.72	
4173.47	Fe II	2.572	4.57	4.59	
4175.60	Fe I	2.833	5.44	5.42	
4178.85	Fe II	2.572	4.62	4.79	
4181.72	Fe I	2.819	4.80	.....	
4183.45	V II	2.041	.....	5.26	
4184.93	Fe I	2.819	5.51	5.63	
4187.02	Fe I	2.439	5.19	5.16	
4187.81	Fe I	2.415	4.76	4.99	
4191.42	Fe I	2.458	5.32	5.13	
4191.65	Fe I	2.846	5.62	.....	
4195.38	Fe I	3.318	.....	5.20	
4210.31	Fe I	2.471	5.51	5.48	
4215.51	Sr II	0.000	4.62	4.76	
4222.23	Fe I	2.439	5.42	5.39	
4224.13	Fe I	3.354	5.04	5.00	
4225.42	Fe I	3.402	5.67	5.51	
4226.71	Ca I	0.000	5.06	4.70	
4227.41	Fe I	3.318	4.83	4.88	
4233.18	Fe II	2.572	4.48	4.63	
4233.61	Fe I	2.471	5.37	5.12	
4235.92	Fe I	2.415	5.00	4.86	
4238.03	Fe I	3.402	5.51	5.36	
4238.81	Fe I	3.382	5.63	5.05	
4244.82	Ni II	4.015	.....	5.37	
4245.32	Fe I	2.846	4.85	5.48	
4246.83	Sc II	0.314	.....	4.74	
4247.41	Fe I	3.354	5.15	5.14	
4248.16	Fe I	3.058	.....	5.78	
4250.10	Fe I	2.958	4.91	4.96	
4250.78	Fe I	1.551	4.88	4.91	
4251.73	Mn II	.....	5.73	.....	
4252.61	Cr II	3.842	4.99	5.40	
4254.33	Cr I	0.000	4.78	4.90	
4259.22	Mn II	.....	6.03	.....	
4260.46	Fe I	2.389	4.69	4.70	
4261.92	Cr II	3.848	4.73	4.91	
4269.22	Cr II	3.837	5.12	4.93	
4271.16	Fe I	2.439	5.00	5.13	
4274.80	Cr I	0.000	5.09	5.22	
4282.41	Fe I	2.167	5.05	5.04	
4283.02	Ca I	1.878	5.48	.....	
4284.20	Cr II	3.837	4.93	4.99	
4287.90	Ti II	1.075	5.17	5.13	
4289.37	Ca I	1.871	5.92	.....	
4289.79	Cr I	0.000	5.24	5.40	
4290.22	Ti II	1.160	4.77	4.66	

TABLE 2—*Continued*

λ	Iden.	Excitation Potential	−log W/λ		Note
			Sirius	γ Gem.	
4296.56	*Fe* II	2.693	4.82	4.81	
4299.21	*Fe* I	2.415	5.06	.....	
4300.04	*Ti* II	1.175	.....	4.60	
4301.92	*Ti* II	1.156	4.95	4.70	
4303.16	*Fe* II	2.693	4.74	4.69	
4312.86	*Ti* II, *Sc* II	1.175	4.80	4.72	
4314.16	*Fe* II	.....	.....	.....	
4316.78	*Ti* II	2.039	.....	5.10	
4325.01b	*Sc* II	0.593	.....	5.19	
4325.76b	*Fe* I	1.601	4.71	4.74	2
4330.72b	*Ti* II	2.039	5.85	5.38	
4337.90b	*Ti* II	1.075	5.74	4.90	
4352.74b	*Fe* I	2.213	5.74	5.54	
4362.22b	*Ni* II	3.976	5.21	5.33	
4369.41	*Fe* II	2.766	5.16	5.04	
4374.44	*Sc* II	0.616	.....	5.08	
4374.85	*Ti* II	2.052	4.89	4.98	
4383.53	*Fe* I	1.478	4.62	4.70	
4384.28	*Fe* II	.....	.....	.....	
4384.63	*Mg* II	.....	4.81	4.89	
4385.38	*Fe* II	2.766	.....	4.77	
4386.85	*Ti* II	2.586	5.34	5.16	
4390.53	*Mg* II	.....	4.87	4.77	
4394.04	*Ti* II	1.216	5.44	5.06	
4395.02	*Ti* II	1.079	4.65	4.62	
4395.86	*Ti* II	1.238	5.80	5.28	
4399.77	*Ti* II	1.230	4.85	4.72	
4400.41	*Sc* II	0.603	.....	5.10	
4404.74	*Fe* I	1.551	4.68	4.70	
4408.37	*Fe* I	2.188	.....	5.20	
4415.08	*Fe* I	1.601	4.88	4.87	
4416.80	*Fe* II	2.766	4.76	4.86	
4417.69	*Ti* II	1.160	4.92	4.81	
4418.32	*Ti* II	1.232	5.96	5.30	
4421.95	*Ti* II	2.052	.....	5.28	
4427.32	*Fe* I	0.051	5.64	.....	
4430.62	*Fe* I	2.213	5.74	.....	
4433.96	*Mg* II	.....	5.12	5.12	
4434.83	*Ca*	1.878	blend	with *Fe*	
4435.16	*Fe* I	0.087	5.49	.....	
4442.35	*Fe* I	2.188	5.17	.....	
4443.20	*Fe* I	2.846	5.47	.....	
4443.89	*Ti* II	1.075	4.66	4.70	
4444.57	*Ti* II	1.111	.....	5.15	
4447.71	*Fe* I	2.213	5.35	5.19	
4450.47	*Ti* II	1.079	4.80	4.84	
4461.67	*Fe* I	0.087	5.10	.....	
4466.59	*Fe* I	2.819	5.31	4.99	
4468.47	*Ti* II	1.126	4.74	4.64	
4470.82	*Ti* II	1.160	5.80	5.00	
4472.90	*Fe* II	.....	.....	5.04	
4476.09	*Fe* I	2.833	5.03	.....	
4481.22	*Mg* II	8.825	4.11	4.02	
4488.28	*Ti* II	3.110	5.10	4.85	
4489.15	*Fe* II	2.816	4.78	4.92	
4491.36	*Fe* II	2.843	4.73	4.71	
4493.55	*Ti* II	1.075	5.62	.....	
4494.51	*Fi* I	2.188	5.05	.....	
4496.93	*Zr* II	0.710	5.57	.....	
4501.24	*Ti* II	1.111	4.73	4.57	
4508.26	*Fe* II	2.843	4.66	4.66	
4515.31	*Fe* II	2.832	4.68	4.71	
4520.21	*Fe* II	2.795	4.68	4.73	
4522.59	*Fe* II	2.832	4.64	4.58	
4528.54	*Fe* I, VII	2.167	4.89	4.94	
4529.48	*Ti* II	1.565	5.36	5.12	
4533.98	*Ti* II	1.232	4.53	4.47	
4540.60	*Cr* I	2.533	5.74	.....	
4541.50	*Fe* II	2.843	4.79	4.84	
4549.51	*Fe* II, *Ti* II	2.816	4.25	4.21	
4553.98	*Ba* II	0.000	4.77	4.92	
4554.90	*Cr* II	4.054	.....	4.97	
4555.84	*Fe* II	2.816	4.88	4.68	
4558.60	*Cr* II	4.056	4.62	4.63	
4563.70	*Ti* II	1.216	4.76	4.62	
4571.92	*Ti* II	1.565	4.63	4.62	
4576.25	*Fe* II	2.832	4.77	4.84	
4582.75	*Fe* II	2.832	4.98	4.94	
4583.79	*Fe* II	2.795	4.50	4.54	
4588.16	*Cr* II	4.054	4.65	4.68	
4589.89	*Ti* II	1.232	5.02	5.08	
4592.00	*Cr* II	4.057	4.78	4.78	
4616.63	*Cr* II	4.055	4.92	5.10	
4618.80	*Cr* II	4.057	4.70	4.75	
4620.48	*Fe* II	2.816	4.89	4.96	
4634.04	*Cr* II	4.055	4.69	4.81	
4656.98	*Fe* II	2.879	5.22	5.29	
4663.63	*Fe* II	2.879	5.39	.....	
4703.00	*Mg* I	4.327	5.01	5.04	
4710.14	*Fe* I	.....	.....	.....	
4714.49	*Ni* I	3.365	5.10	.....	
4731.50r	*Fe* II	2.879	5.01	.....	
4736.79	*Fe* I	3.197	5.60	.....	
4806.85	*Ni* I	3.663	5.20	.....	
4810.47	*Zn*	4.060	5.03	.....	
4812.38	*Cr* II	3.848	5.10	.....	
4836.27b	*Cr* II	3.842	4.80	.....	
4848.23b	*Cr* II	3.848	4.78	.....	
4876.47b	*Cr* II	3.837	4.82	.....	
4883.70	*Y* II	1.079	4.81	.....	
4884.62	*Cr* II	3.842	4.78	.....	
4890.77	*Fe* I	2.863	5.10	.....	
4891.51	*Fe* I	2.839	5.17	.....	
4919.09	*Fe* I	2.853	5.16	.....	
4920.52	*Fe* I	2.820	4.83	.....	
4923.90	*Fe* II	2.879	4.52	.....	
4934.05	*Ba* II	0.000	4.79	.....	
4957.31	*Fe* I	2.839	4.70	.....	
5129.12	*Ti* II	1.884	5.04	.....	
5133.70	*Fe* I	4.160	5.33	.....	

TABLE 2—*Continued*

λ	Iden.	Excitation Potential	−log W/λ		Note
			Sirius	γ Gem.	
5162.30	Fe I, Mg I	2.597	5.25	.....	
5167.35	Fe I	2.697	4.56	.....	
5169.05	Fe II	2.879	4.43	.....	
5171.61	Fe I	1.478	5.39	.....	
5172.67	Mg I	2.700	4.53	.....	
5183.60	Mg I	2.705	4.65	.....	
5185.93	Ti II	1.885	5.13	.....	
5188.79	Ti II	1.575	5.09	.....	
5192.50	Fe I	2.985	4.97	.....	
5195.20	Fe I	4.202	5.18	.....	
5197.56	Fe II	3.217	4.74	.....	
5200.35	V II	0.990	5.48	.....	
5215.16	Fe I	3.252	4.99	.....	
5226.66	Ti II	1.559	4.81	.....	
5227.24	Fe I	1.551	4.65	.....	
5234.62	Fe II	3.207	4.69	.....	
5237.33	Cr II	4.056	4.76	.....	
5245.53	Ni I	.....	5.77	.....	
5253.65	Fe I	3.269	5.77	.....	
5256.94	Fe II	2.879	5.47	.....	
5264.80	Fe II	3.217	4.93	.....	
5266.58	Fe I	2.985	5.06	.....	
5269.54	Fe I	0.855	5.13	.....	
5275.95	Fe II	3.186	4.62	.....	
5281.80	Fe I	3.025	5.40	.....	
5283.59	Fe I	3.227	5.47	.....	
5284.10	Fe II	2.879	5.07	.....	
5302.22	Fe I, Cr II	3.269	5.22	.....	
5305.85	Fe II(?)	3.810	5.01	.....	
5308.44	Cr II	4.054	5.23	.....	
5310.73	Cr II	4.055	5.26	.....	
5316.76	Fe II	3.139 3.207	4.42	.....	3
5324.20	Fe I, Fe I	3.197	5.06	.....	
5328.13	Cr I	0.911	4.88	.....	
5334.95	Cr II	4.055	5.17	.....	
5336.83	Ti II, Cr II, Fe II	1.575	5.45	.....	
5346.57	Cr II	3.217	5.22	.....	2
5362.87	Fe II	3.186	4.80	.....	
5364.80	Fe I	4.294	5.53	.....	
5367.46	Fe I	4.426	5.43	.....	
5370.00	Fe I	4.396	5.12	.....	
5371.55	Fe I	0.954	5.33	.....	
5383.40	Fe I	4.302	5.08	.....	
5393.19	Fe II	.....	.....	.....	
5405.47	Fe I	0.986	5.41	.....	
5414.10	Fe II	3.207	5.34	.....	
5420.99	Cr II	3.742	5.59	.....	
5425.26	Fe II	3.186	5.15	.....	
5446.92	Fe I	0.986	5.34	.....	
5455.65	Fe I	1.007	5.11	.....	
5463.27	Fe I	4.416	5.74	.....	
5502.41	Cr II	4.150	5.36	.....	
5508.85	Cr II	4.138	5.44	.....	
5511.20	Cr II	3.810	5.30?	.....	
5528.47	Mg I	4.327	5.05	.....	
5543.19	Fe I	4.368	5.90	.....	
5569.65	Fe I	3.402	5.60	.....	
5572.86	Fe I	3.382	5.44	.....	
5586.77	Fe I	3.354	4.99	.....	
5615.66	Fe I	3.318	5.20	.....	
5624.56	Fe I	3.402	5.30	.....	
5645.61	Si I	4.908	5.75	.....	
5658.02	Sc II	1.500	5.75	.....	
5658.65	Fe I, Sc II	1.491	.....	.....	2
5853.68	Ba II	0.602	5.51	.....	
5889.96	Na I	0.000	4.62	.....	
5895.93	Na I	0.000	4.70	.....	
5934.68	Fe I	3.912	5.70	.....	
5952.75	Fe I	3.967	5.54	.....	
6024.07	Fe I	4.529	5.08	.....	
6141.70	Fe I	4.814	5.00	.....	
6149.25	Fe II	3.873	5.01	.....	
6169.43	Ca	2.515	5.62	.....	
6238.39	Fe II	3.872	5.10	.....	
6239.97	Fe II	3.873	5.54	.....	
6247.56	Fe II	3.875	4.89	.....	
6301.87	Fe I	3.638	5.13	.....	
6302.61	Fe I	3.671	5.10	.....	
6318.03	Fe I	2.443	4.97	.....	
6347.09	Si II	8.085	4.53	.....	
6371.35	Si II	.....	4.65	.....	
6416.92	Fe II	3.875	5.11	.....	
6432.69	Fe II	2.879	5.19	.....	
6456.40	Fe II	3.887	4.72	.....	
6494.94	Fe I	2.394	5.81	.....	
6496.94	Ba II	0.602	5.43	.....	

NOTES

1. Blend in sun.
2. Blend in A dwarf.
3. Blend of two iron lines.

THE EXCITATION TEMPERATURE

Our observational material consists of a tabulation of the quantity W/λ for a number of selected spectral lines. The curve of growth relates W/λ and X_0[9], the optical depth in the center of the line, which is given by

$$X_0 = N \frac{\pi e^2}{m c} f \frac{c}{\sqrt{\pi}\, v \nu_0}, \tag{1}$$

where v is the most probable kinetic velocity of the atoms (unless turbulence exists) and ν_0 is the frequency of the line, while N is the number of atoms capable of absorbing the line in question and f is the oscillator strength related to the integrated line-absorption coefficient by

$$\int a_\nu d\nu = \frac{\pi e^2}{m c} f.$$

If χ is the excitation potential and ϖ the statistical weight of the ground level of the line in question, we may express X_0 in terms of N_a, the number of neutral or ionized atoms of the given kind above the photosphere, viz.,

$$X_0 = N_a \frac{\varpi}{b(T)} 10^{-5040\chi/T} \frac{\pi e^2}{m c} f \frac{c}{\sqrt{\pi}\nu_0 v}. \tag{2}$$

Menzel and Goldberg have derived values of $\log X_0$ and the quantity

$$\log X_0' = \log X_0 + \frac{5040\chi}{T} \tag{3}$$

from the solar data published by Allen.[10] To determine the excitation temperature we may group the lines of a given ion, e.g., *Fe* I, according to the excitation potentials of their lower levels. Then we may plot $\log W/\lambda$ against $\log X_0'$ for each group and slide the curves together until the best fit is obtained; or we may assume various values of the temperature, e.g., 6000°, 8000°, or 10,000°, and plot $\log W/\lambda$ against $\log X_0$. For the most probable excitation temperature the points corresponding to low-level lines (0–1 volts) will not be displaced with respect to those corresponding to the higher-level lines (3–4 volts). By this latter method I have found an excitation temperature of about 6000° for both γ Geminorum and Sirius. For a number of the *Fe* I lines, laboratory measures of gf values have been made by R. B. and A. S. King,[11] a plot of $\log W/\lambda - \log gf$ for the five lines of the $a^5D - z^5D^0$ multiplet ($\chi = 0.1$ volts) was compared with a plot of the eleven lines of the $a^3F - y^3F$, z^3G^0, z^5G^0 multiplets ($\chi = 1.5$ volts); and with the theoretical curve of growth. A satisfactory fit could be obtained for a temperature of 6000°. There is a large difference between the excitation temperature of about 6000° and the effective temperature which is near 10,000°. Differences of the same character have been found for the sun by King[12] and by Menzel, Baker, and Goldberg,[13] and for Canopus by Greenstein.[14]

The theoretical curve of growth has been calculated with the aid of Menzel's asymptotic formulae. If the value of Nf is so small that $X_0 < 1$, then

$$\frac{w}{\lambda}\frac{c}{v} \sim \sqrt{\pi} X_0 \left(1 - \frac{X_0}{\sqrt{2}} + \frac{X_0}{\sqrt{3}} + \dots\right); \tag{4}$$

[9] We follow here the formulae developed by D. H. Menzel, *Ap. J.*, **84**, 462, 1936.

[10] *Mem. Commonwealth Solar. Obs.*, **1**, No. 5, 1934.

[11] *Ap. J.*, **87**, 24, 1938.

[12] *Ap. J.*, **87**, 40, 1938.

[13] *Ap. J.*, **87**, 81, 1938.

[14] *Ap. J.*, **95**, 161, 1942.

while if $X_0 > 1$, but not so large that wing damping must be considered,

$$\frac{w}{\lambda}\frac{c}{v} \sim 2\,[ln X_0]^{1/2}; \tag{5}$$

while for the damping portion of the curve of growth, when $X_0 >> 1$,

$$\frac{w}{\lambda}\frac{c}{v} \sim \frac{\pi^{1/4}}{2}\left(\frac{c}{v} X_0 \frac{\Gamma}{\nu}\right)^{1/2}, \tag{6}$$

where Γ is generally taken as the damping constant and c, π, λ, and ν have their usual significance. If there is no turbulence, v is simply the most probable kinetic velocity of the atoms. Otherwise, as Struve and his collaborators have shown, we must use for v the turbulent velocities.

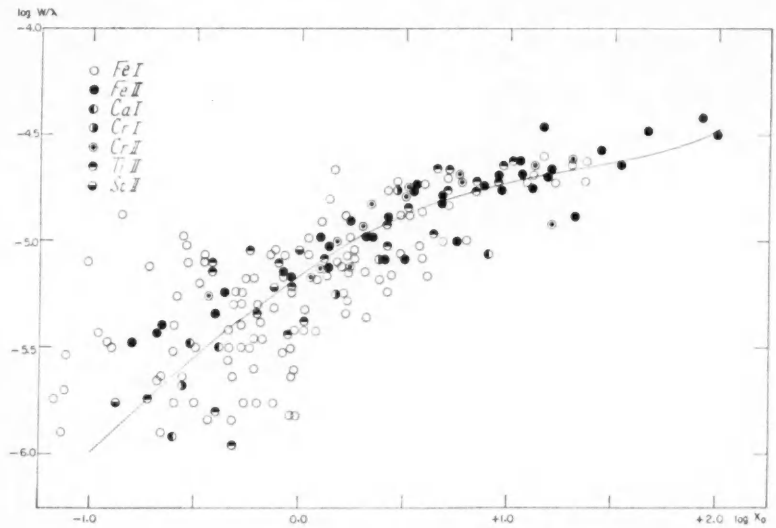

FIG. 1.—The curve of growth for Sirius. The line is the theoretical curve

In constructing the curve of growth for γ Geminorum and Sirius I have assumed an excitation temperature of 6000° and have plotted for each atom in each stage of ionization, log W/λ against the quantity log X_r, where

$$\log X_r = 5040\chi\left(\frac{1}{T_s} - \frac{1}{T_1}\right) + \log X_s. \tag{7}$$

T_s is the excitation temperature of the sun, T_1 is the excitation temperature of an A-dwarf star (adopted as 6000°), and the value of X_0 for the sun is called X_s (see Figs. 1 and 2).

The plots of log W/λ − log X_r are fitted to the curve of growth, vertically to obtain the factor c/v and horizontally to obtain log X_r − log X_1, where we call X_1 the value of X_0 for the star in question. In practice the value of c/v may be found most accurately from the ions whose lines fall on the flat portion of the curve of growth. I found values of $c/v = 1.6 \times 10^5$, and 1.73×10^5 for Sirius and γ Geminorum, respectively. These correspond to kinetic temperatures of 10,000° and 12,000°, respectively. Now, for the sun

$$X_0 = X_s = N_s \frac{\varpi}{b\,(T)_s}\, 10^{-5040\chi/T_s} \frac{\pi\epsilon^2}{mc}\, f \frac{c}{\sqrt{\pi\nu_0 v_s}}, \tag{8}$$

while for the A star

$$X_0 = X_1 = N_1 \frac{\varpi}{b(T_1)} 10^{-5040\chi/T_1} \frac{\pi e^2}{m c} f \frac{c}{\sqrt{\pi}\nu_0 v_1}. \tag{9}$$

Then

$$\frac{X_s}{X_1} = \frac{N_s}{N_1} \frac{b(T_1)}{b(T_s)} 10^{-5040\chi(1/T_s - 1/T_1)} \frac{v_1}{v_s}, \tag{10}$$

whence the relative numbers of atoms of the given kind above the photosphere of the sun and the A star are given by

$$\frac{N_s}{N_1} = \frac{X_r}{X_1} \frac{b(T_s)}{b(T_1)} \frac{v_s}{v_1}. \tag{11}$$

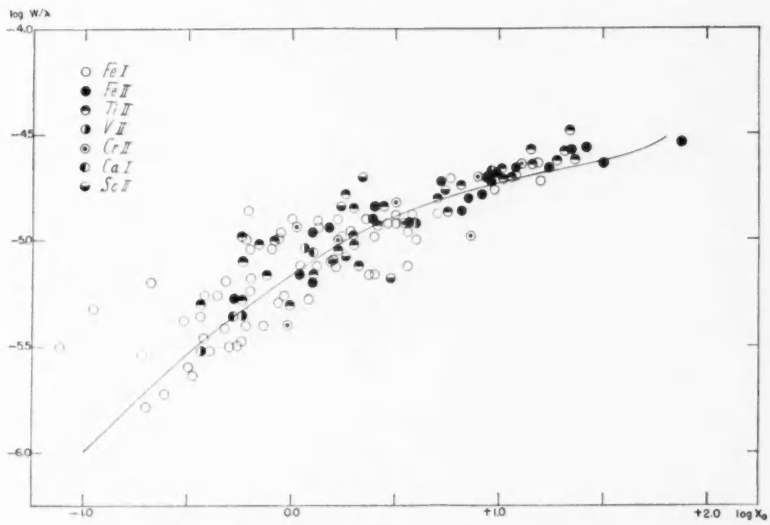

FIG. 2.—The curve of growth for γ Geminorum. The line is the theoretical curve

The ratio, N_s/N_1, depends on several factors: the effective depth of the photosphere, the degree of ionization, the excitation temperature, and the kinetic temperature. The ionization and hence the continuous absorption coefficient depend upon the electron pressure and the ionization temperature. The latter may depend upon the ionization potential, as the star may not radiate like a black body in the ultraviolet. Furthermore, when the continuous absorption coefficient arises chiefly from transitions from excited levels, as is the case with hydrogen in the ordinary spectral regions, we would have to take into account, also, the excitation temperature of the levels involved. The evidence indicates that the excitation temperature of hydrogen is much higher than the 6000° obtained for the metals, and for the discussion of the hydrogen lines I have assumed an excitation temperature of 10,000°. The ionization temperature for the metals has to be evaluated empirically. The effective depth of the photosphere at any wave length will depend upon the structure of the atmosphere, i.e., the variation of electron pressure and temperature with optical depth and the wave-length variation of the continuous absorption coefficient.

A MODEL ATMOSPHERE FOR AN A-TYPE DWARF

Let us now discuss the electron pressure and temperature in a model atmosphere for which the initial parameters of surface gravity and effective temperature are chosen to resemble as closely as possible the known values for an A dwarf. We shall suppose the atmosphere to be in hydrostatic equilibrium, so that the increase in pressure in a distance dh is simply

$$dP = -g\rho dh = -\frac{g d\tau}{\kappa}, \tag{12}$$

since $d\tau = \kappa\rho dh$. Now

$$P = P_g + P_r, \tag{13}$$

i.e., gas pressure plus radiation pressure, and g is the acceleration of gravity. According to the gas law,

$$P_g = nkT. \tag{14}$$

If the gas pressure acted alone, we should have

$$dP_g = -\frac{g d\tau}{\kappa}. \tag{15}$$

We may continue to use this type of equation, provided we redefine an effective surface gravity

$$g_e = g - g', \tag{16}$$

where g' is the acceleration due to the pressure of radiation.

Consider a volume element ρdh exposed to radiation in a stellar atmosphere. The amount of radiation absorbed from an elementary beam $I_\nu(\theta)$ of solid angle $d\omega$, making an angle θ with the outward-directed normal, will be

$$\rho dh\, \kappa_\nu I_\nu(h, \theta)\, d\omega \sec\theta .$$

The factor sec θ enters because of the foreshortening. Now the momentum carried by this radiation of intensity $I_\nu(h, \theta)$ falling upon a surface at an angle θ is $I_\nu \cos^2\theta/c$. Hence the momentum gained by the volume element is $\rho dh\kappa_\nu/c\ I_\nu(h, \theta) \cos\theta\, d\omega$. Integrating over all solid angles and frequencies, we find

$$\frac{\rho dh}{c}\int \kappa_\nu F_\nu d\nu = \rho dh\, g', \tag{17}$$

where

$$F_\nu = 2\pi\int_0^{\pi/2} I_\nu(\theta, h)\cos\theta \sin\theta d\theta$$

and g' is the acceleration of the volume element. We obtain

$$g' = \frac{1}{c}\int \kappa_\nu F_\nu d\nu. \tag{18}$$

If the stellar material is gray, i.e., κ_ν does not depend on ν and the star radiates like a black body, we find

$$g' = \frac{\kappa\sigma}{c} T_e^4. \tag{19}$$

Then we may write

$$dP_g = -(g - g')\frac{d\tau}{\kappa} = -g_e\frac{d\tau}{\kappa}. \tag{20}$$

For a dwarf star radiating like a black body at 10,000° we may easily show that $g' << g$. Now

$$\sigma = 5.75 \times 10^{-5} \text{ erg/cm}^2\text{/sec/deg}^4 ,$$

and we may take $\kappa = 27$ from the computations of Strömgren. Then we find $g' = 5.17 \times 10^2$ dynes, as compared with a surface gravity of $g = 2 \times 10^4$ dynes.

Selective radiation pressure such as appears to be operative in the solar chromosphere is another problem, and the indications are that such selective pressure may play a significant role in supporting the upper layers of the stellar atmosphere. Although in our model star which radiates like a black body at 10,000° we may neglect radiation pressure in comparison with gas pressure, we have no reason to suppose that we can continue to do so for a real star.

Integration of the equation of hydrostatic equilibrium gives the gas pressure, P_g, as a function of the optical depth τ. However, we must know $\bar{\kappa}\ (P_e, T)$. The relation between temperature and optical depth is simply

$$T^4 = \tfrac{1}{2} T_e^4 (1 + \tfrac{3}{2} \bar{\tau}) \tag{21}$$

where

$$\bar{\tau} = \int_0^h \bar{\kappa} \rho dh , \tag{22}$$

and $\bar{\kappa}$ is the Rosseland mean absorption coefficient. The relation between P_g and P_e is less simple. Let N_0 be the total number of atoms of all kinds, and let N_e be the number of electrons. Further, let the N_0 atoms be sorted into groups according to their ionization potential, such that N_j denotes the number of atoms of first ionization potential, χ_j, while x_j denotes the fraction of these atoms that have been ionized once and x_j' the fraction that have been twice ionized. Then

$$\left.\begin{aligned} N_e &= \Sigma N_j (x_j + x_j') , & N_0 &= \Sigma N_j , \\ P_g &= NkT = (N_0 + N_e) kT , \quad \text{and} & P_e &= N_e kT . \end{aligned}\right\} \tag{23}$$

Therefore,

$$\frac{P_g}{P_e} = \frac{N_0 + N_e}{N_e} = \frac{1 + \dfrac{N_e}{N_0}}{\dfrac{N_e}{N_0}} . \tag{24}$$

Our problem is to calculate N_e/N_0 as a function of T and P_e. We must first adopt relative abundances of the various kinds of atoms. In Table 3 we give the element, the adopted abundance, the numbers of atoms, their ionization potentials, and the groups in which they have been placed for the calculations of relative ionizations. I have calculated the ionization in the usual fashion for a series of values of $\theta = 5040/T$ and $\log P_e$. A summation of the $N_j x_j$'s for each value of $\log P_e$ and θ and division by N_0 gives us the quantity N_e/N_0 from which $\log P_g$ is readily calculated as a function of $\log P_e$ and θ (see Table 4).

For the present calculations I have adopted the continuous absorption coefficients given by Strömgren.[15] He tabulates $\log \bar{\kappa}$ against $\log P_e$ and θ. In a star as hot as Sirius or γ Geminorum the bulk of the opacity arises from the continuous absorption of atomic hydrogen. The absorption of negative hydrogen ions is of relatively small importance, except for the higher electron pressures. I have neglected the contribution to the opacity by the metals. Greenstein has shown that one may also neglect the continuous absorption of helium.[16]

[15] *Festschrift für Elis Strömgren*, p. 218, 1940.

[16] *Ap. J.*, **95**, 299, 1942.

TABLE 3

THE ADOPTED RELATIVE ABUNDANCES OF THE ATOMS

Element	Abundance by Weight	Number of Atoms	Ionization Potential	Ionization Group	
				Relative Abundance	Ionization Potential (In Volts)
Helium	800	200	24.46	201	24.5
Neon	25	1.20	21.47		
Hydrogen	1000	1000	13.53	1000	13.53
Oxygen	12	0.75	13.55		
Nitrogen	5	0.36	14.46		
Carbon	2	0.17	11.20		
Iron	0.5	0.009	7.83	0.43	7.9
Silicon	2.5	0.090	8.14		
Magnesium	8.0	0.330	7.61		
Nickel	0.2	0.0034	8.65		
Aluminum	0.1	0.0038	5.95	0.011	5.8
Calcium	0.2	0.0025	6.09		
Sodium	0.1	0.0043	5.11		

TABLE 4

THE RELATION BETWEEN GAS PRESSURE AND ELECTRON PRESSURE AS A FUNCTION OF TEMPERATURE

		log P_g									
	θ =	0.3	0.4	0.5	0.6	0.7	0.8	1.0	1.2	1.4	1.6
log P_e	−2	−1.70	−1.70	−1.68	−1.66	−1.65	−1.53	0.73	1.46	2.13	2.02
	−1	−0.70	−0.70	−0.66	−0.66	−0.62	0.00	2.30	3.68	4.80	5.38
	0	0.30	0.30	0.34	0.47	0.65	1.89	3.46	4.31	5.23	5.08
	1	1.30	1.33	1.35	1.60	2.43	3.78	4.80	5.93	6.85	8.08
	2	2.30	2.34	2.38	2.99	4.36	5.36	6.53	7.59		
	3	3.31	3.35	3.64	4.88	6.15	6.89				
	4	4.34	4.44	5.37	6.78						

TABLE 5

RESULTS OF NUMERICAL INTEGRATIONS FOR THE ATMOSPHERE OF AN A DWARF

θ	$\bar{\tau}$	log Pg	log Pe	log κ
0.59	0.021	3.00	2.00	0.28
.55	0.24	3.30	2.45	0.65
.50	0.67	3.51	2.90	1.08
.45	1.39	3.63	3.10	1.23
.40	2.59	3.72	3.30	1.40
0.35	5.10	3.90	3.50	1.12

The numerical integrations were carried out by successive approximations with $\theta = 5040/T$ as the independent variable. I adopted $\log g = 4.31$ and $T_e = 10{,}000°$ (see Table 5).

We notice that the electron pressure and the absorption coefficient at first increase rapidly with optical depth and then rise relatively slowly. In the layers relevant in the production of the absorption lines, $\bar{\tau} = 0.65$, $P_e \sim 10^3$, and $\bar{\kappa} \sim 10$.

In the Schuster-Schwarzschild approximation of a stellar atmosphere a layer of scattering atoms overlies a sharply defined photosphere at an optical depth τ_0 given by[17]

$$\tau_0 = \frac{1}{1 + \frac{3}{2\beta_0}} \tag{25}$$

where

$$\beta_0 = \frac{\frac{3}{8}\frac{h\nu}{kT_0}}{1 - e^{-h\nu/kT_0}} \frac{\bar{\kappa}}{\kappa_\nu}. \tag{26}$$

T_0 is the boundary temperature, $\bar{\kappa}$ is the Rosseland mean absorption coefficient, and κ_ν is the absorption coefficient at the frequency ν. The latter quantity may be calculated from the absorption coefficients for atomic hydrogen and negative hydrogen ions as a function of temperature and electron pressure.

In a hot star, where the continuous absorption is due mainly to atomic hydrogen, the depth of the photosphere will vary with wave length, that is, the number of atoms above the photosphere will not be the same in the violet and in the red portions of the spectrum. The mass above the photosphere in the Schuster-Schwarzschild model is simply

$$\mathcal{M} = \frac{\tau_0}{\bar{\kappa}_\nu},$$

where $\bar{\kappa}_\nu$ is the average value of κ_ν with depth. Another way of estimating the wavelength variation of the mass above the photosphere is to count only the mass above τ_0, as though no more radiation from the lower levels reached the observer and the atmosphere were transparent above this point. This approximation appears to give an upper limit to the variation. Thirdly, we may calculate the quantity

$$\eta_e = \int \eta\, e^{-\tau \overline{\sec\theta}} dx,$$

where $\overline{\sec\theta} = 1.5$, since the radiation from a volume at the depth τ is weakened in the mean by a factor $e^{-\tau \overline{\sec\theta}}$. From a comparison of the results of these three methods of estimating the numbers of atoms above the photosphere, I have adopted the wavelength variation shown in the accompanying table. The procedure I have adopted is ad-

λ	3750	4000	4500	5000	5500	6000	6500
$N_\lambda/N_{\lambda 0}$	1.48	1.35	1.15	1.00	0.91	0.85	0.80

mittedly rough. Properly, one should take into account the variation of ionization with depth, when one considers any given atom in any specified state of ionization—that is, we should provide a table of $N_\lambda/N_{\lambda 0}$ for each ion. I have not done this because the accuracy of the theory and the precision of the observations seemed scarcely great

[17] Unsöld, *Physik der Sternatmosphären*, pp. 239 and 261, Springer, 1938.

enough to justify the added labor involved. Finally, we may define a corrected X_r for a photosphere of variable depth, as follows:

$$X_r = 10^{5040\chi(1/T_s - 1/T_1)} \left(\frac{N_\lambda}{N_{\lambda 0}}\right) X_s . \tag{27}$$

This quantity is simply the value the solar X_0's would have if the excitation temperature of the sun were increased to T_1 and if the number of atoms above the photosphere varied with wave length as $N_\lambda / N_{\lambda 0}$.

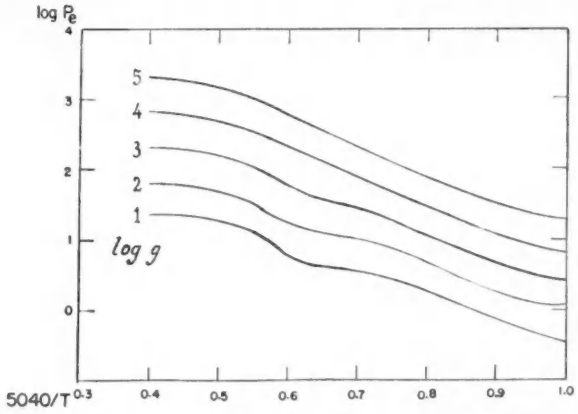

FIG. 3.—Relation between mean electron density, surface gravity, and temperature

VARIATION OF THE THEORETICAL MEAN ELECTRON PRESSURE WITH TEMPERATURE AND SURFACE GRAVITY

We may obtain an idea of the electron pressure in a stellar atmosphere as a function of surface gravity and temperature by setting the absorption coefficient equal to its value at an optical depth τ_0, viz., $\bar{\kappa}_\nu = \kappa_\nu(\tau_0) =$ constant, and integrating the equation of hydrostatic equilibrium for the optical depth τ_0. We obtain

$$P_g = \frac{g \tau_0}{\bar{\kappa}_\nu} . \tag{28}$$

Now τ_0 follows from equation (25), and generally it turns out to be of the order of 0.5–0.7, while $\bar{\kappa}_\nu$ depends on the frequency and is related to the mean optical depth $\bar{\tau}_0$, defined by the Rosseland mean absorption coefficient by

$$\bar{\tau}_0 = \frac{\bar{\kappa}}{\bar{\kappa}_\nu} \tau_0 . \tag{29}$$

We see that $\bar{\tau}_0$ and τ_0 may differ considerably in regions of high transparency ($\bar{\kappa}/\bar{\kappa}_\nu$ large) or low transparency ($\bar{\kappa}/\bar{\kappa}_\nu$ small). From θ, P_g, and Table 4 we may calculate P_e.

Figure 3 gives the electron pressure as a function of effective surface gravity g and effective temperature T_e, as calculated for λ 4000, under the assumption of hydrostatic equilibrium. I have used the Strömgren opacities in these calculations. The Wildt opacities yield electron pressures of the same order of magnitude.

These calculations suggest electron pressures in the atmospheres of A stars of the order of 10^3 dynes and an electron pressure in the atmosphere of the sun of 20 dynes. Fortunately, a rough check on the former estimate is available.

THE HYDROGEN LINES

The most conspicuous spectral features of the A-type stars are, of course, the strong hydrogen lines. These lines are broadened by the interatomic Stark effect, whose magnitude depends on the electron pressure and the temperature.

The absorption coefficient in the line wings is given by[18]

$$l(\Delta\lambda) = C\,\frac{F_0^{3/2}}{\Delta\lambda^{5/2}}, \tag{30}$$

where C is a constant depending on the line of the Balmer series, $\Delta\lambda$ is the distance from the line center in Angstrom units, and F_0 is the mean field acting upon the atom. According to Holtsmark,[19]

$$F = 2.61\epsilon n^{2/3}, \tag{31}$$

where ϵ is the charge on the electron and n is the number of charged particles/cm^3. In electrostatic units

$$F_0 = 46.8\left(\frac{2P_e}{T}\right)^{2/3}. \tag{32}$$

Hence,

$$l(\Delta\lambda) = 640\,\frac{C}{\Delta\lambda^{5/2}}\,\frac{P_e}{T}. \tag{33}$$

The members of the Balmer series in which we are interested arise from transitions from the second to much higher levels. Consider a transition from the second to the fifth level. Once in level 5 the atom has about one chance in five of returning to the second level. The atom absorbs a quantum of one frequency and emits one or more of other frequencies. Transitions of the type $n' - n$, which are not generally followed by the inverse transition, are referred to as transitions of the "absorption" type. On the other hand, the absorption of a Lyman α (or a D-line quantum in the case of sodium) is most likely to be followed by an emission of the same type. Such a process is called a "scattering" transition.

We shall use Unsöld's formula for the line wings[20]

$$A = \frac{l}{\kappa_\nu}\,\frac{1}{1+\dfrac{3}{2\beta_0}}, \tag{34}$$

where A is the amount of light removed from the line wings. Following the notation of Greenstein, we shall let $K_2(\tau)$ denote the absorption coefficient per hydrogen atom in the second energy level. Hence

$$A(\Delta\lambda) = \frac{l(\Delta\lambda)}{K_2(\tau)}\,\frac{1}{1+\dfrac{3}{2\beta_0}}, \tag{35}$$

and

$$P_e = A(\Delta\lambda)\Delta\lambda^{5/2}\left[1+\frac{3}{2\beta_0}\right]\frac{K_2(\tau)T}{640C}. \tag{36}$$

Now $A(\Delta\lambda)\Delta\lambda^{5/2}$ may be determined from the observed profiles, $(1 + 3/2\beta_0)$ and $K_2(\tau)$ can be computed from theory, and hence P_e can be estimated (see Table 6).

[18] *Ibid.*, p. 183.

[19] *Ann. d. Phys.*, **58**, 576, 1919.

[20] *Op. cit.*, p. 241.

We find that the electron pressures estimated in this way are somewhat smaller than those predicted by our theory. Possibly the assumption of hydrostatic equilibrium is not completely valid, and the neglect of the effects of stratification in our discussion of the line profiles may be serious. In subsequent discussions we shall adopt electron pressures of the order of 10^2 dynes/cm^2.

Pannekoek's calculations[21] of model stellar atmospheres indicate that for the wings of the lines in dwarf stars, the mean log P_e is 2.28 and 2.14 for λ 4000 and λ 5000, respectively for a temperature of 10,000°. On the other hand, from a discussion of the discontinuity at the limit of the Balmer series in A-type stars, Wildt[22] concludes that the theoretical values of the discontinuity may be brought into agreement with the observed values if an electron pressure of about 10^3 dynes/cm^2 be assigned. For the late F stars and the sun the electron pressure is somewhat less than 10^2 dynes/cm^2, according to his calculations.

TABLE 6

λ	C×10^{17}	$A(\Delta\lambda)\Delta\lambda^{5/2}$		P_e (Dynes/Cm^2)$\theta=0.5$	
		γ Gem.	Sirius	γ Gem.	Sirius
4861	8.85	.....	160	.....	100
4340	4.42	136	160	103	121
4101	3.09	138	200	114	170

In Figures 4–8 we compare the profiles of $H\beta$, $H\gamma$, and $H\delta$ in Sirius and γ Geminorum with those measured by E. G. Williams[2] and also with those predicted by Verweij[23] for log g = 4.4 and T = 10,000°. Verweij's profiles are based on Pannekoek's work, and a comparison of the observations with them again suggests an electron pressure of the order of 10^2 dynes/cm.[2]

Out to about 5 A from the line center the Verweij theory predicts a wider core than is actually observed, while the observed wings are broader than the calculated ones. This result agrees with those of A. Vibert Douglas and D. C. West[2] for two class-B stars. The observed cores are not only narrower but also less deep than the theoretical ones, and the shapes of the theoretical profiles are not similar to those observed.[24]

BLENDS

In many cases lines fall in the broad wings of the hydrogen lines. In most cases these lines are weak, and accidental errors in the measurement of their equivalent widths are large. Hence a comparison of the observed and theoretical weakening is difficult to

[21] *Pub. Astronomical Inst. Amsterdam*, No. 4, 1935, and Addendum.

[22] *Ap. J.*, **93**, 47, 1941.

[23] *Pub. Astronomical Inst. Amsterdam*, No. 5, 1936.

[24] Verweij's theory is based upon the Holtsmark theory of atomic fields produced by charged particles. In this point of view one regards the atom at any instant as subject to some static field F produced by a near-by charged particle. It is supposed that the duration of the encounter is much greater than the reciprocal of the frequency change of the radiated quantum, i.e., $T >> 1/\Delta\nu$. Otherwise, we cannot calculate the broadening of the line by supposing the atom to radiate under the influence of a static electric field. Unsöld (*op. cit.*, p. 184) remarks that for electron-atom encounters in the atmosphere of an A star, the Holtsmark theory is no longer accurate and should give only an order-of-magnitude result. Verweij calculates the profiles for lines formed in an atmosphere in which the ionization, kinetic, and excitation temperatures are all the same. Accordingly, its application is further restricted by this limitation. His profiles are also sensitive to surface gravity; if we adopt a surface gravity low enough to represent the cores of the line, the representation of the wings is poor.

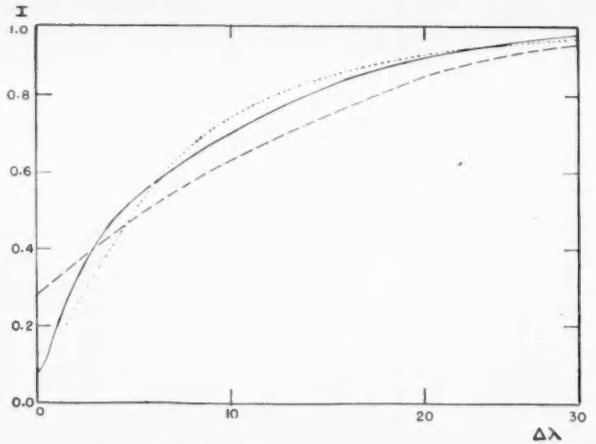

FIG. 4.—Profile of $H\beta$ in Sirius. Dotted curves, Verweij theory; dashed curve, observations by E. G Williams; solid curve, present observations.

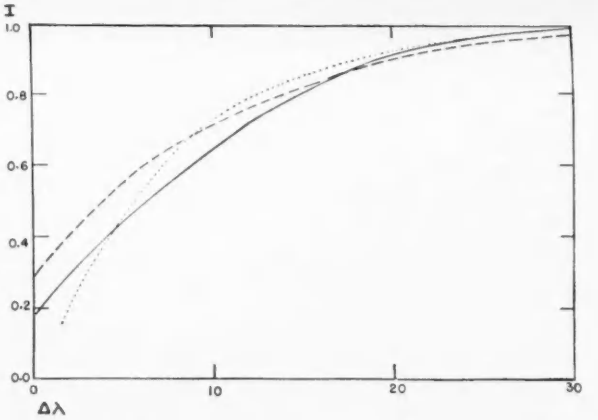

FIG. 5.—Profile of $H\gamma$ in Sirius. Dotted curve, Verweij theory; dashed curve, observations by E. G. Williams; solid curve, present observations.

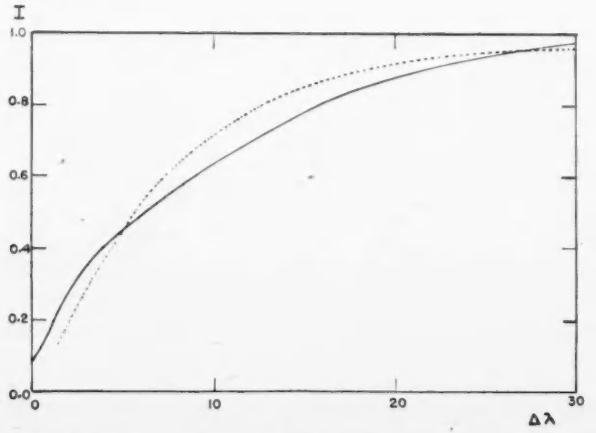

FIG. 6.—Profile of $H\delta$ in Sirius. Dotted curve, Verweij theory; solid curve, observed profile.

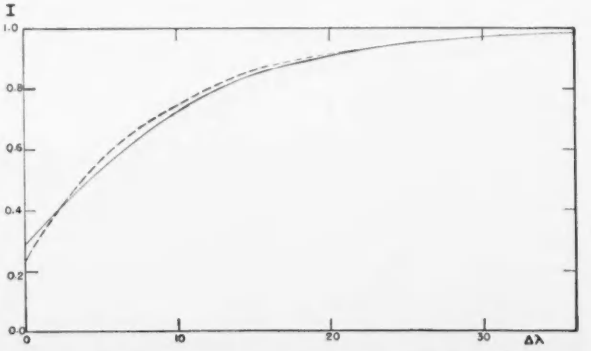

FIG. 7.—Profile of $H\gamma$ in γ Geminorum. The observations of E. G. Williams (dashed curve) are compared with the present observations (solid curve).

undertake. Only in the case of the H and K lines of *Ca* II are the lines sufficiently strong to merit a worth-while comparison.

In the wings of a strong line the depth to which we can see in the stellar atmosphere is diminished, i.e., the effective level of the photosphere is raised. Hence the number of atoms above the photosphere as measured by means of the curve of growth, should be cut down by an amount calculable from theory. Let I_0 be the central intensity of the hydrogen line in question (the intensity of the continuous spectrum is taken as 1.0), and I be the intensity of the wing at the point where the line is formed. Then the ratio of the number of atoms above the raised level of the photosphere to the number of atoms which would be present if the hydrogen line were not there is[25]

$$\frac{N}{N_0}=\frac{\tau}{\tau_0}=\frac{1}{I}\left(\frac{I-I_0}{1+I_0}\right)^2. \tag{37}$$

Let us apply this formula to the weakening of the H line in γ Geminorum. The provisional equivalent width of the K line is 1.05, while that of the H line, measured with

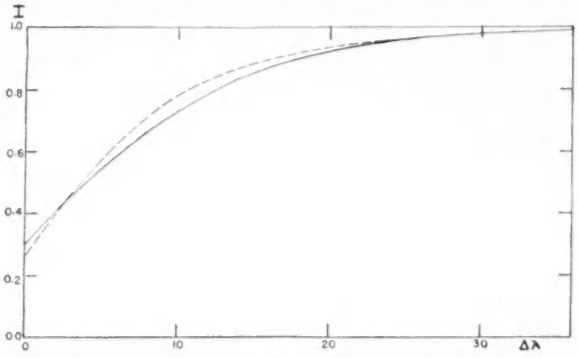

FIG. 8.—Profile of $H\delta$ in γ Geminorum. The observations of E. G. Williams (dashed curve) are compared with the present observations (solid curve).

respect to the $H\epsilon$ line is 0.31, $I = 0.38$, and $I_0 = 0.27$. Hence the predicted ratio is $N/N_0 = 0.06$. Now, both the H and the K lines probably lie on the radiation-damping portion of the curve of growth, and their f-values are in the ratio 2:1. The K line is not affected by the hydrogen-wing absorption to an appreciable degree and the ratio of the equivalent widths of the H and K lines is related to N/N_0 by

$$\frac{N}{N_0}=2\left(\frac{W_H}{W_K}\right)^2. \tag{38}$$

Hence the observed value of N/N_0 is 0.175, which is about three times larger than the predicted value—a result in agreement with those of Swings and Struve,[26] who studied the weakening of H by $H\epsilon$ in a number of stars. The discrepancy between observed and computed values may be interpreted by supposing that the H and K lines are produced in higher levels of the atmosphere than are the Balmer lines. Swings and Chandrasekhar[27] have investigated the problem of blended absorption lines in a stratified atmosphere and have shown that the abnormal weakening of the H line of *Ca* II could be explained by supposing that the ionized calcium is principally in the upper part of the reversing layer, where the optical depth is less than about one-sixth. The Balmer lines, on the other hand, are produced in the deeper layers.

[25] Unsöld, *op. cit.*, p. 314. [26] *Ap. J.*, **83**, 238, 1936. [27] *M.N.*, **97**, 27, 1936.

A number of iron and titanium lines fall in the wings of the hydrogen lines, but the uncertainties in their intensities and strengths make any discussion of the stratification of iron or titanium impracticable.

DISCUSSION OF THE CURVE OF GROWTH

To construct the final curve of growth, I have calculated the quantity X_r for the temperature 6000° and the variation of $N_\lambda/N_{\lambda 0}$ previously given. Log X_r is plotted against log W/λ. The amount of horizontal shift necessary to bring the log W/λ − log X_r curve into coincidence with the curve of growth yields log X_r/X_1, which is related to the relative numbers of atoms above the photosphere of the sun and the A dwarf. The wave-length correction for the depth of the photosphere introduces a very small difference in the resultant values of log X_r/X_1. The uncertainty in the excitation temperature is a more serious source of error.

The quantity adopted for comparison with theory is log X_r/X_1 for each ion involved. Because of the uncertainty in the excitation temperature T_1 and, to a lesser degree, the assumed variation of the depth of the photosphere, X_r is not strictly an observed quantity; but I feel that the uncertainty in X_r is not so great as to preclude its use as a quantity to compare with a value to be computed entirely from theory. The information we are looking for is the ionization temperature and the electron pressure in the A dwarf. In this investigation I have assumed the Strömgren opacities. Let ξ be the fraction of all atoms of a given kind in a specified state of ionization. Let τ_{01} be the optical depth of the photosphere in the A star, τ_{0s} the optical depth of the solar photosphere; let $\bar{\kappa}_s$ be the mean absorption coefficient in the atmosphere of the sun and $\bar{\kappa}_\lambda$ the absorption coefficient in the atmosphere of the A star at wave length λ, while $\bar{\kappa}_1$ is the Rosseland mean absorption coefficient. If μ_0 is the mean molecular weight of the atoms of which the stellar atmosphere is composed, $\mu_0 = 1.54$ for the mixture we have assumed, and m_H is the mass of the hydrogen atom, the number of all atoms above the photosphere of the sun will be

$$\eta_s = \frac{1}{\mu_0 m_H} \frac{\tau_{0s}}{\bar{\kappa}_s}, \tag{39}$$

while that above the atmosphere of the A star at λ will be

$$\eta_\lambda = \frac{1}{\mu_0 m_H} \frac{\tau_{01}}{\kappa_\lambda}, \tag{40}$$

while

$$\eta_1 = \eta_{\lambda_1} = \frac{1}{\mu_0 m_H} \frac{\tau_{01}}{\bar{\kappa}_1}. \tag{41}$$

Let N_1 and N_s be the numbers of atoms in the stage of ionization we are considering, above the photospheres of the A star and the sun, respectively. Then

$$N_1 = N_s \frac{\xi_1 \tau_{01} \bar{\kappa}_s}{\xi_s \tau_{0s} \bar{\kappa}_\lambda} = N \frac{\xi_1 \tau_{01} \bar{\kappa}_s}{\xi_s \tau_{0s} \bar{\kappa}_1} \left(\frac{\eta_\lambda}{\eta_{\lambda_1}} \right). \tag{42}$$

Now

$$\frac{X_r}{X_1} = \frac{N_s}{N_1} \frac{b(T_1)}{b(T_s)} \frac{\eta_\lambda}{\eta_{\lambda_1}} \frac{v_1}{v_s} = \frac{\eta_s \xi_s}{\eta_1 \xi_1} \frac{b(T_1)}{b(T_s)} \frac{v_1}{v_s}, \tag{43}$$

where $\lambda_1 = 5000$ A, for $\theta = 0.5$ is the point where $\kappa_\lambda \sim \bar{\kappa}_1$. I have taken $\kappa = \kappa_{5000}$ in this section of the discussion.

Table 7 gives the observed values of log X_r/X_1 for γ Geminorum and Sirius and also the value of log $\eta_s\xi_s/\eta_1\xi_1$ derived from this quantity. Now in the calculation of log $b(T_1)v_1/b(T_s)v_s$ we should use the excitation temperatures of the A star and the sun, respectively, in the partition functions $b_1(T_1)$, $b(T_s)$, while the velocity ratio, v_1/v_s, depends on the square root of the ratio of the gas kinetic temperatures,

$$\frac{v_1}{v_s}=\sqrt{\frac{T_1}{T_s}},$$

where $T_1 = 10{,}000°$ and $T_s = 5700°$ are the adopted values of the kinetic temperatures. The excitation temperature of Sirius and γ Geminorum was found to be somewhere in the neighborhood of 6000°, while that of the sun is 4400°. The ionization temperatures seem to be somewhat higher. The Saha equation, of course, refers to thermodynamic equilibrium and, when we have to deal with excitation and ionization temperatures that are not the same, the situation becomes a trifle puzzling. One might suppose that the ioniza-

TABLE 7

OBSERVED LOG X_r/X_1

Ion	Sirius		γ Geminorum		Ion	Sirius		γ Geminorum	
	log $\frac{\eta_s\xi_s}{\eta_1\xi_1}$	log $\frac{X_r}{X_1}$	log $\frac{\eta_s\xi_s}{\eta_1\xi_1}$	log $\frac{X_r}{X_1}$		log $\frac{\eta_s\xi_s}{\eta_1\xi_1}$	log $\frac{X_r}{X_1}$	log $\frac{\eta_s\xi_s}{\eta_1\xi_1}$	log $\frac{X_r}{X_1}$
Na	2.03	2.15	.....	.....	*Cr* I	2.70	3.04	2.86	3.20
Mg I	3.88	4.00	4.28	4.40	*Cr* II	.....	.....	1.12	1.40
Mg II	0.32	0.45	0.11	0.23	*Mn* I	3.18	3.40	3.04	3.28
Al I	3.26	3.38	4.14	4.26	*Fe* I	3.23	3.48	3.23	3.48
Si I	1.97	2.13	.....	.....	*Fe* II	1.03	1.28	1.07	1.32
Si II	0.11	0.23	.....	.....	*Ni* I	2.44	2.56	.....	.....
Ca I	3.73	4.00	3.05	3.32	*Ni* II	0.89	1.07	0.90	1.08
Ca II	.....	.....	2.23	2.46	*Sr* II	1.30	1.50	2.05	2.25
Sc II	2.00	2.24	1.91	2.15	*Zr* II	0.63	0.89	.....	.....
Ti II	1.63	1.84	1.35	1.56	*Y* II	0.58	0.80	1.69	1.91
V II	2.03	2.28	1.79	2.04	*Ba* II	1.57	1.88	1.96	2.27

tion temperature could be used in the exponential term and the lower excitation temperatures of 6000° and 4400° in the calculation of the partition functions. Presumably, if we plotted log X/X^1 against χ, we should not get a straight line but a curve, the slope of which at the lower end would correspond to the excitation temperature we have found, while the slope at the upper end would correspond to some higher temperature. Actually, we have no very satisfactory information on this point. In the calculation of the partition function I have adopted excitation temperatures of 7200° and 4600°, respectively. Fortunately, our results are not unduly sensitive to the choice of excitation temperature in the partition function. Now the quantity $\eta_s\xi_s/\eta_1\xi_1$ is the ratio of the number of atoms of the given kind above the photosphere of the sun to the number of the same kind of atoms or ions above the photosphere of the A star. For the theoretical calculation of log X_r/X_1 I have taken the ionization temperature of the sun as 5600°, the electron pressure as 20 dynes, and the mass-absorption coefficient as 0.234 on the basis of the Strömgren opacity calculations and the assumed composition of the solar atmosphere. The mean optical depth of the solar atmosphere in the Schuster-Schwarzschild model is taken as 0.60.

For comparison with the observed log X_r/X_1 I have calculated ξ_s/ξ_1 and η_s/η_1 for $\theta = 0.5, 0.6$, and 0.7 and log $P_e = 2.0$ and 2.4. The results are given in Table 8. In comparing observed and computed log X_r/X_1, I have used the values for *Fe* I, *Fe* II, *Ti* II, and *Cr* II to determine the ionization in Sirius and γ Geminorum. This ionization temperature turns out to be about 8700° for an assumed electron pressure of either 100 or 250 dynes. The discrepancies between observed and computed log X_r/X_1 is sometimes large, owing to inaccuracies in the measured log W/λ and the solar log X_0's. Consequently, only if the abundance of an atom were greatly different in an A-type star than in the sun, would the result show up in the curve-of-growth analysis. The value of log X_r/X_1 derived from ions like *Fe* II or *Ti* II which fall on the flat portion of the curve of growth is likely to be uncertain. Other elements are represented by few lines, and esti-

TABLE 8

CALCULATED LOG X_r/X_1

	log P_e=2.0				log P_e=2.4			
θ	0.5	0.58	0.6	0.7	0.5	0.58	0.6	0.7
Na	3.29	2.50	2.33	1.20	3.18	2.28	2.09	1.11
Mg I	4.42	3.48	3.21	1.82	4.31	3.21	2.97	1.71
Mg II	1.64	1.27	1.16	0.59	1.76	1.32	1.22	0.90
Al I	3.50	2.87	2.69	1.45	3.60	2.67	2.45	1.36
Si I	4.34	3.42	3.08	1.52	4.23	3.12	2.84	1.57
Si II	1.17	0.93	0.87	0.43	1.44	1.10	1.03	0.75
Ca I	3.62	2.87	2.61	0.39	3.51	2.60	2.37	1.26
Ca II	2.85	1.72	1.56	0.74	2.84	1.84	1.63	1.05
Sc II	2.41	1.50	1.31	0.74	2.37	1.51	1.41	1.05
Ti II	2.16	1.40	1.23	0.71	2.16	1.52	1.35	1.02
V II	2.16	1.38	1.22	0.75	2.15	1.49	1.38	1.06
Cr I	4.07	3.20	2.96	1.64	3.96	2.97	2.72	1.55
Cr II	1.82	1.37	1.24	0.77	1.94	1.49	1.39	1.10
Mn I	4.28	3.38	3.10	1.72	4.17	3.13	2.86	1.63
Fe I	4.32	3.38	3.11	1.71	4.27	3.15	2.87	1.64
Fe II	1.57	1.16	1.07	0.72	1.78	1.42	1.34	1.04
Ni I	3.36	2.36	2.12	0.77	3.25	2.16	1.89	0.70
Ni II	1.40	1.20	1.14	0.68	1.68	1.35	1.28	0.98
Sr II	3.34	2.16	1.90	0.79	3.26	2.15	1.88	1.05
Zr II	2.13	1.40	1.25	0.76	2.14	1.53	1.39	1.07
Y II	1.84	1.54	1.46	0.72	2.73	1.64	1.47	1.03
Ba II	3.53	2.67	2.42	0.96	3.69	2.38	2.05	1.20

mates of their abundances are subject to considerable uncertainty. The lower levels of the *Mg* II lines have high excitation potentials (about 9 volts), and the Boltzmann correction for them is very uncertain. Despite the scatter of the individual points, the value of log X_r/X_1 for *Fe* I is probably the best determined of them all. The excitation temperature is probably the greatest source of uncertainty here.

In order to estimate the relative abundances of the metals and hydrogen, I shall suppose that the relative abundances of the various metals are the same in Sirius and γ Geminorum as in the sun, and I shall attempt to compare the abundances of iron and hydrogen.

The observed value of log X_r/X_1 for *Fe* I is 3.48 in both Sirius and γ Geminorum, whence log $\eta_s\xi_s/\eta_1\xi_1 = 3.23$. If we suppose $\theta = 0.58$, and log $P_e = 2.0$, we derive log $\xi_s/\xi_1 = 2.10$, whence log $\eta_s/\eta_1 = 1.13$ with uncertainties introduced by the assumed

values of P_e and T_i for the sun and the A dwarfs. This result means that about 0.074 as much material is above the photosphere of the A dwarf as above that of the sun. In a recent paper R. B. King[28] has derived the number of neutral iron atoms above the photosphere of the sun. He finds $N_{Fe\,I} = 4.3 \times 10^{18}$ or a mass of neutral iron of 4.0×10^{-4} gm/cm^2 above the photosphere of the sun. If the fraction α is in the neutral condition, the mass of iron above the photosphere of the sun will be $4.0 \times 10^{-4}/\alpha$ gm/cm^2, and above the photosphere of Sirius or γ Geminorum the amount will be

$$\frac{4.0 \times 10^{-4}}{\alpha} \times 0.076 \text{ gm}.$$

We estimate the amount of hydrogen above the photosphere of the A dwarf by noting that the opacity arises from this element. With the assumed values of P_e and T, the absorption coefficient per gram of hydrogen amounts to 3.80, the optical depth of the photosphere being taken as 0.54. It should be emphasized that this value is very sensitive to the excitation temperature of hydrogen. Hence the amount of hydrogen above the photosphere amounts to $0.54/3.80 = 0.142$ gm. The ratio of hydrogen to iron will depend on the factor α. If $\alpha = 0.10$ (as our assumed P_e and T for the sun would indicate), then $H/Fe \sim 500$.

We may also employ the lines of *Fe* II. If we suppose the iron in the sun to be nine-tenths ionized, the *Fe* II data show that $\eta_s/\eta_1 = 12.5$ and the amount of iron above the photosphere of the A dwarf will again be about 3×10^{-4} gm/cm^2. On the other hand, if the iron is only half-ionized in the sun, it turns out that the ratio of the total number of iron atoms above the photosphere of the sun to that above the photosphere of Sirius is about twenty.[29] The masses will be 8×10^{-4} and 4×10^{-5} gm, respectively, and, with our previous estimate of the abundance of hydrogen, the ratio of hydrogen to iron will be about 3000. These results show that the abundance ratio of hydrogen to iron depends critically on the degree to which iron is ionized in the sun. For the present we may adopt the hydrogen-iron ratio as about 1000/1 by weight.[30]

The very large scatter of the individual points on the curve of growth is disappointing. This scatter probably arises from three causes: (1) observational errors in determining equivalent widths as small as 0.01; (2) errors in the solar log X_0's, which are likely to be quite uncertain when estimated from the flat portion of the curve of growth; and (3) the effects of interlocking between the various lines. The first source of error may be minimized by taking a large number of plates, and the second type of error may be reduced when improved f-values are available. The evaluation of interlocking effects would require detailed studies for each line. To some extent we have taken them into account empirically by the use of the solar log X_0's, for, if a line is affected by interlocking in Sirius, it may be so affected in the sun.

In any case the curves of growth and the equivalent widths upon which they are

[28] *Ap. J.*, **95**, 82, 1942.

[29] In their analysis of stellar spectra, W. S. Adams and H. N. Russell (*Ap. J.*, **68**, 9, 1928) assumed *Fe* I and *Fe* II to be equally abundant in the sun (see their Table X) and concluded that the amount of material above the photosphere of Sirius was about 0.05 as much as that above the solar photosphere. This latter result, based on eye estimates, is in excellent agreement with the conclusions of the present study.

[30] P. ten Bruggencate and H. von Klüber (*Zs. f. Ap.*, **18**, 284, 1939) have derived the relative numbers of neutral iron and titanium atoms above a sunspot and the photosphere. They find $n_s/n_p = 9.1$. Unsöld (*op. cit.*, p. 367) suggests that the electron pressure in a sunspot is about half that in the photosphere and that the relative numbers of atoms above a spot and the photosphere is about 1.7. With our adopted values of P_e and T for the solar photosphere and an assumed ionization temperature of 4200° for the sunspot, we find about twenty times as many neutral atoms above the spot as above the photosphere. To fit the observations it seems reasonable to suppose that about 20 instead of 8 per cent of the iron atoms above the photosphere are neutral. The hydrogen-iron ratio then turns out to be about a thousand.

based are to be regarded as provisional. Improved data may become available at some later date. Nevertheless, the present material seems to have yielded information of a sufficient interest to merit its discussion at the present time.

In conclusion I should like to express my gratitude to Director W. S. Adams and Dr. Theodore Dunham of the Mount Wilson Observatory for allowing me to use their data on Sirius. I am also grateful for the opportunity to use the Lick Observatory material on Sirius. I am indebted to Dr. Louis Berman, who traced the Mount Wilson plates and reduced a number of them. To Director O. Struve and Dr. Jesse Greenstein of Yerkes and McDonald observatories, who made available to me the plates of γ Geminorum, I am deeply grateful. Thanks are also due to Dr. Leo Goldberg and Dr. Donald Menzel for reading the manuscript and making helpful suggestions.

HARVARD COLLEGE OBSERVATORY
July 17, 1942

A SURVEY OF THE SPECTRA AND RADIAL VELOCITIES OF THE LESS REGULAR M-TYPE VARIABLE STARS*

ALFRED H. JOY

ABSTRACT

The spectra of 118 variable M-type stars characterized by small and irregular light-changes and by the absence or weakness of emission lines were examined with respect to their spectral classification, spectroscopic absolute magnitude, and radial velocity. Of these stars, 105 were previously unobserved spectroscopically.

Distribution.—The supergiants have a mean galactic latitude of 11°, but the normal giants, like the Me variables, show little galactic concentration.

Spectroscopic absolute magnitude.—The 1935 Mount Wilson curves were used. For the supergiants the absolute magnitudes are scattered from −2.0 to −4.5; for the normal giants the mean is −0.9, which corresponds closely with that of the Me variables.

Spectral type.—The stars are largely concentrated in classes M5 and M6. The supergiants are found in the earlier types from M0 to M5. For a given type the periods are much shorter than in the Me variables.

Radial velocities.—The mean residual velocity of the supergiants is 18.2 km/sec; of the giants, 26.1 km/sec. The stars with shorter period show a larger mean velocity and greater scatter.

Displacements of emission lines.—Emission at certain phases is shown by 19 stars. The mean violet displacement of the bright lines is 8.9 km/sec with respect to the absorption lines. The relationship between shift and spectral type corresponds closely with that of the Me variables.

Giant M-type stars are particularly subject to fluctuations in light. It has been suspected that practically all red stars vary more or less in total luminosity.[1] About two-thirds of all known intrinsic variable stars have titanium oxide bands in their spectra and show strong hydrogen emission except at minimum light. In their light-changes and general behavior these emission stars resemble Mira and are known as long-period, or Me, variables. Although considerable irregularity is often present in their light-curves, the period is fairly definite. The variation in visual light is several magnitudes, but the velocity-changes are small and have been detected in few stars. The motions and spectroscopic characteristics of the Me variables are well known, largely through the studies of P. W. Merrill.

The remaining variables with M-type spectra showing little or no emission may not form a homogeneous group, but they can be readily separated from the Mira stars, because of their irregular light-curves, smaller magnitude ranges, and the absence of strong emission lines in their spectra. Their periods, in general, are poorly defined, and often no certain regularities in their light-changes can be found. Usually the periods which have been deduced are between 50 and 150 days and in the mean are markedly shorter than those of the Mira stars. For this reason it might be expected that the physical properties of this group would be intermediate between the long-period and the Cepheid classes. The results of this investigation, however, indicate that these less regular stars are closely related to long-period variables in most of their characteristics.

In the region of the sky suitable for observation at Mount Wilson, Schneller's *Catalogue and Ephemeris of Variable Stars* for 1939[2] lists 202 semiregular and irregular M-type variables without bright lines and, in addition, 67 stars, which, on account of small magnitude range or intermediate period (50–150 days), might be expected to fall outside the Mira class, even though no spectral classification was available.

* *Contributions from the Mount Wilson Observatory, Carnegie Institution of Washington*, No. 668.

[1] Joel Stebbins, *Pub. A.A.S.*, **6**, 244, 1928.

[2] *Kleinere Veröff. Sternwarte Berlin-Babelsberg*, No. 20, 1938.

The spectral types and mean radial velocities for 13 of the brightest of these variables have been previously published[3] and are given in Table 1. In the column headed V' is given the radial velocity corrected for a solar motion of 20 km/sec. No certain changes in spectra during the cycle of light-variation were recorded, and velocity-changes, except for V UMi, are not much greater than the errors of measurement. Several of the stars will be recognized as supergiants of a much higher order of luminosity than the ordinary giant M or Me stars.

Selection of stars.—This study was begun some ten years ago for the purpose of determining the motions and spectral features of those M-type variables which had not been included in the lists of other observers. The program was limited for the most part

TABLE 1

PUBLISHED DATA FOR IRREGULAR M-TYPE VARIABLES

Star	m_v	Sp.	Meas. V	V'	Vel. Range	Observer
			km/sec	km/sec	km/sec	
RS Cnc	5.3–6.8	M6	+ 12.8	+ 6.8	6	McLaughlin*
μ Cep	4.0–4.8	M2	+ 20.5	+ 34.2	14	Campbell†
η Gem	3.2–4.2	M3	+ 19.4	+ 6.9	10	Reese‡
α Her	3.1–3.9	M5	− 32.6	− 13.6	6	Lick§
g Her	4.4–5.6	M6	+ 3.3	+ 21.6	5	Lick,§ Mt. Wilson‖
R Lyr	4.0–4.5	M5	− 28.3	− 9.3	6	Lick,§ Sanford¶
α Ori	0.1–1.2	M2	+ 21.0	+ 5.0	4	Lick,§ Cape,** Sanford††
CI Ori	4.5–5.5	M0	+ 7.5	− 10.0	10	Lick,§ Mt. Wilson‖
SX Pav	5.3–6.3	M6	+ 42.9	+ 37.4	8	Lick§
ρ Per	3.2–4.1	M4	+ 28.2	+ 24.6	1	Lick§
TV Psc	5.1–5.5	M3	+ 5.2	+ 6.6	10	Lick,§ Mt. Wilson‡‡
α Sco	0.9–1.8	M1	− 3.0	+ 6.8	4	Lick,§ Cape**
V UMi	7.1–8.9	M4	−165	−154	27	Redman,§§ Sanford‖‖

* *Pub. Univ. of Michigan*, **8**, 118, 1941.
† *Lick Obs. Bull.*, **7**, 102, 1912.
‡ *Lick Obs. Bull.*, **1**, 158, 1902.
§ *Lic Obs. Pub.*, **16**, 1928.
‖ *Mt. W. Contr.*, No. 387; *Ap. J.*, **70**, 207 1929.
¶ *Mt. W. Contr.*, No. 394; *Ap. J.*, **71**, 209, 1930.
** *M.N.*, **88**, 660, 1928.
†† *Mt. W. Contr.*, No. 464; *Ap. J.*, **77**, 110, 1933.
‡‡ *Mt. W. Contr.*, No. 105; *Ap. J.*, **42**, 175, 1915.
§§ *M.N.*, **92**, 118, 1931.
‖‖ *Mt. W. Contr.*, No. 481; *Ap. J.*, **79**, 77, 1934.

to stars north of declination −26° and brighter than twelfth magnitude which could be observed with the one-prism spectrograph of the 60-inch reflector and was intended to include a variety of nonemission variable stars with intermediate periods or with small light-ranges. Some preference was, perhaps, given to stars with assigned periods and recent discoveries may be somewhat neglected. As far as our present knowledge goes, the list is fairly representative of this class of stars. It contains about half of the known variables of this kind having assigned periods, together with a moderate sampling of the more irregular stars. While the program is in no sense complete, it serves as a preliminary basis for the study of a group of stars about which little precise information has heretofore been available.

Although one of the criteria of selection was the absence of bright lines, no stars being retained which showed emission on all plates, nevertheless, weak or moderately strong

[3] Since this paper was written, P. C. Keenan has published (*Ap. J.*, **95**, 461, 1942) the spectral types and luminosity classes of 67 semiregular or irregular variables of types K and M observed in November and December, 1941, with the McDonald reflector. Thirty-seven of his stars are common to this Mount Wilson list. His spectral types are about 0.4 of a subdivision earlier than those given here, and his absolute magnitudes of supergiants, based largely on standards taken from the Perseus double cluster, are more than a magnitude brighter than those determined from the Mount Wilson curves. In general, the results of the two papers are in satisfactory agreement.

hydrogen emission lines were found on one or more spectrograms of 19 stars of the list, and emission lines of neutral silicon also appear on a few. In addition, emission was previously detected in 3 of the stars (RS Cnc, AF Cyg, X Her) by D. B. McLaughlin at the University of Michigan and in 11 stars (RV And, RU Aqr, S Crt, AB Cyg, UW Her, ST Peg, RW Psc, Y Ser, V UMa, RY UMa, W Vul) by observers at the Harvard College Observatory. At one time or another, then, 33 of the 118 stars observed have shown bright lines. The presence of emission does not seem to be correlated with other physical characteristics, but it usually occurs near maximum or during increasing light.

I am indebted to my colleagues, Mr. P. W. Merrill, who was kind enough to turn over to me 24 plates of 17 stars which he found to lack the emission characteristics of the Me variables, and Messrs. W. S. Adams, R. F. Sanford, and G. Strömberg, who obtained a number of the plates used in this study.

The observations.—Two or more spectrograms of each star on the program were obtained as opportunity permitted, without much consideration of phase. The dispersion depended on the brightness of the star and the observing conditions at the time. Many lines or blends were identified even with low dispersion, and 15 or 20 were measured on each good plate. Radial velocities were determined with the aid of Merrill's wave lengths.[4] The results for 105 stars previously unobserved are listed in Table 2. The first column gives the name of the star and its period (in parenthesis), its positional designation according to the Harvard system, and the visual magnitude at maximum and minimum from Harvard publications or from Schneller's *Catalogue*. The spectral types (fifth column) are based on the strength of the titanium oxide bands. The velocities (sixth column) are determined by measurement of the absorption lines. The dispersions given in the eighth column are approximately: $a=36$, $b=70$, and $c=120$ A/mm at $H\gamma$. The weights in the last column are arbitrarily assigned with reference to the dispersion, the number of lines measured, and the quality of the plate.

The elements from which the phases (fourth column) are computed may be found in the notes to the table. Periods have been assigned for 89 stars, and phases are computed for 46, but for most of them the irregularities of the light-changes make the elements quite unreliable. The phases should be used with caution. They are entered in the table to show the distribution of the observations over the cycle of the light-variation. In very few of the stars is it possible to detect any correlation between light- and velocity-variations; but for a proper study of such relationships it is imperative that simultaneous observations of light- and velocity-changes should be carried out. The velocity-range is small; hence it is difficult to separate any variation of velocity during the cycle from errors of observation. Additional evidence of variation can be obtained only at the expense of a many fold increase in the number of observations of each star.

Collected data for the irregular M-type variables.—A summary of the astrophysical data now available for 118 irregular M-type variables is in Table 3. This table includes the galactic co-ordinates, the apparent visual magnitude at maximum light, the spectroscopic absolute magnitude, the corresponding photometric parallax, the spectral type, the mean measured and residual radial velocity (corrected for a solar motion of 20 km/sec toward the usual apex), and the period of light-variation.

Distribution of stars.—The lack of observations of stars in the southern skies results in an unbalanced distribution, which makes the material unsuitable for many statistical investigations. There is little galactic concentration for the stars observed. The average latitude is 29° for the giants, which is closely the same as that of the Me stars[5] but widely different from that of the δ Cepheids,[6] for which the value is 5°. The average latitude of the 13 supergiants, however, is only 11°.

[4] *Mt. W. Contr.*, Nos. 265 and 644; *Ap. J.*, **58**, 195, 1923; **93**, 381, 1941.

[5] P. W. Merrill, *Mt. W. Contr.*, No. 649; *Ap. J.*, **94**, 208, 1941.

[6] A. H. Joy, *Mt. W. Contr.*, No. 607; *Ap. J.*, **89**, 361, 1939.

TABLE 2

OBSERVATIONS OF IRREGULAR M-TYPE VARIABLES

Star, Period, Designation, Magnitude	Plate	JD 242	Phase	Spectrum	Vel.	Disp.	Wt.
			days		km/sec		
RU And (231[d])							
013238	C 7216	9183	38	M6	.....	b	0.0
10.0–13.7	E 61	9913	75	6e	− 43	c	0.6
	C 7658	0029*	190	6	.....	c	0.0
	E 250	0248*	178	6e	− 39	c	0.6
	318	0298*	228	5e	− 45	c	0.6
					− 42		
RV And (229)							
020448	γ17729	6222	.....	M5	− 14	b	1.0
8.7–11.4	C 6588	7763	.....	5	− 14	b	1.0
	γ20874	8117	.....	5	− 6	b	1.0
	C 7155	8936	.....	5	− 4	c	0.4
					− 10		
SS And (160)							
230752	γ21248	8852	.....	M6	− 23	c	0.6
8.9–9.9	22204	9562	.....	6	− 32	c	0.4
	C 7541	9854	.....	6	− 15	c	0.6
	γ22999	9894	.....	5	− 22	b	1.0
					− 22		
TV And (114)							
225342	C 2387	3652	.....	M5	.....	b	0.0
8.8–11.1	7517	9826	.....	5e	− 47	c	0.6
	γ22857	9858	.....	4e	− 51	b	1.0
					− 50		
TY And (150)							
231040	γ20791	7971	.....	M6	.....	b	0.0
8.2–10.0	22994	9893	.....	6e	− 8	b	1.0
	23134	9927	.....	5e	− 3	b	1.0
	23839	0301*	.....	6	− 9	c	0.4
					− 6		
TZ And (280)							
234546	γ12878	4014	.....	M6	.....	b	0.0
8.5–9.5	22205	9562	.....	5	− 28	c	0.6
	C 7552	9856	.....	6	− 33	b	1.0
					− 31		
RU Aqr (69)							
231917	C 2938	4013	31	M6	+ 22	b	1.0
9.0–10.3	5808	6557	33	5	+ 32	b	1.0
	γ23154	9943	53	6	+ 22	c	0.6
					+ 26		
TW Aqr (79)							
205802	γ22776	9827	63	M5	− 41	c	0.6
9.3–10.3	C 7544	9854	11	6	− 34	c	0.6
					− 38		

* The first three figures of the JD number are 243.

TABLE 2—*Continued*

Star, Period, Designation, Magnitude	Plate	JD 242	Phase	Spectrum	Vel.	Disp.	Wt.
			days		km/sec		
BM Aqr (—)							
22016	C 6953	8409	.....	M4	− 18	c	0.4
9.0–10.2	γ22777	9827	.....	5	− 33	c	0.6
	22851	9856	.....	5	− 11	c	0.6
					− 21		
TZ Aql (90)							
202505	C 4467	5165	.....	M6	+ 52	b	1.0
8.5–9.5	γ21867	9414	.....	6	+ 48	c	0.6
	E 51	9912	.....	6	+ 50	b	1.0
					+ 50		
WX Aql (105)							
194303	C 7506	9806	86	M6	− 21	c	0.6
8.8–9.9	7548	9855	30	6	− 29	c	0.6
	γ22996	9894	69	6	− 33	c	0.6
					− 28		
KN Aql (139)							
202501	C 7516	9825	58	M5	−140	b	1.0
7.7–9.2	γ22997	9894	127	5e	−148	b	1.0
	E 312	0297*	113	5	−128	c	0.6
					−140		
LU Aql (50)							
193415	C 7091	8733	.....	M4	− 1	b	0.7
9.2–10.3	γ21866	9414	.....	4	+ 3	c	0.2
	C 7505	9806	.....	4	+ 6	c	0.6
					+ 2		
NO Aql (66)							
194004	γ23143	9932	62	M3	− 96	c	0.6
9.9–11.2	23155	9944	7	4	− 91	c	0.6
	23205	9970	33	4e	−105	c	0.4
	E 477	0515*	50	3	−108	c	0.6
					− 99		
PX Aql (—)							
195209	C 6273	7267	.....	M5	− 34	c	0.6
9.2–10.7	γ22736	9803	.....	5	− 36	c	0.6
					− 35		
TU Aur (75)							
062845	γ21674	9293	.....	M5	+ 12	b	1.0
7.7–9.1	22418	9647	.....	5	+ 5	b	1.0
					+ 8		
UX Aur (90)							
050849	C 4439	5159	.....	M5	+ 34	b	1.0
8.0–8.8	γ21275	8910	.....	5	+ 33	b	1.0
					+ 34		
UZ Aur (66)							
050840	E 56	9912	.....	M4	+ 15	c	0.6
7.7–9.3	C 7650	0002*	.....	4	+ 24	b	1.0
					+ 21		

TABLE 2—*Continued*

Star, Period, Designation, Magnitude	Plate	JD 242	Phase	Spectrum	Vel.	Disp.	Wt.
			days		km/sec		
RV Boo (138)							
143532	C 5139	5671	.....	M6	− 7	b	1.0
7.6–8.6	γ17376	6076	.....	6e	− 9	b	1.0
	17424	6104	.....	6e	+ 1	b	1.0
	17473	6130	.....	6	+ 3	b	1.0
	17541	6154	.....	5	− 5	b	1.0
	17571	6168	.....	6e	− 5	b	1.0
	17634	6198	.....	6	− 1	b	1.0
					− 3		
RW Boo (373)							
143632	γ22589	9764	.....	M5	− 9	b	1.0
7.3–7.7	22739	9804	.....	5	− 13	b	1.0
					− 11		
RX Boo (78)							
141926	γ21688	9322	.....	M7	− 15	b	1.0
7.0–9.2	21722	9351	.....	8e	− 8	a	1.5
	C 7277	9379	.....	8	− 8	b	1.0
					− 10		
RR Cam (123)							
052372	γ19190	6992	.....	M6	− 61	b	1.0
9.2–10.6	21285	8935	.....	6	− 60	c	0.4
					− 61		
RS Cam (89)							
083679	γ12291	3746	.....	M6	− 30	b	0.3
8.1–9.5	17137	5960	.....	6	− 35	b	0.3
	17375	6076	.....	5	− 38	b	0.7
	17478	6131	.....	6	− 37	c	0.2
	18029	6343	.....	6	.....	b	0.0
	18143	6427	.....	5	− 42	b	0.7
	18752	6784	.....	5	− 47	b	1.0
					− 41		
RV Cam (103)							
042257	γ22209	9563	.....	M6	− 16	b	1.0
7.9–9.0	C 7649	0002*	.....	5	− 26	b	1.0
					− 21		
RY Cam (135)							
042164	γ13247	4186	.....	M3	− 14	b	0.3
8.0–9.2	14545	4781	.....	4	− 18	b	0.3
	22208	9562	.....	4	− 27	b	1.0
	22421	9648	.....	3	− 23	b	1.0
	22478	9679	.....	4	− 22	b	1.0
					− 23		
Z Cnc (80)							
081615	C 2582	3772	.....	M7	+ 8	b	1.0
8.5–9.8	5133	5669	.....	7	+ 5	b	1.0
	5159	5722	.....	6	+ 7	b	1.0
	5368	5959	.....	6	0	b	1.0
	5399	6019	.....	6	− 4	b	1.0
	γ17944	6316	.....	6	+ 14	b	1.0
	C 5653	6338	.....	7	+ 1	b	1.0
					+ 4		

TABLE 2—*Continued*

Star, Period, Designation, Magnitude	Plate	JD 242	Phase	Spectrum	Vel.	Disp.	Wt.
			days		km/sec		
RS Cnc (239)							
090431	γ19524	7137	113	M6	+ 13	a	1.5
5.3–6.8	21858	9413	0	6	+ 15	a	1.5
	C 7326	9440	26	5	+ 2	b	1.0
	γ22419	9647	233	6	+ 12	a	1.5
					+ 11		
RT Cnc							
085211	C 7293	9393	89	M5	+ 13	b	1.0
7.3–8.6	γ21863	9414	15	5	+ 38	b	1.0
	C 7662	0029*	64	6	+ 27	b	1.0
	E 86	0090*	31	6	+ 43	b	1.0
	104	0119*	60	6	+ 44	b	1.0
	147	0148*	89	5	+ 51	b	1.0
					+ 36		
RV CMa (—)							
065*14*	γ19456	7105	.....	M6	+ 29	c	0.4
8.9–9.7	C 7666	0030*	.....	6	+ 26	c	0.6
					+ 27		
VY CMa (—)							
071*825*	C 7450	9670	.....	M4	.....	b	0.0
7.8–9.8	7667	0030*	.....	4e	+ 45	b	0.7
	γ23338	0070*	.....	3e	+ 42	c	0.6
	E 419	0443*	.....	4e	+ 67	c	0.4
					+ 49		
UX CMi (151)							
074005	γ22555	9736	138	M5	+ 25	c	0.6
8.5–9.5	23313	0034*	134	5	+ 25	c	0.6
					+ 25		
UY Cas (102)							
225757	γ19261	7021	6	M4	− 10	b	0.7
9.6–11.5	22106	9505	30	3e	− 1	b	1.0
	E 347	0326*	31	4e	− 1	c	0.6
					− 4		
VY Cas (100)							
004562	γ21249	8852	.....	M6	− 92	c	0.6
9.0–10.2	23001	9894	.....	6	− 92	b	1.0
					− 92		
SS Cep (98)							
033380	γ17937	6314	48	M6	− 36	b	1.0
6.7–7.8	22416	9647	66	6	− 46	b	1.0
					− 41		
T Cet (160)							
001*620*	γ12874	4012	.....	M5	+ 29	a	0.5
5.2–6.0	12924	4037	.....	5e	+ 28	a	1.0
	13017	4073	.....	5e	+ 17	a	1.5
	13500	4333	.....	5	+ 37	a	0.5
	13594	4365	.....	5	+ 26	a	0.5
	13680	4393	.....	5	+ 26	a	1.5
	13727	4404	.....	5	+ 28	a	1.5

TABLE 2—*Continued*

Star, Period, Designation, Magnitude	Plate	JD 242	Phase	Spectrum	Vel.	Disp.	Wt.
			days		km/sec		
T Cet (160) *Cont.*							
	13827	4432	.....	M5	+ 35	a	1.5
	13848	4450	.....	5	+ 40	a	1.0
					+ 29		
Y CrB (300)							
154338	γ22481	9679	.....	M8	− 19	c	0.6
9.8–10.8	22560	9737	.....	8	− 22	c	0.6
					− 20		
RR CrB (57)							
153738	C 5978	6783	11	M5	− 54	b	1.0
7.2–8.4	5992	6811	39	5	− 38	b	1.0
	6256	7226	56	5	− 57	b	1.0
					− 50		
RU CrB (436)							
153126	C 6048	6880	.....	M5	− 15	c	0.2
8.8–11.4	γ21856	9412	.....	5	− 27	c	0.6
	21988	9469	.....	5	− 31	c	0.6
					− 27		
X Crv (127)							
124*318*	γ22425	9649	.....	M6	+ 6	b	0.7
7.8–8.8	C 7452	9670	.....	6	− 5	b	1.0
	γ23336	0070*	.....	6	+ 7	c	0.4
					+ 1		
S Crt (152)							
114*707*	C 5137	5670	.....	M6	.....	b	0.0
8.4–9.5	7663	0029*	.....	6	+ 35	c	0.6
	γ23329	0069*	.....	6	+ 27	c	0.4
					+ 32		
RZ Cyg (546)							
204846	C 7372	9508	538	M7	.....	b	0.0
9.6–13.6	γ23156	9944	428	7	− 51	c	0.6
	E 94	0091*	30	7	− 42	c	0.6
	316	0298*	236	7	.....	c	0.0
					− 47		
AB Cyg (482)							
213231	γ17778	6233	405	M4	− 17	b	1.0
7.7–8.9	C 5748	6494	184	5	− 8	b	1.0
	5804	6555	245	4	0	b	1.0
	6532	7680	451	4	− 4	b	0.7
					− 7		
AF Cyg (94)							
192745	γ12819	3987	43	M6	− 20	a	1.5
6.4–8.4	12877	4014	70	6	− 7	b	0.3
	13458	4313	69	6	− 9	b	1.0
	C 3889	4719	69	6	− 12	a	1.5
	γ17482	6131	15	6	− 19	b	1.0
	17530	6140	24	6	− 12	b	1.0
	17772	6232	22	6	− 24	b	0.7
	17789	6255	55	6	− 2	b	0.3
					− 15		

TABLE 2—*Continued*

Star, Period, Designation, Magnitude	Plate	JD 242	Phase	Spectrum	Vel.	Disp.	Wt.
			days		km/sec		
AI Cyg (140)							
202732	C 7296	9393	74	M6	− 50	c	0.6
8.4–9.7	7519	9826	86	6	− 64	b	1.0
	E 58	9913	34	6	− 56	c	0.6
					− 58		
BC Cyg (—)							
201737	C 7550	9855	.....	M4	− 6	b	0.7
9.8–10.8	γ22993	9893	.....	3	+ 1	c	0.6
					− 3		
CH Cyg (101)							
192150	γ12914	4036	39	M7	− 53	a	1.5
6.4–7.4	13578	4362	64	6	− 51	a	1.5
	C 3480	4393	95	6	− 52	a	1.5
	γ17477	6130	21	6	− 59	b	1.0
	17726	6222	12	6	− 51	b	1.0
					− 53		
U Del (—)							
204017	γ22757	9824	.....	M5	− 19	a	1.5
5.6–7.5	23142	9932	.....	5	− 23	b	1.0
					− 21		
S Dra (—)							
164055	C 7457	9703	.....	M6	+ 10	b	1.0
7.5–9.3	γ22557	9736	.....	6	− 2	c	0.6
					+ 6		
SS Dra (48)							
122169	γ22424	9648	.....	M5	+ 28	b	1.0
8.6–10.0	22480	9679	.....	5	+ 38	b	1.0
					+ 33		
SZ Dra (120)							
190965	γ22559	9736	.....	M5	− 41	b	1.0
8.0–8.6	22590	9764	.....	5	− 42	b	1.0
					− 42		
TT Dra (107)							
171157	C 4255	5011	71	M6	− 38	b	0.7
8.5–9.3	5456	6111	97	6	− 26	b	0.3
	γ17572	6168	47	6	− 9	b	0.7
	C 5716	6459	16	6	− 24	b	0.3
	6054	6881	88	6	− 16	b	0.7
					− 23		
TX Dra (134)							
163360	γ12815	3986	59	M5	.....	b	0.0
6.8–8.1	13457	4313	118	4	+ 58	b	1.0
	13483	4331	2	4	+ 42	a	1.0
	13583	4364	35	5	+ 51	a	0.5
	C 3717	4574	111	5	+ 58	b	1.0
	3769	4631	34	4	+ 40	a	1.0
	γ14208	4658	61	5	+ 60	a	0.5
	C 3842	4689	92	5	+ 54	a	1.0
	3878	4714	117	5	+ 54	a	1.0

TABLE 2—*Continued*

Star, Period, Designation, Magnitude	Plate	JD 242	Phase	Spectrum	Vel.	Disp.	Wt.
			days		km/sec		
TX Dra (134) *Cont.*							
	3896	4720	123	M4	+ 51	a	1.5
	γ15002	5023	24	4e	+ 52	a	1.5
					+ 52		
UU Dra (234)							
202574	γ22585	9763	81	M8	− 17	b	0.3
8.7–10.3	22743	9804	122	8	− 45	b	1.0
	22754	9823	141	8	− 34	b	1.0
					− 37		
UV Dra (77)							
144156	C 1600	3124	4	M5	− 46	b	0.3
8.8–9.4	3855	4692	24	6	− 34	b	1.0
	4766	5362	75	5	− 23	b	0.7
	γ16575	5750	76	5	− 21	b	0.3
	C 5394	6019	35	5	− 46	b	0.7
	5455	6111	50	5	− 21	b	1.0
	γ17484	6132	71	5	− 33	b	0.7
	C 5692	6427	57	5	− 37	b	1.0
	5720	6461	13	5	− 36	b	1.0
	5752	6515	67	5	− 47	b	0.3
	6011	6840	5	5	− 41	b	1.0
	γ18913	6882	47	5	− 37	b	1.0
					− 35		
Z Eri (—)							
024*31*2	γ17632	6197	.....	M5	+ 3	b	1.0
6.4–7.7	22477	9679	.....	5	− 22	b	1.0
	E 289	0269*	.....	5	− 24	c	0.6
					− 14		
RW Eri (91)							
041*705*	C 5386	6017	6	M6	+118	b	0.3
8.6–9.6	5631	6312	27	6	+106	b	1.0
	γ23820	0280*	64	6	+108	b	0.7
	23903	0327*	20	6	+101	c	0.6
					+107		
Y Gem (—)							
073520	C 5380	5961	.....	M6	+ 18	a	1.0
8.5–10.0	7456	9703	.....	6e	+ 18	b	1.0
					+ 18		
TV Gem							
060521	E 409	0416*	.....	M2	+ 16	b	1.0
7.0–7.8	γ24052	0423*	.....	2	+ 18	b	1.0
					+ 17		
X Her (100)							
155947	C 298	2388	.....	M6	− 93	a	1.5
5.8–7.2	304	2389	.....	6	− 92	a	1.5
	γ 9054	2392	.....	6	− 91	a	1.5
	10130	2806	.....	6	− 89	a	1.5
					− 91		

TABLE 2—*Continued*

Star, Period, Designation, Magnitude	Plate	JD 242	Phase	Spectrum	Vel.	Disp.	Wt.
			days		km/sec		
ST Her (167)							
154748	C 297	2387	.....	M7	− 33	a	1.5
6.8–8.5	γ21859	9413	.....	7	− 23	b	1.0
					− 29		
UW Her (229)							
171036	C 5189	5754	102	M5	− 13	b	1.0
7.5–8.5	5490	6165	55	5	− 15	b	1.0
	γ17635	6198	88	5	− 24	b	1.0
					− 17		
CX Her (90)							
170627	C 6223	7135	.....	M6	− 24	b	0.3
7.8–8.8	7278	9379	.....	7	− 42	b	1.0
	γ21864	9414	.....	7	− 48	b	0.3
	C 7349	9471	.....	7	− 46	b	1.0
					− 42		
Z Leo (57)							
094627	C 2044	3423	23	M4	− 22	b	0.7
8.6–10.0	4769	5364	34	3	− 24	b	0.7
	γ17308	6044	33	3	.....	b	0.0
	C 5454	6111	43	2	+ 6	b	0.3
	5633	6313	17	3	− 22	b	1.0
	5661	6339	44	3	− 16	b	1.0
	γ18073	6401	50	3	− 25	b	0.7
	C 5714	6459	51	3	− 9	b	1.0
					− 17		
RY Leo (155)							
095814	γ19427	7080	.....	M3e	+ 37	c	0.4
9.1–10.0	21276	8910	.....	2e	+ 16	c	0.6
	C 5157	8936	.....	3	+ 11	c	0.2
					+ 22		
S Lep (96)							
060124	C 7254	9292	.....	M5	+ 16	b	1.0
6.0–8.0	γ23326	0069*	.....	5	+ 8	b	1.0
					+ 12		
V Lyn (87)							
062061	C 2048	3423	.....	M6	− 43	b	0.3
8.6–9.8	5406	6046	.....	6	− 28	b	0.3
	5908	6649	.....	6	− 25	b	1.0
					− 29		
SZ Lyr (133)							
183146	C 7090	8733	55	M6	.....	c	0.0
10.5–12.5	7295	9393	48	6	− 33	c	0.2
	7308	9411	66	6	− 35	c	0.4
	γ23330	0070*	57	6	− 49	c	0.4
	E 89	0090*	78	6	− 85	c	0.6
	305	0296*	17	6	− 49	c	0.2
					− 54		

TABLE 2—*Continued*

Star, Period, Designation, Magnitude	Plate	JD 242	Phase	Spectrum	Vel.	Disp.	Wt.
			days		km/sec		
XY Lyr (—)							
183439	γ22558	9736	.....	M4	− 25	a	1.5
5.8–6.8	22591	9764	.....	4	− 12	a	1.0
					− 20		
RT Mon (115)							
0803*10*	C 5947	6726	33	M5	.....	b	0.0
8.5–9.3	7275	9379	34	5	.....	c	0.0
	γ22391	9644	69	4	+ 45	b	1.0
	C 7451	9670	95	3	+ 42	b	1.0
					+ 44		
SW Mon (110)							
062105	γ19272	7023	.....	M5	+ 42	b	0.7
9.1–10.6	23311	0032*	.....	5	+ 34	c	0.4
					+ 39		
BQ Ori (129)							
055122	C 7253	9292	.....	M6	+ 22	b	0.7
7.4–8.9	γ23244	9974	.....	5e	+ 37	b	1.0
					+ 31		
DP Ori (—)							
055610	γ23138	9928	.....	M7	− 11	c	0.6
8.6–11.2	C 7651	0002*	.....	7	− 8	c	0.6
					− 10		
ST Peg (136)							
224426	γ18903	6879	105	M6	+ 4	b	1.0
8.3–9.4	C 7551	9855	13	6	− 2	b	1.0
					+ 1		
TT Peg (158)							
000126	C 7154	8850	19	M6e	− 29	b	0.3
9.0–10.3	E 42	9896	114	6	− 34	b	0.6
					− 32		
TW Peg (90)							
215927	γ11283	3298	.....	M7	− 33	a	1.5
6.5–9.2	11313	3325	.....	6	− 23	a	0.5
	11994	3634	.....	6	− 12	a	0.5
					− 27		
TX Peg (132)							
221313	C 7065	8702	11	M6e	+ 12	b	1.0
8.5–9.2	7134	8831	8	6	+ 13	b	1.0
	7135	8831	8	6	+ 10	b	1.0
					+ 12		
UW Peg (106)							
221302	γ21161	8734	.....	M5	+ 28	c	0.6
8.7–9.7	C 7331	9440	.....	5	+ 21	b	1.0
					+ 23		

TABLE 2—*Continued*

Star, Period, Designation, Magnitude	Plate	JD 242	Phase	Spectrum	Vel.	Disp.	Wt.
			days		km/sec		
AF Peg (52)							
224617	C 4963	5492	24	M6	− 44	b	1.0
8.9–9.9	5259	5817	34	6	− 40	b	1.0
	5512	6199	50	6	− 40	b	0.3
					− 42		
BC Peg (100)							
223620	γ19770	7287	37	M6	− 12	c	0.6
7.8–8.5	21206	8765	15	6	− 20	c	0.4
	22759	9824	74	6	− 10	c	0.6
					− 13		
BD Peg (—)							
223827	C 7089	8732	.....	M6	− 9	b	1.0
6.8–7.8	γ21264	8881	.....	6	− 21	b	1.0
	21375	9147	.....	6	+ 10	b	0.7
	23818	0280*	.....	6	− 25	c	0.6
					− 12		
BI Peg (120)							
225217	γ19771	7287	3	M6	− 19	c	0.6
8.0–8.8	21374	9147	63	6e	− 20	b	1.0
					− 20		
RS Per (—)							
021556	C 2536	3742	.....	M4	− 36	b	1.0
8.0–9.4	2633	3803	.....	4	− 39	b	0.3
	2672	3829	.....	4	− 41	b	0.3
					− 38		
RU Per (181)							
032339	E 46	9897	12	M7	− 35	c	0.6
9.5–10.5	62	9913	28	6e	− 43	c	0.6
					− 39		
SU Per (116)							
021556	C 2535	3742	.....	M4	− 39	b	1.0
7.4–8.4	2632	3803	.....	4	− 39	b	1.0
	2671	3829	.....	3	− 44	b	0.7
	γ17724	6221	.....	3	− 36	b	1.0
	18050	6373	.....	4	− 43	b	1.0
	C 5899	6646	.....	4	− 34	b	1.0
					− 39		
SW Per (83)							
040441	C 5005	5519	15	M6	+ 52	b	1.0
8.2–9.8	7641	9971	68	5	+ 57	b	1.0
					+ 54		
TT Per (91)							
014453	C 7099	8763	9	M6	− 3	c	0.6
8.0–9.2	γ23310	0032*	89	6	− 5	c	0.6
					− 4		

TABLE 2—*Continued*

Star, Period, Designation, Magnitude	Plate	JD 242	Phase	Spectrum	Vel.	Disp.	Wt.
			days		km/sec		
UZ Per (90)							
031331	γ22472	9678	.....	M5	− 8	c	0.6
7.8–9.0	C 7660	0029*	.....	5	+ 10	c	0.6
					+ 1		
AA Per (130)							
030846	C 6963	8422	11	M6	+ 21	c	0.6
9.2–10.3	7659	0029*	50	6	+ 14	c	0.4
					+ 18		
AD Per (—)							
021356	C 1974	3358	.....	M2	− 34	a	1.0
7.7–8.4	2124	3475	.....	3	− 45	a	1.0
	5689	6373	.....	2	− 51	b	0.7
					− 43		
RW Psc (100)							
011821	E 45	9897	.....	M3	+ 6	c	0.6
9.1–10.3	60	9913	.....	3	− 6	c	0.6
					0		
T Sge (157)							
191717	γ22561	9738	.....	M4	+ 7	b	1.0
8.3–9.5	C 7487	9765	.....	3	+ 2	b	1.0
					+ 4		
SU Sgr (88)							
185*22*	γ18367	6553	77	M6	+ 41	b	1.0
8.3–8.5	21861	9413	33	6	+ 44	b	1.0
					+ 42		
AX Sco (—)							
163*26*	C 7463	9705	.....	M6	.....	b	0.0
7.1–8.1	7486	9765	.....	6	− 50	b	0.3
	7504	9806	.....	6	− 40	c	0.6
					− 45		
Y Ser (385)							
150*801*	C 5192	5755	65	M5	− 67	b	1.0
8.0–9.1	7320	9439	284	5	− 51	b	1.0
					− 59		
Z Ser (88)							
151002	γ17425	6104	10	M5	− 26	b	0.3
9.4–10.4	18806	6814	20	5	− 32	b	0.3
	C 6047	6880	86	5	− 16	b	0.3
					− 25		
TV Tau (120)							
040226	γ21439	9176	66	M6	+ 82	c	0.2
10.9–11.7	23162	9945	115	6	+ 62	c	0.6
	E 315	0297*	107	6	+ 68	c	0.4
					+ 67		

TABLE 2—*Continued*

Star, Period, Designation, Magnitude	Plate	JD 242	Phase	Spectrum	Vel.	Disp.	Wt.
			days		km/sec		
TX Tau (84)							
040226	C 5591	6281	17	M5	− 13	c	0.4
10.6–12.3	7445	9669	45	5	− 20	b	0.7
					− 17		
W Tri (148)							
023534	γ22099	9505	.....	M5	+ 12	c	0.6
8.2–9.0	23145	9932	.....	5	+ 2	b	1.0
	23195	9957	.....	5	+ 6	b	1.0
					+ 6		
V UMa (207)							
090151	γ22556	9736	206	M5	− 13	c	0.2
9.6–11.2	22587	9764	27	5	− 34	c	0.6
	C 7645	9972	27	6	− 42	c	0.6
	7652	0003*	58	5	− 33	c	0.6
	γ23328	0069*	124	5	− 43	c	0.4
					− 35		
RY UMa (41)							
121561	C 5176	5729	18	M3	− 9	a	1.5
7.2–8.3	γ21965	9450	12	2	− 13	b	1.0
	22475	9678	33	3	− 11	b	1.0
					− 11		
RZ UMa (136)							
080165	γ20679	7791	.....	M5	− 33	c	0.6
8.8–10.2	21277	8911	.....	6	− 36	c	0.6
					− 34		
ST UMa (81)							
112245	C 7251	9290	.....	M5	− 10	a	1.5
6.5–7.3	γ21790	9381	.....	5	− 24	a	1.5
	C 7297	9409	.....	5	− 15	a	1.5
	7302	9410	.....	5	− 16	b	1.0
					− 16		
R UMi (326)							
163172	γ12875	4014	208	M7	.....	b	0.0
8.6–10.5	14175	4631	173	7	− 22	b	1.0
	21966	9450	102	7e	− 22	b	1.0
					− 22		
RT Vir (—)							
125705	C 296	2387	.....	M8	+ 21	a	1.0
8.0–9.0	γ 9051	2391	.....	8	.....	a	0.0
	C 9298	5757	.....	8	+ 6	b	1.0
	γ22476	9679	.....	8	+ 11	b	1.0
					+ 13		
SW Vir (—)							
130*802*	C 302	2388	.....	M7	− 11	a	1.0
6.8–8.1	γ 7299	9409	.....	7	− 19	b	1.0
					− 15		

TABLE 2—*Continued*

Star, Period, Designation, Magnitude	Plate	JD 242	Phase	Spectrum	Vel.	Disp.	Wt.
			days		km/sec		
W Vul (239)							
200525	γ20789	7971	113	M5	+ 51	b	1.0
8 8–10 2	23133	9927	21	6	+ 48	b	1.0
					+ 50		

NOTES TO TABLE 2

Bright lines are mentioned in order of their intensity on the spectrograms.

RU And. Max. = JD 2429377 + 231^{d}2 E, Schneller, *Catalogue*, 1939. *Hδ* and *Hγ* are fairly strong bright lines on plate E318. E61 and E250 show very faint emission lines. C7216 and C7658 are weak and do not definitely prove the absence of emission. This star has a large magnitude range but considerable irregularity in period and light-variation.

RV And. A single Harvard observation, M3e, *Harvard Ann.*, **79**, 196, 1928.

TV And. *Hδ*, *Hγ*, *Hζ*, and *Hη* are fairly strong bright lines on plate γ22857. C7517 shows very faint bright *Hδ* and *Hγ*.

TY And. *Hδ*, *Hγ*, *Hζ*, *Hβ*, *Hη*, and λ 3905 *Si* I are fairly strong bright lines on plate γ23134. γ22994 shows faint bright *Hδ*, *Hζ*, and λ 3905 *Si* I. Two of four Harvard plates have hydrogen emission, *Harvard Ann.*, **79**, 204, 1928.

RU Aqr. Max. = JD 2415601 + 68^{d}7E, Ryves, *M.N.*, **92**, 132, 1932. One of two Harvard plates has hydrogen emission, *Harvard Ann.*, **79**, 204, 1928.

TW Aqr. Max. = JD 2425103 + 79^d E, Schneller, *Catalogue*, 1939.

WX Aql. Max. = JD 2423210 + 105^d E, Leiner, *A.N. Beob.-Zirk.*, **4**, 51 (No. 29), 1922.

KN Aql. Max. = JD 2426153 + 139^d E, Schneller, *Catalogue*, 1939. Very faint bright *Hδ* shows on the second plate, which was taken shortly before predicted maximum.

NO Aql. Max. = JD 2428419.2 + 63^d E, Schneller, *Catalogue*, 1939. Very faint bright *Hδ* shows on plate γ23205. This star resembles the RV Tauri stars in some respects.

RV Boo. Very faint bright *Hδ* shows on three plates. One of five Harvard exposures has bright hydrogen, *Harvard Ann.*, **79**, 200, 1928. λ 4226 *Ca* I is strong on the first two and the last plates.

RX Boo. Faint hydrogen lines, together with fairly strong λ 3905 and λ 4102 *Si* I, show in emission on the second plate. λ 4102 is stronger than *Hδ*.

RS Cnc. McLaughlin reports that bright lines appear during increasing light and weaken before maximum. Emission was found to be strongest in cycles when the light-variation was greatest. The light-elements Min. = JD 2425351 + 239^d E were determined. The maximum velocity of recession occurred one-fourth period after light-minimum. A mean velocity of +12.8 km/sec with a range of 6 km/sec was found. *Pub. Univ. of Michigan*, **8**, 118, 1941.

RT Cnc. Max. = JD 2426756 + 94^{d}4 E, Schneller, *Catalogue*, 1939. The variation in type and velocity are apparently real.

VY CMa. This star, HD 58061 = ADS 6033 A, is imbedded in bright nebulosity, which possibly is responsible for the emission lines of hydrogen. It is described by Perrine, *Pub. A.S.P.*, **35**, 233, 1923. Several near-by companions or nuclei are recognized by double-star observers. M-type stars are not usually connected with nebulosity. The variation in light may well be of a nature very different from the other stars in this list. The emission lines are on the red edge of moderately strong absorption lines of hydrogen, which are displaced an angstrom or more toward the violet. The aluminum band head near *Hβ* is unusually strong.

UX CMi. Max. = JD 2425370 + 151^d E, Schneller, *Catalogue*, 1939.

UY Cas. Max. = JD 2419328 + 102^{d}5 E, Schneller, *Catalogue*, 1939. Fairly strong bright *Hβ*, *Hγ*, *Hδ*, and *Hζ* show on the second and third plates.

SS Cep. Max. = 2425779.5 + 97^{d}5 E, Schneller, *Catalogue*, 1939.

T Cet. Boss 60. Bright *Hβ*, *Hγ*, and *Hδ* show on the second and third plates. *Hβ* is remarkably strong for a type so late, and the decrement is steep. The variation in velocity is probably real.

RR CrB. Max. = JD 2426148 + 56^{d}8 E, Schneller, *Catalogue*, 1939.

S Crt. Two Harvard observations of type are M7e and M6e, *Harvard Ann.*, **79**, 199, 1928.

RZ Cyg. Max. = 2429516 + 546^d E, Schneller, *Catalogue*, 1939. In this peculiar star high and low maxima alternate. The light-curve resembles that of R Cen. The magnitude range is large for variables without bright lines.

AB Cyg. Observed maximum on JD 2426310 and JD 2427711, Loreta, *A.N.*, **261**, 263, 1936. Of three Harvard exposures, one shows bright lines, M4e, *Harvard Ann.*, **79**, 204, 1928.

AF Cyg. The light-curve is sometimes of the RV Tau type. McLaughlin reports bright lines, *Pub. A.A.S.*, **8**, 15, 1933. The phases are taken from O'Connell's observed maxima, *Harvard Bull.*, No. 888, 1933. There is some correlation of velocity with phase.

AI Cyg. Max. = JD 2420080 + 140^d E, Schneller, *Catalogue*, 1939.

BC Cyg. R. F. Sanford found that this red star is M-type and not N as suggested in Schneller's *Catalogue*. The star is located in an obscured region, and the spectra are markedly weak in the violet. The nature of its variation is not known.

CH Cyg. Boss 4966. Max. = 2422991 + 100^{d}6 E, Schneller, *Catalogue*, 1939.

TT Dra. Max. = 2424727 + 107^{d}4 E, Schneller, *Catalogue*, 1939.

TX Dra. Max. = 2425267 + 134^d E, *Harvard Ann.*, **79**, 175, 1928. Very faint bright $H\delta$ and $H\gamma$ show on the last plate.

UU Dra. Max. = JD 2418745 + 234^{d}4 E, *Harvard Ann.*, **79**, 190, 1928.

UV Dra. Max. = JD 2424436.4 + 77^{d}4 E, Schneller, *Catalogue*, 1939.

RW Eri. Max. = JD 2416780 + 91^{d}4 E, Schneller, *Catalogue*, 1939.

Y Gem. Strong bright $H\beta$ and weak $H\gamma$ show on the second plate. The decrement is steep, and $H\delta$ is not seen. One of three Harvard exposures has bright lines, M6e, *Harvard Ann.*, **79**, 198, 1928.

X Her. McLaughlin reports bright hydrogen lines at or just betore maximum, *Pub. A.A.S.*, **7**, 94, 1932.

UW Her. Max. = JD 2419011 + 229^d E, *Harvard Ann.*, **79**, 176, 1928. One of two Harvard exposures has bright hydrogen lines, M4e, *Harvard Ann.*, **79**, 201, 1928.

Z Leo. Max. = JD 2424592.2 + 56^{d}77 E, Schneller, *Catalogue*, 1939.

RY Leo. Fairly strong bright $H\beta$, $H\gamma$, and $H\delta$ show on the first and second plates. The decrement toward the violet is gradual.

S Lep. Type Me, Gaposchkin and Gaposchkin, *Variable Stars*, 1938.

SZ Lyr. Max. = JD 2424410 + 133^{d}4 E, Schneller, *Catalogue*, 1939.

RT Mon. Max. = JD 2424618 + 115^{d}3 E, Schneller, *Catalogue*, 1939.

BQ Ori. Fairly strong bright $H\beta$, $H\gamma$, $H\delta$, and $H\zeta$, together with λ 3905 *Si* I, show on the second plate.

ST Peg. Max. = JD 2424562 + 115^{d}3 E, Schneller, *Catalogue*, 1939. One of two Harvard plates shows bright lines, M6e, *Harvard Ann.*, **79**, 204, 1928.

TT Peg. Max. = JD 2419321 + 158^{d}5 E, *Harvard Ann.*, **79**, 163, 1928. Faint bright $H\delta$ and $H\gamma$ show on the first plate.

TX Peg. Max. = JD 2423804 + 132^d E, Schneller, *Catalogue*, 1939. Faint bright $H\delta$ and $H\gamma$ show on the first plate.

AF Peg. Max. = JD 2423006 + 52^{d}4 E, Schneller, *Catalogue*, 1939.

BC Peg. Max. = JD 2426650 + 100^d E, Schneller, *Catalogue*, 1939.

BI Peg. Max. = JD 2426565 + 120^d E, Schneller, *Catalogue*, 1939. Faint bright $H\delta$ shows on the second plate.

RS Per, SU Per, and AD Per. Members of the double cluster (h and χ Per). The mean parallax of the cluster determined from the spectroscopic absolute magnitudes of the three stars, neglecting absorption in space, is 0".00073.

RU Per. Max. = JD 2416814 + 180^{d}7 E, Schneller, *Catalogue*, 1939. Fairly strong bright $H\delta$, $H\gamma$, $H\zeta$, and λ 3905 *Si* I show on the second plate.

SW Per. Max. = JD 2419362 + 83^d E, *Harvard Ann.*, **79**, 165, 1928.

TT Per. Max. = JD 2423721.5 + 91^{d}5 E, Schneller, *Catalogue*, 1939.

AA Per. Max. = JD 2424890 + 130^{d}4 E, Schneller, *Catalogue*, 1939.

SU Sgr. Max. = JD 2416620 + 88^d E, Schneller, *Catalogue*, 1939.

Y Ser. Max. = JD 2419145 + 385^d E, *Harvard Ann.*, **79**, 174, 1928. Two of six Harvard plates show $H\gamma$ and $H\delta$ faintly bright, *Harvard Ann.*, **79**, 200, 1928.

Z Ser. Max. = JD 2423204.3 + 87^{d}57 E, Schneller, *Catalogue*, 1939.

TV Tau. Max. = JD 2425870 + 120^d E, Schneller, *Catalogue*, 1939.

TX Tau. Max. = JD 2419384 + 80^d E, *Harvard Ann.*, **79**, 165, 1928.

V UMa. Min. = JD 2429530 + 207^{d}5 E, Schneller, *Catalogue*, 1939. Faint bright lines are suspected on Harvard plates, *Harvard Ann.*, **79**, 198, 1928.

RY UMa. Min. = JD 2429894 + 41^{d}42 E, Schneller, *Catalogue*, 1940. One of six Harvard plates shows bright hydrogen lines, M4e, *Harvard Ann.*, **79**, 199, 1928.

R UMi. Min. = JD 2429348 + 326^d E, Nielsen, *A.N.*, **270**, 42, 1940. Faint bright $H\delta$ and $H\gamma$ show on the third plate.

W Vul. Max. = JD 2417017 + 238^{d}7 E, *Harvard Ann.*, **79**, 189, 1928. One Harvard exposure shows bright lines, M4e. *Harvard Bull.*, **79**, 203, 1928.

TABLE 3

ABSOLUTE MAGNITUDES AND VELOCITIES OF IRREGULAR M-TYPE VARIABLES

STAR	l	b	m_v AT MAX.	SPEC. M_v	π_{ap} UNIT = 0".001	SPEC.	VELOCITY		PERIOD
							Meas.	Residual	
							km/sec	km/sec	days
RU And.	101°	−23°	10.0	−0.6	0.8	M5e–6e	− 42	− 41	231
RV And.	104	−11	8.7	−0.3	1.6	5	− 10	− 9	229
SS And.	76	− 7	8.9	−1.3	0.9	5 –6	− 22	− 12	160
TV And.	70	−16	8.8	−0.5	1.4	4e–5e	− 50	− 40	114
TY And.	72	−19	8.2	−0.9	1.5	5e–6e	− 6	+ 3	150
TZ And.	81	−14	8.5	−0.7	1.4	5 –6	− 31	− 23	280
RU Aqr.	24	−69	9.0	−1.0	1.0	5 –6	+ 26	+ 27	69
TW Aqr.	16	−31	9.3	−0.9	0.9	5 –6	− 38	− 26	79
BM Aqr.	10	−51	9.0	−1.0	1.0	4 –5	− 21	− 15	. . . . .
TZ Aql.	8	−25	8.5	−0.6	1.5	6	+ 50	+ 63	90
WX Aql.	10	−12	8.8	−0.8	0.5	6	− 28	− 12	105
KN Aql.	14	−22	7.7	−1.0	1.8	5e	−140	−125	139
LU Aql.	20	− 4	9.2	−0.9	1.0	4	+ 2	+ 20	50
NO Aql.	11	−11	9.9	−1.6	0.5	3 –4e	− 99	− 82	66
PX Aql.	0	−20	9.2	−0.6	1.1	5	− 35	− 21	. . . . .
TU Aur.	138	+18	7.7	−0.9	1.9	5	+ 8	+ 3	75
UX Aur.	128	+ 7	8.0	−1.3	1.4	5	+ 34	+ 30	90
UZ Aur.	135	+ 2	7.7	−1.0	1.8	4	+ 21	+ 24	66
RV Boo.	18	+65	7.6	−0.9	2.1	5 –6e	− 3	+ 11	138
RW Boo.	16	+65	7.3	−0.7	2.5	5	− 11	+ 3	373
RX Boo.	1	+68	7.0	−0.6	3.0	7 –8e	− 10	+ 3	78
RR Cam.	108	+21	9.2	−0.5	1.1	6	− 61	− 56	123
RS Cam.	101	+33	8.1	−0.4	2.0	5 –6	− 41	− 34	89
RV Cam.	117	+ 7	7.9	−1.0	1.7	5 –6	− 21	− 21	103
RY Cam.	112	+12	8.0	−0.7	1.8	3 –4	− 23	− 21	135
Z Cnc.	177	+28	8.5	−0.5	1.6	6 –7	+ 4	− 8	80
RS Cnc.	163	+43	5.3	−1.5	4.4	5 –6	+ 11	+ 5	239
RT Cnc.	186	+34	7.3	−1.3	1.9	5 –6	+ 36	+ 25	94
RV CMa. . . .	194	− 3	8.9	−0.9	1.1	6	+ 27	+ 8	. . . . .
VY CMa. . . .	206	− 4	7.8	−2.9	0.7	3e–4e	+ 49	+ 30	. . . . .
UX CMi. . . .	183	+16	8.5	−1.2	1.1	5	+ 25	+ 10	151
UY Cas.	77	− 2	9.6	−1.1	0.7	3e–4e	− 4	+ 7	102
VY Cas.	90	0	9.0	−0.6	1.2	6	− 92	− 85	100
SS Cep.	97	+21	6.7	−1.1	2.7	6	− 41	− 34	98
μ Cep.	68	+ 4	4.0	−4.5	2.0	2	+ 20	+ 34	. . . . .
T Cet.	54	−80	5.2	−1.8	4.0	5e	+ 29	+ 27	160
Y CrB.	27	+51	9.8	−0.4	0.9	8	− 20	− 3	300
RR CrB.	27	+52	7.2	−0.5	2.9	5	− 50	− 33	57
RU CrB.	7	+52	8.8	−0.9	1.1	5	− 27	− 10	436
X Crv.	271	+44	7.8	−1.2	1.6	6	+ 1	+ 1	127
S Crt.	248	+53	8.4	−1.1	1.3	6	+ 32	+ 30	152
RZ Cyg.	54	+ 1	9.6	−1.4	0.6	7	− 47	− 31	546
AB Cyg.	49	−16	7.7	−0.7	2.1	4 –5	− 7	+ 7	482
AF Cyg.	45	+12	6.4	−0.8	3.6	6	− 15	+ 3	94
AI Cyg.	41	− 5	8.4	−0.8	1.4	6	− 58	− 41	140

TABLE 3—*Continued*

Star	l	b	m_v at Max.	Spec. M_v	π_{sp} Unit = 0".001	Spec.	Velocity		Period
							Meas.	Residual	
							km/sec	km/sec	days
BC Cyg	43°	0°	9.8	−1.8	0.5	M3 –4	− 3	+ 15	.....
CH Cyg	49	+15	6.4	−1.4	2.7	6	− 53	− 35	101
U Del	30	−17	5.6	−2.0	3.0	5	− 21	− 5	.....
S Dra	50	+40	7.5	−1.0	2.0	6	+ 6	+ 23	.....
SS Dra	93	+49	8.6	−1.1	1.1	5	+ 33	+ 43	48
SZ Dra	63	+22	8.0	−1.2	1.4	5	− 42	− 26	120
TT Dra	52	+35	8.5	−0.9	1.3	6	− 23	− 6	107
TX Dra	56	+40	6.8	−1.9	1.8	4e–5	+ 52	+ 68	134
UU Dra	75	+20	8.7	−0.2	1.7	8	− 37	− 24	234
UV Dra	61	+55	8.8	−1.1	1.0	5	− 35	− 21	77
Z Eri	157	−57	6.4	−0.9	3.5	5	− 14	− 27	.....
RW Eri	166	−34	8.6	−1.0	1.2	6	+107	+ 90	91
Y Gem	168	+21	8.5	−0.7	1.4	6e	+ 18	+ 6	.....
TV Gem	157	+ 3	7.0	−3.1	1.0	2	+ 17	+ 4	.....
η Gem	157	+ 4	3.3	−0.9	14.5	3	+ 19	+ 7	.....
X Her	40	+47	5.8	−1.1	4.2	6	− 91	− 74	100
ST Her	42	+49	6.8	−0.7	3.2	7	− 29	− 12	167
UW Her	27	+34	7.5	−1.3	1.7	5	− 17	+ 2	229
CX Her	16	+32	7.8	−0.5	2.2	7	− 42	− 22	90
α Her	3	+26	3.1	−2.2	8.7	5	− 33	− 14	.....
g Her	33	+43	4.4	−1.0	8.3	6	+ 3	+ 22	.....
Z Leo	174	+52	8.6	−0.6	1.4	2 –4	− 17	− 22	57
RY Leo	192	+50	9.1	−0.9	1.0	2e–3e	+ 22	+ 15	155
S Lep	198	−19	6.0	−1.3	3.5	5	+ 12	− 8	96
V Lyn	121	+22	8.6	+0.1	2.0	6	− 29	− 29	87
R Lyr	41	+17	4.0	−1.1	9.6	5	− 28	− 9	.....
SZ Lyr	42	+21	10.5	−0.8	0.5	6	− 54	− 35	133
XY Lyr	35	+18	5.8	−2.6	2.1	4	− 20	− 1	.....
RT Mon	199	+13	8.5	−0.9	1.3	3 –4	+ 44	+ 27	115
SW Mon	173	− 2	9.1	−0.5	1.2	5	+ 39	+ 22	110
BQ Ori	155	0	7.4	−0.4	2.7	5e–6	+ 31	+ 18	129
CI Ori	172	−17	4.7	+0.1	12.0	0	+ 8	− 10	.....
DP Ori	166	− 5	8.6	−0.4	1.6	7	− 10	− 26	.....
α Ori	167	− 7	0.1	−4.1	14.5	2	+ 21	+ 5	.....
SX Pav	290	−39	5.3	.....	.....	6	+ 43	+ 37	.....
ST Peg	60	−29	8.3	−1.4	1.1	6	+ 1	+ 9	136
TT Peg	79	−35	9.0	−1.5	0.8	6e	− 32	− 28	158
TW Peg	51	−23	6.5	−0.9	3.3	6 –7	− 27	− 15	90
TX Peg	44	−36	8.5	−0.4	1.7	6e	+ 12	+ 22	132
UW Peg	34	−44	8.7	−1.4	1.0	5	+ 23	+ 31	106
AF Peg	55	−37	8.9	−1.3	0.9	6	− 42	− 34	52
BC Peg	55	−33	7.8	−1.1	1.7	6	− 13	− 3	100
BD Peg	59	−28	6.8	−0.8	3.0	6	− 9	+ 1	.....
BI Peg	57	−38	8.0	−1.0	1.6	6e	− 20	− 12	120
RS Per	103	− 4	8.0	−2.6	0.8	4	− 38	− 35	.....

TABLE 3—*Continued*

Star	l	b	m_v at Max.	Spec. M_v	π_{sp} Unit = 0".001	Spec.	Velocity		Period
							Meas.	Residual	
							km/sec	km/sec	days
RU Per	121°	−13°	9.5	−1.3	0.7	M6e–7	− 39	− 43	181
SU Per	103	− 4	7.4	−3.5	0.7	3 –4	− 39	− 36	116
SW Per	126	− 7	8.2	−1.0	1.4	5 –6	+ 54	+ 49	83
TT Per	100	− 8	8.0	−0.9	1.7	6	− 4	− 1	91
UZ Per	125	−21	7.8	−1.5	1.4	5	+ 1	− 5	90
AA Per	115	− 9	9.2	−1.8	0.6	6	+ 18	+ 16	130
AD Per	103	− 3	7.7	−3.1	0.7	2 –3	− 43	− 40	.....
ρ Per	117	−16	3.2	−0.9	15.1	4	+ 28	+ 25	.....
RW Psc	102	−40	9.1	−2.0	0.6	3	0	− 2	100
TV Psc	84	−44	5.2	−1.4	4.8	3	+ 5	+ 7	.....
T Sge	19	0	8.3	−2.3	0.8	3 –4	+ 4	+ 23	157
SU Sgr	342	−14	8.3	−0.8	1.5	6	+ 42	+ 54	88
AX Sco	322	+12	7.1	−0.8	2.6	6	− 45	− 35	.....
α Sco	320	+14	0.9	−3.7	12.0	1	− 3	+ 7	.....
Y Ser	327	+44	8.0	0.0	2.5	5	− 59	− 47	385
Z Ser	331	+46	9.4	−1.1	0.8	5	− 25	− 12	88
TV Tau	137	−18	10.9	−0.7	0.5	6	+ 67	+ 58	120
TX Tau	137	−18	10.6	−0.8	0.5	5	− 17	− 26	84
W Tri	116	−22	8.2	−0.7	1.7	5	+ 6	+ 2	148
V UMa	135	+43	9.6	−0.4	1.0	5 –6	− 35	− 36	207
RY UMa	96	+57	7.2	−0.5	2.9	2 –3	− 11	− 2	41
RZ UMa	118	+34	8.8	−1.2	1.0	5 –6	− 34	− 32	136
ST UMa	127	+67	6.5	−1.3	2.7	5	− 16	− 12	81
R UMi	71	+36	8.6	−0.3	1.7	7e	− 22	− 8	326
V UMi	85	+43	7.5	−0.5	2.5	4	−165	−154	70
RT Vir	281	+67	8.0	0.0	2.5	8	+ 13	+ 18	.....
SW Vir	284	+59	6.8	−1.0	2.7	7	− 15	− 11	.....
W Vul	32	− 5	8.8	−0.8	1.2	5 –6	+ 50	+ 68	239

Figure 1 shows the galactic distribution of the stars of Table 3. The center of the figure represents longitude 90° and latitude 0°. The scarcity of stars in the general direction of the center of the galaxy at longitude 325° is probably without significance. This region may have been somewhat neglected on account of its southern declination. In longitude the greatest density is in the region between 40° and 120°, but this concentration may be the result of selection.

Apparent magnitude.—In order to be comparable with the general practice for Me stars, the maximum apparent brightness has been used. Photographic magnitudes have been reduced to visual by the appropriate correction for color index, 1.7 mag. The average magnitude range is 1.3 mag., which is much smaller than that of the Mira variables.

Spectroscopic absolute magnitudes.—For the determination of absolute magnitude by the Mount Wilson spectroscopic method the reduction tables used in 1935[7] were employed without change. The zero point for the normal giants is fairly well determined, but for the supergiants the calibration is less certain on account of the lack of suitable standards. Distinct supergiant characteristics are shown by 13 stars (μ Cep, α Ori, α Sco SU Per, TV Gem, AD Her, VY CMa, XY Lyr, RS Per, T Sge, α Her, RW Psc, U Del),

[7] *Mt. W. Contr.*, No. 511; *Ap. J.*, **81**, 187, 1935.

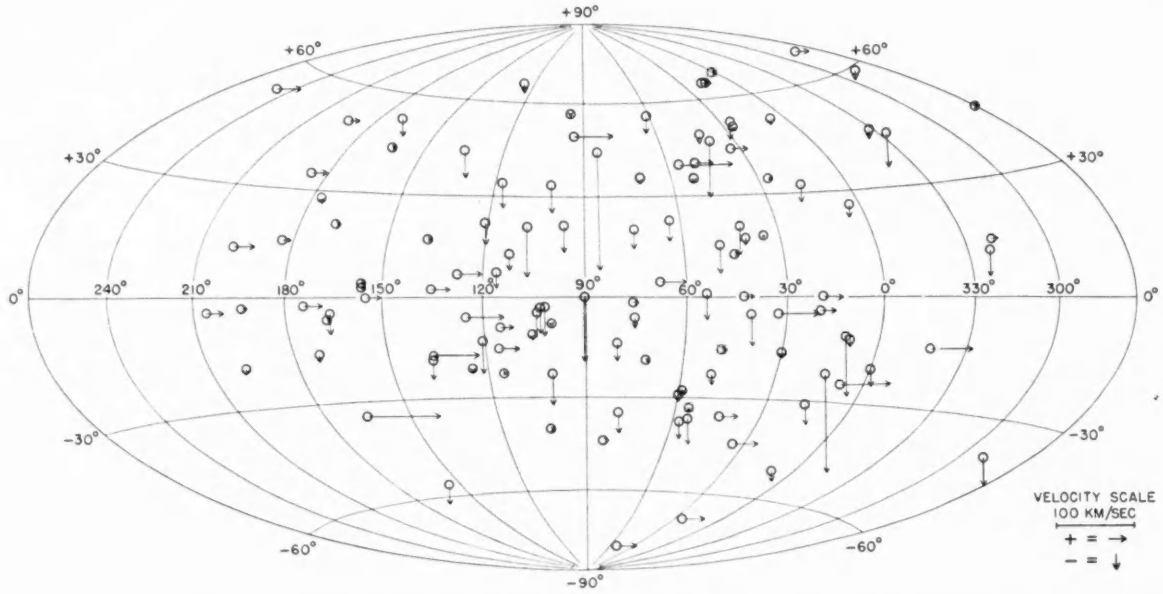

FIG. 1.—Galactic distribution and residual radial velocities of irregular M-type variables. The horizontal arrows indicate positive velocities; the vertical arrows, negative.

whose absolute magnitudes range from −4.5 to −2.0. The remainder of the variables are normal giants with a dispersion of about 1 mag. from the mean absolute magnitude of −0.9. This mean corresponds closely with −1.0 found by Wilson and Merrill[8] for the Me variables. Figure 2 shows the distribution of absolute magnitudes. The stars are mainly concentrated in the giant group, and the scattered supergiants are compara-

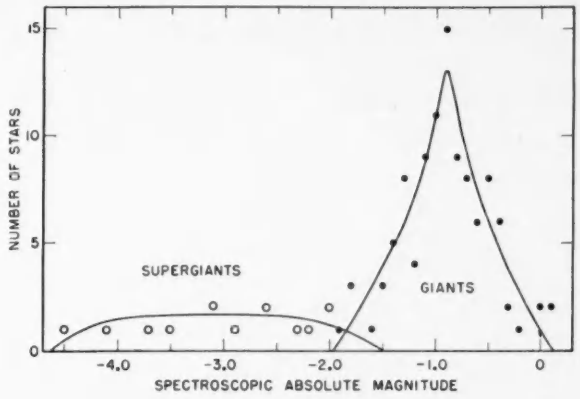

FIG. 2.—Distribution of absolute magnitudes of irregular M-type variables

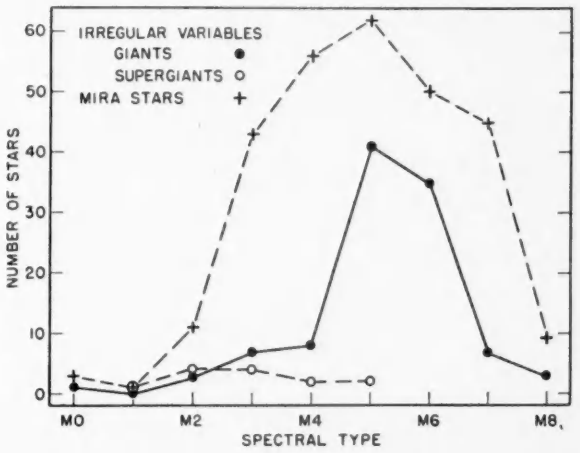

FIG. 3.—Distribution of spectral type among the irregular M-type variables. Merrill's estimates of the Mira stars are included for comparison.

tively few. Numerical values of the relative percentage in each group cannot be given until the effect of selection is known, but it seems clear that about nine-tenths of the irregular M-variables belong to the normal giant group and that their luminosities are much the same as those of the Mira variables.

Spectral type.—As shown in Figure 3, the irregular variables are predominantly of spectral types M5 and M6. Two-thirds of the observed stars fall in these two classes. As compared with the long-period variables,[9] the maximum frequency is at about the

[8] *Mt. W. Contr.*, No. 658; *Ap. J.*, **95**, 255, 1942.

[9] Merrill, *Mt. W. Contr.*, No. 649; *Ap. J.*, **94**, 208, 1941.

same spectral type, but the irregular stars have a much greater concentration. Of the 13 supergiant irregular variables, 11 are M4 or earlier. The stars having emission lines show no preference for any particular type.

Although the full range in type during a cycle may not always be covered by the scattered observations, it is evident that the change is small. For 82 stars the estimates indicate no change in type; for 35, the variation, including the error of estimation, is only one subdivision of type; and for one star only, Z Leo, the difference in type amounts to as much as two subdivisions.

Radial velocities.—The velocities of Table 3 are the weighted means of the observed values for each star. The variation with phase is small compared with the errors of observation and may be neglected. In order to free the velocities from the effect of the

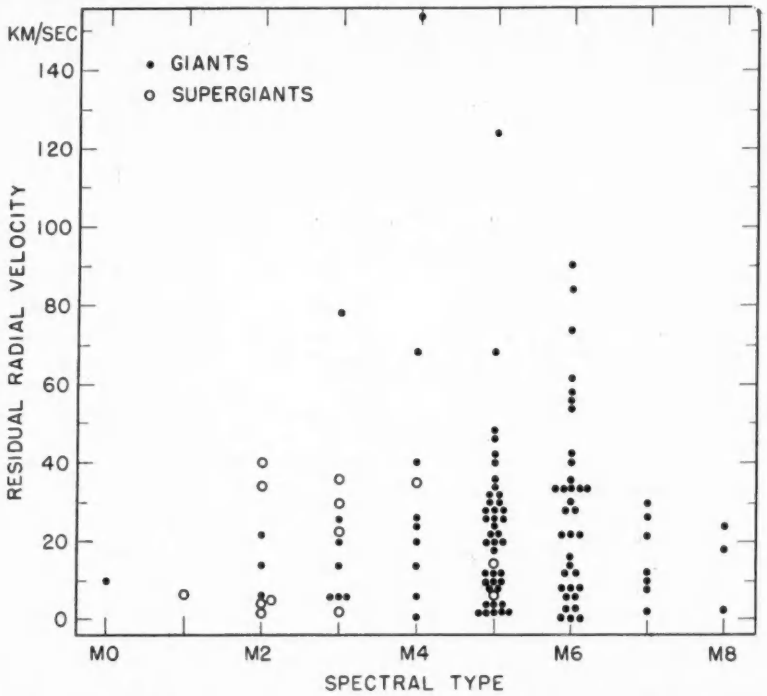

FIG. 4.—Residual radial velocity and spectral type for the irregular M-type variables

sun's motion relative to the near-by stars they have been corrected for a solar motion of 20 km/sec toward the usual apex, and the residual values are in the next to the last column. The direction and relative values of the residual velocities are displayed in Figure 1.

The average residual velocity for 118 irregular stars is 25.3 km/sec, which is definitely smaller than the value 36.1 km/sec found by Merrill[10] for the long-period variables. The average velocity for the 13 irregular supergiants is 18.2 km/sec and for 105 giants, 26.1 km/sec. The distribution of residual velocities with respect to spectral type is shown in Figure 4. The wide scatter of velocities in the earlier spectral types from M0 to M4, which was found for the long-period variables, is not present among the irregular stars, probably for the reason that there are few normal giants of early spectral types.

[10] *Mt. W. Contr.*, No. 649; *Ap. J.*, **94**, 209, 1941.

The mean residual velocities for the various spectral types appear in Table 4, where the number of stars in each group is in parenthesis.

The relationship between radial velocity and period is shown in the second half of the table, the individual values being plotted in Figure 5. The scatter in the residual

TABLE 4

RESIDUAL RADIAL VELOCITY AND DISPLACEMENT OF EMISSION LINES FOR DIFFERENT SPECTRAL TYPES AND PERIODS

Spectrum	Mean Residual Vel.	Displacement Abs.−Em.	Period	Mean Residual Vel.	Displacement Abs.−Em.
	km/sec	km/sec	days	km/sec	km/sec
M0–2	15(9)	+ 6.0(1)	41– 74	44(10)	+16 (1)
M3	23(11)	+ 8.0(2)	75– 99	25(33)	+ 8 (1)
M4	39(10)	+ 8.6(4)	100–124	31(18)	+ 7.5(2)
M5	23(43)	+ 5.8(5)	125–149	31(13)	+ 6.8(5)
M6	28(35)	+10.0(7)	150–199	20(10)	+ 8.8(5)
M7	17(7)	+12.0(1)	200–249	21(15)	+10.1(2)
M8	15(3)	+ 9.0(1)	>250		+12 (1)
Mean	25.3(118)	+ 8.9(21)	Mean	27.7(89)	+ 8.9(17)

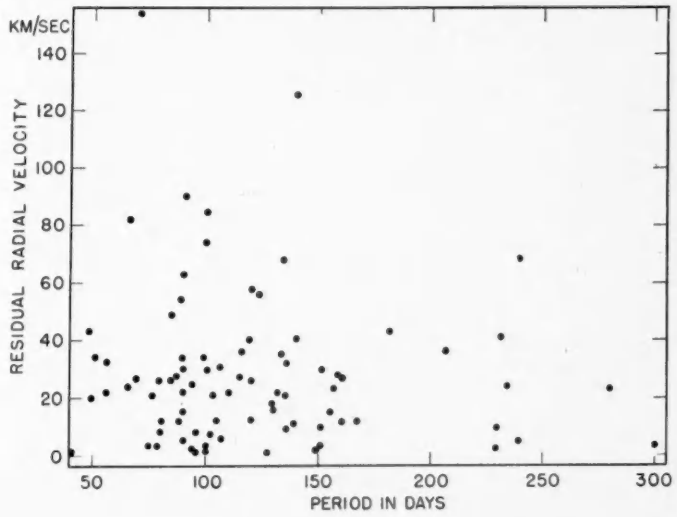

FIG. 5.—Residual radial velocity and period

velocities is greater among the stars having shorter periods. A similar correlation was obtained by Merrill from the Mira stars, although the periods involved are very different.

Displacements of emission lines.—Emission lines of hydrogen were measured in 17 stars. Their displacements, which are toward the violet with reference to the absorption lines, are listed in Table 5. The means for various spectral types and periods are given in Table 4, where the number of stars used in the mean is given in parenthesis. In Figures

TABLE 5

DISPLACEMENT OF EMISSION LINES

Star	Spec.	Period	No. Lines	Abs.—Em.	Star	Spec.	Period	No. Lines	Abs.—Em.
		days		km/sec			days		km/sec
RU And.....	M6e M5e	231	3 2	+15 + 8	T Cet....	M5e	160	2	+ 8
TV And.....	M4e	114	2	+ 5	TX Dra....	M4e	134	2	+13
TY And.....	M5e	150	4	+ 6	Y Gem...	M6e	.....	2	+15
KN Aql.....	M5e	139	1	+ 3	RY Leo....	M3e M2e	155	2 2	0 + 6
NO Aql.....	M4e	66	1	+16	BQ Ori....	M5e	129	4	+ 4
RV Boo.....	M6e	138	1	+ 8	TT Peg....	M6e	158	2	+21
RX Boo.....	M8e	78	3	+ 8	TX Peg....	M6e	132	2	+ 6
RS Cnc.....	M6e	239	21	+ 8.7*	RU Per....	M6e	181	2	+ 6
UY Cas.....	M3e M4e	102	2 2	+16 + 4	R UMi...	M7e	326	2	+12

* McLaughlin, *Pub. Obs. Univ. of Michigan*, **8**, 120, 1941.

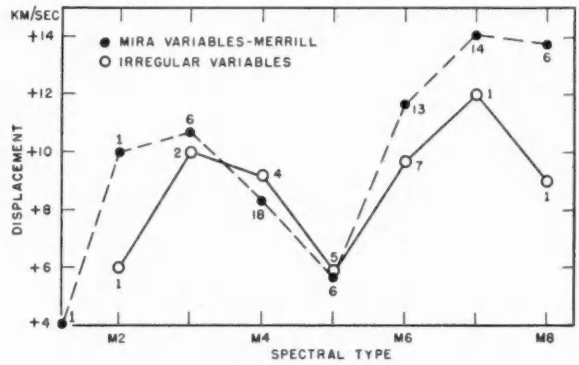

FIG. 6.—Spectral type and relative displacement (A–E) of emission in M-type variables. The number of stars in each normal point is indicated.

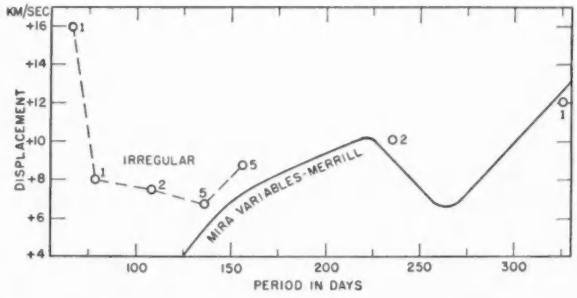

FIG. 7.—Period and relative displacement (A–E) of emission in M-type variables. The number of stars in each normal point is indicated for the irregular variables. Merrill's curve for the Mira stars is shown.

6 and 7 these values are plotted, together with the comparable mean displacements determined by Merrill[11] for the long-period variables. Although the material is rather limited, there is a striking similarity in the two groups, especially in the correlation between displacement of the bright lines and spectral type. The displacement seems to be more intimately related to spectral type or temperature than to other parameters, such as period, range, and regularity of light-changes.

Correlations with period.—For variable stars in general the period of variation is a definite and fundamental parameter to which other characteristics may be referred, but

TABLE 6

DISTRIBUTION OF PERIODS OF 89 OBSERVED STARS

Period	No.	Period	No.
days		days	
40– 59	6	160–179	3
60– 79	8	180–199	1
80– 99	19	200–219	1
100–119	14	220–239	6
120–139	15	240–299	1
140–159	8	>300	7

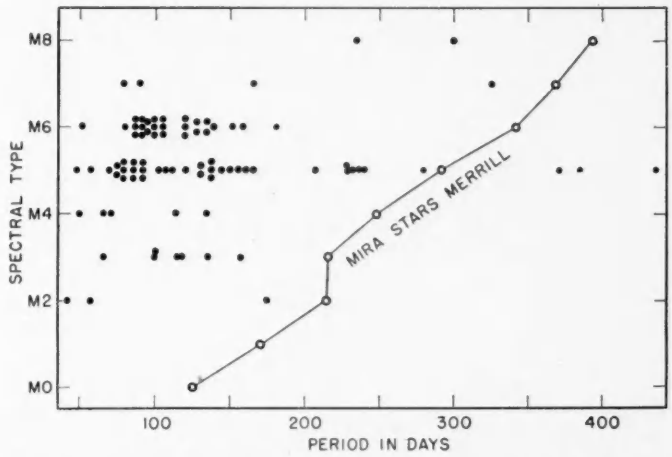

FIG. 8.—Spectral type and period of M-type variables observed at Mount Wilson. The normal points for Merrill's Mira stars, grouped according to type, are plotted.

for causes at present not fully understood periodicities in the less regular variables are followed in a loose and uncertain fashion. In some stars there may be a multiplicity of cycles which overlap one another and thus conceal the underlying periodicities. The period which has been assigned to the irregular M-type stars by the variable-star observers is usually a mean of the intervals between maxima or minima which may differ greatly in magnitude. The ingenuity of the observers in deducing periods from the observations is most commendable, but it should be kept in mind that the periods determined for stars considered in this paper have quite a different significance from the periods of the Mira stars or the Cepheids.

The periods for 89 of the stars observed are distributed as shown in Table 6. The greatest frequency lies between 80 and 140 days, with a mean at 108 days.

[11] *Mt. W. Contr.*, No. 644; *Ap. J.*, **93**, 383, 1941.

There are also 15 stars with periods between 200 and 546 days, with a secondary frequency maximum at 233 days. Few supergiants are included because their light-changes are too irregular to justify the assignment of periods. Of the giants, the stars with periods between 40 and 200 days have slightly fainter absolute magnitudes, somewhat earlier spectral types, and residual radial velocities which are 8 km/sec greater in the mean than those of the stars with longer periods. It is probable that the variables with periods shorter than 200 days are considerably different in nature from those with longer periods.

In Figure 8, spectral type is plotted against period for the irregular stars, and the corresponding mean values for the Mira variables[12] are included for comparison. The lack of agreement between the two groups is very striking. Later spectral type goes with longer period in both groups, but in the irregular variables the periods are of an entirely different order from those of the Mira stars. In the irregular stars the higher harmonics of the cycle appear to be enhanced, but in the Mira stars the fundamental period with its greater regularity prevails and induces a greater range in luminosity and temperature.

CARNEGIE INSTITUTION OF WASHINGTON
MOUNT WILSON OBSERVATORY
June 1942

[12] Merrill, *Mt. W. Contr.*, No. 649; *Ap. J.*, **94**, 199, 1941.

MEAN ABSOLUTE MAGNITUDES AND SPACE MOTIONS OF THE IRREGULAR VARIABLE STARS*

RALPH E. WILSON

ABSTRACT

The radial velocities and proper motions of the irregular variable stars of spectral type M have been used to determine the mean absolute magnitude, $\overline{M}$. The average value, $\overline{M}=-1.1$, is essentially the same as that previously found for the long-period variables of type Me. About 10 per cent of the stars are supergiants, for which $\overline{M}=-3.4$; the remainder are ordinary giants, $\overline{M}=-0.9$. Among the giants no correlations of M with type, period, or character of light-variation were found. The intensities of the critical absolute-magnitude lines in the spectra of the irregular variables behave as they do among the nonvariable stars of type M; hence the calibration-curves for determining individual absolute magnitudes of the latter may be used for the variables.

Space motions derived with the aid of the spectroscopic parallaxes indicate that the irregular variables move with an average speed, $S=54$ km/sec, definitely greater than that of the nonvariable giants of type M but much less than that of the long-period variables. The group motion, $V_0=28.1$ km/sec, likewise lies between that of the nonvariable giants and the faster-moving Me stars. The preferential motion is in the direction indicated by the stars in general. In spite of the weak concentration of the irregular variables toward the plane of the galaxy, the radial velocities show definite effects of the galactic rotation. The space motions show some effects of the velocity asymmetry associated with high-speed stars. These are reasonably explained by the hypothesis of galactic rotation. In their kinematic properties the irregular variables seem to be related to the long-period variables; in their physical properties the relation to the nonvariable stars of the same spectral types appears more definite.

Absolute magnitudes of irregular variable stars of spectral type M have been determined by A. H. Joy[1] from the relative intensities of certain lines in their spectra, on the assumption that these lines behave as they do in the nonvariable stars of the same spectral class. It is desirable to test the validity of this assumption.

The data available are the magnitudes, types, and radial velocities from Joy's paper and the proper motions listed in Table 1. For the stars not in Joy's list the apparent magnitudes at maximum have been taken in order of preference from the lists of *Variable Stars*,[2] the "Harvard Catalogue of Long-Period Variables,"[3] the *Henry Draper Catalogue*,[4] and Schneller's *Catalogue and Ephemerides of Variable Stars for 1939*.[5] Whenever photographic magnitudes only were available, the color index -1.7 was applied in order to reduce to visual magnitude. The spectra in parentheses are from the *Henry Draper Catalogue*, the lettered subclassifications being used as follows: Ma = M3, Mb = M5, Mc = M7.

The proper motions are mainly from determinations by the writer, many of them heretofore unpublished. Seventeen were taken from the *Albany General Catalogue*[6] and a like number from determinations at Lund by Frida Palmer.[7] The Lund values and five from scattered sources were reduced to the system of the *Albany General Catalogue*.

* *Contributions from the Mount Wilson Observatory, Carnegie Institution of Washington*, No. 669.

[1] *Mt. W. Contr.*, No. 668; *Ap. J.*, **96**, 344, 1942.

[2] C. P. and S. Gaposchkin, *Harv. Monograph*, No. 5, 1938.

[3] *Harv. Ann.*, **79**, Part 3, 161, 1928.

[4] *Harv. Ann.*, **91–99**, 1918–24.

[5] *Kleinere Veröff., Sternwarte Berlin-Babelsberg*, No. 20, 1938.

[6] *Carnegie Institution of Washington Pub.*, No. 468, 1938. [7] *Lund Medd.*, Ser. II, No. 66, 1932.

TABLE 1

PROPER MOTIONS OF IRREGULAR VARIABLES

Star	Desig.	l	b	m_v Max.	Sp.	Cl.*	Per.	μ	r	ψ	Auth.†
							days				
T Cet	001620	54°	−80°	5.2	M5	S	159	0".076 ±	5	90°	W
TV Psc	002217	84	−44	5.2	M3	I	.....	.117	2	82	GC
T Psc	002714	85	−48	9.3	M5	R	258	.021	6	295	Lu
RT Psc	010826	98	−35	8.3	M0	S	550	.050	8	175	Lu
AA Cas	011355	95	− 6	9.0	(M5)	I	.....	.009	10	306	Lu
TT Per	014453	100	− 8	8.0	M6	S	92	.009	5	144	W
T Per	021258	102	− 1	8.0	K5	I	.....	.048	14	254	Lu
AD Per‡	021356	103	− 3	7.7	M2	I	.....	.004	7	166	W
SU Per‡	021556	103	− 4	7.4	M4	S	477	.003	6	135	W
RS Per‡	021556	103	− 4	8.0	M4	I	.....	.028	13	41	W
S Per	021558	103	− 2	7.2	M5	I	.....	.004	8	76	W
YZ Per	023156	105	− 2	7.6	M2	I	.....	.009	5	307	Lu
W Tri	023534	116	−22	8.2	M5	S	148	.019	11	58	Lu
T Ari	024217	127	−36	7.4	M6	R	314	.025	5	249	W
Z Eri	024312	157	−57	6.4	M5	S	66	.031	5	173	W
W Per	024356	106	− 2	8.9	M9	R	477	.007	10	135	W
RR Eri	024708	154	−54	7.2	(M5)	I	.....	.042	6	149	W
ρ Per	025838	117	−16	3.2	M4	I	.....	.171	1	129	GC
V Hor	030159	242	−51	5.6	(M5)	U	.....	.061	9	99	GC
UZ Per	031331	125	−21	7.8	M5	S	90	.001	8	90	W
SS Cep	033380	97	+21	6.7	M6	S	100	.019	8	344	GC
V Eri	035916	176	−42	6.9	(M7)	I	.....	.014	9	330	W
SW Per	040441	126	− 7	8.2	M6	S	84	.037	10	204	W
W Tau	042215	148	−21	9.1	M4	R	266	.016	6	325	Mc
RV Cam	042257	117	+ 7	7.9	M6	S	107	.038	11	220	W
R Dor	043562	239	−39	5.3	M7	R	335	.098	5	215	W
UZ Aur	050840	135	+ 2	7.7	M4	S	66	.058	5	13	W
UX Aur	050849	128	+ 7	8.0	M5	S	90	.011	1	153	W
CI Ori	052401	172	−17	4.7	M0	I	.....	.023	2	159	GC
TW Aur	054945	134	+12	8.0	(M7)	I	.....	.032	7	187	W
α Ori‡	054907	167	− 7	0.1	M2	S	2070	.031	1	73	GC
BQ Ori	055122	155	0	7.4	M6	S	130	.016	5	248	W
S Lep	060124	198	−19	6.0	M5	S	96	.003	5	288	W
TV Gem‡	060521	157	+ 3	7.0	M2	S	425	.008	5	14	W
η Gem	060822	157	+ 4	3.3	M3	R	236	.063	1	258	GC
VW Aur	061033	146	+10	8.1	M6	S	219	.045	9	57	W
TU Aur	062845	138	+18	7.7	M5	S	75	.021	6	152	W
SX Mon	064604	176	+ 4	8.7	(M5)	I	.....	.036	9	256	W
TW Gem	070122	162	+15	7.7	K5	U	.....	.025	5	217	W
Y Lyn	072046	140	+26	6.9	M6	I	.....	.014	7	168	W
Y Gem	073520	168	+21	8.5	M6	I	.....	.023	6	223	W
SU Mon	073710	197	+ 8	8.0	S	I	.....	.014	5	4	W
RX Cnc	080825	166	+30	8.4	M8	I	.....	.017	4	213	W
Z Cnc	081615	177	+28	8.5	M6	S	80	.032	1	196	W
RV Hya	083409	203	+20	7.6	(M5)	I	.....	0.019	9	168	W

* Symbols in column headed "Cl.": R, fairly regular; S, semiregular; I, irregular; U, unknown.

† Authorities: C, Cape; GC, *Albany General Catalogue;* Lu, Lund; Mc, McCormick; W, Wilson; and Y, Mount Holyoke.

‡ Supergiants.

TABLE 1—*Continued*

Star	Desig.	l	b	m_v Max.	Sp.	Cl.*	Per.	μ	r	ψ	Auth.†
							days				
RS Cam	083679	101°	+33°	8.1	M6	S	166	0".025±	6	95°	W
RT Cnc	085211	186	+34	7.3	M5	S	94	.051	5	239	W
TT UMa	085760	122	+41	8.9	(M5)	I	.....	.011	7	128	Lu
RS Cnc	090431	163	+43	5.3	M6	S	239	.031	3	191	W
SY Vel	090*843*	234	+ 4	6.8	M5	I	.....	.028	6	315	C
N Vel	092*856*	246	− 4	3.4	K5	U	.....	.034	3	277	GC
U Vel	092*945*	238	+ 5	8.1	(M5)	I	.....	.001	6	225	W
R Sex	093*707*	212	+33	9.5	M5	I	.....	.030	14	40	W
Z Leo	094627	174	+52	8.6	M3	S	57	.009	9	96	W
RR Car	095*458*	250	− 3	7.8	M6	I	.....	.021	9	313	GC
U UMa	100860	117	+49	6.1	(M3)	I	.....	.018	3	56	W
BZ Car	105*261*	257	− 2	9.0	K5	I	.....	.023	9	200	GC
R Crt	105*517*	238	+37	9.0	(M7)	I	.....	.016	5	300	W
ST UMa	112245	127	+67	6.5	M5	S	81	.039	5	211	W
S Crt	114*707*	248	+53	8.4	M6	R	152	.009	9	12	W
TZ Vir	115903	247	+63	8.6	(M3)	I	.....	.022	13	98	Lu
RW Vir	120*206*	253	+55	7.0	(M5)	I	.....	.022	4	326	W
TZ UMa	120458	99	+58	9.1	(M3)	S	179	.022	10	114	Lu
V368 Cen	120*749*	265	+12	8.5	M5	R	175	.026	6	241	C
RY UMa	121561	96	+57	7.2	M3	R	311	.034	4	244	W
Y UMa	123556	91	+62	7.7	(M7)	I	.....	.013	7	18	W
RT Vir	125705	281	+67	8.0	M8	I	.....	.038	5	119	W
SW Vir	130*802*	284	+59	6.8	M7	I	.....	.047	6	251	W
UY Cen	131*044*	276	+17	7.1	K5	R	186	.019	5	82	W
RV Vir	133*618*	288	+42	8.0	(M5)	I	.....	.043	7	243	W
V UMi	133674	85	+43	7.5	M4	S	70	.043	5	97	W
θ Aps	135*576*	275	−15	5.5	(M5)	I	.....	.097	2	246	GC
RX Boo	141926	1	+68	7.0	M8	S	78	.046	3	158	W
Y Cen	142*529*	296	+27	6.0	(M7)	I	.....	.040	12	212	W
RV Boo	143532	18	+65	7.6	M6	I	.....	.021	5	119	W
RW Boo	143632	16	+65	7.3	M5	I	.....	.047	5	247	W
UV Dra	144156	61	+55	8.8	M5	S	77	.025	1	302	W
Y Ser	150*801*	327	+44	8.0	M5	I	.....	.050	6	253	W
RU CrB	153126	7	+52	8.8	M5	I	.....	.053	10	267	Lu
RR CrB	153738	27	+52	7.2	M5	S	57	.049	4	151	W
ST Her	154748	42	+49	6.8	M7	I	.....	.013	6	122	W
RS CrB	155436	24	+48	7.6	M5	R	333	.042	8	262	W
X Her	155947	40	+47	5.8	M6	I	.....	.080	6	309	W
V Nor	160*248*	300	+ 1	7.2	M5	I	.....	.006	6	141	C
BE Her	162129	16	+42	8.2	M3	I	.....	.073	8	256	Lu
α Sco‡	162*326*	320	+14	0.9	M1	I	.....	.029	1	196	GC
g Her	162542	33	+43	4.4	M6	S	40	.031	2	105	GC
TX Dra	163360	56	+40	6.8	M5	S	77	.052	4	287	W
TV Dra	170764	61	+35	7.4	(M7)	U	.....	.007	9	30	W
α Her‡	171014	3	+26	3.1	M5	S	120	.029	1	350	GC
UW Her	171036	27	+34	7.5	M5	I	.....	.016	7	162	W
TT Dra	171157	52	+35	8.5	M6	R	107	.004	10	236	W
UW Dra	175554	50	+29	7.0	K5	I	.....	.038	5	153	W
XY Lyr‡	183439	35	+18	5.8	M4	I	.....	.011	3	112	W
T Aql	184008	8	+ 4	8.8	(M5)	I	.....	0.032	15	118	Lu

TABLE 1—*Continued*

Star	Desig.	l	b	m_v Max.	Sp.	Cl.*	Per.	μ	r	ψ	Auth.†
							days				
UX Sgr	1849*16*	346°	−10°	7.6	(M5)	I	.....	0".006 ±	7	211°	W
RW Sct	1851*10*	352	− 7	8.5	(M7)	U	.....	.008	9	310	W
R Lyr	185243	41	+17	4.0	M5	S	50	.078	1	19	GC
UW Aql	185200	2	− 2	8.7	M0	I	.....	.013	8	222	W
CH Cyg	192150	49	+15	6.4	M6	R	101	.020	3	183	W
AF Cyg	192745	45	+12	6.4	M6	S	182	.037	4	101	W
QZ Cyg	195537	42	+ 4	9.5	M3	I	.....	.060	10	249	Lu
AA Cyg	200036	46	+ 2	8.4	S	R	202	.037	9	216	W
W Vul	200525	32	− 5	8.8	M6	R	239	.029	11	178	W
AC Cyg	200949	52	+ 8	7.5	(M7)	S	118	.023	7	73	W
RS Del	202415	27	−14	7.5	(M7)	I	.....	.033	6	83	W
TZ Aql	202*505*	8	−25	8.5	M6	I	.....	.039	10	207	W
RW Cyg	202539	46	0	7.6	M1	R	631	.034	6	230	W
AD Cyg	202732	41	− 5	8.5	S	S	73	.025	6	225	W
AI Cyg	202732	41	− 5	8.4	M6	R	140	.020	6	160	W
Y Aqr	203*905*	10	−28	9.4	M7	R	381	.020	12	70	W
U Del‡	204017	30	−17	5.6	M5	I	.....	.003	6	90	W
RZ Cyg	204846	54	+ 1	9.6	M7	R	546	.032	12	344	Y
AZ Cyg	205446	55	0	8.1	M3	I	.....	.009	5	162	W
RS Cap	2101*16*	0	−39	6.9	(M7)	I	.....	.029	6	188	W
RX Aqr	2107*14*	3	−39	8.0	(M7)	U	.....	.041	6	142	W
SX Pav	2119*69*	290	−39	5.3	M6	I	.....	.096	5	125	GC
SW Cep	212362	69	+ 8	8.0	(M7)	I	.....	.012	11	99	W
AB Cyg	213231	49	−16	7.7	M4	S	482	.034	5	73	W
μ Cep‡	214058	68	+ 4	4.0	M2	S	750	.011	3	158	W
TW Peg	215927	51	−23	6.5	M6	S	90	.021	2	90	W
SV Peg	220134	57	−17	8.4	(M7)	I	.....	.003	6	18	W
UW Peg	221302	34	−44	8.7	M5	S	106	.011	9	319	Lu
TX Peg	221313	44	−36	8.5	M6	R	132	.052	7	174	W
π_1 Gru	221*646*	317	−56	5.8	S	U	.....	.015	6	157	W
RW Cep	221955	71	− 1	6.8	(M3)	I	.....	.004	3	34	W
ST Cep	222656	72	− 1	7.7	M0	U	.....	.013	9	261	Lu
BD Peg	223827	59	−28	6.8	M6	I	.....	.013	6	145	Lu
UY Peg	224029	61	−25	9.0	M1	I	.....	.021	9	121	W
U Lac	224354	74	− 4	8.5	M4	S	659	.062	12	214	Lu
ST Peg	224426	60	−29	8.3	M6	R	136	.007	7	188	W
RX Lac	224540	68	−17	8.5	M5	R	321	.016	9	104	W
AR Cep	225384	87	+23	7.1	(M5)	S	.....	.033	5	67	GC
TV And	225342	70	−16	8.8	M5	S	115	.011	1	124	W
RZ And	230552	76	− 7	8.7	M0	S	336	.065	13	276	Lu
TY And	231040	72	−19	8.2	M6	I	.....	.014	6	120	W
RU Aqr	2319*17*	24	−69	9.0	M6	S	170	.011	6	63	W
SV Cas	233451	80	− 9	7.8	M5	R	295	.018	6	164	W
TZ And	234546	81	−14	8.5	M6	I	.....	.007	11	352	W
TZ Cas	234860	84	− 1	9.0	M2	I	.....	.021	7	208	W
RS And	235048	81	−13	7.0	(M7)	I	.....	0.005	9	68	W

The corrections to the system determined by Wilson and Raymond[8] were applied to give the total proper motions and position angles in the ninth and eleventh columns in Table 1. The proper motions are in general well determined, the few found with probable errors greater than 0".015 per annum having been omitted. The dispersion in proper motion, from 0".171 for ρ Persei (3^m2) to 0".001, is small in comparison with that among the Me stars,[9] as was found by Joy for the dispersion in radial velocity.

In all, we have to deal with 189 stars—119 with radial velocities and 141 with proper motions. The distribution of these stars in type, together with the average galactic latitudes, is shown in Table 2. Over half are of types M5 and M6, the mean being

TABLE 2

TYPE AND AVERAGE GALACTIC LATITUDE OF IRREGULAR VARIABLES

Type	No.	$\lvert\bar{b}\rvert$	Type	No.	$\lvert\bar{b}\rvert$
K5	6	11.3°	M5	54	29.5°
M0	5	12.4	M6	51	24.7
M1	3	13.0	M7	24	29.0
M2	6	3.3	M8	6	39.7
M3	15	30.9	S	4	17.8
M4	15	11.6			
K5–M4	50	16.5	M5–M8	135	28.0
Super giant (K5–M5)	13	11.1	Giant (K5–S)	176	25.4

M4.7, whereas that of the long-period variables is M4.9e. While the concentration of the irregular variables toward the galactic plane is not marked, it is somewhat stronger than that of the long-period variables, the respective average latitudes being 24.4° and 29.1°.[10] Moreover, the irregular variables with early types and those to which Joy assigns absolute magnitudes equal to or brighter than −2.0 lie considerably closer to the galaxy than do those with later types and fainter luminosities.

GENERAL MOTIONS

Radial velocities.—Although the concentration of the irregular variables toward the galactic plane is not sufficient to lead one to expect a priori an appreciable effect of galactic rotation on the radial velocities, the rotation terms were included in a preliminary analysis of the 116 radial velocities available in 1941. Equations of the form

$$V = K + x \cos b \cos l + Y \cos b \sin l + z \sin b + du + ev , \qquad (1)$$

where

$$u = \bar{r}A \cos 2l_0 , \qquad d = \sin 2l \cos^2 b ,$$
$$v = \bar{r}A \sin 2l_0 , \qquad e = -\cos 2l \cos^2 b ,$$

were used. The results are in Table 3. The apex of the motion is somewhat nearer the standard apex ($A_0 = 270°$; $D_0 = +30°$) than that usually shown by stars of late type and certainly close enough to justify the use of the standard apex in the computation of group and peculiar motions. The average value of the peculiar motion resulting from this solution is 23.2 km/sec. The values of both the group and the peculiar motions are about two-thirds of the corresponding values for the long-period variables. The rotation effect, $\bar{r}A$, is large; and the center of rotation, l_0, is fortuitously close to the galactic cen-

[8] *A.J.*, **47**, 57, 1938. [9] Wilson and Merrill, *Mt. W. Contr.*, No. 658; *Ap. J.*, **95**, 253, 1942.

[10] *Mt. W. Contr.*, No. 649; *Ap. J.*, **94**, 208, 1941.

ter of 325°. If the writer's value of the rotational constant, $A = 17.7$ km/sec/kpc,[11] is employed with the value of $\bar{r}A$ found above, the mean distance of the 116 stars is 536 parsecs. Since their mean apparent magnitude at maximum is 7.7, the mean absolute magnitude at maximum, derived from the rotation, is -1.0.

Proper motions.—An analysis of the proper motions reduced to visual magnitude 7.5 gave the results in the second column of Table 4. The large difference between the apex

TABLE 3

LINEAR GROUP MOTION AND GALACTIC ROTATION OF IRREGULAR VARIABLES

	km/sec		
K	-1.1 ± 3.3	L_a	29.8°
X	$-26.6 \quad 4.3$	B_a	$+28.1$
Y	$-15.2 \quad 6.1$	A_0	265.
Z	$-16.4 \quad 4.4$	D_0	$+37.$
u	$+3.5 \quad 4.7$	l_0	325.7
v	-8.8 ± 4.7		
V_0	34.7		
$\bar{r}A$	9.48		

TABLE 4

ANGULAR GROUP MOTION

Quantity	Reduced P.M.	Unreduced P.M.
A_0	303°	294°
D_0	$+74$	$+51$
L_a	74	51
B_a	$+21$	$+13$
$100q$	1".13	1".21

given by this solution and that given by the radial velocities is disturbing. Although reduced to about half by using the unreduced proper motions (third column), it is still large. The difference is probably due mainly to the poor distribution of the stars; the fact that it exists warns us not to expect good agreement between results based upon the comparisons of linear and angular motions in the direction of and at right angles to the standard apex. Comparison of the group motions in Tables 3 and 4 gives a mean parallax, $\bar{\pi}_q = 0''.0016$. The average peculiar motion at right angles to the standard apex, $100\,\bar{\tau}$, is 1".06. Comparing this with the peculiar radial motion above, we find $\bar{\pi}_\tau = 0''.0022$. The mean, $\frac{1}{2}(\bar{\pi}_q + \bar{\pi}_\tau)$, is 0".0019 for a variable of apparent magnitude 7.5, whence we derive a mean absolute magnitude at maximum, $\bar{M}_\tau = -1.1$, in substantial agreement with that derived from the rotation effect. The mean absolute magnitude at maximum of the irregular variables of class M is, therefore, essentially the same as that of the long-period variables of class Me.

MEAN ABSOLUTE MAGNITUDES BY CLASSES

Among the long-period Me variables there exist correlations between luminosity, type, and period, such that the mean luminosities of the stars with earlier types and shorter periods are about 2 mag. brighter than those of the later types and longer periods. It is well, therefore, to inquire whether or not similar correlations occur among the non-emission variables. It has long been known that α Orionis, α Scorpii, and μ Cephei are

[11] *Mt. W. Contr.*, No. 631; *Ap. J.*, 92, 170, 1940.

much brighter than $M = -1.0$. Joy lists 13 stars equal to or brighter than -2.0. For 11 of these we have proper motions, all considerably smaller than the average for stars of corresponding apparent magnitudes. The linear group motion of these stars is but 22.5 km/sec, and their linear peculiar motions are appreciably smaller than average. They are too few to affect materially the general solutions, but they should be segregated in the determinations of mean absolute magnitudes. Joy shows that these stars fall largely in types K5–M3, none having spectra later than M5. We have, therefore, divided the data according to type, K5–M3 and M4–S (II–III), and, according to Joy's values of absolute magnitude, classing as supergiants all stars for which $M \gtrsim -2.0$ (IV) and as giants all stars fainter than -2.0 (V). In their discussions the Gaposchkins recognize three types of variation among these stars: R, in which the light-curves are more or less regular; SR, the semiregular, in which two or more oscillations may appear; and I, the totally irregular. For most of the R and SR stars estimates of periods have been made. Five divisions of the data (VI–X) have been made to indicate possible variations in $\bar{M}$ with the character of light-variation and with period, the division point in period being at 125 days.

The angular and linear parallatic and peculiar motions referred to the standard apex were determined for each group of stars and for all. True values of the mean angular peculiar motion, $\bar{\tau}$, were determined by the methods used for the long-period variables.[9] The linear group and peculiar motions and the rotation factors, $\bar{r}A$, were determined from the relations

$$V = K + V_0 \cos \lambda + \bar{r}A \sin 2(l - 326°) \cos^2 b \ ,$$
$$\theta = | V - V_c | \ .$$

The mean values of these components of the stellar motions for each of the subdivisions of the data are given in the first two sections of Table 5. The third section gives the computed parallaxes for a star of apparent magnitude 7.5. The weakness of the data is here very apparent; in nearly every group the value $\bar{\pi}_r$ is much greater than $\bar{\pi}_q$. A corresponding but much smaller difference was found for the Me stars. Here again the difficulty may be due partly to poor distribution of the stars, although a difference between the actual and the adopted apices may be a contributory factor. Since no reason for assigning unequal weights to the two determinations of parallax was apparent, the straight means were used. The values of $\bar{M}_\pi$, derived from the mean parallaxes, and of $\bar{M}_r$, derived from the rotation factors, $\bar{r}A$, are in the fourth section of Table 5. The values of $\bar{r}A$,

TABLE 5

MEAN ABSOLUTE MAGNITUDES OF IRREGULAR VARIABLES

Quantity	I All	II K5–M3	III M4–S	IV Super-giant	V Giant	VI R	VII SR	VIII I	IX $P<125^d$	X $P>125^d$
No. P.M.	141	31	110	11	130	23	45	65	29	38
$\bar{\tau}$	0".0139	0".0156	0".0113	0".0032	0".0149	0".0124	0".0167	0".0126	0".0134	0".0191
q	0.0090	−0.0014	0.0118	0.0031	0.0095	0.0028	0.0049	0.0120	0.0072	0.0021
No. R.V.	119	15	104	13	106	29	61	29	52	37
θ (km/sec)	23.5	12.0	24.3	19.2	23.9	23.2	25.3	19.8	26.8	21.5
V_0 (km/sec)	29.3	4.4	33.1	18.0	31.5	36.4	29.8	22.	33.8	27.3
$\bar{r}A$	11.9	17.2	12.2	14.8	10.3	6.6	14.0	12.0	10.5	15.2
r (kpc)	0.67	0.97	0.69	0.84	0.58	0.37	0.79	0.68	0.59	0.86
m_s	7.67	5.89	7.92	5.86	7.91	8.40	7.60	7.06	8.01	7.67
$\bar{\pi}_r$	0".0028	0".0067:	0".0022	0".0008:	0".0030	0".0025	0".0031	0".0030	0".0024	0".0042
$\bar{\pi}_q$	.0015	−.0015:	.0017	.0008:	.0014	.0004	.0008	.0025	.0010	.0004
$\bar{\pi}$	0.0021	0.0026:	0.0020	0.0008:	0.0022	0.0014	0.0020	0.0028	0.0017	0.0023
$\bar{M}_\pi$	−0.85	−0.4:	−1.1	−3.0:	−0.8	−1.7	−1.0	−0.2	−1.4	−0.7
$\bar{M}_r$	−1.46	−4.0:	−1.5	−3.8:	−0.9	+0.6:	−1.9:	−2.1:	−0.8:	−2.0:
M (Wilson)	−1.16	−2.2	−1.3	−3.4:	−0.85	−0.9	−1.3	−0.8	−1.2	−1.1
M (Joy)	−1.13	−2.1	−1.0	−3.0	−0.89	−0.9	−1.1	−1.3	−1.0	−1.2

$\bar{r}$, and $\bar{M}_r$ are significant; but only those values of $\bar{M}_r$ based upon at least 100 stars are deemed of equal weight with values of parallax derived from the group and peculiar motions, in spite of the uncertainties in these motions. In Table 5 a colon indicates that half-weight was assigned in taking a mean. In the next to the last line are the mean absolute magnitudes determined in this investigation. All weights were assigned and final means obtained before comparison with the means of Joy's spectroscopic absolute magnitudes in the last line of the table. Not only are the mean values based upon a fairly representative number of stars (I, III, V) essentially the same, but there is excellent agreement between the results from groups containing only a few stars, much better agreement, in fact, that one would expect in view of the uncertainties involved. This investigation confirms Joy's conclusions that the great majority of the irregular variables of class M are ordinary giants with $\bar{M} = -0.9$ (V), with a few supergiants for which $\bar{M} = -3.0$ (IV) approximately. The values of M in the other subdivisions are roughly correlated with the proportion of supergiants (II, 5; III, 6; VI, 0; VII, 6; VIII, 5; IX, 2; X, 4). There seems to be no dependence in M upon type, character of light-variation, or period.

TABLE 6

TRIGONOMETRIC PARALLAXES OF IRREGULAR VARIABLES

Star	m_v	μ	π_t
	Supergiants		
α Ori	0.1	0".031	0".012
α Sco	1.2	.029	.028
α Her	3.1	.029	− .001
μ Cep	4.0	.011	.016
XY Lyr	5.8	0.011	0.003
	Giants		
ρ Per	3.2	0".171	0".032
η Gem	3.3	.063	.011
N Vel	3.4	.034	.020
CI Ori	3.7	.023	.005
R Lyr	4.0	.078	− .010
g Her	4.4	.031	.019
TV Psc	5.2	.117	.014
SX Pav	5.3	.096	.022
UV Dra	8.1	.025	− .011
RT Psc	8.3	.050	.014
RU CrB	8.8	0.053	0.004

TRIGONOMETRIC PARALLAXES

The available trigonometric parallaxes of type-M variables, compiled by A. van Maanen, are given in Table 6. Values of $\bar{M}$ derived from these by means of G. Strömberg's formula,[12]

$$\bar{M} = 5 + 5\,(\log \Sigma\pi - \log \Sigma\, 10^{-0.2m}) ,$$

[12] *Mt. W. Contr.*, No. 267; *Ap. J.*, 59, 98, 1924.

are -0.3 for the giants and -2.7 for the supergiants. For the same 5 supergiants, $\bar{M}_{sp} = -3.4$. Eight of the giants are in Joy's list; for these $\bar{M}_{tr} = -0.8$, $\bar{M}_{sp} = -0.9$.

The values of $\bar{M}$ for supergiants and giants derived from the motions, the rotation factors, and the trigonometric parallaxes agree well with the $\bar{M}$ derived from the relative intensities of the spectral lines. The conclusion is that the spectroscopic absolute magnitudes are essentially correct and that the critical lines in the spectra of the irregular variables of class M behave as they do among the nonvariable stars of the same spectral class.

SPACE MOTIONS

The spectroscopic values of M were used to derive parallaxes by means of the relation

$$\log \pi = -0.2\,(m - M) - 1\ .$$

With these parallaxes the directions and amounts of the space motions were computed for all the stars whose radial velocities and proper motions are known. Values of the average residual radial velocity and total speeds are given in Table 7. The over-all

TABLE 7

AVERAGE RADIAL AND SPACE VELOCITIES OF IRREGULAR VARIABLES

Group	No.	$\bar{V}'$	No.	$\bar{S}$
		km/sec		km/sec
I All	119	23.5	74	54
II Supergiant	13	19.2	11	36
III Giant	106	23.8	63	57
IV K5–M3	15	12.0	11	36
V M4–M8	104	24.3	63	58
VI Periodic	90	24.6	50	59
VII Irregular	26	19.8	23	54
VIII $P<125$ d	47	26.8	28	57
IX $P>125$ d	30	21.5	22	53

average speed, 54 km/sec, is about midway between that of the nonvariable class-M giant, 36 km/sec,[13] and that of the faster-moving Me stars, 74 km/sec, as would be expected from the velocity dispersions of the three classes of stars. The supergiants are evidently moving more slowly than the giants, but there is no progression in speed that can be correlated with type, character of light-variation, or period.

The distribution of the apices (Fig. 1) is quite similar to that exhibited by the long-period variables. With a single exception, UZ Aurigae, the stars with the greater speeds are moving toward the hemisphere opposite to the direction of the solar motion and the direction in which the stars in the vicinity of the sun are being carried by the rotation of the galaxy. The irregular variables, therefore, share in the asymmetry of motion usually associated with high velocities. The abnormal motion of UZ Aurigae is almost wholly tangential, but the proper motion is well determined.

The group motion derived from the space motions is 28.1 km/sec in the direction $A_0 = 266°$, $D_0 = +47°$ ($L_a = 40°$, $B_a = +29°$). The maximum concentrations of apices are approximately at right angles to this direction and sensibly radial with respect to the galactic center.

Determinations of preferential motion from the space motions are seriously affected by the distribution of the stars; objects for which radial velocities have been measured lie almost wholly in the northern half of the sky; the distribution of the stars with

[13] R. E. Wilson and H. Raymond, *A.J.*, **40**, 125, 1930.

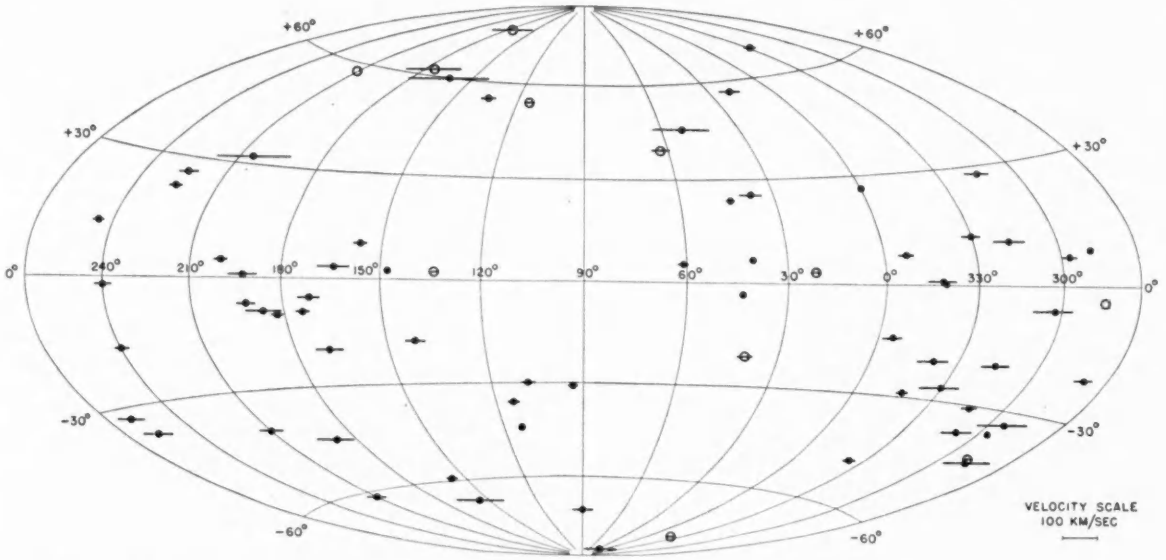

FIG. 1.—Distribution in galactic co-ordinates of the apices of motion of irregular variables. Apices marked by circles are of supergiants; all others are of giants. The lengths of the lines indicate speed.

known proper motions is somewhat more even and should give a better picture of the velocity distribution. Separate analyses of the proper motions and the space motions give the co-ordinates of the velocity ellipsoids in Table 8. These indicate that the preferential motion of the irregular variables, although not marked, is in the direction of the vertex indicated by the stars in general. As was found for the long-period variables, the shortest axis of the velocity ellipsoid lies in or near the galactic plane, and the intermediate axis lies in the general direction of the galactic poles. Thus the irregular variables share in the stream motion of the stars in general; but among them, as among the long-period variables, the motion away from the galactic plane is more pronounced than that in the plane at right angles to the stream motion.

TABLE 8

PREFERENTIAL MOTIONS OF IRREGULAR VARIABLES

Quantity	Preferential		Quantity	Intermediate		Quantity	Avoidance	
	P.M.	S.M.		P.M.	S.M.		P.M.	S.M.
A_1	98°	101°	A_2	190°	221°	A_3	357°	355°
D_1	+ 4	+ 25	D_2	+ 20	+ 48	D_3	+ 69	+ 32
L_1	176	158	L_2	270	48	L_3	85	+ 75
B_1	0	+ 12	B_2	+ 82	+ 58	B_3	+ 7	− 28
a	2".74	45 km/sec	b	1".84	39 km/sec	c	1".17	27 km/sec

In kinematic properties, such as relatively high speed with its concomitant properties —asymmetric motion and motion away from the galactic plane—the irregular variables resemble the long-period variables. In physical properties, evidenced by the spectra, the variation in the intensities of certain lines with absolute magnitude, and the absence of correlations between luminosity, type, character of light-variation, and period, they appear to be more closely associated with the nonvariable giants of the same spectral types. These facts indicate that the irregular variables as a class are intermediate between the nonvariable stars and the regular variables with long periods. This conclusion is corroborated by the small amplitudes of their light-variation and the occasional appearance of emission lines in their spectra.

CARNEGIE INSTITUTION OF WASHINGTON
MOUNT WILSON OBSERVATORY
July 1942

INVESTIGATIONS ON PROPER MOTION. XXII. THE PROPER MOTION OF THE OPEN CLUSTER MESSIER 67*

ADRIAAN VAN MAANEN

ABSTRACT

On two pairs of plates of Messier 67 taken at the Cassegrain focus of the 60-inch reflector with an interval of 21 years, 343 stars were measured for proper motion. The probable error of a final motion in each co-ordinate is, in the mean, 0".0008. The 284 stars probably belonging to the cluster give, as a final relative motion with respect to the stars of mean magnitude 14.5: $\mu_\alpha = -0".0046$; $\mu_\delta = +0".0003$.

In 1930 I measured two pairs of plates of the open cluster NGC 2264,[1] taken at the 80-foot focus of the 60-inch reflector with an interval of about 11 years. The probable error, while small, was still not quite good enough to enable us to separate the cluster stars from the noncluster stars. Recently it seemed worth while to make a trial on another cluster with an increased time interval. The object chosen was NGC 2682, or Messier 67, for which two pairs of plates were available with intervals of 21.10 and 21.04 years, respectively. The cluster offers the advantage of being so rich in stars that by far the majority of those measured must be members of the group; accordingly, we can derive the motions of all the stars by computing the plate constants from a large number of the cluster stars. We are also able to find a magnitude correction, as the motions of the cluster stars are naturally independent of their magnitudes.

Another advantage of measuring this particular cluster is that Shapley has published in *Mount Wilson Contributions*, No. 117, photographic magnitudes to about 15.0. On my plates, however, several fainter stars were measured; in fact, all the stars visible on the Wolf-Palisa Chart No. 40 could be measured. Shapley states that the limit of the Wolf-Palisa chart is approximately 1 mag. fainter than that of the plates used in his paper. From my measures of parallax plates, which in general have an exposure of 15 minutes, both Willis and I came to the conclusion that the limiting magnitude of measurable stars is about 15.0; for exposures of 30 minutes this would give a limiting measurable magnitude of about 15.6; from my earlier measures on plates in the Pleiades region I derived 15.7; from a few Selected Areas, taken under normal conditions, 15.6 or 15.7. It is therefore pretty safe to conclude that our limiting magnitude for astrometric measures is 15.6 or 15.7 on half-hour exposures.

In Table 1 Shapley's magnitudes have been used when available, his catalogue numbers being given for convenience in the second column; for stars not in Shapley's list but within his limits of magnitude the magnitude has been interpolated from stars in the neighborhood, and the value then given with one decimal; for fainter stars, the letters "f" and "vf" (faint and very faint) apply to stars of about magnitude 15.0–15.4 and magnitude 15.5–15.6 or 15.7, respectively. In the fourth and fifth columns the co-ordinates of the stars are given in minutes of arc from star 193. In the last two columns, for twenty stars found difficult to measure, the motions have been marked by a colon; in the reductions as well as in the conclusions drawn from the results these stars have been excluded.

Shapley's counts of the Wolf-Palisa chart seem to indicate that the cluster may be a degree in diameter; outside of that region the number of stars per square of 10 minutes of arc is fairly constant, being in the mean 10.7; in the region which I measured we may then expect about 35 stars that are not members of the cluster. As I have measured 343 stars, it is evident that by far the majority must belong to the cluster.

* *Contributions from the Mount Wilson Observatory, Carnegie Institution of Washington*, No. 670; *Mt. W. Contr.* No. 653; *Ap. J.*, **94**, 399, 1941, was numbered XXII by mistake instead of XXI.

[1] *Mt. W. Contr.*, No. 405.

TABLE 1

PROPER MOTIONS OF STARS MEASURED
(Unit = 0".001)

No.	Shapley No.	m_{ph}	x	y	$\bar{\mu}_\alpha$	$\bar{\mu}_\delta$
1		f	−9".6	+2".9	+13	−20
2		vf	−9.5	+3.2	0	0
3		vf	−9.4	+4.7	0	+ 1
4		f	−9.4	+3.8	− 1	+ 2
5	14	14.52	−9.2	−3.8	− 2	+ 1
6	15	14.16	−9.2	−1.2	+ 1	0
7	16	13.38	−9.2	−4.3	0	0
8		f	−9.0	+0.6	− 1	− 2
9	19	14.64	−8.7	+5.4	− 2	0
10	20	13.95	−8.6	+0.1	0	− 1
11	23	13.36	−8.2	−0.9	− 3	+12
12		f	−7.9	−4.1	− 1	0
13		vf	−7.8	+5.1	+12:	+11:
14		vf	−7.7	+0.7	0	− 1
15		f	−7.7	−0.1	− 3	÷ 2
16		f	−7.6	−5.5	0	− 1
17	24	13.97	−7.7	−1.6	0	0
18	27	14.25	−7.6	−4.5	0	− 1
19		vf	−7.6	+6.2	0	− 2
20	28	13.93	−7.6	+7.4	− 2	0
21	29	14.00	−7.5	+2.1	+ 2	+ 1
22		f	−7.4	+2.2	+ 5	+ 2
23	30	12.84	−7.2	+3.2	0	− 3
24		f	−7.2	+3.8	+ 1	− 2
25		f	−7.1	+2.8	+11	− 4
26	31	13.95	−7.2	+4.8	0	− 1
27	33	14.67	−7.1	+2.4	− 1	− 2
28		f	−7.0	+0.8	− 1	− 2
29		vf	−6.9	+7.7	0	− 1
30	36	13.83	−6.8	+6.2	0	− 1
31	39	13.93	−6.5	−6.9	− 2	+12
32	37	13.85	−6.7	+3.3	+ 2	0
33	40	14.46	−6.4	−0.8	+ 1	+ 1
34	41	13.45	−6.4	+7.5	+ 1	0
35	42	14.11	−6.4	−0.1	+ 1	0
36	43	14.09	−6.3	−2.9	0	− 1
37		f	−6.2	−4.9	− 1	+ 1
38		vf	−6.3	+5.8	+11:	− 6:
39		f	−6.2	+2.1	+ 1	0
40		vf	−6.3	+7.5	0:	0:
41	46	13.43	−6.1	+5.5	− 1	− 1
42		f	−5.9	−0.2	+ 2	0
43		f	−5.9	+4.1	− 1	+ 2
44	48	13.55	−5.9	+1.1	+ 2	0
45	50	13.95	−5.7	−7.1	0	0

TABLE 1—*Continued*

No.	Shapley No.	m_{ph}	x	y	$\bar{\mu}_\alpha$	$\bar{\mu}_\delta$
46	51	13.34	−5.″7	+0.″5	− 1	0
47	.....	f	−5.7	+0.3	+ 9	+ 7
48	52	14.15	−5.7	−1.2	0	+ 2
49	.....	f	−5.7	+6.2	− 2	+ 2
50	.....	f	−5.6	−3.8	− 1	0
51	53	13.95	−5.6	−0.1	0	0
52	.....	f	−5.5	−1.2	+ 5	+10
53	.....	f	−5.5	+2.3	+ 5	− 2
54	.....	vf	−5.5	+3.3	+ 4	+ 1
55	54	13.46	−5.3	−3.3	− 1	0
56	55	12.08	−5.2	−4.1	− 1	0
57	56	13.91	−5.1	−8.6	0	0
58	.....	f	−5.1	−6.7	+ 3	+ 1
59	.....	vf	−5.2	+3.3	+ 9:	0:
60	58	14.54	−5.0	+2.6	+ 1	0
61	59	14.33	−4.9	+3.3	+ 2	+ 2
62	61	14.12	−4.9	−3.1	− 1	− 1
63	.....	vf	−4.9	+0.5	+ 8:	+ 2:
64	.....	vf	−4.8	+3.4	+ 2:	− 3:
65	63	13.97	−4.7	+2.1	+10	+ 4
66	62	14.32	−4.8	+0.4	0	0
67	64	14.72	−4.7	−5.3	− 1	− 2
68	.....	vf	−4.7	+4.1	+ 1	+ 4
69	65	13.37	−4.4	+3.9	− 1	− 1
70	66	14.54	−4.3	+3.8	0	0
71	.....	f	−4.3	+2.8	− 1	0
72	.....	vf	−4.3	+7.4	+10	0
73	70	12.40	−4.2	−0.9	+ 5	+ 4
74	.....	vf	−4.2	+0.9	+ 3:	− 4:
75	71	14.20	−4.1	+1.0	0	0
76	72	13.74	−4.1	−1.9	− 2	0
77	.....	vf	−4.1	+0.7	+ 2	− 4
78	73	14.40	−4.0	+1.8	+ 2	+ 1
79	75	14.14	−4.0	−2.9	0	+ 2
80	.....	f	−4.0	+0.4	+ 9	−24
81	76	14.70	−3.9	−0.5	− 1	+ 8
82	77	14.16	−3.8	−0.8	0	0
83	.....	f	−4.0	+8.8	− 1	0
84	.....	f	−3.9	+7.9	− 2	+ 1
85	.....	f	−3.7	−2.8	0	0
86	79	13.44	−3.7	−7.4	0	0
87	.....	f	−3.4	−9.3	− 1	− 2
88	.....	vf	−3.2	−3.2	+ 3	+ 4
89	80	14.38	−3.3	−0.2	+ 2	+ 2
90	81	10.39	−3.2	−3.7	0	0
91	.....	f	−3.2	−0.7	0	+ 1
92	82	14.66	−3.2	−0.5	− 1	0
93	.....	vf	−3.2	+1.0	+ 4	− 4
94	.....	vf	−3.1	−1.9	− 1	0
95	83	14.02	−3.1	−2.7	0	0

TABLE 1—*Continued*

No.	Shapley No.	m_{ph}	x	y	$\bar{\mu}_\alpha$	$\bar{\mu}_\delta$
96		f	−3.″2	+1.″5	+ 1	0
97		vf	−3.2	+5.6	− 4	+ 4
98		f	−3.2	+5.3	− 1	+ 1
99	84	12.14	−3.0	+3.6	+ 1	− 4
100	85	14.32	−3.0	+1.5	+ 1	0
101		f	−3.0	+7.9	− 1	0
102	86	14.64	−2.8	+2.6	+ 1	− 2
103	87	14.19	−2.8	+2.2	+ 2	0
104	88	13.21	−2.8	+1.5	0	0
105		14.7	−2.7	+0.9	+ 6	+ 7
106		vf	−2.8	+8.5	0	+ 3
107	90α	12.04	−2.6	−4.1	− 1	0
108	90β	13.42	−2.6	−4.0	− 1	0
109		f	−2.5	−7.9	− 2	+ 2
110		f	−2.5	−4.5	− 1	− 1
111		vf	−2.5	−4.4	+ 2:	0:
112	91	13.67	−2.5	−1.7	0	0
113	92	14.28	−2.5	+9.6	+10	−13
114	89	14.26	−2.6	+1.5	0	0
115		vf	−2.5	−0.1	0	− 3
116	93	14.68	−2.5	+0.3	− 1	0
117	94	13.62	−2.4	+1.1	0	0
118	95	13.48	−2.3	−1.6	− 1	+ 1
119		f	−2.2	−8.6	+ 1	+ 2
120	96	13.98	−2.4	+1.9	+ 2	0
121	97	14.76	−2.3	−0.8	+19	+ 2
122		f	−2.3	+2.9	− 1	+ 2
123	98	13.49	−2.3	+3.9	+ 1	0
124	99	14.10	−2.1	+5.2	+ 1	− 1
125	100	14.20	−2.1	−4.5	+ 1	+ 1
126		f	−1.8	−6.5	− 1	− 2
127	101	14.00	−2.0	+1.6	+ 2	0
128	102	13.50	−2.0	−3.6	+ 1	0
129	102a	14.69	−2.0	−3.4	0	0
130	103	14.00	−2.0	+1.1	+ 1	0
131	104	12.70	−2.0	+1.7	0	− 2
132	105	12.13	−1.9	−0.8	− 1	− 2
133	106	13.95	−1.9	−2.1	− 2	0
134	107	14.58	−1.8	−3.0	+ 1	+ 1
135	108	11.68	−1.8	−3.7	0	0
136	109	14.28	−1.8	+1.0	0	0
137	110	14.20	−1.7	−9.4	+ 1	0
138	111	13.58	−1.7	−3.1	+ 1	+ 2
139	112	14.03	−1.6	−6.1	0	0
140	113	14.70	−1.6	+6.8	0	− 2
141	114	14.13	−1.5	−5.6	− 2	0
142	115	13.34	−1.6	+0.3	+ 1	+ 1
143		14.8	−1.6	+1.3	− 1	+ 2
144	92a	13.38	−1.6	+9.1	− 1	− 1
145	137b	15.06	−1.5	+2.2	− 1	+ 2

TABLE 1—*Continued*

No.	Shapley No.	m_{ph}	x	y	$\bar{\mu}_\alpha$	$\bar{\mu}_\delta$
146	117	13.77	−1′.5	− 2′.0	− 2	+ 2
147	118	14.52	−1.5	− 8.5	+ 5	− 2
148	119	13.47	−1.5	− 1.0	− 1	0
149	120	14.48	−1.4	− 1.2	− 1	− 2
150	121	14.48	−1.4	+ 0.3	− 1	+ 1
151	122	14.22	−1.4	− 8.8	0	− 2
152	123	14.64	−1.4	+ 3.1	+ 1	0
153	124	13.00	−1.3	− 2.1	−1	0
154	125	14.40	−1.3	− 3.7	+ 1	0
155	126	14.71	−1.2	+ 1.3	0	− 2
156	127	13.61	−1.2	− 2.4	− 2	0
157	128	13.91	−1.1	− 3.2	− 1	0
158	129	13.94	−1.1	− 3.0	− 1	0
159	130	13.55	−1.1	− 2.8	− 1	+ 1
160	131	12.05	−1.1	+ 2.4	+ 1	0
161	132	13.98	−1.0	− 4.0	− 1	− 1
162	.....	14.7	−1.2	+ 2.0	0	+ 2
163	134	13.35	−0.9	− 3.2	0	0
164	133	14.28	−1.0	− 9.4	0	+ 2
165	135	13.15	−0.8	− 2.9	− 1	+ 1
166	.....	14.8	−0.7	− 5.0	− 1	+ 1
167	136	12.30	−0.8	+ 3.6	− 1	− 4
168	.....	vf	−0.8	+ 4.1	− 1	+ 2
169	.....	f	−0.7	− 5.8	0	− 1
170	137	14.71	−0.8	+ 2.6	− 1	+ 1
171	138	14.16	−0.7	−10.0	+ 4	+ 5
172	137a	14.04	−0.7	+ 2.5	0	0
173	139a	14.58	−0.9	+10.0	− 3	0
174	139	14.41	−0.8	+10.1	− 7	+21
175	.....	vf	−0.8	0.0	− 4	− 1
176	143a	13.98	−0.5	+ 0.2	+ 2	0
177	143b	13.48	−0.5	− 0.2	0	0
178	.....	vf	−0.7	− 0.6	− 2:	− 6:
179	.....	14.8	−0.4	− 0.6	+ 1	− 1
180	145	13.74	−0.2	− 0.7	− 1	0
181	140	14.00	−0.7	− 2.4	− 1	0
182	141	12.13	−0.5	− 1.0	0	0
183	142	14.68	−0.5	+ 5.1	− 1	0
184	143	12.86	−0.3	+ 0.8	0	0
185	.....	f	−0.2	+ 0.8	+ 3	− 2
186	.....	f	+0.3	+ 0.9	− 1	+ 2
187	144	13.91	−0.3	− 1.8	0	0
188	146α	14.43	−0.3	− 1.9	+10	− 4
189	146β	14.46	−0.2	− 1.9	− 1	+ 1
190	.....	f	−0.1	− 1.6	− 4	0
191	.....	f	0.0	− 5.9	+ 1	− 2
192	.....	14.7	0.0	− 3.3	0	0
193	147	14.08	0.0	0.0	0	0
194	.....	14.8	0.0	− 1.0	− 3	+ 2
195	.....	14.6	+0.1	− 0.8	− 1	− 1

TABLE 1—*Continued*

No.	Shapley No.	m_{ph}	x	y	$\bar{\mu}_\alpha$	$\bar{\mu}_\delta$
196	148	13.93	+0.″1	+ 3.″6	− 2	+ 2
197	149	13.45	+0.1	− 1.5	− 1	0
198	150	14.08	+0.3	+ 0.1	+ 1	0
199	.....	vf	+0.2	+ 4.3	+ 2:	− 6:
200	151	12.08	+0.3	+ 4.8	+ 1	− 1
201	152	14.16	+0.3	+ 0.3	0	+ 2
202	153	11.80	+0.4	− 5.2	− 2	− 1
203	.....	14.7	+0.4	− 8.9	−24	+ 6
204	.....	vf	+0.4	− 4.7	+ 8	−10
205	.....	f	+0.3	+ 8.1	+ 9	− 5
206	155	11.42	+0.4	− 0.3	− 2	+ 2
207	156	11.45	+0.4	+ 2.8	0	0
208	.....	14.6	+0.6	− 1.5	+ 7	+ 1
209	157	13.40	+0.6	+ 4.4	0	0
210	157a	14.68	+0.6	+ 4.0	+ 1	+ 2
211	159	13.83	+0.6	+ 6.7	+ 1	− 1
212	.....	14.6	+0.7	+ 1.1	0	+ 2
213	161	13.40	+0.7	+ 0.4	− 1	+ 1
214	.....	vf	+0.8	− 2.2	0	− 4
215	.....	14.4	+0.9	− 1.0	+ 2	− 1
216	.....	vf	+1.0	− 5.9	0:	− 2:
217	.....	vf	+1.0	− 6.8	+12:	0:
218	.....	f	+0.7	+ 2.8	+ 1	+ 2
219	162	13.42	+0.7	+ 3.3	+ 2	0
220	163	13.44	+0.8	+ 2.9	+ 1	0
221	.....	f	+0.9	+ 3.2	− 1	+ 2
222	164	12.06	+0.9	+ 1.5	− 1	− 1
223	.....	14.6	+1.1	+ 1.4	− 1	+ 2
224	165	13.37	+1.0	+ 5.2	0	0
225	166	14.00	+1.1	− 3.6	+ 2	0
226	168	13.93	+1.2	+ 2.5	0	0
227	169	14.68	+1.2	+ 2.1	0	0
228	.....	f	+1.3	+ 2.3	+ 1	0
229	167	14.32	+1.2	+ 9.3	+12	+ 1
230	170	11.76	+1.2	− 1.8	+ 2	0
231	171	13.81	+1.3	− 5.2	0	0
232	173α	13.55	+1.3	0.0	+ 1	− 1
233	173β	13.97	+1.3	− 0.1	+ 1	0
234	174	13.46	+1.3	+ 0.2	+ 1	− 2
235	175	14.20	+1.4	+ 4.2	+ 2	0
236	176	13.42	+1.5	− 3.2	− 1	0
237	.....	vf	+1.6	− 3.9	0:	− 3:
238	177	13.85	+1.6	+ 4.1	− 1	0
239	.....	f	+1.6	+ 2.9	+15	+ 4
240	178	14.76	+1.6	+ 2.2	+ 1	0
241	179	14.05	+1.6	+ 6.1	+ 1	+ 1
242	180	13.38	+1.6	+ 1.0	− 1	+ 1
243	181	13.84	+1.8	− 1.0	0	0
244	182	13.42	+1.8	− 1.2	+ 1	0
245	.....	14.6	+1.8	− 0.6	0	0

TABLE 1—*Continued*

No.	Shapley No.	m_{ph}	x	y	$\bar{\mu}_\alpha$	$\bar{\mu}_\delta$
246	.....	f	+1.8	− 2.3	− 2	0
247	184	13.02	+1.8	+ 1.6	− 1	− 1
248	185	11.84	+1.8	− 0.2	+ 1	0
249	185a	13.60	+2.0	− 0.2	+ 1	0
250	.....	vf	+2.0	− 3.0	0	− 3
251	187	14.06	+2.1	+ 2.7	0	0
252	.....	f	+2.2	− 2.1	+ 1	0
253	188	14.31	+2.2	+ .9	+ 2	0
254	189	13.65	+2.2	+ 0.7	− 1	0
255	.....	f	+2.3	− 5.2	0	0
256	.....	vf	+2.3	− 3.1	0	0
257	.....	f	+1.9	− 7.0	+ 1	− 4
258	.....	f	+2.6	− 9.2	− 1	+ 1
259	190	11.61	+2.2	+ 2.2	+ 2	− 3
260	192	13.40	+2.5	+ 8.9	+ 1	0
261	193	13.52	+2.6	+ 4.6	+ 1	0
262	194	14.39	+2.6	− 0.1	0	0
263	195	13.77	+2.7	− 2.5	− 3	+ 1
264	.....	14.8	+2.7	− 1.2	+ 1	− 2
265	196	14.52	+2.6	+ 7.7	0	0
266	.....	vf	+2.7	+ 5.5	− 1	+ 2
267	.....	vf	+2.8	+ 5.8	+ 2:	0:
268	199	13.50	+2.8	+ 6.0	+ 1	0
269	200	11.96	+2.9	+10.0	−19	+ 2
270	201	14.67	+3.0	− 2.1	− 1	0
271	202	13.42	+3.0	+ 1.1	− 1	0
272	.....	f	+3.0	+ 7.6	− 3	+ 3
273	205	14.13	+3.1	+ 1.9	+ 2	0
274	206	13.57	+3.1	+ 9.8	−25	− 4
275	208	14.40	+3.4	− 6.4	+ 2	0
276	.....	14.6	+3.7	− 6.1	+ 1	−19
277	209	14.44	+3.5	− 1.1	0	− 1
278	210	13.24	+3.5	+ 1.0	− 1	0
279	217a	13.43	+3.5	+ 2.7	− 1	0
280	.....	vf	+3.6	− 4.0	+ 6:	+ 3:
281	211	14.42	+3.6	+ 3.7	− 1	+ 1
282	213	14.40	+3.8	− 2.3	+ 1	− 1
283	214	14.46	+3.8	+ 0.1	− 1	0
284	215	13.40	+3.9	+ 5.5	+ 1	0
285	.....	14.6	+4.0	− 1.4	+ 1	− 1
286	.....	f	+4.0	− 4.1	+ 7	+ 4
287	216	13.37	+4.2	− 5.4	+ 2	0
288	.....	f	+4.1	+ 0.6	− 2	+ 2
289	217	12.67	+4.2	+ 2.4	0	0
290	218	13.24	+4.3	+ 1.1	− 1	− 1
291	219	13.40	+4.3	+ 0.9	+ 1	+ 1
292	.....	vf	+4.4	− 0.1	− 2:	+ 6:
293	221	13.28	+4.3	− 2.3	+ 3	− 7
294	223	11.96	+4.6	+ 7.7	− 1	− 2
295	224	12.57	+4.6	− 4.6	− 2	− 2

TABLE 1—*Continued*

No.	Shapley No.	m_{ph}	x	y	$\bar{\mu}_\alpha$	$\bar{\mu}_\delta$
296	225	13.81	+4′.6	− 3′.7	0	− 2
297	226	13.81	+4.7	− 2.6	− 1	− 2
298	227	14.03	+4.8	− 2.2	+ 1	0
299	228	13.84	+4.8	− 7.1	0	+ 2
300	229	14.01	+4.8	− 4.0	0	− 1
301	230	13.95	+4.9	+ 7.9	0	0
302	231	13.10	+4.9	− 1.2	− 2	0
303	233	14.03	+5.2	− 4.8	− 1	− 2
304	.....	vf	+5.2	− 0.4	+14	− 1
305	235	14.00	+5.2	− 2.5	+ 2	− 2
306	229a	13.42	+5.3	− 4.0	+13	−12
307	.....	f	+5.4	− 4.3	+ 3	+ 4
308	.....	vf	+5.4	− 6.5	− 2:	− 5:
309	.....	f	+5.5	− 1.8	0	− 1
310	236	13.40	+5.7	+ 2.2	− 1	0
311	237	14.05	+5.8	+ 7.8	+ 2	0
312	238	11.54	+5.8	+ 0.3	0	− 2
313	.....	f	+5.8	− 1.4	− 1	+ 2
314	.....	f	+5.9	− 1.0	+ 1	− 1
315	239	14.62	+5.8	− 6.6	− 1	0
316	241	13.44	+5.9	+ 0.7	− 1	0
317	242	9.30	+5.9	+ 4.7	− 7	+ 2
318	243	13.42	+6.1	+ 0.5	− 1	0
319	244	12.12	+6.2	− 2.9	− 1	− 2
320	245a	14.05	+6.2	− 4.0	+ 1	0
321	245β	14.20	+6.2	− 4.1	0	0
322	.....	f	+6.7	+ 5.0	+ 9	+ 3
323	255	13.40	+6.9	− 0.6	− 1	0
324	.....	f	+7.1	− 2.4	− 1	0
325	.....	f	+6.9	+ 5.4	− 1	0
326	.....	f	+6.9	+ 7.4	− 1	0
327	259	14.60	+7.5	− 0.3	+ 1	0
328	261	11.17	+7.5	+ 2.5	− 1	− 8
329	262	14.02	+7.6	+ 1.3	0	0
330	263	14.50	+7.7	− 0.7	+ 1	0
331	.....	14.7	+7.7	− 1.5	+ 1	0
332	265	13.10	+8.2	− 2.1	− 7	+ 9
333	.....	vf	+8.3	− 0.7	+ 2:	+ 9:
334	.....	f	+8.3	+ 1.1	− 1	0
335	.....	vf	+8.2	+ 2.3	+ 1:	− 3:
336	.....	vf	+8.2	+ 3.3	+ 2	+ 2
337	.....	f	+7.5	+ 4.7	+ 1	0
338	.....	vf	+7.5	+ 4.9	− 2:	−10:
339	267	13.43	+8.4	+ 4.0	− 1	− 2
340	.....	f	+8.7	+ 3.6	− 1	0
341	268	14.14	+9.1	+ 0.2	0	0
342	269	13.74	+9.2	− 2.9	0	0
343	.....	f	+9.4	− 1.1	+ 1	0

NOTES

Numbers 11, 31, and 206 are close double stars.
Numbers 107 and 108 are so close that the images overlap on one pair of plates.

To increase the accuracy of the results I have restricted the measures to the best part of the plates, a circle with a radius of about 10 minutes of arc. The results are very satisfactory. The distances measured between the images of each pair of plates showed at once that, except for a scale correction, the reductions would involve only small corrections, so small that with a first rough reduction of scale it would be possible to determine whether a star belongs to the cluster. It was then decided to derive the proper motions with respect to the cluster, as such a procedure would enable us to use a great many more stars for the determination of the plate constants. Excluded were the following:

a, 3 double stars, Nos. 11, 31, and 206
b, 2 stars close together, Nos. 107 and 108, whose images were overlapping on one of the plates
c, 20 stars, marked "difficult" during the measuring
d, 24 stars, marked vf (very faint)
e, 13 stars, whose magnitudes were brighter than 12
f, 56 stars, which from the preliminary reductions showed proper motions differing from that of the cluster

Since No. 206 is included in both categories *a* and *e* and since 27 stars under *f* are also included in *c* or *d*, the total number of stars excluded is 90, leaving 253 probable cluster stars for the derivation of the plate constants. The final results show that only one star (No. 167, which was excluded on account of a possible motion) might have been retained. On the other hand, No. 73, although included in the reductions, does show a motion just exceeding 0".005, later accepted as the limit for possible members of the cluster; it should, therefore, have been excluded. But as 253 stars were used for this reduction, one noncluster star of small motion cannot have changed the results by any appreciable amount.

In order to get the best results, quadratic terms were included in the reductions. We have therefore solved four sets of equations of condition of the form

$$M = a + bx + cy + dx^2 + exy + fy^2 + \mu_\alpha \text{ or } \mu_\delta ,$$

one for each pair of plates in both right ascension and declination, where M is the measured quantity, reduced to 0".001 per year as a unit; x and y are the co-ordinates; a, b, c, d, e, and f are the plate constants; and μ is the resulting motion in α or δ.

The resulting motions $\mu_{\alpha 1}$, $\mu_{\alpha 2}$, $\mu_{\delta 1}$, and $\mu_{\delta 2}$ were first used for a derivation of the probable errors of the mean motions $\bar{\mu}_\alpha$ and $\bar{\mu}_\delta$. The results are given in Table 2.

TABLE 2

PROBABLE ERRORS FOR DIFFERENT CATEGORIES OF STARS
(Unit = 0".001)

Objects	P.E. in $\bar{\mu}_\alpha$	P.E. in $\bar{\mu}_\delta$	n	Objects	P.E. in $\bar{\mu}_\alpha$	P.E. in $\bar{\mu}_\delta$	n
All stars	0.8	0.8	343	12	0.8	1.8	15
Stars marked:	1.9	1.5	20	13	0.5	0.5	91
All others	0.7	0.8	323	14	0.6	0.6	110
Double stars	1.1	1.4	5	f	0.9	0.8	66
$m_{ph} < 11$	2.8	3.4	2	vf	1.3	1.1	24
11	1.3	2.7	10				

The differences between $\mu_{\alpha 1}$ and $\mu_{\alpha 2}$ and between $\mu_{\delta 1}$ and $\mu_{\delta 2}$ show the possibility of a slight magnitude error (which is not surprising, since the photographic magnitudes range from 9.3 to about 15.7); but, because we are dealing with an abundance of stars belonging to the cluster, for which the motions should be identical, we are fortunately able to overcome this difficulty.

When we plot the proper motions for different magnitudes, the relatively few stars with motions different from the cluster stand out decidedly; we can therefore easily select the probable members of the cluster. After excluding from the mean for each magnitude the double stars, stars marked with a colon, and stars with $\Delta\mu > 0''.005$, we find the mean motions for different magnitudes given in Table 3. It is evident that the motions

TABLE 3

MEAN MOTION OF CLUSTER STARS FOR DIFFERENT MAGNITUDES
(Unit = 0".001)

Ph. Mag.	Mean Mag.	Mean μ_α	Mean μ_δ	n	Ph. Mag.	Mean Mag.	Mean μ_α	Mean μ_δ	n
10.0–11.0	10.39	−4.0	0.0	1	13.5–14.0	13.76	−0.4	0.0	50
11.0–11.5	11.40	−4.0	0.0	1	14.0–14.5	14.19	+0.7	+0.1	59
11.5–12.0	11.74	−3.4	−1.1	7	14.5–15.0	14.65	+0.7	0.0	39
12.0–12.5	12.13	−3.2	−1.6	9	f	f	+0.6	+0.3	55
12.5–13.0	12.74	−2.4	−1.4	5	vf	vf	+0.3	0.0	19
13.0–13.5	13.34	−1.3	−0.1	36					

in declination do not require a correction; on the other hand, those in right ascension show such a smooth correlation with magnitude that the following corrections are applied to reduce them all to the mean motion of the stars of magnitude 13.0–15.5.

CORRECTIONS TO BE APPLIED TO $\bar{\mu}_\alpha$
(Unit 0".001)

$m_{ph} < 10.0$	+5	13.01–13.60	+1
10.01–11.80	+4	13.61–14.40	0
11.81–12.50	+3	14.41–15.40	−1
12.51–13.00	+2	> 15.40	0

The last two columns of Table 1 contain the corrected motions.

The distribution of the final motions, after this magnitude correction has been applied, is shown in Figure 1. Not including the stars marked uncertain, the deviations are as follows:

≦ 1".00	136	3".01–4".00	8
1".01–2.00	75	4.01–5.00	10
2.01–3.00	55	> 5.00	39

If we accept all the stars within 0".005 as members of the cluster, we derive an external probable error of 0".0084 in α and 0".0087 in δ, only slightly larger than the internal probable error given in Table 2, while for the total mean motion of each star the probable error is 0".0012. The stars with motions exceeding 0".005 are arranged according to magnitude in Table 4. Before we try to derive the relative and the absolute motion of the cluster, we may compare the number of noncluster stars with that computed by means of *Groningen Publications*, No. 27, Table 4. In the circle with radius 10 minutes of arc we may expect, according to that table, the numbers given in the second column of Table 5. The 39 stars whose motions show that they are not members of the cluster are given in the third column. These figures are in such excellent agreement that we may accept the magnitude adopted on page 382 for the f and vf stars as fairly correct. This leaves for probable members of the cluster the figures in the fourth column of Table 5. Some of the stars included here as cluster stars may, in reality, not be members of the group; but the number is undoubtedly small. Finally, in the last column are the differences, which would therefore represent the number of stars of different magnitudes be-

longing to the cluster; the very steep rise at the top suggests that Shapley's magnitudes may need a scale correction.

From the motions in Tables 1 and 4 relative to the cluster it is now our task to derive the motion of the cluster with respect to the field stars, and, finally, its absolute motion. As we can make a fairly good guess at the parallactic motion of the stars between magnitudes 13 and 15.7, we may use the 35 stars of these magnitudes not belonging to

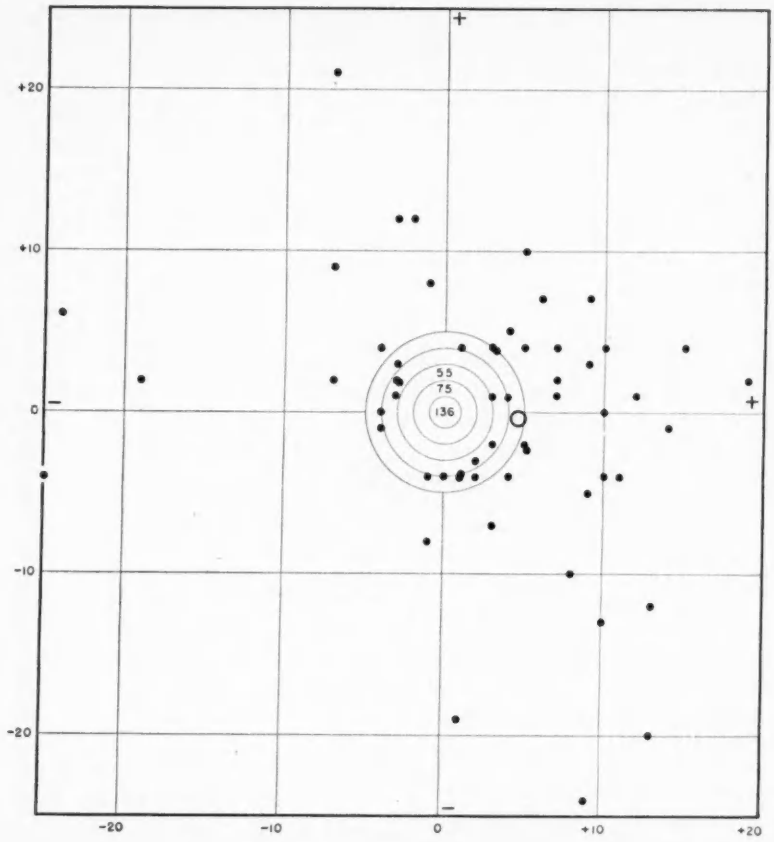

FIG. 1.—Distribution of the proper motions in Messier 67. The unit is 0".001. In order to avoid crowding, the total numbers are given for the central zones with 0".001, 0".002, and 0".003 as radii. The small heavy circle represents the mean motion of the noncluster stars of magnitude 13–15.7.

the cluster; but we exclude the 4 brighter stars, because for such a limited number the parallactic motion is rather uncertain. For the 35 stars $\mu_\alpha = +0''.0046 \pm 0''.0011$, and $\mu_\delta = -0''.0003 \pm 0''.0011$. A few stars, included as cluster stars, may after all be field stars. As the number of field stars in the region measured can hardly exceed 40, only a few stars can have been excluded; if we suppose their number to be 5, with motions in the mean equaling 0 in each co-ordinate, μ_α and μ_δ would change only to $+0''.0040$ and $-0''.0002$, respectively. The relative motion of the cluster with respect to the field stars of magnitude 13–15.7 may therefore be accepted as

$$\mu_\alpha = -0''.0046 \; ; \qquad \mu_\delta = +0''.0003 \; .$$

In Figure 1 this mean motion is indicated by a small circle. The main difficulty is to reduce this value to absolute motion. However, for the mean apparent magnitude 14.5 of the field stars we have a fair idea of the parallactic motion for different galactic latitudes from Oort's[2] result and from some unpublished motions by H. C. Willis. For the

TABLE 4

PROBABLE FIELD STARS
(Unit for $\bar{\mu}_\alpha$ and $\bar{\mu}_\delta$=0".001)

No.	m_{ph}	$\bar{\mu}_\alpha$	$\bar{\mu}_\delta$	No.	m_{ph}	$\bar{\mu}_\alpha$	$\bar{\mu}_\delta$
317	9.30	− 7	+ 2	105	14.7	+ 6	+ 7
328	11.17	− 1	− 8	203	14.7	−24	+ 6
269	11.96	−19	+ 2	121	14.76	+19	+ 2
73	12.40	+ 5	+ 4	1	f	+13	−20
332	13.10	− 7	+ 9	22	f	+ 5	+ 2
293	13.28	+ 3	− 7	25	f	+11	− 4
11	13.36	− 3	+12	47	f	+ 9	+ 7
306	13.42	+13	−12	52	f	+ 5	+10
274	13.57	−25	− 4	53	f	+ 5	− 2
31	13.93	− 2	+12	80	f	+ 9	−24
65	13.97	+10	+ 4	205	f	+ 9	− 5
171	14.16	+ 4	+ 5	239	f	+15	+ 4
113	14.28	+10	−13	286	f	+ 7	+ 4
229	14.32	+12	+ 1	322	f	+ 9	+ 3
174	14.41	− 7	+21	72	vf	+10	0
188	14.43	+10	− 4	93	vf	+ 4	− 4
147	14.52	+ 5	− 2	97	vf	− 4	+ 4
208	14.6	+ 7	+ 1	204	vf	+ 8	−10
276	14.6	+ 1	−19	304	vf	+14	− 1
81	14.70	− 1	+ 8				

TABLE 5

NUMBERS OF FIELD AND CLUSTER STARS

Lower Limit of Mag.	$n_{comp.}$	$n_{obs.}$	$n_{cluster}$	Diff.
12	3	3	10	
13	6	4	25	15
14	12	11	112	87
15	24	23	210	98
15.5	34	34	265	55
15.7	39	39	284	19

galactic latitude of the cluster Oort's value is 0".0066; Willis', 0".0071. If we accept the apex for these faint stars as $\alpha = 6^h40^m$, $\delta = -50°$ and use the mean of 0".0068, we derive, for the field stars in our field, a parallactic motion of

$$-0''.0021 \text{ in } \alpha\,, \qquad -0''.0059 \text{ in } \delta\,.$$

This gives for the absolute motions of Messier 67

$$-0''.0067 \text{ in } \alpha\,, \qquad -0''.0056 \text{ in } \delta\,, \qquad \text{or } 0''.0087 \text{ in } p = 230°\,.$$

[2] *Bull. Astr. Inst. Netherlands*, **8**, 75, 1936.

The main uncertainty of this result is felt to be in the reduction from relative to absolute motion. Since in the future we are planning a better determination of the parallactic motion of the faint stars, not too much emphasis should be put on the values given here for the absolute motions.

Comparison with other observers.—Two other determinations of the motion of Messier 67 are available:

$\mu = 0''.0073$ in $p = 287°$, P. J. van Rhyn,[3]

$\mu = 0''.0090$ in $p = 220°$, E. G. Ebbighausen.[4]

Van Rhyn measured two Carte du ciel plates with an interval of 27 years; the probable error of a μ_α or μ_δ is $0''.0054$. On account of the smallness of the actual motion of the cluster it was impossible to decide which stars are members of the cluster.

Ebbighausen used four pairs of plates, secured with the 40-inch Yerkes refractor, with a mean interval of 26 years. For the 45 stars (28 per cent of those measured) of weight 4 and 3, the internal probable error is $0''.0009$. For these stars the external probable error, determined as in the present paper, is the same as that for the Mount Wilson plates based on two exposures with a mean interval of 21 years, viz., $0''.0011$ for a total motion. For the stars of weight 2 (52 per cent) the external probable error is $0''.0021$; for those of weight 1 (20 per cent), $0''.0028$. The accuracy of the present results can best be

TABLE 6

PERCENTAGES OF DEVIATIONS OF PROBABLE CLUSTER STARS

Deviations	Ebbighausen	van Maanen	Deviations	Ebbighausen	van Maanen
$\leqq 0''.001$	17	48	$0''.003$–$0''.004$	22	3
$0''.001$–$0''.002$	21	26	.004– .005	8	4
.002– .003	32	19			

appreciated from Table 6, which shows the percentages of motions for the determinations by Ebbighausen and by the present writer.

Using Ebbighausen's measures for the 33 stars to which he gave weights 3 and 4 and for which the probability that the star is a member of the cluster is high, I have made a solution including the quadratic terms. We then find that the percentages of the smaller deviations increase considerably, while those exceeding $0''.002$ decrease accordingly. The sums of the squares of the deviations are reduced by this process from 6605 to 3580 in μ_α and from 4728 to 3734 in μ_δ. It therefore seems that the relatively small amount of routine computing involved should not be omitted, particularly if the motions are given with $0''.0001$ as unit.

CARNEGIE INSTITUTION OF WASHINGTON
MOUNT WILSON OBSERVATORY
July 1942

[3] *Pub. Kapteyn Astr. Lab. Groningen*, No. 33, 1922.

[4] *Ap. J.*, **91**, 255, 1940.

THE WAVE LENGTHS OF NEW CORONAL LINES

WILLIAM PETRIE AND DONALD H. MENZEL

ABSTRACT

The wave lengths of all coronal lines have been measured on photographs taken with three instruments at the 1936 eclipse. Seven lines obtained from three jumping-film spectra are believed to be new; five lines measured on one ultraviolet moving-film spectrum are new; ten lines measured on five moving-film spectra of high dispersion are probably also new. However, it is possible that these latter features may originate from photographic effects of undetermined origin. Every effort has been made to exclude the lines of the chromosphere, so that the tabulated wave lengths may be definitely attributed to the corona.

It is well known that the coronal spectrum varies considerably. The relative intensities of the emission lines change from eclipse to eclipse, and, on certain occasions, several of the lines have been absent from the spectrum. The line[1] λ 3601 was never observed until 1908; yet it is one of the strongest lines in the coronal spectrum, and the instrumental equipment used in 1905 was adequate to record a spectral feature of such intensity.[2] Grotrian reported three lines missing from the spectrum secured during the 1929 eclipse, those at λλ 3643, 4586, and 5536. The green line at λ 5303 is generally the strongest in the spectrum; but in 1932 the red line at λ 6374 exceeded the former in intensity. These examples of the variation of the emission spectrum should indicate that the appearance of a line at only one eclipse does not mean that the line is not real.

On low-dispersion spectra it is difficult to differentiate between chromospheric and coronal lines. Observations indicate that the coronal lines are most intense in regions close to the solar limb, and the chief distinguishing feature from an objective viewpoint is the relatively slow intensity decrement with height of the coronal lines. The fact that *He* lines, especially λ 4686 of *He* II, show the slowest decrement of all the chromospheric lines has made it especially difficult to distinguish whether the helium emission is partly coronal or entirely chromospheric. With the low dispersion usually employed for the recording of the coronal spectrum, the high intensity of the coronal continuum produces an added difficulty; it is difficult to distinguish the faint patches of coronal emission against a background that offers so little contrast. For this reason results from more than one plate taken at the same eclipse are especially desirable for purposes of checking. A recent study of the spectrograms taken at the 1936 eclipse by the[3] Harvard–Massachusetts Institute of Technology expedition has revealed numerous new lines; and this paper presents the results of the wave-length measures. Table 1 summarizes the observational material.

We measured the grating spectrograms with the coast and geodetic survey machine of the Harvard Observatory—an instrument that may be read to the nearest micron. On the jumping-film spectra the coronal lines show as monochromatic images of the corona. They appear as arcs or complete circles, but the most striking feature is the occurrence of "flares" having a definite resemblance to ordinary prominences. They do not show, however, in the light of the ordinary chromospheric lines. It seems to us that the term "coronal prominences," employed by Pettit and McMath to describe ordinary prominences forming in and cascading down from the coronal regions, would be better applied to the phenomenon here described. Provisionally, we shall call these prominence-like coronal formations "flares." The flares show a very strong continuum. The cross-

[1] Campbell and Moore, *Lick Obs. Bull.*, No. 318, p. 12, 1918.

[2] *Zs. f. Ap.*, **2**, 106, 1931.

[3] *Harvard Ann.*, **105**, 1936.

hairs were set on the concave edges of the coronal lines, since the moon's limb defines a definite boundary. It is much easier to detect the boundary between line emission and continuous emission for the strong lines. For this reason we took care to measure the coronal lines with respect to several chromospheric lines of comparable intensity. We made our measures on the region of the plate where the continuum is strongest, since the emission lines have their greatest intensity in this region. We found the same lines on several of the jumping-film spectra and took a weighted mean of our measures. It is difficult to estimate the accuracy of the wave lengths determined, because of the faint

TABLE 1

LIST OF OBSERVATIONAL DATA

MOVING-FILM SPECTRA				JUMPING-FILM SPECTRA			
Film No.	Type	Wave-Length Range (I.A.)	Disp. (A/Mm.)	Film No.	Type	Wave-Length Range (I.A.)	Disp. (A/Mm.)
S.P. No. 0.....	Grating	3196–3787	2.46	3:0.....	Grating	3281–4910	6.95
1.....	Grating	4162–4752	2.46	5:0.....	Grating	5551–7507	8.20
2.....	Grating	5085–5611	2.46	6:0.....	Grating	4169–6784	11.02
3.....	Grating	4329–5129	3.72				
5.....	Grating	3517–3964	1.86*				
Ultraviolet plate.	Prism	3277–5550	7.7†				

* Second order. † At λ 3850.

character of the lines involved. The largest discrepancy, however, between the measured and accepted values for the known lines was never greater than 0.8 A.

The moving-film spectra revealed what appeared to be a number of new lines, but the absence of several of the known coronal lines casts some doubt on the reality of the former. It may be, however, that the specific region observed lay just on the edge of one of the bright coronal flares and, in consequence, included a region of intermediate coronal excitation. The appearance of the lines here measured was similar to that of the known lines recorded. Nevertheless, there is still a possibility that the features we observed are simply photographic effects arising from an undetermined origin. In the moving-film instrument the film was slid against a layer of felt; but none of the numerous test spectra showed spurious lines of this character which could be interpreted as arising from a mechanical source. It may be that these lines are not seen on spectra of low dispersion but appear on the moving films of relatively high dispersion, which makes the lines stand out more clearly against the reduced background continuum.

The prism spectrum of the moving-film type taken primarily for the records of the chromosphere proved to have an exceptionally large number of new and known coronal lines recorded. This feature is all the more remarkable in that the effective exposure was of the order of only 1 second. Fortunately, the region of the sun recorded upon it was extremely rich in coronal lines and continuum. As a matter of fact, the continuum recorded itself with appreciable intensity throughout totality. This moving-film spectrum had a defect of a very peculiar character, which rendered it somewhat unsatisfactory for the original purpose of chromospheric photometry. The exposures of one of the instruments on the same mounting were manually controlled. At each exposure the entire mounting was subjected to a minute torque, which caused a break in the otherwise straight lines running perpendicular to the dispersion. These breaks, however, proved to be most providential in the identification of coronal lines. Their appearance made it possible to distinguish unquestionably lines of true solar origin from any possible instru-

mental effect, such as scratches. On this spectrum were recorded five new lines of sufficient intensity for position measurement.

Dr. George R. Harrison kindly placed at our disposal the wave-length analyzing machine of the Spectroscopic Laboratory at the Massachusetts Institute of Technology. Mr. Norman Oliver, of the Institute, made runs of the analyzer at six different points along the plate. Since we were working with a prism plate, the machine did not record

TABLE 2

WAVE LENGTHS OF CORONAL LINES

JUMPING-FILM SPECTRA	ULTRAVIOLET MOVING-FILM SPECTRUM	JUMPING-FILM SPECTRA	ULTRAVIOLET MOVING-FILM SPECTRUM
Wave Length (I.A.)	Wave Length (I.A.)	Wave Length (I.A.)	Wave Length (I.A.)
3328.6	3389.0	5536.7	4359.3
3387.9	3454.9	5899.1*	5116.8
3454.3	3601.9	5912.4*	5303.2
3601.8	3801.5	5937.1*	
3800.4	3980.9*	6294.9*	
3987.2	3987.6	6336.9*	
4085.6	4003.5*	6374.8	
4230.6	4056.3*	6513.0*	
4359.4	4087.0	6524.1*	
4566.8	4170.8*	6701.5	
5115.8	4231.6	7060.2	
5303.4	4272.9*		

* New lines.

TABLE 3

WAVE LENGTHS OF CORONAL LINES
(MOVING-FILM SPECTRA)

Wave Length (I.A.)	Wave Length (I.A.)
3216.5*	4429.8*
3296.1*	4674.4*
3388.5	4705.7*
3577.2*	4783.9*
3586.6*	5094. *
3600.7	5116.2
3630.7*	5303.0
4231.5	

* New lines.

wave lengths directly; nevertheless, it measured the relative positions of all lines very accurately.

We determined the wave lengths from the Hartmann formula in the usual manner. The differences between the observed and the calculated values of the wave lengths of forty chromospheric lines defined a correction-curve for the coronal wave lengths. The differences between the coronal wave lengths so obtained and the true wave lengths for the known lines defined another curve, which we applied as a second correction. Finally, we calculated a weighted mean of the measures from the various runs.

As was mentioned previously, coronal lines have often been mistaken for faint chromospheric lines, but the authors do not think that a similar error has occurred here. In

every case the lines studied on the jumping-film spectra were relatively strong in the flares, where the chromospheric emission was either weak or absent.

One difficulty arises in measurement of the moving-film plates. The slit is placed so as to isolate one small section of the coronal and chromospheric rings. The corona, however, shows on both sides of the sun, giving double lines, and one must decide which set of chromospheric lines to use as reference. One is aided by the fact that the spectrograph is focused for one side of the sun only; consequently, the lines from the other side lack sharpness. Since the coronal lines are naturally broad and fuzzy, this criterion is not infallible; but the authors feel that they were able to differentiate between the lines in focus and those not in focus. There is a second and more powerful criterion. Moving-film spectra give a continuous record of the gradient of the coronal and chromospheric lines with height; consequently, the intensity decrement of the former enables one to associate these lines with the proper side of the sun.

We feel reasonably sure that the seven lines measured on the jumping-film spectra and the five lines on the moving-film spectrum are truly coronal in origin. The wave lengths of the known and the new lines obtained from these films are given in Table 2. The remaining lines found on the moving-film grating spectra certainly have the appearance of coronal emission; but the absence of many of the known lines, as mentioned previously, casts some doubts on the reality of these apparently new lines. The wave lengths are given in Table 3.

We wish to thank Dr. George R. Harrison of the Massachusetts Institute of Technology for allowing us the use of the wave-length analyzing machine and Mr. Norman Oliver of the same institution for the operation of the instrument.

HARVARD COLLEGE OBSERVATORY
August 1942

A STUDY OF THE ALGOL SYSTEM

ZDENĚK KOPAL

ABSTRACT

New photometric elements of the eclipsing system of Algol are derived from an analysis of combined photoelectric light-curves by Stebbins and Smart. In doing so we assume the B8 component to be darkened at the limb to a degree compatible with its spectrum and the effective wave length of the observations. Preliminary elements, as well as their uncertainty, are determined by a method recently proposed by the writer. These elements are subsequently refined by taking into account effects arising from the difference in form of both components, as well as those due to the gravity darkening of the B8 star. The resulting set of elements differs significantly from that derived by Stebbins. The changes of light exhibited by Algol between eclipses are finally found to be compatible with elements derived from the light-curve within minima.

The mass ratio of the eclipsing system of Algol is specified from the rotational effect exhibited by lines of the B8 spectrum during primary minimum. In the course of its derivation the B8 star is again assumed to be partially darkened at the limb. By a combination of this mass ratio with McLaughlin's single-spectrum orbit we then derive the absolute dimensions of the eclipsing orbit. It is pointed out that the temporary asymmetry of the rotational effect observed at Ann Arbor may be tentatively explained by an inclined axis of rotation of the B8 star executing precessional motion under the gravitational influence of the eclipsing companion.

The combined light of Algol in the blue is completely dominated by the bright B8 star. Neither the secondary component nor the third body appears to be spectroscopically observable at any time. The B8 component is a genuine main-sequence star. The third body is probably a star of approximately 1 solar mass and of average (or possibly subnormal) luminosity. The eclipsing companion, on the other hand, appears to be less massive than the third body, but, like other similar subgiants, it is so much more luminous for its mass that its total luminosity actually exceeds that of the third star.

The periodic variability of Algol was discovered in 1782 by Goodricke;[1] and, although its binary character was suggested at once by the discoverer, it was not safely established until in 1889 by Vogel.[2] A vast amount of observational material has been accumulated since that time, and the significant facts concerning Algol are well known. It is a single-spectrum binary of a period of 2.8673 days, the components of which revolve around the common center of gravity in orbits that are practically circular and slightly inclined to the line of sight, so that at each conjunction one star partially eclipses the other. The resulting minima are very unequal in depth; while during the primary minimum the brightness of Algol diminishes by more than 1 mag., the depth of the secondary minimum amounts to only a few hundredths of a magnitude—suggesting that the surface brightnesses of both components differ widely. The deep minimum is due to the eclipse of the bright component of spectral class B8 by its companion, slightly larger in size, whose spectrum has thus far not been observed but which, judging from the surface brightness, should be similar to that of the sun. Periodic variations of radial velocity of the center of mass of the eclipsing system have revealed that, furthermore, the eclipsing system is attended by a distant third body of appreciable mass, which revolves around the common center of gravity in a period of 1.873 years. The absolute orbit of the eclipsing pair around the center of gravity of the triple system proved large enough to be detected astrometrically. Colorimetric observations have, however, failed, thus far, to disclose any trace of the third body in the combined light of Algol.

I

The spectrum of Algol has, on closer scrutiny, revealed many complex features. Its dominant character is that of a normal B8 star of approximately zero absolute spectro-

[1] *Phil. Trans. Roy. Soc.*, **73**, 474, 1783. [2] *A.N.*, **123**, 289, 1890.

scopic magnitude. In studying the spectrograms secured by Schlesinger and others at the Allegheny Observatory in the years 1907–12, Miss Barney[3] detected, however, a number of faint lines, mostly of metallic origin, which led to velocities following in phase the velocity-curve derived from hydrogen and other prominent lines of the B8 spectrum, but with an amplitude diminished to about one-third. These "extra" lines were reportedly best seen at the time of primary minimum, but the visibility of most of them persisted throughout the whole cycle. Their origin could scarcely be associated with the third body of the Algol system, for the material examined by Miss Barney, extending over an interval of five years, failed to show any variation commensurable with the orbital period of the third body. Miss Barney concluded that the extra lines must be due to both the primary and the secondary components of the eclipsing pair; for the lines appeared relatively strongest when the radial velocities of both components coincided, and their lines should be expected to reinforce one another.

In addition to the wide difference in spectral classes, the components of the eclipsing system differ, however, approximately 3 mag. in brightness in the blue, and even at mid-primary minimum this difference decreases to but 1.8 mag. The visibility of a number of extra lines in full light therefore makes the participation of the secondary component in the composite spectrum extremely dubious. In view of this, as well as of the fact that the extra lines follow in phase the velocity-curve of the B8 star, it seems logical to conclude that they are associated with the primary star alone. The peculiar fact that their velocity amplitude is only about one-third of that derived from the "normal" (i.e., strongest) lines of the B8 spectrum remains unexplained—though it is no longer unique. Quite recently Joy[4] discovered lines of *Ca* I of similar behavior in the spectrum of WW Draconis. Here the *H* and *K* lines in emission were found to follow in phase the velocity-curve of the secondary (less massive) component, but also with much diminished amplitude. It is likely that the "extra" lines in the spectra of these two eclipsing systems are of similar origin, which can be tentatively associated with outer atmospheres surrounding the respective stars and extending far in the direction of the center of gravity of the eclipsing system.

Another peculiarity exhibited by certain lines of the Algol spectrum is their doubling. Struve and Elvey[5] were the first to suspect the duplicity of *Mg* II 4481, which was subsequently studied by Morgan[6] on the basis of Yerkes spectrograms taken within primary minimum. He found that the relative intensities of the blue and the red components of *Mg* II 4481 were comparable and fluctuated somewhat with the phase. Their separation appeared to remain unchanged. Arithmetical means of the radial velocities of the two components showed variation conforming to the velocity-curve of the primary star as derived from the hydrogen lines, but without exhibiting the rotational effect. If so, the lines could scarcely originate in the reversing layer of the B8 star. In addition to *Mg* II 4481, *Fe* II 4549 was also found to exhibit a similar doubling. It may be pointed out that, while *Mg* II 4481 is a "normal" line which follows the velocity-curve derived from the hydrogen lines, *Fe* II 4549 is one of the "extra" lines exhibiting the greatly reduced velocity range. The phenomenon of doubling is therefore not confined to either group of lines. Whether or not the hydrogen and other broad lines of the B8 spectrum exhibit similar structure remains conjectural. Algol would decidedly be a gratifying object for spectroscopic study with an apparatus of high resolving-power attached to a large reflector, for instruments employed so far have been of only moderate size (apertures not exceeding 40 inches).

As to the origin of the duplicity, Morgan[6] advanced a hypothesis that the doubling is only apparent and due in some way to the effect of the secondary component on the profiles of lines of the primary star. This might be conceivable, were the doubling con-

[3] *A.J.*, **35**, 95, 1923.

[4] *Ap. J.*, **94**, 407, 1941.

[5] *M.N.*, **91**, 663, 1931.

[6] *Ap. J.*, **81**, 348, 1935.

fined to phases around the mid-primary minimum only. But Melnikov,[7] examining the spectrograms secured by Belopolsky at Pulkovo, found the doubling to persist throughout the whole cycle, with the separation of both components unchanged and their intensities nearly equal. This again absolves the secondary component from any responsibility for the observed facts. The origin of the doubling, as well as the origin of the "extra" lines, remains, thus, an open problem which we shall not at present attempt to solve. The spectroscopic investigations point, however, to one important conclusion: namely, that none of the spectral characteristics detected so far—whatever the mechanism of their origin—can be traced back with certainty to any star other than the bright B8 component. The secondary component of the eclipsing system, as well as the third body attending the eclipsing pair, seem to be spectroscopically invisible in photographic light, even at the time of maximum eclipse.[8] Hence, both the secondary component and the third body must be at least 1 mag. fainter than the crescent of the B8 star visible at the moment of mid-primary minimum. This permits us, in the first approximation, to neglect the light of the third body altogether and carry out a solution for orbital elements as if it were absent. A discussion of the observational evidence pertaining to its possible luminosity will be taken up at a later stage (sec. V).

II

The two best existing light-curves of Algol are undoubtedly the photoelectric curves by Stebbins[9] and Smart.[10] Stebbins also carried out a solution of his light-curve, while Smart's curve has thus far not been solved for orbital elements. There are, however, several reasons why Stebbins' elements published in 1920 cannot at present be regarded as entirely satisfactory. First, Stebbins carried out his solution by Russell's method in its original form, which involved some equations of approximate validity,[11] and the accuracy of the three-figure tables of the χ-functions, then available, was inadequate for the interpretation of so precise a light-curve. Second, Stebbins' solution presumed uniformly bright disks, which is scarcely the case in reality; both components are expected to display some darkening at the limb as well as gravity darkening due to gravitational distortion. Third, no attention was paid in Stebbins' solution to effects arising from the difference in form of the two components, which prove to be conspicuous. Many of the deficiencies of the older methods of approach have been gradually met by subsequent investigations. New and more complete sets of χ-tables are in preparation at Princeton; until they are available the use of the χ-functions can be avoided by a method recently proposed by the writer.[12] Moreover, the effects upon light-curves of gravity darkening and difference in form of both components have also recently been investigated quantitatively and expressed in terms of the geometry of the eclipse.[13] The theoretical background for a rigorous interpretation of light-curves like that of Algol being now complete, an application of the new methods of solution to Algol suggests itself.

[7] *Poulkovo Circ.*, No. 30, 1940.

[8] A report of the Dominion Astrophysical Observatory for 1938 (*M.N.*, **99**, 354, 1939) contains a statement, in reference to Pearce's spectroscopic observations of Algol, that "during eclipse the spectrum of the class *A* companion star has been repeatedly photographed." Pending further elaboration, the writer considers it probable that the superposed A spectrum proved to be, on closer scrutiny, identical with the extra lines studied by Miss Barney, which as a whole correspond to a slightly later spectral type than that of the bright star.

[9] *Ap. J.*, **53**, 105, 1921.

[10] *M.N.*, **97**, 396, 1937.

[11] In particular, that expressing the linear dependence of the $\chi(k, a_0, n)$ functions for uniform disks.

[12] *Ap. J.*, **94**, 145, 1941.

[13] *Proc. Amer. Phil. Soc.*, **85**, 399, 1942; cf. also *Ap. J.*, **94**, 159, 1941, and **96**, 20, 1942.

The photoelectric light-curves by Stebbins and Smart were both observed with a potassium hydride cell and their effective wave lengths should be closely similar, namely, about 4500 A. The epochs of both series are nearly two decades apart; but there appears to be no evidence of any secular change. Therefore, for the purposes of the present investigation we shall combine Stebbins' and Smart's series of observations in a single light-curve which will then be subjected to orbital analysis. Stebbins, cutting down the light of Algol by a neutral shade glass, referred his measurements to l Persei as a comparison star and found the difference in magnitudes between l and β Persei between minima to vary as

$$m(l) - m(\beta) = 0.0285 - 0.0164 \cos\theta - 0.0148 \cos^2\theta - \ldots\ , \qquad (1.0)$$
$$\pm 0.0015 \quad \pm 0.0011 \qquad \pm 0.0027 \text{ (p.e.)}\ ,$$

where θ denotes the mean anomaly (phase angle) in the relative orbit of the faint component around the bright star, reckoned from mid-primary minimum. Smart, on the other hand, used δ Persei as his comparison star. A harmonic analysis of his measurements between minima yields

$$m(\delta) - m(\beta) = 0^m.8383 - 0^m.0162 \cos\theta - 0^m.0029 \cos^2\theta - \ldots\ , \qquad (2.0)$$
$$\pm 0.0007 \quad \pm 0.0012 \qquad \pm .0025 \text{ (p.e.)}\ .$$

Therefore, if we subtract $0^m.810 \pm 0^m.001$ from Smart's values of M, given in Table IV, column 2, of his paper, and subtract $2^d.0491$ from his time readings, his light-curve is reduced to the system of Stebbins.[9] If, in order to remove the constant term of Stebbins' series, we further subtract from all measurements a value of $0^m.0285$ and convert magnitudes into intensity units, we find the light l of Algol between minima to vary as

$$l = 1.0000 - 0.0151 \cos\theta - 0.0136 \cos^2\theta \qquad (1.1)$$
$$\pm .0016 \pm .0010 \qquad \pm .0024 \text{ (p.e.)}\ ,$$

according to Stebbins, and

$$l = 1.0000 - 0.0149 \cos\theta - 0.0027 \cos^2\theta \qquad (2.1)$$
$$\pm .0007 \pm .0012 \qquad \pm .0023 \text{ (p.e.)}\ ,$$

according to Smart.

A comparison of equations (1.1) and (2.1) reveals that the coefficients of $\cos\theta$ (reflection constants) of both series are closely concordant; but Stebbins' ellipticity constant (coefficient of $\cos^2\theta$) is several times as large as Smart's, and their discrepancy widely exceeds the probable errors of the respective quantities. As often happens, later observations may enable us to decide which of the two values is likely to be more correct. In the case of Algol the ellipticity of the system should be almost entirely due to the tidal distortion of its late-type companion and should therefore be expected sensibly to increase toward the red. A recent series of photoelectric observations of Algol made with a cesium oxide cell (effective wave length of 8660 A) by Hall[14] failed, however, to detect any noticeable ellipticity in the infrared. Since it is, then, all the more unlikely that any should be apparent in the blue, we have to conclude that Stebbins' value, although statistically significant, has probably no real existence. The photometric ellipticity of Algol at 4500 A is apparently too small for reliable determination, and in the following it will be neglected.

The dispersion of individual observations between minima furnishes a testimony on their precision. If—in the absence of any indication to the contrary—we assume that Stebbins' "sets" are comparable with Smart's "observations," both series are apparently

[14] *Ap. J.*, **90**, 449, 1939.

of equal precision, for a single normal based, on the average, on seven "sets" or "observations" carries a probable error of $\pm 0^m.0039$ (Stebbins) and $\pm 0^m.0037$ (Smart).

The basic data for the determination of orbital elements of an eclipsing system are naturally the observations within minima. In order to avoid an undue amount of work at various later stages of the orbital analysis we find it expedient to combine Stebbins' and Smart's normals on the ascending and descending branches of both minima into a limited number of supernormals which will be used for actual solution later on. Table 1

TABLE 1

OBSERVATIONAL DATA

No.	d	θ	Δm	l_{rec}	w	$(O-C)_I$	$(O-C)_{II}$
1	$0^d.0011$	$0^\circ.14$	$-1^m.214$	0.3517	1.1	−0.0034	−0.0027
2	.0128	1 61	1.180	.3620	2.7	− .0006	+ .0008
3	.0237	2 98	1.116	.3821	3.1	+ .0015	+ .0029
4	.0364	4 57	1.033	.4101	3.4	+ .0018	+ .0028
5	.0457	5 74	0.950	.4403	1.4	− .0068	− .0059
6	.0531	6 67	0.886	.4654	2.6	− .0043	− .0040
7	.0624	7 83	0.794	.5038	3.3	+ .0031	+ .0029
8	.0715	8 98	0.703	.5452	3.4	+ .0033	+ .0025
9	.0834	10 47	0.613	.5897	3.0	+ .0035	+ .0016
10	.0948	11 90	0.518	.6410	3.1	− .0007	− .0026
11	.1022	12 83	0.459	.6750	2.0	+ .0009	− .0014
12	.1123	14 10	0.393	.7155	4.0	− .0031	− .0038
13	.1220	15 32	0.327	.7583	3.3	+ .0012	+ .0010
14	.1319	16 56	0.262	.8034	2.4	+ .0057	+ .0068
15	.1451	18 22	0.196	.8516	4.6	− .0019	− .0004
16	.1601	20 10	0.138	.8967	4.6	− .0003	+ .0006
17	.1722	21 62	0.092	.9341	2.3	+ .0007	+ .0008
18	.1832	23 00	0.056	.9646	3.0	+ .0031	+ .0038
19	0.2007	25 20	−0.027	0.9895	1.9	−0.0021	−0.0034

contains a summary of the observational data relative to the primary minimum. The first column gives the number of the respective supernormal; the second column the interval (in days) from mid-primary minimum; the third column the corresponding phase angle θ; and the fourth column the magnitude difference $m(l) - m(\beta)$ as observed through Stebbins' shade glass and diminished by $0^m.0285$. The observed magnitude differences are then converted into light-intensities and rectified for reflection by means of the formula

$$l_{rec} = \frac{l_{obs} + 0.0150\,(1 + \cos\theta)}{1.0150}, \qquad (3)$$

which reduces the light between minima to unity. The rectified intensities of the individual supernormals are then given in the fifth column and their observational weights (proportional to the number of normals included) in the sixth column; unit weight corresponds to a probable error of $\pm 0^m.0038$. The average weight of a supernormal is 2.9, which should correspond to a probable error of $\pm 0^m.0023$.

The rectified loss of light at primary minimum becomes $1^m.135 \pm 0^m.003$. The secondary minimum is too shallow to be used for an independent determination of the orbital elements and need not be treated with the same detail. The only characteristic of the secondary minimum required later is again its rectified depth, which amounts to $0^m.040 \pm 0^m.003$. If, therefore, λ_1, λ_2 denote the fractional intensities (expressed in terms of light between minima taken as unit) of Algol at the moments of mid-primary and mid-secondary minimum, respectively, then

$$\lambda_1 = 0.352 \pm 0.003\,, \qquad \lambda_2 = 0.964 \pm 0.003\,.$$

III

In deriving the elements of the eclipsing system of Algol we avail ourselves of a method recently proposed by the writer,[12] which consists in improving a preliminary set of elements by rapidly convergent successive approximations. This method can be applied with advantage to systems where good preliminary elements (such as Stebbins' for Algol) are available. At no stage does it require recourse to freehand curves, the basic material being the observed normal points; and it calls for tables of no special functions other than of $p(k, \alpha)$. Its analytical principles need not be repeated here; in the following only those equations will be quoted that are used for actual computations.

The following notations will be employed:

θ, the longitude in the orbital plane reckoned from mid-primary minimum,
i, the inclination of the plane of the orbit to the celestial sphere,
$r_{1,2}$, the fractional radii of the bright (smaller) and faint (larger) component, respectively,
k, the ratio of radii r_1/r_2,
p, the geometrical depth of the eclipse,
p_0, the geometrical depth at the moment of maximum obscuration,
α^U, the fractional loss of light, at any moment, due to the eclipse of a uniformly bright disk,
α^D, the fractional loss of light due to the eclipse of a disk that is completely darkened at the limb by another disk which is larger (α_1^D) or smaller (α_2^D) than the one eclipsed,
α_0, the fractional loss of light of the eclipsed star at the moment of maximum obscuration,
q, the fractional loss of light at the moment of internal tangency of an eclipse of a larger star by a smaller one, when the former is uniformly bright (q^U) or completely darkened at limb (q^D),
u, the coefficient of limb darkening of the respective star.

As usual, the rectified intensity between minima is taken as the unit of light and the radius of the orbit as the unit of length.

The quantities α^U, as well as α_1^D or α_2^D, can be made to depend on two suitably chosen independent parameters—such as k and p—and tabulated for practical use. By inversion of such tables, p may be found in terms of k and α for any distribution of brightness (degree of darkening) of the eclipsed star. Computers of orbits of eclipsing binaries have recently been put under a deep debt of obligation to Professor Zessewitsch of the University of Leningrad for the completion of extensive tables of α-functions accurate to five decimal figures and of p-functions accurate to four decimals,[15] which will be used for the purposes of the present investigation. The references to the individual tables are as follows:

$\alpha^U(k, p)$ . . . . . Zessewitsch II, Table 5,
$\alpha_1^D(k, p)$ . . . . . Zessewitsch I, Table 1,
$\alpha_2^D(k, p)$ . . . . . Zessewitsch I, Table 3,
$p(k, \alpha)$ . . . . . Zessewitsch II, Table 6 (uniform disks), and Tables 7–14 (partial darkening); I, Tables 2 and 4 (complete darkening).

During primary eclipse, at any moment, we have

$$\sin^2\theta \sin^2 i + \cos^2 i = r_2^2(1 + kp)^2 , \qquad (4.0)$$

[15] *Bull. Inst. Astr. Leningrad*, No. 45, 1939, and No. 50, 1940. These papers will hereafter be referred to as Zessewitsch I and II, respectively.

which at mid-primary minimum reduces to

$$\cos i = r_2(1 + k p_0). \tag{4.1}$$

Subtracting equation (4.1) from equation (4.0), we obtain

$$\sin^2 \theta = 2(p - p_0)C_1 + (p^2 - p_0^2)C_2, \tag{A}$$

where we have abbreviated

$$C_1 = r_1 r_2 \operatorname{cosec}^2 i \qquad \text{and} \qquad C_2 = r_1^2 \operatorname{cosec}^2 i .$$

On the other hand, the maximum fractional loss of light α_0 of the B8 star is given by

$$\alpha_0 = (1 - x_1)\alpha^U(k, p_0) + x_1 \alpha_1^D(k, p_0) = 1 - \lambda_1 + \frac{1 - \lambda_2}{Q(k, p_0)}, \tag{B}$$

where

$$Q(k, p_0) = \frac{q^U(1 - x_2)\alpha^U(k, p_0) + q^D x_2 \alpha_2^D(k, p_0)}{(1 - x_1)\alpha^U(k, p_0) + x_1 \alpha_1^D(k, p_0)}. \tag{5}$$

In these equations

$$x = \frac{2u}{3 - u},$$

and

$$q^U = k^2, \qquad q^D = \tfrac{3}{2}k^2 \Phi(k),$$

where $\Phi(k)$ is a function which had also been tabulated by Zessewitsch (II, Table 5).

Equations (A) and (B) are fundamental for the specification of orbital elements in partially eclipsing systems, and their solution may proceed as follows: Of the quantities entering in equation (B) λ_1, λ_2 are obtained directly from observations, and x_1, x_2 (resp., u_1, u_2) may be estimated from the general physical evidence. When this is done, equation (B) reduces to a relation between k and p which can be solved with the aid of appropriate tables for any of these quantities, provided that the other is known.

In the case of Algol the fractional losses of light at the moments of mid-primary and mid-secondary minima are

$$1 - \lambda_1 = 0.648 \pm 0.003, \qquad \text{and} \qquad 1 - \lambda_2 = 0.036 \pm 0.003.$$

The spectrum of the primary component is B8. That of the secondary is not accessible to direct observation; but from a comparison of its surface brightnesses in the blue and infrared Hall[14] derived a color temperature of approximately 5600°, which would correspond to an early G spectrum. At the effective wave length of 4500 A the degree of darkening of the bright star should be in the vicinity of $u_1 = 0.32$,[16] while the darkening of its companion should be practically equal to that of the sun; we adopt $u = 0.74$.[17] Hence,

$$x_1 = 0.24 \qquad \text{and} \qquad x_2 = 0.66 .$$

If the value of k as derived by Stebbins is adopted as provisional and is to be improved by successive approximations, then, to start with, we have $k = 0.85$, $q^U = 0.723$, and $q^D = 0.830$. Equation (B), solved by trial and error, then yields $p_0 = -0.448 \pm 0.005$ and $\alpha_0 = 0.695 \pm 0.003$. Thus, to a first approximation, we have

$$k = 0.85 \text{ (assumed)}, \qquad \alpha_0 = 0.695 \pm 0.003, \qquad p_0 = -0.448 \pm 0.005 .$$

[16] Cf. Kopal, *Pub. A.A.S.*, **10**, 134, 1941.

[17] Abbot, Fowle, and Aldrich, *Ann. Astr. Obs. Smithsonian Inst.*, **4**, 221, 1922.

If α represents the fractional loss of light of the B8 star at any moment during the primary minimum and l the corresponding rectified loss of light of the whole system then, evidently,

$$\alpha = \frac{1-l}{1-\lambda_1}\,\alpha_0\,, \tag{6}$$

and the values of α for any observed value of l follow immediately. The corresponding geometrical depths $p(k, \alpha)$ can then be obtained by means of tables. Since, according to Stebbins, the component eclipsed at the time of primary minimum is the smaller of the two, the p's appropriate for the adopted degree of darkening of the B8 star are found by interpolation in Zessewitsch II, Tables 7 and 8. In this way the coefficients of C_1 and C_2 in equation (A) can be evaluated for every normal point within primary minimum. If, for the purposes of numerical computations, equation (A) is re-written as

$$2C_1 + (p + p_0)C_2 = \frac{\sin^2\theta}{p - p_0} \tag{A'}$$

and the first three normals of Table 1 are omitted as unreliable on account of small divisors on the right-hand sides, equations of the type (A') for the sixteen remaining normals within Algol's primary minimum take the forms shown below.

No.	Equation	No.	Equation
4	$2C_1 - 0.800\,C_2 = 0.0657$	12	$2C_1 - 0.267\,C_2 = 0.0943$
5	$2C_1 - 0.750\,C_2 = 0.0689$	13	$2C_1 - 0.183\,C_2 = 0.0978$
6	$2C_1 - 0.709\,C_2 = 0.0719$	14	$2C_1 - 0.090\,C_2 = 0.1008$
7	$2C_1 - 0.644\,C_2 = 0.0736$	15	$2C_1 + 0.018\,C_2 = 0.1069$
8	$2C_1 - 0.575\,C_2 = 0.0758$	16	$2C_1 + 0.132\,C_2 = 0.1149$
9	$2C_1 - 0.497\,C_2 = 0.0826$	17	$2C_1 + 0.235\,C_2 = 0.1200$
10	$2C_1 - 0.405\,C_2 = 0.0868$	18	$2C_1 + 0.342\,C_2 = 0.1234$
11	$2C_1 - 0.343\,C_2 = 0.0891$	19	$2C_1 + 0.458\,C_2 = 0.1340$

They may be used as equations of condition for determining the constants C_1 and C_2 by the method of least squares. After imposing proper weights, the normal equations take the forms

$$\begin{aligned} 63.2\,C_1 - 16.695\,C_2 &= 2.5290\,, \\ - 5.4678\,C_2 &= 0.6133\,, \end{aligned}$$

and their solution yields

$$C_1 = 0.0537 \pm 0.0002\,, \qquad C_2 = 0.0518 \pm 0.0007\,;$$

hence,

$$k = \frac{C_2}{C_1} = 0.965 \pm 0.015\,.$$

Probable errors are used throughout this paper.

The resulting value of k differs significantly from Stebbins' value adopted at the outset, and the procedure is therefore to be repeated. With the new value of k, $q^v = 0.931$, and $q^p = 0.978$, equation (B) now yields

$$k = 0.965 \pm 0.015\,, \qquad \alpha_0 = 0.685 \pm 0.003\,, \qquad p_0 = -0.463 \pm 0.005\,.$$

A new set of equations of condition of the type (A') is formed exactly as above; and its solution gives

$$C_1 = 0.0540 \pm 0.0002\,, \qquad C_2 = 0.0519 \pm 0.0007\,.$$

The ratio

$$\frac{C_2}{C_1} = 0.961 \pm 0.014$$

is now practically identical with that found previously, and hence no further repetition of the iterative process is necessary. Equation (B) then yields the final set

$$k = 0.961 \pm 0.014\,, \qquad a_0 = 0.684 \pm 0.003\,, \qquad p_0 = -0.460 \pm 0.005\,,$$

which, together with the above values of C_1 and C_2, represents the solution of our problem. An inspection of successive approximations leading to it reveals that a relatively large initial change in k resulted only in a minor change in p_0 (or a_0), which shows that k in the present case depends but little on p. The convergence of the iterative process is then rapid, with the second approximation giving ample results. This is bound to be true in general for eclipses of a small bright star by a larger faint one (that is, for Algol-like systems),[18] but not necessarily so if the reverse is the case.

The conventional geometrical elements r_1, r_2, and i are then obtained from the relations

$$r_1 = \sqrt{C_2}\sin i\,, \qquad r_2 = \frac{C_1}{\sqrt{C_2}}\sin i\,, \qquad \cos i = \frac{C_1 + C_2 p_0}{\sqrt{C_2}}\,, \tag{7}$$

while the ratios of surface brightnesses J_1/J_2 and of relative luminosities of both components L_1/L_2 follow from

$$\frac{J_1}{J_2} = k^2\left(\frac{L_1}{L_2}\right) \quad \text{and} \quad \frac{L_1}{L_2} = Q(k, p_0)\frac{1-\lambda_1}{1-\lambda_2}. \tag{8.0}$$

If, consistent with our choice of the maximum brightness of a system as the unit of light, we put

$$L_1 + L_2 = 1\,,$$

the values of L_1 and L_2 follow readily. In reality, however, the total light of an eclipsing system consists of the proper luminosities of the two components plus a fraction of light of each star incident on the other and "reflected" from its surface in the direction of the line of sight. Hence the fractional luminosities, L_1, L_2, derived by means of the above formulae from the rectified intensities, λ_1 and λ_2, differ from the proper luminosity of each star by the amount of light reflected when the phase is "full." In the case of Algol and similar eclipsing systems the fraction of light of the companion reflected from the bright star is negligible compared with that of the bright star reflected from the companion; and the amount of the latter at full phase is known to be equal to twice the observed reflection constant, c_1. Hence, if the proper luminosity and surface brightness of the companion in the absence of incident radiation are denoted by asterisks, we have

$$L_2^* = L_2 - 2c_1\,, \qquad \frac{J_1}{J_2^*} = k^2\left(\frac{L_1}{L_2^*}\right); \tag{8.1}$$

and the ratio of the average surface brightness on the illuminated and dark hemispheres of the companion results,

$$\frac{J_2}{J_2^*} = \frac{L_2}{L_2 - 2c_1}\,.$$

[18] Cf. Russell, *Ap. J.*, **95**, 345, 1942.

Now, according to Stebbins and Smart, $c_1 = 0.015 \pm 0.001$. Making use of results obtained in the preceding paragraphs, we finally obtain

$$r_1 = 0.226 \pm 0.002, \quad \frac{J_1}{J_2} = 18.0 \pm 1.5, \quad L_1 = 0.943 \pm 0.005,$$
$$r^2 = 0.235 \pm 0.002, \quad L_2 = 0.057 \pm 0.005,$$
$$i = 82°.5 \pm 0°.3, \quad \frac{J_2}{J_2^*} = 2.1 \pm 0.3, \quad L_2^* = 0.027 \pm 0.005.$$

These elements differ significantly from those derived by Stebbins in 1920. They agree, however, strikingly well with elements derived in 1914 by Shapley,[19] assuming practically the same degree of darkening ($u = \frac{1}{3}$), from an analysis of Stebbins' selenium light-curve.

The probable errors of the geometrical elements r_1, r_2, and i account for all sources of observational errors, except for uncertainty in assumed degrees of darkening of the two components. The light-curves, within minima, of partially eclipsing systems (such as Algol) do not lend themselves to an empirical determination of limb darkening of the star undergoing eclipse; the differential corrections for u would result with too small a weight. It is, moreover, difficult to estimate at present the error of the assumed values; and to incorporate it in our procedure would entail considerable labor. The probable errors attached to the foregoing elements need therefore not be rigorously true but are certainly of the correct order of magnitude.

A comparison of the theoretical light-curve defined by the foregoing elements yields residuals given in the seventh column of Table 1. The probable error of a single supernormal consisting, on the average, of about 20 "sets" or "observations" is ± 0.0026 in intensity units, or $\pm 0^m.0028$ in magnitudes. The empirical probable error of an average supernormal (based on deviations from a freehand curve) is $\pm 0^m.0023$. The difference of the latter two values is hardly significant—which means that the theoretical light-curve fits the observations about as closely as it possibly can.

IV

In spite of this apparently perfect agreement between theory and observations there are weighty reasons to consider the solution of the preceding section still as a preliminary one. In the course of derivation of the above elements we assumed both components to be spherical and to appear as circular disks of fractional radii r_1 and r_2. The reality is, however, likely to be more complex. The components of an eclipsing system can be regarded as approximately spherical only if their dimensions, expressed in terms of their separation, are very small. If not, the free surfaces of the components will deviate sensibly from a sphere on account of their rotational distortion and mutual tidal action. The amount of distortion depends on the relative dimensions (fractional radii), structure, and mass ratio of the two components and is predictable on theoretical grounds as far as the axial rotation is slow and the tidal action of each star upon its mate can be regarded as that of a mass point. The photometric consequences of distortion upon light-curves of close eclipsing systems within minima have recently been investigated by the writer[13] and are now sufficiently well understood to be applied to practical cases.

Of the quantities required to specify the amount of distortion of each component in the Algol system, the relative dimensions r_1 and r_2 are, at least approximately, known from the photometric solution of the preceding section. There appears to be no way of determining the structure of the components from observations; but, unless their density concentrations are low—which is unlikely—the actual model according to which they are built up plays but a very minor role. Therefore, the only other quantity required is the mass ratio of the eclipsing system.

[19] *Ap. J.*, **40**, 221, 1914.

In view of large disparity in luminosities of both components and of the consequent absence of lines of the secondary component from the spectrum, a study of the rotational effect exhibited by the principal lines of the B8 component during primary minimum appears to be the only possible method by which, under certain conditions, an approximate value of the mass ratio can be obtained. More precisely, an interpretation of the rotational effect yields the velocity of rotation at the equator of the eclipsed star and—if rotation and revolution are in synchronism—its radius in absolute units. Since, however, the latter is a known fraction of the orbital radius and the radius of the absolute orbit of the rotating star is independently known from spectroscopic observations, the ratio of radii of the absolute and relative orbit should specify the mass ratio.

Let V_e denote the velocity at equator of the rotating star, and V_r the observed rotational effect (i.e., the deviation of observed radial velocity of the eclipsed star from simple orbital motion). Then V_e and V_r are related by

$$V_r = FV_e \sin i\,, \tag{9}$$

where F, the rotation factor, depends on the geometry of the eclipse and distribution of intensity over the disk of the eclipsed star. If the latter can be regarded as spherical and darkened at the limb to any arbitrary degree, then[20]

$$F = -\frac{\sin\theta}{\delta}\left\{\frac{(1-u)\,a_0^1 + u a_1^1}{(1-u)\,(1-a_0^0) + u\,(\frac{2}{3} - a_1^0)}\right\}, \tag{10}$$

where u denotes the coefficient of limb darkening; δ, the apparent separation of centers of the two components; and the a_n^m's are associated a-functions, depending on the geometry of the eclipse, whose explicit forms have recently been evaluated by the writer.[20] This formula for F is exact, provided that the axis of rotation of the eclipsed star is perpendicular to the orbital plane, in which case the rotational effect is symmetrical with respect to maximum eclipse.

An extensive study of the rotational effect in Algol was carried out at Ann Arbor Observatory by McLaughlin.[21] He found that a conspicuous rotational effect, attaining nearly 20 km/sec, was indeed symmetrical with respect to conjunction in 1924 (and probably in 1913), but in 1923 it exhibited a definite asymmetry. A blending of lines of the B8 star and the third body was found inadequate to account for the observed facts and was discarded by McLaughlin. The possibility, therefore, remains that the asymmetry might be due to an inclined axis of rotation. If so, the rotational effect need no longer be symmetrical with respect to conjunction nor does it necessarily disappear at mid-primary minimum. The asymmetry should, moreover, vanish and reappear periodically, as the apparent inclination of the axis of rotation of the B8 star (i.e., the projection of its true axis of rotation on the celestial sphere) oscillates in the course of its precessional motion invoked by the disturbing action of the eclipsing companion. As this explanation appears to be a promising one, it will be examined in some detail.

Since the true inclination of the axis of rotation to the orbital plane is not known a priori, it is evident that the observed rotational effect can be utilized for the determination of the equatorial velocity only at a time when it is symmetrical with respect to conjunction. McLaughlin grouped the observations of the rotational effect at phases that were free of asymmetry into eight normal points, which will serve as a basis for the present investigation. The first three columns of Table 2, giving, successively, the interval d from mid-primary minimum in fractions of a day, the observed rotational effect V_r (in km/sec), and its observational weight w, have been taken directly from McLaughlin. The fourth column gives the geometrical depth p, and the fifth to eighth columns con-

[20] Cf. Kopal, *Proc. Nat. Acad. Sci.* **28**, 133, 1942.

[21] *Michigan Obs. Pub.*, **6**, 3, 1934.

tain the numerical values of the respective associated α-functions. The ninth column gives the values of the rotation factors F, computed by means of equation (10) for one-third darkening of the B8 star, and the tenth column finally contains the resulting values of $V_e \sin i$. The intrinsic weights of the individual determinations of $V_e \sin i$ can be reasonably set proportional to the magnitude of the rotation factor itself; for the smaller the latter, the more an error inherent in the observed value of V_r is going to be magnified.

TABLE 2

ROTATIONAL EFFECT IN ALGOL

d	V_r	w	p	α_0^0	α_1^0	α_0^1	α_1^1	F	$V_e \sin i$
−0^{d}113.....	+ 7.3	3	+0.182	0.297	0.193	0.175	0.105	0.222	32.9
− .090.....	+13.0	5	− .003	.397	.276	.197	.120	.278	46.8
− .057.....	+15.5	5	− .242	.535	.388	.201	.116	.307	50.5
− .025.....	+ 7.6	3	− .411	.637	.465	.186	.104	.206	36.9
+ .060.....	−16.2	3	− .223	.524	.376	.202	.116	.309	52.4
+ .081.....	−16.7	5	− .071	.434	.304	.195	.122	.286	58.7
+ .109.....	− 9.9	3	+ .150	.314	.206	.179	.109	.232	42.7
+0.125.....	− 7.8	2	+0.283	0.246	0.152	0.159	0.090	0.188	41.5

The total weight of each value of $V_e \sin i$ should then be equal to the observational times the intrinsic weight.

A weighted mean of the individual values of $V_e \sin i$ gives 47.6 ± 1.9 km/sec. Since the preliminary photometric solution yields $\sin i = 0.9914 \pm 0.0007$, we have

$$V_e = 48 \pm 2 \text{ km/sec}.$$

If we now assume that the B8 star rotates about its axis in the same period as it revolves around the common center of gravity—an assumption probably legitimate for components describing circular orbits—this velocity of rotation at the equator of the B8 star corresponds to an absolute radius of 1,890,000 km. But the radius of the B8 star is known from the photometric solution to be 0.226 ± 0.002 times the radius of the eclipsing orbit. The latter should, therefore, amount to 8,370,000 km. On the other hand, the radius of the absolute orbit of the B8 star is, according to McLaughlin, $a \sin i$ = 1,740,000 km. These last two values lead to a mass ratio of

$$\frac{m_1}{m_2} = 3.8 \pm 0.3 .$$

If this value is accepted, the masses and absolute dimensions of the components of the eclipsing system now follow without difficulty. According to McLaughlin,

$$\frac{m_2^3 \sin^3 i}{(m_1 + m_2)^2} = 0.0256 \odot .$$

Since, very approximately, $i = 82^\circ.5 \pm 0^\circ.3$, the masses m and radii R of the two components are

$$m_1 = 2.3 \pm 0.3 \odot , \qquad R_1 = 2.7 \pm 0.2 \odot ,$$
$$m_2 = 0.61 \pm 0.08 \odot , \qquad R_2 = 2.8 \pm 0.2 \odot .$$

The bright component is a genuine main-sequence star; but the secondary appears to be a typical subgiant of very low mean density.

The above value of the mass ratio is based essentially on Ann Arbor observations of the rotational effect in 1924 when it was symmetrical with respect to the moment of conjunction. A year before, however, the effect was distinctly asymmetric. An analysis of observations from 1923 by trial and error showed that the observed asymmetry could be reproduced fairly well by an inclined axis of rotation deviating from perpendicularity to the orbital plane by approximately 15°. If this were the maximum elongation (i.e., the true inclination of the axis of rotation to the orbital plane) and the asymmetry was to disappear from 1923 to 1924, the period of precessional motion would have to be in the neighborhood of four years. This is a point which lends itself to further examination.

Unlike the solids, the fluid bodies possess no free period of precession; while the forced period differs but little from that of a rigid spheroid of the same form, provided that the precessional period of the spheroid, expressed in terms of period of its axial rotation, is large compared with the reciprocal of its ellipticity.[22] This applies to the B8 component of Algol. If we assume that it is built up according to a centrally condensed model (the actual degree of its central condensation being of very little consequence), the ratio of the period P of axial rotation to the precessional period U is

$$\frac{P}{U} = \frac{3}{4}\frac{m_2}{m_1} r_1^3 \cos\phi\,, \tag{11}$$

where ϕ denotes the deviation of the axis of rotation from perpendicularity to the orbital plane. From the foregoing analysis we have $m_2/m_1 = 0.26 \pm 0.02$, $r_1 = 0.226 \pm 0.002$, and ϕ is likely to be in the neighborhood of 15°. Therefore,

$$\frac{P}{U} = 0.0022 \pm 0.0002\,,$$

and, since P can be reasonably identified with the orbital period of 2.8673 days,

$$U = 1310 \pm 120 \text{ days} = 3.6 \pm 0.3 \text{ years}\,.$$

This demonstrates that, if the axis of rotation of the principal component of Algol is inclined to the plane of the eclipsing orbit, its apparent inclination is bound to oscillate, on account of precession, in a period of just under four years. If, therefore, the asymmetry of the rotational effect is due to this cause, we should expect it to vanish and reappear periodically from year to year. This is, indeed, what seems to be borne out by the Ann Arbor observations in 1923–24. Unfortunately, Algol never has been observed spectrographically for more than two successive seasons. But if future observations should establish that the asymmetry really appears alternately in opposite directions—which is the crucial point of the precession hypothesis—there will be little room for doubt that the precession actually takes place. The period of the precessional motion, which could be determined spectroscopically from the fluctuation of the rotational effect, may then lead to another determination of the mass ratio by means of equation (11), independently of the magnitude of the rotational effect or of the distribution of brightness on the disk of the eclipsed star.

V

Before proceeding to evaluate the actual distortion of the components of the eclipsing system of Algol and its effects upon the light-curve, let us examine more closely the observational evidence pertaining to the third body. The absence of its lines from the combined spectrum at the time of mid-primary minimum shows that its luminosity can be only a minute fraction of that of the B8 star. On the other hand, its mass must be large enough to produce the variation of radial velocity of the center of mass of the eclipsing

[22] Cf. G. H. Darwin, *Scientific Papers*, **2**, 36, Cambridge, 1908.

system, which was discovered by Belopolsky and Curtiss[23] and investigated subsequently by several writers. The following elements of the absolute orbit of the eclipsing pair around the center of gravity of the triple system have been derived by McLaughlin,[21]

$$P' = 1.873 \text{ years},$$

$$a \sin i' = 88{,}000{,}000 \text{ km},$$

and lead to a mass function

$$\frac{m_3^3 \sin^3 i'}{(m_1 + m_2 + m_3)^2} = 0.058 \odot ,$$

where m_3 stands for the mass of the third body and i' denotes the inclination of the third orbit to the celestial sphere.

The distance of Algol being about 30 parsecs, the apparent ellipse of the absolute orbit of the eclipsing system is large enough to be measurable on long-focus parallax plates. A provisional determination of the photographic orbit by Alden[24] led to $i' = 58°$. A renewed investigation, based on several hundred plates, has recently been undertaken at Sproul Observatory by A. Thomas. The writer is much indebted to Mr. Thomas for advance information that a revised value of i' comes closer to that of the eclipsing pair, being in the neighborhood of 72°. If so and if the combined mass of the eclipsing system $m_1 + m_2 = 2.9 \pm 0.3 \odot$, the above mass function yields

$$m_3 = 1.0 \pm 0.3 \odot ,$$

and the semi-major axis of the relative orbit of the third body becomes 360,000,000 km. The apparent separation of the eclipsing pair and the third body at the time of maximum elongation should then amount to 0".10. If it were not too faint, the third body should be a relatively easy object for an interferometer.

The mass of the third body comes out practically equal to that of the sun and exceeds, therefore, the mass of the secondary component of the eclipsing system. If it is a genuine main-sequence star, it should resemble the sun in luminosity, spectrum, and color. Let us therefore investigate whether the combined color of the Algol system bears this out. A thorough spectrophotometric study of Algol has recently been carried out by Hall.[14] He measured with the aid of a photoelectric photometer the differences in magnitude between Algol and β Tauri (a normal B8 star) in thirteen different wave lengths ranging from 4200 to 8660 A and found that in short wave lengths the composite color of Algol is sensibly that of a genuine B8 star; but a positive color excess, increasing toward the red, was found exactly in an amount expected by the presence of the eclipsing companion. The observations revealed, however, no trace of any further admixture of color in the combined light; or, in Hall's own words, "the spectrophotometric observations can be satisfactorily predicted from the data derived from the light curves if we assume that the third body is completely dark." This, however, cannot be literally true. If the mass can be any guide, the third body should be somewhat brighter than the eclipsing companion and of similar spectrum or color. Yet Hall's observations were accurate enough to detect the presence of such a star even if its luminosity were but one-fifth of that of the companion; and he found no trace of it.

Two alternatives can explain this result. Either the color of the third body is so similar to that of the B8 star that colors of both stars cannot be distinguished, or its luminosity is too small to produce any noticeable effect upon the color of the combined light. It is, however, unlikely that a main-sequence star of solar mass could closely match a B8 star in color. On the other hand, the latter alernative is not a priori improbable; and,

[23] *Ap. J.*, **28**, 150, 1908.

[24] *Pop. Astr.*, **60**, 30, 1924.

if true, the luminosity of the third body should be less than about one-fifth of that of the eclipsing companion. In order to find out whether or not this is compatible with their masses, let us investigate the absolute magnitudes of the individual components.

The apparent magnitude of Algol in full light is $+2^m.2$. Since the proper luminosity of the secondary component was found to be approximately 3 per cent of that of the bright star, the apparent photoelectric magnitudes of the two components become $+2^m.3$ and $+6^m.0$, respectively.[25] The trigonometric parallax of Algol given in Schlesinger's *General Catalogue of Stellar Parallaxes* is $0''.031 \pm 0''.004$, while a more recent redetermination at Sproul by Thomas[26] gave $\pi_a = 0''.033 \pm 0''.003$. This latter value leads to the following (proper) photoelectric absolute magnitudes,

$$M_1 = -0^m.1 \pm 0^m.2, \qquad M_2 = +3^m.6 \pm 0^m.2,$$

of the two components. If these are converted into absolute bolometric magnitudes, the B8 star is found to conform fairly closely to the empirical mass-luminosity law, but the secondary component becomes some 3 mag. too bright for its mass. Since its absolute magnitude seems fairly well established, this discrepancy could be lessened only by an increase of its mass, which in turn would require a mass ratio considerably in excess of 3.8. Such a value would, however, be definitely at variance with the observed rotational effect; and hence the mass of the secondary component cannot greatly exceed the value derived above. On the other hand, we may recall that overluminosity seems a common feature of subgiant components of several other eclipsing systems (U Sagittae, U Cephei, RS Canum Venaticorum, etc.), and stars are known (such as the bright component of ζ Herculis) which exhibit an excess of luminosity of a similar order of magnitude. Hence the behavior of the secondary component of Algol need not be unduly disturbing.

As to the third body, an average absolute bolometric magnitude of a main-sequence star of its mass is $+5^m.2$.[27] A considerable dispersion in this part of the mass-luminosity relation makes this value somewhat uncertain; but in the absence of any indication to the contrary we have no right to consider the luminosity of the third body to be unusual. Since its spectral type is then probably close to that of the sun, its absolute photoelectric magnitude should be in the vicinity of $+5^m.7$—which would make it nearly 6 mag. fainter than the B8 star and 2 mag. fainter than the eclipsing companion. The spectroscopic and colorimetric evidence pertaining to the third body (or rather the lack of it) is therefore compatible with its being a main-sequence star of average luminosity. If so, its brightness would amount to only about 0.004 of the combined light of Algol, which is less than the probable errors of L_1 or L_2 and can therefore be neglected. On the other hand, the third body need not necessarily be a main-sequence star. The observational evidence would be satisfied equally well if it were, for example, a subdwarf or a white dwarf or a main-sequence binary of combined mass 1.0 $\odot$—none of these possibilities can be ruled out on grounds of probability. In any of these cases the fractional luminosity of the third body would, however, be less than 0.004 and possibly less than 0.001. The conclusion seems inevitable that its luminosity is too small to be significant, and we are justified in neglecting it in the derivation of final elements of the eclipsing system.

VI

After this digression let us return to the evaluation of the effects of distortion of both components upon the light-curve of Algol within primary minimum. The approximate relative dimensions and mass ratio now being known, the form of both components can

[25] The latter value refers to the proper light of the secondary component. If the companion could actually be seen in a telescope, the reflected radiation would tend to increase its apparent brightness to $5^m.3$ near the secondary minimum.

[26] Private communication. [27] Russell and Moore, *The Masses of the Stars*, p. 112, Chicago, 1940.

be predicted theoretically, as far as terms of the order of r^5 are concerned. Let $v_{1,2}$ denote the polar flattenings of the components arising from their axial rotation with Keplerian angular velocity and $w_{1,2}(j)$ their equatorial ellipticities arising from the jth tidal harmonic distortion. If the components are supposed to be built up according to a centrally condensed model, then

$$v_{1,2}(2) = \left(1 + \frac{m_{2,1}}{m_{1,2}}\right) r_{1,2}^3 \quad \text{and} \quad w_{1,2}(j) = \frac{m_{2,1}}{m_{1,2}} r_{1,2}^{1+j}. \tag{12}$$

In the case of Algol we obtain

$$\begin{aligned} v_1(2) &= 0.015\,, & v_2(2) &= 0.062\,, \\ w_1(2) &= 0.003\,, & w_2(2) &= 0.049\,, \\ w_1(3) &= 0.0007\,, & w_2(3) &= 0.012\,, \\ w_1(4) &= 0.0002\,, & w_2(4) &= 0.003\,. \end{aligned}$$

Since the probable error of an average supernormal constituting our light-curve is close to 0.002, it is evident that quantities of the order of $w_1(2)$ or $w_2(4)$ and smaller can be neglected. The term $w_2(3)$ is probably significant, but since it would enter with a small coefficient it can also be neglected. Hence, to the order of accuracy to which we shall be working, the primary component of Algol will be regarded as a rotational spheroid flattened at the poles because of its rotation with Keplerian angular velocity and the secondary as a three-axial ellipsoid. Effects arising from the third and fourth tidal harmonic distortions will be neglected.

During eclipse of the bright star the fractional loss of light can be expressed as

$$l = 1 - fL_1\,, \tag{13.0}$$

where

$$f = \alpha^U + x_1(\alpha_1^D - \alpha^U) + R\,. \tag{13.1}$$

If both components were spherical, R would naturally vanish. If, however, the components became appreciably distorted, a difference in their polar flattenings will give the term

$$+\{v_1 - v_2\}\left(\frac{r_2}{r_1}\right)^2 I_{1,0}^0\,, \tag{14}$$

while the gravity darkening due to the rotational distortion of the primary adds

$$-\frac{c_2 v_1}{2\lambda T(1 - e^{-c_2/\lambda T})}[A_2^0 + A_0^2]\,, \tag{15}$$

where λ denotes the effective wave length, $c_2 = 1.432$ cm deg., and the tidal distortion of the eclipsing component contributes

$$+3w_2(2)\,\delta I_{-1,0}^2\,, \tag{16}$$

where $I_{\beta,\gamma}^{\alpha}$ or A_{α}^{β} denote rather complicated functions of k and p, whose explicit forms have been evaluated by the writer,[13] and δ, the apparent separation of the centers of the two components, becomes

$$\delta^2 = \sin^2\theta \sin^2 i + \cos^2 i\,.$$

Numerically, during the primary minimum of Algol

$$R = -0.052 I_{1,0}^0 - 0.022(A_2^0 + A_0^2) + 0.148\,\delta^2 I_{-1,0}^2 + \ldots\ldots \tag{17}$$

None of the three terms on the right-hand side of equation (17) causes any variation of light between minima and cannot consequently be removed by rectification. The problem therefore arises to incorporate them now in the solution for orbital elements.

In order to do so we shall follow a suggestion recently made by Russell[18] to employ the "method of false position." With the aid of elements obtained in section III under the assumption of circular disks we compute from equations (13.0), (13.1), and (17) the true theoretical light-curve, including the effects of distortion, and compare it with the observations. Let O be the observed curve and C the computed one. Construct now a new fictitious light-curve C', defined by

$$f' = a^U + x_1(a_1^D - a^U) - R, \qquad (13.2)$$

which is at every point as far below O as C is above it. From this curve derive a new set of elements by the same method as in section III. This should generally come much closer to reality than the former set was; and if R is small enough no further approximations may be necessary.

This applies to the case of Algol. In order to save unnecessary computations we are not going to employ at this stage the observed normals, but a set of fewer points com-

TABLE 3

EFFECTS OF DISTORTION

d	C	$I^2_{-1,0}$	$I^0_{1,0}$	$A^0_0+A^0_2$	R	C'
0^{d}000	0.3553	0.2454	0.1418	0.0224	−0.0073	0.3415
.025	.3838	.2446	.1365	.0242	− .0069	.3707
.050	.4582	.2420	.1221	.0284	− .0059	.4470
.075	.5578	.2368	.1015	.0322	− .0045	.5493
.100	.6652	.2278	.0783	.0334	− .0027	.6601
.125	.7709	.2133	.0551	.0304	− .0007	.7696
.150	.8646	.1908	.0336	.0220	+ .0013	.8652
.175	.9407	.1553	.0154	.0129	+ .0025	.9442
0.200	0.9908	0.0905	0.0027	0.0038	+0.0027	0.9955

puted with the aid of the provisional elements for regular intervals of time. By this we give up the possibility of reascertaining the probable errors of the elements we seek to determine; but, since R will prove to be small, the errors of the individual elements will be practically identical with those arrived at for the respective quantities in section III, and a duplication of this work seems superfluous. Table 3 will illustrate the procedure. Its successive columns indicate (1), the phase of the respective point reckoned from mid-primary minimum; (2), the intensities computed from the set of elements derived in section III without regard to distortion and practically identical with the observed light; (3), (4), and (5), the numerical values of functions associated with effects of distortion at the respective phases; (6), the combined effect of distortion, R, in intensity units, computed by means of equation (17); and (7), the fictitious light-curve, C', whose solution will yield the refined elements.

An inspection of the preceding columns shows that R has its maximum at the moment of conjunction, reaching 0^{m}008—which is a small but observationally significant amount. A closer examination reveals that throughout most part of the eclipse R is dominated by the term (14) arising from the difference in polar flattenings of both components, which effectively similates decreased limb darkening. At the beginning of eclipse the tidal distortion of the star in front tends to do the opposite, but with diminishing light its effect rapidly becomes insignificant. Term (15), representing the effect of gravity darkening due to the rotational distortion of the eclipsed star, is minor throughout.

The refined elements now follow from the solution of the fictitious light-curve C' tabulated in the seventh column of Table 3 by the method of section III. Since, according to the fictitious curve, $1 - \lambda_1 = 0.659$, the relation (B) between k and p_0 now takes the form

$$0.761 a^U(k, p_0) + 0.239 a_1^D(k, p_0) = 0.659 + \frac{0.036}{Q(k, p_0)}$$

and yields

$$k = 0.96 \text{ (assumed)}, \qquad a_0 = 0.697, \qquad p_0 = -0.480.$$

Equations of condition of the type (A′) are then formed with the aid of Zessewitsch's tables for nine points listed in Table 3 in exactly the same manner as in section III. Since these points now do not correspond to the observed normals, the solution of the resulting set of equations need not be performed by the method of least squares. We find it more convenient merely to divide the equations into two groups of approximately equal weights and form the "normal" equations by addition. Solving them, we obtain

$$C_1 = 0.0532, \qquad C_2 = 0.0488,$$

and, in consequence,

$$\begin{aligned} k &= 0.92, & r_1 &= 0.219, & L_1 &= 0.938, \\ a_0 &= 0.695, & r_2 &= 0.238, & L_2 &= 0.062, \\ p_0 &= -0.465, & i &= 82^\circ.1, & L_2^* &= 0.032. \end{aligned}$$

The uncertainty of these elements should be practically equal to that of the respective quantities in section III. The final elements thus differ slightly, yet significantly, from those obtained previously under the assumption of circular disks.

Since at this stage we no longer regard both components as spheres, the fractional radii r_1 and r_2 require redefinition. A little consideration shows that these quantities as determined from observations are, in fact, effectively equal to the geometric means of the polar and diametral semi-axes of the distorted components. If $a > b > c$ denote the semi-axes of the actual ellipsoids, then the ellipticities v and w of their different cross-sections, evaluated above, lead to

$$\begin{aligned} a_1 &= 0.220 \pm 0.002, & a_2 &= 0.261 \pm 0.002, \\ b_1 &= 0.220 \pm 0.002, & b_2 &= 0.241 \pm 0.002, \\ c_1 &= 0.218 \pm 0.002, & c_2 &= 0.235 \pm 0.002, \end{aligned}$$

and to the mean densities of the two components

$$\bar{\rho}_1 = \frac{0.01344}{a_1 b_1 c_1 P^2} \frac{m_1}{m_1 + m_2} \odot = 0.123 \pm 0.004 \odot,$$

$$\bar{\rho}_2 = \frac{0.01344}{a_2 b_2 c_2 P^2} \frac{m_2}{m_1 + m_2} \odot = 0.023 \pm 0.002 \odot.$$

On the basis of the final set of elements a new theoretical light-curve has been computed, including the effects of distortion, and compared with the observed normals. The eighth column of Table 1 gives the final residuals. The resulting fit is good; but, as the reader may easily verify, a transition from spherical to distorted components has scarcely diminished the residuals. Similar agreement could, however, probably have been obtained by forcing through the observed normals a theoretical light-curve based on a different set of elements derived under the assumption of uniformly bright disks. The consideration of distortion, like that of limb darkening, is manifestly not prompted by a

discrepancy between theory and observations but by its intrinsic reasonableness. In eclipsing systems like Algol, spherical components, like uniform disks, constitute a model which might formally represent a light-curve but which is physically inadmissible, and the elements it leads to cannot therefore correspond to reality.

VII

The investigation of the light-curve of Algol within minima now being complete, we shall find whether or not the changes of light between eclipses, isolated in section II, are consistent with the above model. In section II we found, that, between minima,

$$l = 1 - c_1 \cos\theta - c_2 \cos^2\theta - \ldots ,$$

where $c_1 = 0.015 \pm 0.001$ and c_2 is probably too small to be reliably determined.

As is well known, c_1 measures the difference of light falling on each component from its mate and re-radiated in the direction of the line of sight. Provided that this "reflected" radiation is of black-body quality, the theory yields[28]

$$c_1 = L_1\left(\frac{T_1}{T_2}\right)^4\frac{J_2}{J_1}\left\{\tfrac{1}{3}r_2^2+\tfrac{1}{4}r_2^3+\ldots\right\}\sin i - L_2\left(\frac{T_2}{T_1}\right)^4\frac{J_1}{J_2}\left\{\tfrac{1}{3}r_1^2+\tfrac{1}{4}r_1^3+\ldots\right\}\sin i , \quad (18)$$

where the temperatures and surface brightnesses of both components refer naturally to the illuminated hemispheres. Of the quantities entering on the right-hand side of equation (18) the ratio of effective temperatures, T_1/T_2, appears to be least accurately known from the observations; and the idea suggests itself to utilize equation (18) for determining it. Equation (18) is quadratic in $(T_1/T_2)^4$; with its left-hand side directly known from observations and with the coefficients of $(T_1/T_2)^4$ expressible in terms of quantities which have already been determined, it can be solved at once and yields $T_1/T_2 = 1.92$.

The effective temperature T_1 of the B8 component now follows directly from the known parallax and the absolute dimensions. The bolometric correction for a B8 star being approximately -1^m1,[29] we obtain $T_1 = 13{,}000° \pm 800°$, with an error about equally divided between the uncertainty in absolute bolometric magnitude (i.e., of the parallax and bolometric correction) and the uncertainty in radius. Hence the mean effective temperature of the illuminated hemisphere of the secondary component, as derived from the reflection effect, gives $T_2 = 6800°$. Another way of determining T_2, still under the assumption of black-body radiation, is from the ratio of surface brightnesses using Planck's formula. The observed value of J_1/J_2 referring to the illuminated hemispheres is 18.0 ± 1.5 and leads to $T_2 = 6500°$, which agrees satisfactorily with the value previously obtained. The observed reflection constant is therefore consistent with the rectified depths of both minima and the elements derived therefrom.

The mean temperature of the dark hemisphere of the secondary component, which is its proper temperature, is considerably lower. The ratio of surface brightnesses of the dark hemispheres $J_1/J_2^* = 35 \pm 3$ leads to $T_2^* = 5500°$. The radiation of the B8 star incident upon the secondary component thus increases the mean temperature of its illuminated hemisphere by approximately 1000°.

As to the ellipticity constant, an observed value of c_2 is known to represent the net outcome of two different effects—one due to the ellipticity proper, the other to reflection—which are of opposite signs and tend to cancel. The distortion of the components invokes a term varying as $\cos^2\theta$ of the form

$$-(z_1L_1 + z_2L_2^*)\sin^2 i , \quad (19.0)$$

[28] Cf. Kopal, *Ann. New York Acad. Sci.*, **41**, 13, 1941.

[29] Kuiper, *Ap. J.*, **88**, 429, 1938.

where $z_{1,2}$, the photometric ellipticities of individual components built up according to a centrally condensed model and radiating like black bodies, are given by[13]

$$z_i = \frac{3(15+u)}{10(3-u)} \left\{ 1 + \frac{c_2}{4\lambda T(1-e^{-c_2/\lambda T})} \right\} \frac{m_j}{m_i} r_i^3 + \ldots . \qquad (19.1)$$

The ellipticities of the two components, weighted in proportion to their proper luminosities, represent the mean ellipticity of a system. On the other hand, the reflection effect also generates a term varying as $\cos^2 \theta$, of the form

$$+ \sum_{i=1}^{2} L_i \left\{ \frac{1}{3\pi} r_j^2 + \tfrac{3}{8} r_j^3 + \frac{3}{2\pi} r_j^4 + \ldots . \right\} \left(\frac{T_i}{T_j} \right)^4 \frac{J_j}{J_i} \sin i , \qquad (20)$$

which is of opposite sign from the photometric ellipticity and therefore tends to mask it.

Now, in the case of Algol, the elements obtained above lead to $z_1 = 0.008 \pm 0.001$, $z_2 = 0.229 \pm 0.023$, and hence

$$(z_1 L_1 + z_2 L_2) \sin^2 i = 0.015 \pm 0.003 .$$

As could have been anticipated, the photometric ellipticity of the smaller and massive B8 component is minute. The ellipticity of the companion is conspicuous; but, since its luminosity is small, it impresses but a small effect on Algol's combined light. Nevertheless, the mean ellipticity of Algol would still be appreciable, were it not masked almost entirely by the reflection effect; for the term (20), due to reflection, is found to assume a numerical value of 0.012 ± 0.004; and, since it is of an opposite sign than the ellipticity proper, we should expect

$$c_2 = 0.015 \pm 0.003 - 0.012 \pm 0.004 = 0.003 \pm 0.005 .$$

The error of the ellipticity proper is about equally divided between the uncertainty of the fractional radii and of the mass ratio, while the error of the correction for reflection depends predominantly upon the uncertainty of the ratio of temperatures. If, as in the case of Algol, the temperatures of both components differ widely, this latter correction cannot be determined with sufficient accuracy, and hence the ellipticity proper cannot be satisfactorily isolated. The observed values of c_2 are 0.014 ± 0.003 (Stebbins) and 0.003 ± 0.002 (Smart). The theory thus favors definitely a value as small as Smart's and justifies our neglect of the ellipticity at earlier stages of the orbital analysis.

VIII

The present investigation of the system of Algol is now complete. The individual results are, however, scattered over various parts of the preceding sections so that it seems advisable to collect them in the following tabulation.

ELEMENTS OF THE ECLIPSING ORBIT

Mean observed period of the eclipsing system	$P = 2^d.86731$
Eccentricity of the eclipsing orbit (photometric)	$e < 0.01$
Ratio of radii of the two components	$k = 0.92 \pm 0.01$
Fractional loss of light of the B8 star at mid-primary minimum	$a_0 = 0.695 \pm 0.003$
Inclination of the orbital plane	$i = 82°.1 \pm 0°.3$
Ratio of surface brightnesses of illuminated hemispheres of both components at 4500 A	$J_1/J_2 = 18.0 \pm 1.5$
Ratio of proper surface brightnesses (dark hemispheres)	$J_1/J_2^* = 35 \pm 3$
Velocity of rotation at the equator of the B8 star	$V_e = 48 \pm 2$ km/sec
Mass ratio	$m_1/m_2 = 3.8 \pm 0.3$
Semi-major axis of the relative orbit	$a_1 + a_2 = 8{,}400{,}000$ km
Parallax of Algol (Thomas)	$\pi = 0''.033 \pm 0''.003$

		Primary	Secondary
Spectrum		B8	(G)
Degree of limb darkening at the effective wave length of 4500 A (assumed)	u	0.32	0.74
Longest semi-axis	a	0.220 ± 0.002	0.261 ± 0.002
Diametral semi-axis	b	0.220 ± 0.002	0.241 ± 0.002
Polar semi-axis	c	0.218 ± 0.002	0.235 ± 0.002
Longest semi-axis in solar units	R	2.7 ± 0.2 ⊙	2.8 ± 0.2 ⊙
Fractional luminosity (freed from reflected light)	L^*	0.938 ± 0.005	0.032 ± 0.005
Effective temperature (proper)	T^*	13,300° ± 800°	5500°
Effective temperature of illuminated hemisphere	T	.....	6500°
Photoelectric absolute magnitude	M	$-0^m1 \pm 0^m2$	$+3^m6 \pm 0^m2$
Mass	m	2.3 ± 0.3 ⊙	0.61 ± 0.08 ⊙
Mean density	$\bar{\rho}$	0.123 ± 0.004 ⊙	0.023 ± 0.002 ⊙

ELEMENTS OF THE THIRD ORBIT

Period	1.873 years
Eccentricity of the orbit	0.26
Inclination (provisional value communicated by Thomas)	72°
Mass	1.0 ± 0.3 ⊙
Semi-major axis of the relative orbit	360,000,000 km
Apparent separation at maximum elongation	0".10

The uncertainty, whenever given, approximates the probable errors of the respective quantities.

The observed mean period of the eclipsing system is 2.86731 days. Since the triple system as a whole is receding from us at present with a velocity of approximately 5 km/sec, the true period is shorter by 4 seconds. The light-curve of Algol with minima is symmetrical, and there is no evidence of displacement of the secondary minimum compatible with an orbital eccentricity exceeding 0.01. The first contact of the eclipse occurs at the phase $\theta = 26°.1 \pm 0°.2$, or $0^d208 \pm 0^d002$ before the moment of conjunction. The whole eclipse lasts, therefore, 10 hours ± 5 minutes.

The masses and absolute dimensions of components of the eclipsing system appear to be quite normal. The B8 component appears slightly above the empirical mass-luminosity law, and the secondary—a typical low-density subgiant—is much too luminous and actually brighter than the third body, which is almost certainly more massive than the eclipsing companion. The third body must, however, possess only an average luminosity for its mass if it is to be a main-sequence star, for otherwise it could not have escaped observations.

It is of interest, in this connection, to compare the properties of the three stars as shown in the accompanying table. All three stars exhibit practically the same spectra

Star	Spectrum	Abs. Vis. Mag.	Mass	Authority
WW Draconis A	G2	$+3^m2$	4.0 ⊙	Joy, *Ap. J.*, **94**, 407, 1941
ζ Herculis A	G0	+3.3	0.86	Van de Kamp, *A.J.*, **47**, 168, 1938
Algol B	(G)	+3.1	0.61	Present investigation

and absolute magnitudes, but their masses range from 0.6 to 4.0 ⊙. Their deviations from an empirical mass-luminosity law are naturally conspicuous; and it is disconcerting to note that the number of similar stars has in recent years exhibited a tendency to increase.

In conclusion, it may be pointed out that the present investigation was not intended to deal exhaustively with every aspect of the observational evidence pertaining to Algol; and some rather puzzling phenomena will require further study. Thus the radial velocity of the center of mass of the triple system is probably not constant and appears at present to be slowly increasing.[21] A serious and thus far unexplained discrepancy exists between the values of the parallax derived from observations in right ascension and declination.[26] Finally, the orbital period of the eclipsing system has long been known to exhibit periodic variations of very complex nature which have defied explanation. Until these problems are disposed of, it cannot be denied that the system of Algol conceals still more unexpected information than we have been able to decipher.

In conclusion, the writer takes pleasure in expressing his sincere thanks to Dr. Harlow Shapley for stimulating interest and valuable suggestions.

HARVARD COLLEGE OBSERVATORY
August 1942

THE TOTAL LIGHT OF THE SOLAR CORONA OF SEPTEMBER 21, 1941

Y. C. Chang and K. T. Li

ABSTRACT

The total light of the corona was measured with a Weston exposuremeter. By comparison with measurements on the full moon a fortnight later, it was found that the ratio of corona to full moon was 0.39.

The total light of the solar corona of September 21, 1941, was compared with that of the full moon a fortnight later by means of a Weston exposuremeter. The choice of an exposuremeter for this purpose was simply because it happened to be the only apparatus we could get hold of during the war.

The Weston exposuremeter is not sensitive enough to give any noticeable deflection when directed toward the full moon. We increased its sensitivity by: (1) placing the photocell of the exposuremeter in the focus of a camera with an objective 9 cm in aperture and 33 cm in focal length, (2) by connecting the photocell directly to a Leeds and Northrup galvanometer of high sensitivity, and (3) by placing the telescope and scale to be used with the galvanometer at a distance of about 6 meters so as to obtain a larger deflection reading.

TABLE 1*a*

CALIBRATION OF THE EXPOSUREMETER

Lamp I	Dark	Deflection	Shunt	Distance	Intensity	Lamp I	Dark	Deflection	Shunt	Distance	Intensity
9°.80	8°.85	0°.95	1	291 cm	12	10°.80	9°.05	1°.75	1	191 cm	28
9.80	8.90	0.90	1	291	12	15.00	9.05	5.95	1	118	72
10.85	9.05	1.80	1	191	28	15.00	9.05	5.95	1	118	72

TABLE 1*b*

Lamp II	Dark	Deflection	Shunt	Distance	Intensity	Lamp II	Dark	Deflection	Shunt	Distance	Intensity
15°.05	15°.90	0°.85	10	389 cm	6.6	14°.85	15°.70	0°.85	100	151 cm	44
15.10	15.95	0.85	10	389	6.6	14.85	15.70	0.85	100	151	44
7.50	15.55	8.05	10	151	44	13.75	15.95	2.20	100	102	96
7.35	15.65	8.30	10	151	44	13.75	15.95	2.20	100	102	96
−7.40	15.80	23.20	10	92	118	13.20	15.80	2.60	100	92	118
−7.35	15.80	23.15	10	92	118	13.20	15.80	2.60	100	92	118

In order that this arrangement may be used to measure a wide range of light intensities, two diaphragms of 8.66-cm and 0.493-cm aperture are introduced in front of the camera lens. Furthermore, a universal shunt is connected in parallel to the galvanometer so that the fraction of the total photocurrent going through the galvanometer may be varied at will. The exposuremeter then measures the light of the unobstructed sun, as well as that of the corona during totality.

We made the following calibration to test how the galvanometer deflection varies with light intensity. A small incandescent lamp was placed at different distances from the exposuremeter and the deflections of the galvanometer were recorded. The aperture was 8.66 cm.

TABLE 2

MEASURES OF SOLAR INTENSITY BEFORE AND AFTER TOTALITY

Time	Deflection	Shunt and Aperture	Reduced Deflection	Log. of Reduced Deflection
	Before Totality			
$8^h 32^m5$	8.6	Shunt 100	2.75×10^5	5.44
8 41.5	8.2	Aper. 0.49	2.62	5.42
8 50.9	8.3		2.66	5.42
9 1.1	8.4		2.69	5.43
9 12.9	8.5		2.72	5.43
9 21.8	7.6		2.43	5.39
9 28.5	8.3		2.66	5.42
9 33.1	7.5		2.40	5.38
9 36.2	8.1		2.59	5.41
9 40.5	7.4		2.37	5.37
9 45.8	7.6		2.43	5.39
9 51.8	7.9		2.53	5.40
9 55.6	7.3		2.34	5.37
10 0.6	6.8		2.18	5.34
10 5.6	6.3		2.02	5.31
10 10.0	6.3		2.02	5.31
10 15.2	5.7		1.82	5.26
10 20.4	4.8		1.54	5.19
10 27.2	4.1		1.31	5.12
10 30.6	3.3		1.06×10^5	5.03
10 35.0	2.7		8.65×10^4	4.94
10 39.7	22.4	Shunt 10	7.80	4.89
10 41.7	18.0		6.26	4.80
10 44.3	15.6		5.43	4.74
10 48.0	10.3		3.58	4.55
10 49.3	7.6		2.64	4.42
	After Totality			
11 0.6	13.4	Shunt 10	4.66	4.67
11 3.5	20.8		7.25	4.86
11 7.7	2.8	Shunt 100	8.95	4.95
11 11.3	2.8		8.95×10^4	4.95
11 15.4	3.4		1.09×10^5	5.04
11 21.7	3.5		1.12	5.05
11 22.4	4.5		1.44	5.16
11 25.7	4.2		1.34	5.13
11 30.7	5.1		1.63	5.21
11 36.0	5.6		1.79	5.25
11 41.2	4.9		1.57	5.20
11 46.2	6.5		2.08	5.32
11 55.8	7.1		2.27	5.36
11 56.9	7.1		2.27	5.36
12 0.6	7.2		2.30	5.36
12 6.4	7.4		2.36	5.37
12 10.9	7.4		2.36	5.37
12 15.8	7.4		2.36	5.36
12 21.7	7.2		2.30	5.36
12 31.4	7.7		2.46	5.39
12 41.6	7.6		2.43	5.39
12 52.4	7.2		2.30	5.36
13 1.2	7.3		2.34×10^5	5.37

In Table 1*a* and *b*, the columns from left to right give the galvanometer reading when measuring the lamp intensity, the zero reading, the deflection produced, the shunt reading, the distance from exposuremeter to lamp, the intensity denoted by 1,000,000/(distance)^2. When this intensity is plotted against deflection even from the few points a linear relationship is evident.

The exposuremeter with its camera was mounted on a Zeiss altazimuth telescope with the optical axes parallel to each other. This arrangement enabled the observer to point the exposuremeter quickly at any celestial body. Our observing station was located at Lintao, Kansu (longitude, 103°52′14″ E.; latitude, 30°22′33″ N.). The times of contact (Standard Time for longitude 105° E.) are given below:

	Observed	Calculated	O−C		Observed	Calculated	O−C
First contact...	$9^h29^m42^s.1$	$9^h29^m32^s.3$	$+9^s.8$	Third contact.	$10^h53^m38^s.8$	$10^h53^m37^s.6$	$+1^s.2$
Second contact.	10 50 36.6	10 50 38.0	−1.4	Last contact..	12 18 36.0	12 18 31.0	−5.0

The observation began 1 hour before the first contact and stopped 1 hour after the last contact. Observations were made at intervals of a few minutes, except during totality when we tried to get as many determinations as possible. Zero readings of the galvanometer were also determined by pointing the exposuremeter at the sky 8° from the sun. On account of the slow damping of the suspended mirror, the number of observations at the time of totality could not be further increased. The results of the observations are given in Tables 2 and 3.

TABLE 3

MEASURES OF CORONA DURING TOTALITY

	Reading	Deflection	Log (Deflection)		Reading	Deflection	Log (Deflection)
Dark.....	2.3			Sky.....	2.7		
Corona.....	4.2	1.7	0.23	Corona.....	4.3	1.7	0.23
Sky.....	2.7			Dark.....	2.6		
Corona.....	4.4	1.7	.23				

Under the column of reduced deflection we put down the value which the deflection would have if shunt 1 and aperture 8.66 cm were employed. These values of shunt and aperture were used in the observations of the corona.

Figure 1 shows the variation of illumination during the eclipse of September 21, 1941;

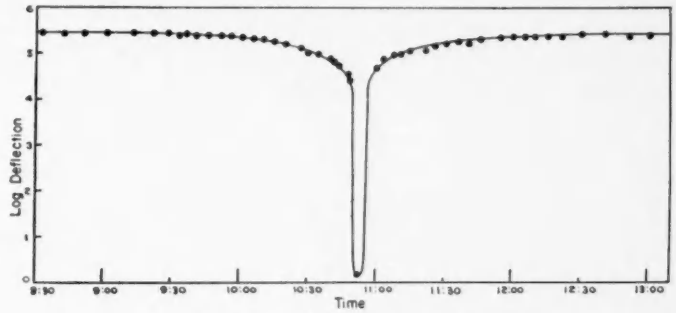

FIG. 1.—Illumination during the eclipse, September 21, 1941

in it the logarithm of the deflection is plotted against time. Near the minimum the curve is not accurate, owing to the small number of observations.

On account of unfavorable weather, we were not able to observe the full moon before the eclipse at Lintao. Such observations were made a fortnight afterward, on our return to Langchow, about 110 km to the north of Lintao. The measures are given in Table 4.

TABLE 4

MEASURES OF FULL MOON ON OCTOBER 5, 1941

Time	Zero Reading	Moon	Sky	Deflection	Mean	Time	Zero Reading	Moon	Sky	Deflection	Mean
8^h23^m	14.8	10.7	14.8	4.1		9^h21^m	16.0	11.4	16.0	4.6	
8 24	14.9	10.7	14.9	4.2		9 22	16.0	11.5	16.0	4.5	4.58
8 24	15.0	11.1	15.0	3.9	4.04	9 23	16.0	11.5	16.0	4.5	
8 25	14.9	10.9	14.9	4.0		9 24	16.0	11.4	16.0	4.6	
8 26	15.0	11.0	15.0	4.0		Average					4.31
9 20	16.0	11.3	16.0	4.7							

The moon was observed at about 3° from the antisolar point. The properties of the exposuremeter and galvanometer were checked by the same incandescent lamp and at the same amperage as used at Lintao. It was found that, if the instruments suffered any deterioration during this interval, the variation would amount to 10 per cent at the most. Comparing the average deflection due to the moon (4.31) with that due to the corona (1.7), we conclude that the total light of the corona at this eclipse was 0.39 times that of full moon.

NATIONAL INSTITUTE OF ASTRONOMY
KUNMING, CHINA
May 1942

THE COMPOSITE SPECTRUM OF ζ TAURI

J. A. HYNEK AND O. STRUVE

ABSTRACT

Radial velocities from one hundred plates taken at the Yerkes and Perkins observatories show marked changes from cycle to cycle for any one line and from line to line within each cycle. There is a disturbance in the smooth velocity-curves (referred to as secondary variation) at phase 75 days, where the smooth curves would cross the gamma axis from positive to negative values. This disturbance shows secular changes. The rotational velocities of the lines suggest stratification in the shell which surrounds the star. The radius of the largest shell is about 10^{12} cm, while the semimajor axis of the orbit is about 10^{13} cm, if the smooth velocity-curve is interpreted in terms of binary motion. It is suggested that prominence action near that point of the shell which is directed toward the invisible companion accounts for the secondary variation of the curves at phase 75 days.

When the spectrum of ζ Tauri (B4ne, $\alpha = 5^h32^m$, $\delta = 21°05'$, 1900), which contains both extremely sharp and extremely wide lines, was first systematically observed, the evidence seemed to be strong that the velocity-curve indicated simple orbital motion. From measures of the sharp line $H\gamma$ Adams[1] obtained reasonable elements for the system; but, when later Miss Losh[2] made a thorough examination of the Michigan plates of this star, she showed plainly that more than orbital motion was involved, though the constancy of the period and the reported 180° out-of-phase behavior of the helium velocities made it feasible to keep the binary hypothesis. Thus, in the classification of composite spectra attempted by one of the authors several years ago,[3] the best that could be done with this star was to state: "Class II (spectroscopic binary with two spectra) and probably also Class VI (composite spectrum arising from peculiar conditions in one body)." This unsatisfactory and contradictory classification led to the present investigation.

ζ Tauri belongs to the growing list of shell or envelope stars, along with 17 Leporis, ϕ Persei, 25 Orionis, and many others. Two stars of this list, ϕ Persei and ζ Tauri, have often been cited as equivalent examples of the shell phenomena; yet detailed investigation by the writers has shown that the observed differences in behavior are very marked, although it is, of course, probable that the physical interpretations of the two stars will be similar.

It may be helpful to compare ζ Tauri and ϕ Persei to clarify the present problem. Their spectral classes are similar, in so far as a classification is possible, B4ne and B0ne, respectively; their periods are constant, 132^d91 and 126^d67, respectively. It is hardly a coincidence that in Merrill's[4] recent list of early-type binaries with periods greater than 50 days these two stars appear side by side if the material is arranged in order of period. Both spectra contain sharp as well as broad Balmer absorption lines and emission features, and both indicate an underlying, rapidly rotating photosphere with reversing layer and above it an extensive shell giving rise to the emission and the sharp Balmer absorption lines. Here, however, the similarity ends. ζ Tauri varies from cycle to cycle in the velocity of the shell lines and in the number and intensity of the shell lines present. It is impossible to state with any certainty what the true mean velocity-curve is for even the remarkably sharp Balmer lines. The amplitudes and the range of the velocity-curve vary secularly; yet the period of variation is constant within the limits of observation.

In ϕ Persei the lines vary to a far greater degree, both in velocity and in intensity, but they are strictly periodic within the limits of observation. This characteristic is most marked in the emission features; the V/R variation is pronounced and periodic, while in

[1] *Ap. J.*, **22**, 115, 1905.

[2] *Pub. Univ. Michigan Obs.*, **4**, 1, 1931.

[3] Hynek, *Contr. Perkins Obs.*, No. 10, 1938.

[4] *Ap. J.*, **95**, 269, 1942.

ζ Tauri the Balmer emission is entirely secular in its intensity variation. In ϕ Persei the shell lines undergo a marked periodic broadening, and their velocity has a constant over-all period and repeats itself strictly periodically except during the broad-line phase.

The helium velocities are in phase with the Balmer velocities in ζ Tauri and out of phase in ϕ Persei, except that those helium lines which arise from metastable levels are in phase in both stars. In ϕ Persei, further, the nonmetastable helium lines vary greatly in intensity during the period, while in ζ Tauri no variation has been detected. Both stars show sharp helium lines arising from metastable levels, but they undergo no measurable periodic variation in ζ Tauri, while they broaden very perceptibly at certain phases in ϕ Persei.

OBSERVATIONAL MATERIAL AND REDUCTIONS

A series of one hundred Eastman Process plates were taken, some at the Yerkes Observatory with the Bruce spectrograph attached to the 40-inch refractor and the rest at the Perkins Observatory with the two-prism spectrograph attached to the 69-inch reflector. The dispersions were similar (about 30 A/mm at $H\gamma$), and enough overlapping plates were obtained to reduce the Bruce plates to the Perkins system, which was arbitrarily adopted as standard. The measures were made by Mr. Hynek. To check the personal equation Mr. Struve independently measured some twenty-five Yerkes and Perkins plates, with the gratifying result: Struve-Hynek = 0.03 km/sec. In order to establish the reality of the small changes in velocity from cycle to cycle it was necessary to give special attention to the probable errors of the normal places used in the velocity-curves.

Table 1 lists the plates used. A number of fast-emulsion plates were included, because the means of several such plates taken in rapid succession were found to give Balmer velocities of a high order of accuracy. The plates were limited to the photographic region except for a number taken to check the emission at $H\alpha$. The dispersion in the red is so small that velocity measures would not be comparable to those made in the photographic region. The first column gives the plate numbers, Y designating a Yerkes plate and P a Perkins plate; the second column gives the Julian date of mid-exposure, and the third column gives the cycle designation and the phase of the plate. A period of $132^d.91$ was assumed, which has satisfied observations over the last forty years, and the epoch of the estimated time of zero relative velocity for the first cycle observed by Adams was taken as JD 2415754.00. Numbering the cycles successively since that epoch and, for the sake of convenience, calling the one hundred and first cycle A, the proper designations are found in the third column. The observations by Adams cover the first ten cycles incompletely, while the Michigan observations used by Miss Losh and by Baldwin[5] cover a part of cycle 36 in 1914, a part of cycle 53, cycles 59–62 and 66–70, but not completely. The majority of the present plates cover cycles G, H, and J (107, 108, and 110). Since secular variations prevent the lumping-together of cycles in the discussion of this star, it is suggested that this method of numbering be followed in the future until a definite period is obtained.

By comparing the hydrogen velocity-curves derived by Adams[1] and Miss Losh[2] with that given in the present work (Fig. 2), the over-all period appears to be constant, $P = 132.91$ days—a value close to that given by Miss Losh ($133^d.0$). Because of the secular variations in the curve it is impossible to regard this value as definitive. The constancy of the period seems to be well established.

A typical spectrogram of ζ Tauri is shown in Plate XXIII. The most prominent features are the sharp Balmer lines, which must arise in the shell. Emission is present at $H\alpha$ and $H\beta$. The underlying Balmer lines are extremely wide and weak, but the sharp Balmer lines have been measured to $H32$ by Miss Losh.[2] Next in order of prominence are the

[5] *Ap. J.*, **93**, 420, 1941.

PLATE XXIII

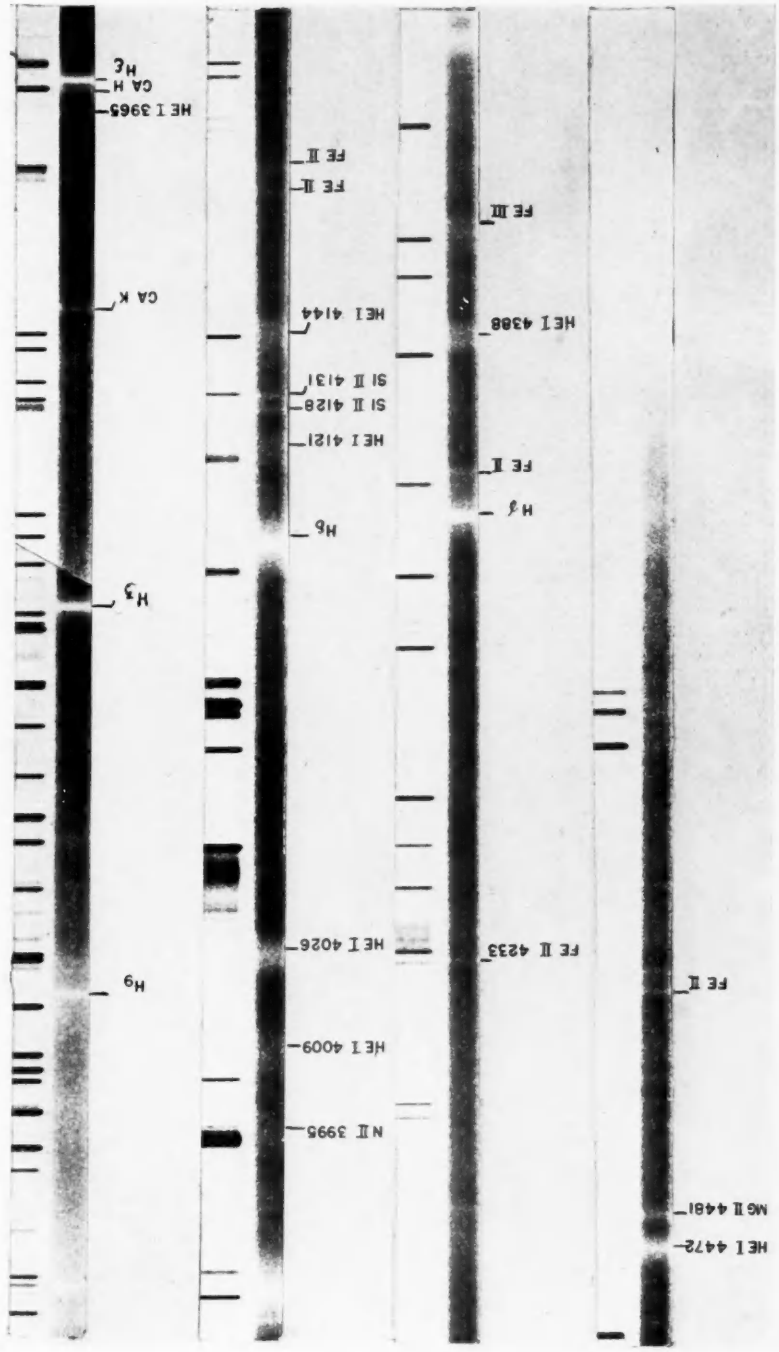

THE SPECTRUM OF ζ TAURI ON JAN. 22, 1941

TABLE 1

RADIAL VELOCITIES OF ζ TAURI

Plate No.	JD 24+	Phase	Wt.	*H*	*Ca* II K	*He* I 3965	*He* I 4026 4471	*Si* II 4128 4130	*He* I 4144	*Fe* II 4173 4179	*Fe* II 4233 4352	*Mg* II 4481
Y 12253	28798.0	99 18.9	a	+30.3	+19.0	+29.2	+14.8	+35.0	+19.5	+24.6*	+41.8	+27.6
Y 12313	29154.9	A 109.9	b	17.8	.....	.....	+21.6*	.....	.....	+ 4.3	.....	+14.3
Y 12320	29185.8	B 8.0	a	24.0	+22.2	+26.8	+28.6	+18.9	+18.1	+16.1*	+33.6	+14.1
Y 12325	29199.0	B 21.2	a	25.4	.....	+35.6	+21.2	+27.4	+23.4	+24.4	+40.0	+19.2
Y 12381	29885.9	G 43.4	b	29.9	.....	.....	+38.6	+27.8	+70.2	+25.4*	+19.4	+35.1
Y 12385	29892.8	G 50.4	b	29.0	.....	+44.9	+41.7	+21.9	+67.4	+15.1	+26.7	+14.4
P 370	29893.9	G 51.4	a	26.2	+21.3	.....	+ 3.2	+31.1	.....	+33.4	+31.4	+24.9
P 371	29893.9	G 51.4	b	28.6	.....	.....	+37.9*	+24.3	.....	+32.6	.....	+15.0
Y 12397	29893.9	G 51.4	b	24.4	.....	.....	+ 4.8	+23.2	+ 8.8	.....	+37.4*	+41.2
Y 12398	29894.0	G 51.5	a	27.5	.....	.....	− 2.1	+29.6	+30.3	+26.8	+34.1	+18.9
Y 12410	29894.8	G 52.3	a	27.2	.....	+18.4	+15.6	+23.5	− 1.4	+16.0	+43.6	+26.3
Y 12423	29895.9	G 53.4	a	27.3	.....	+19.8	+ 8.4	+17.2	+23.8	+15.2*	+34.4	+22.2
P 390	29899.9	G 57.4	a	24.4	+31.6	+26.2	+ 9.3	+16.0	+84.7	+16.1	+19.5	+39.4
Y 12441	29904.8	G 62.3	a	22.5	.....	.....	−25.7	+29.6	+27.5	+ 9.2	+24.2	+ 9.5
Y 12442	29904.9	G 62.4	a	23.4	+23.1	+27.4	− 6.3	+27.3	+10.0	− 4.9	+26.1	+18.7
†P 409	29905.8	G 63.3	b	19.0	.....	.....	+ 5.0*	.....	.....	.....	.....	+13.3
P 416	29910.9	G 68.4	a	15.2	+17.1	+14.8	− 3.4	+12.1	+51.6	+15.0	+22.3	− 5.8
P 451	29919.8	G 77.3	a	15.8	+14.3	+24.7	−21.6	+19.3	+17.6	+25.4	+27.9	+ 5.1
P 452	29919.8	G 77.3	a	18.5	+16.7	+ 8.5	+ 0.6	+13.9	+20.5	.....	+35.4	−15.0
†P 454	29919.9	G 77.4	b	17.3	+20.4	.....	+ 3.8	.....	.....	.....	.....	.....
P 461	29924.8	G 82.3	a	18.4	+20.9	+23.6	+ 7.2	+15.8	+26.3	+20.5*	+16.8	+13.0
Y 12449	29925.8	G 83.3	a	17.2	+ 5.9	+ 6.8	− 9.1	+27.1	+ 3.2	+ 3.4*	+15.3	+16.0
Y 12454	29926.8	G 84.3	b	15.4	+22.2	+14.6	+12.4	+10.6	+25.9	.....	+10.2*	+ 9.6
P 470	29932.9	G 90.4	a	15.9	+ 9.6	+25.4	+ 6.9	+16.7	+50.3	+ 7.1*	+ 3.7*	+ 4.1
P 476	29933.9	G 91.4	a	15.2	+16.0	+13.7	−15.7	+15.2	+21.7	+16.0*	+31.0	+ 7.3
Y 12458	29936.8	G 94.3	a	16.9	.....	+ 7.1	− 6.6	+10.6	+10.3	.....	+33.2	+ 0.3
Y 12459	29936.9	G 94.4	a	15.4	+14.2	+ 2.2	+ 5.4	+12.7	− 2.1	− 4.1*	+19.6	+ 3.5
Y 12465	29937.8	G 95.3	a	13.6	+18.4	− 1.3	−11.8	+19.6	− 2.5	− 0.1*	+14.4	+17.9
P 487	29940.8	G 98.3	a	11.5	+15.7	+19.4	− 0.8	+19.9	+38.7	.....	.....	+25.4
†P 490	29940.8	G 98.3	b	11.1	+14.7	.....	+ 6.9	.....	.....	.....	.....	− 0.7*
P 505	29942.9	G 100.4	a	14.4	+14.8	−11.0	−18.7	+11.7	+19.0	+ 7.0	+20.4	− 2.0
†P 506	29943.0	G 100.5	b	13.9	+18.2	+ 6.8	+ 2.2	.....	.....	.....	.....	−16.2*
P 511	29946.8	G 104.3	a	12.7	+19.4	+ 5.8	−12.9	+16.0	.....	+15.3*	+19.0	− 8.5
†P 512	29946.8	G 104.3	b	10.1	+20.1	.....	+14.6*	.....	.....	.....	.....	.....
P 524	29951.8	G 109.3	a	13.4	+12.5	+ 8.7	− 1.6	+ 7.9	.....	.....	+ 7.3*	− 3.4
†P 525	29951.8	G 109.3	b	10.1	+13.5	.....	.....	.....	.....	.....	.....	.....
P 527	29956.7	G 114.2	b	13.4	.....	.....	+ 2.4*	.....	.....	.....	.....	+ 2.4
Y 12469	29958.7	G 116.2	a	15.9	+22.1	+17.8	+28.8	+ 5.8	+38.3	+ 1.9*	+29.5	+ 8.1
Y 12470	29958.8	G 116.3	a	12.7	+17.6	+ 3.1	+30.9	+12.1	+33.8	+14.3*	+22.5	+12.7
Y 12477	29966.8	G 124.3	a	14.1	+20.4	+12.0	+ 5.2	+12.5	+44.3	+ 6.6*	+20.1*	+ 6.7
Y 12478	29966.8	G 124.3	a	8.5	+13.7	+13.7	+ 8.0	− 1.8	+24.6	.....	+26.4	+ 5.2
P 534	29967.8	G 125.3	a	19.8	+19.8	+23.3	+ 6.7	+29.3	+31.0	+20.1*	+20.7	+11.4
P 542	29969.7	G 127.2	a	18.6	+25.0	+18.7	+19.6	.....	.....	.....	.....	+19.2
Y 12485	29971.9	G 129.4	a	16.4	+13.6	+12.0	+15.9	+17.8	+25.4	.....	+22.8*	+25.8
P 544	29972.8	G 130.3	a	20.4	+24.4	+19.2	+14.2	+22.0	+19.8	.....	+29.6	+15.5
Y 12489	29972.8	G 130.3	b	16.7	.....	.....	+17.6	+ 7.7	+16.4	.....	+18.3*	+32.9
P 547	29982.7	H 7.4	a	25.3	+21.2	+27.7	+15.2	+23.8	+20.4	.....	+41.9*	+21.8
P 548	29982.7	H 7.4	a	22.6	+18.2	.....	+21.1	+19.4	+25.5	.....	+22.5	+31.2
P 550	29982.7	H 7.4	b	25.9	+21.0	.....	.....	.....	.....	.....	.....	+23.6*
Y 12490	29984.6	H 9.3	a	22.0	+ 9.6	+20.8	−10.0	+15.1	.....	.....	+25.6*	− 6.6
P 554	29987.7	H 12.3	a	26.7	+21.4	+27.3	+ 0.9*	+34.2	.....	.....	.....	.....
P 555	29987.7	H 12.3	a	27.0	+26.0	+36.4	+ 9.1	+38.5	+36.6	+29.0*	+32.3	+ 4.4
P 557	30015.8	H 40.4	a	28.1	+26.0	+31.6	+29.8	+32.5	+33.5	+28.8	+20.2	+ 5.9
P 558	30016.6	H 41.2	a	31.6	+26.8	+37.2	+28.5	+43.1	+50.1	+35.9	+46.3	+21.3
P 559	30016.6	H 41.2	a	30.8	+24.0	+27.6	+16.7	+26.6	+25.5	.....	+49.1	+23.2
Y 12491	30025.8	H 50.4	a	23.9	+19.8	.....	+ 7.9	+23.2	+16.2	.....	.....	+20.1
Y 12494	30034.6	H 59.2	a	18.6	+ 2.9	+14.5	+18.1	+12.2	.....	.....	.....	+12.7
Y 12495	30034.6	H 59.2	a	18.3	+ 3.4	+24.0	+17.6	+12.8	.....	.....	+37.6*	+19.2
Y 12500	30035.7	H 60.3	a	18.6	+18.8	+16.1	+10.8	+18.9	+10.8	.....	.....	+24.2
Y 12501	30035.8	H 60.4	b	26.3	+18.7	.....	+22.2	+ 6.8	+36.0	.....	.....	+36.1
P 563	30037.6	H 62.2	a	18.6	+18.1	+18.1	+21.2	+14.5	+52.1	.....	+36.9	+12.6
Y 12506	30040.5	H 65.1	a	18.4	+17.1	+17.5	+ 4.8	+18.6	.....	.....	+26.1*	+32.0
P 565	30044.6	H 69.2	a	19.1	+ 9.0	+16.6	+ 3.8	+27.0	+48.8	+ 6.6*	+21.5*	+ 2.7
P 567	30045.6	H 70.2	a	17.4	+17.9	+17.8	+ 5.6	+20.2	+32.8	+ 7.2*	+33.3	− 5.5
P 568	30051.6	H 76.2	a	20.3	+24.2	+22.6	− 4.6	+ 7.4	+ 7.6	.....	+20.3*	−10.9
Y 12524	30051.7	H 76.3	a	21.0	+11.5	+ 9.7	+ 8.0	+12.4	.....	.....	.....	.....
Y 12529	30054.7	H 76.3	a	21.4	+19.5	+13.0	−24.0	+14.2	.....	.....	+20.3*	+10.9
P 570	30055.6	H 80.2	a	21.4	+22.2	+25.9	− 0.1	+22.3	+47.0	.....	+39.8*	+ 4.9
P 571	30055.6	H 80.2	a	20.0	+27.1	+26.2	+ 7.3	+15.8	+27.5	.....	+28.5*	− 3.8
P 572	30059.6	H 84.2	a	17.6	+11.4	+ 6.3	+12.1	+21.9	.....	.....	+29.1	+19.3
P 573	30059.6	H 84.2	a	19.1	+20.2	+20.3	+15.8	+12.1	+ 8.3	.....	+22.3*	+17.2
P 574	30067.6	H 92.2	a	17.6	+10.1	+13.4	− 4.8	+20.1	− 1.4	.....	+30.2	+17.6
P 575	30067.6	H 92.2	a	19.0	+ 7.6	+17.6	− 6.8	+10.6	+11.6	.....	+ 8.5	+19.5
P 576	30075.5	H 100.1	a	16.2	+15.9	+ 7.1	− 3.6	+ 7.2*	+ 4.5	.....	+33.5*	− 2.4
Y 12537	30076.6	H 101.2	a	18.1	+18.9	+13.2	+ 9.2	+ 8.2	+25.8	.....	.....	+19.0
Y 12543	30078.7	H 103.3	a	+13.6	+10.1	+11.4	+ 0.6	+ 7.0	.....	.....	+30.8	− 0.3

* Mean has one or more measures missing.

† Mean of several plates taken in rapid succession.

TABLE 1—*Continued*

Plate No.	JD 24+	Phase	Wt.	*H*	*Ca* II K	*He* I 3965	*He* I 4026 4471	*Si* II 4128 4130	*He* I 4144	*Fe* II 4173 4179	*Fe* II 4233 4352	*Mg* II 4481
Y 12556	30108.6	I 0.3	a	+19.5	+13.9	+21.2	− 0.3	.....	+13.5	.....	+16.2*	+15.5
Y 12563	30109.6	I 1.3	a	21.1	+12.7	+16.2	+ 6.9	+13.5	.....	.....	+26.5*	− 7.7
Y 12571	30110.6	I 2.3	a	23.8	+ 3.1	+19.5	+ 8.7	.....	.....	.....	+60.6*	+16.1
Y 12589	30243.9	J 2.8	a	22.9	+25.7	+22.7	+16.7	+21.3	+28.2	+ 7.2	+23.2	+12.5
Y 12594	30252.9	J 11.7	a	26.9	+27.7	+41.4	+23.6	+20.8	+38.1	+12.7	+38.7	+17.7
P 683	30253.9	J 12.7	b	30.9	+20.7	+50.2	+16.6	+37.8	.....	+11.9	+38.6	+22.5
Y 12598	30256.9	J 15.7	a	30.9	.....	.....	+25.8	+25.8	+15.6	+10.4	+28.9	+14.3
P 687	30257.9	J 16.7	b	29.4	.....	.....	− 5.7*	+28.7	.....	+21.1	+35.8	+15.0
Y 12606	30257.9	J 16.7	a	33.6	+17.5	+41.3	+ 8.4	+25.0	+15.6	+26.2	+38.2	+14.3
P 693	30260.9	J 19.7	b	28.8	+19.8	.....	+ 2.6	.....	+48.1	+43.2	+21.8	+19.6
Y 12610	30263.9	J 22.7	a	29.1	+22.7	+26.6	+25.4	+24.6	+47.9	+18.0	+34.6	+10.6
Y 12614	30264.8	J 23.6	a	32.1	+22.7	.....	+12.2	+20.4	+21.1	+ 9.0	+36.6	+32.1
P 696	30264.9	J 23.7	b	31.5	.....	.....	.....	.....	.....	.....	.....	.....
P 700	30276.8	J 35.6	a	32.3	+32.3	+26.1	+ 0.0	+42.6	.....	+32.8	+38.4	+12.2
P 701	30276.9	J 35.7	a	33.7	+23.1	+24.5	+ 2.4	+32.4	+26.6	+17.0	+41.0	+20.9
†P 708	30278.8	J 37.6	a	33.2	.....	.....	.....	.....	.....	.....	.....	.....
Y 12624	30283.8	J 42.6	a	29.9	+24.8	+30.1	+27.9	+38.5	+43.1	+35.8	+29.8	+40.1
P 713	30288.8	J 47.6	a	27.9	+31.7	+30.0	+21.4	+44.5	.....	.....	.....	+21.5
Y 12633	30291.8	J 50.6	b	31.8	+27.8	.....	+ 4.0	+24.6	.....	+19.2	+56.0*	+ 1.0
Y 12639	30292.8	J 51.6	a	25.1	+27.6	+29.9	+26.6	+13.4	+26.9	+ 7.6	+35.9	+16.9
P 721	30293.8	J 52.6	a	23.6	+18.8	+34.6	+17.4	+12.1	+28.8	+16.2	+28.8	+13.3
P 725	30302.8	J 61.6	a	21.6	+27.0	+28.4	− 4.2	+36.2	+27.8	− 1.3	+15.0	+19.4
Y 12668	30339.8	J 98.6	a	+ 9.7	− 0.5	+22.2	− 3.6	+17.8	.....	− 3.6	+15.0	+ 4.5

triplet *He* I lines, λ 4026 and λ 4471, and *Mg* II λ 4481, which is nearly as strong. All three lines remain sensibly constant in intensity and show marked rotational broadening. The lines of *He* I, λ 3888 and λ 3965, which arise from metastable levels are strong and sharp shell lines and are constant in appearance. As in ϕ Persei, λ 3888 is blended with $H\zeta$, causing this Balmer line to stand out conspicuously. *Ca* II H and K complete the list of prominent features.

The less prominent features comprise the rest of the normal helium series, the *Si* II lines λ 4128, λ 4130 and the *Fe* II lines λλ 4173, 4178, 4233, and 4352 showing faint emission edges. These lines of the ionized metals are moderately broad but must be ascribed to the shell, since, judging from the weak Balmer lines of the reversing layer, they would be rendered invisible by the rapid rotation. Finally, there remains a host of faint, moderately sharp lines which appear on some of the plates. These are compared in Table 3 with those found by Baldwin[5] on earlier plates.

RADIAL-VELOCITY MEASURES

Radial-velocity measures can be made with profit only on the sharp Balmer lines, *He* I λλ 4026, 4471, 3965, and *Mg* II λ 4481. The faint metallic lines yield velocities of a low order of accuracy. The lines λλ 4026, 4471, and 4481 give velocities of a higher order of accuracy, but they are poor in comparison with the Balmer lines. These three lines are very wide, though strong, and have no semblance of a core on which to set the micrometer wire. The probable error of a mean velocity from $H\gamma$, $H\delta$, $H\epsilon$ on a single plate is of the order of ± 1 km/sec, while for a *He* I line the probable error of a normal place formed from grouped plates is five or more times as large. Thus, only for the Balmer lines can the variations from cycle to cycle be distinguished with certainty, and a mean curve must be used for *He* I and the other lines. These latter velocities have a meaning only when normal places formed from a large number of measures are used. In Figures 3 and 4 the cycle designation of the normal places has been given, and smooth curves are indicated whenever possible. The evidence is strong that real variations from cycle to cycle occur also for these lines. No attempt was made to measure the very broad underlying hydrogen absorption lines. Table 1 gives the measured velocities for all the accessible lines.

The only trustworthy velocities are those from the stronger circumstellar lines produced in the shell. Hence the true radial velocity of the star itself is not directly determined and is merely inferred from the velocity-curve of the sharp Balmer lines, which we shall use as a standard of reference.

The sharp Balmer lines lend themselves to a more critical analysis than do the broader lines; hence in Figure 1 the velocity-curve for $H\gamma$, $H\delta$, and $H\epsilon$ is given during the period of the present series of observations. Normal places have been formed for conveniently grouped observations during each cycle. The length of the vertical lines through each point has been made equal to the probable error of the normal place. There can be no question as to the reality of the changes in the shape of the velocity-curve from cycle to cycle. Cycle G is certainly different from cycle H, especially in that the latter exhibits a marked secondary variation (similar to that in ϕ Persei), while cycle G does not.

The establishment of these changes within the cycle and from cycle to cycle, already commented upon by Miss Losh, is very important, for it suggests a type of prominence activity in the shell. Such sporadic changes must influence the probable errors of the

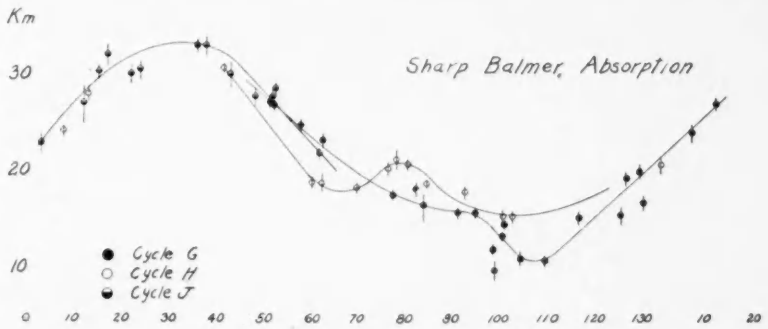

FIG. 1.—Radial velocities of ζ Tauri

normal places, making them somewhat larger than would be expected from these extremely sharp lines.

The existence of secular changes in the velocity-curve makes it of interest to reanalyze the velocity measures made by the earlier observers. This has been done in Figure 2. Only individual cycles are given, taken from the measures by Adams and by Losh. Cycles G, H, and J have been included for comparison.

Cycle 3 (along with a part of 4) is the only one measured reasonably completely by Adams, and it comprises the only measures by Adams given in Figure 2. If one compares the remaining measures made by Adams with those of Figure 2, the cycle-to-cycle variation is apparent even from those few measures. The measures by Miss Losh, when studied separately, also show clearly the secular variations in the shape of the velocity-curve.

The variations in the gamma axis might be ascribed to systematic differences between plates and measures made at Yerkes and at Michigan, were it not for the fragmentary evidence given by the Michigan measures of cycle 36 (Fig. 2). If these are real, it is tempting to suggest that the strong positive displacement is related to the prominent shell activity which occurred at that epoch.

As in the case of ϕ Persei, the (2^1S-4^1P) line, *He* I λ 3965, arising from a metastable level, is much sharper than the triplet lines and follows closely the Balmer velocity-

curve (Fig. 3). The probable errors are about four times as large as for the combined Balmer lines. Individual cycles have been designated in Figure 3; and, though the scatter is great, the indication is that λ 3965 also varies in velocity from cycle to cycle.

Figure 3 also shows the velocity-curves for *He* I λ 4026, λ 4471, and *Mg* II λ 4481. It was reported as possible by Miss Losh that the velocity-curves of the *He* I triplet lines λ 4026, λ 4471 were out of phase with the Balmer velocities. The present measures suggest that they are in phase but are displaced, in the mean, by some 13 km/sec toward the violet side. The negative displacement appeared consistently throughout the series of measures for both λ 4026 and λ 4471 and must be considered real, despite the large probable errors of the individual measures. As Figure 3 shows, all cycles exhibit this negative displacement. Furthermore, both cycles G and H show a decided

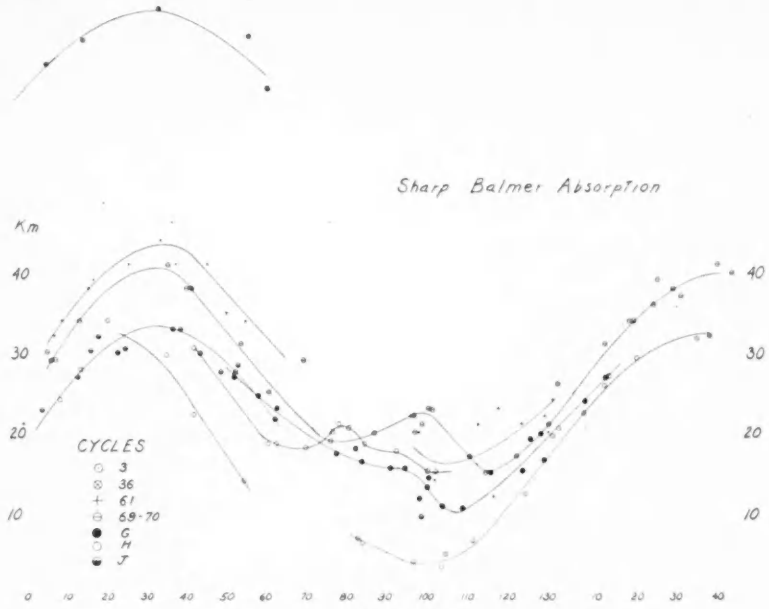

FIG. 2.—Radial velocities of ζ Tauri

secondary variation at 70 days, whereas the variation was absent in cycle G for the Balmer lines.

This secondary variation and the greater velocity of approach are also exhibited by the strong, broad line *Mg* II λ 4481 (Fig. 3). The negative displacement with respect to the Balmer lines is not so prominent as for the *He* I triplet lines, but the secondary variation is more pronounced than for any other element. *Mg* II shows a mean velocity which is 8 km/sec less than the Balmer velocity, but 5 km/sec greater than the *He* I triplet velocity. The velocity of *He* I λ 3965 is essentially the same as the Balmer velocity.

The marked secondary variation is of decided interest. It would be difficult to state from the *Mg* II curve alone whether the secondary variation represents a dip to greater negative velocities at 70^d or a rise to greater positive velocities at 85^d or both, but the rise at 75^d seems to be the more likely case. The evidence of the other elements tends to support the conclusion that the departure from a smooth curve represents a secondary rise at 75^d. This is different from φ Persei, in which the secondary variation is clearly a dip to greater negative velocities; but, since the origin of the primary velocity-curve is not known, the form of the secondary variation in ζ Tauri remains uncertain.

The varying displacements of the gamma axis for the different elements indicate a stratified atmosphere. The existence of a strong secondary variation for *Mg* II λ 4481 and for the normal *He* I lines in cycles G and H, the absence of this variation in the Balmer velocity-curve in cycle G, and its presence in cycle H indicate a disturbance which occurs more or less regularly in the lower strata but which is not always transmitted to the higher levels.

Fe II is most clearly represented in the observed region of the spectrum by λλ 4173, 4179, 4233, and 4352. The lines are very difficult to measure, and much weight cannot be attached to them. The first two and the last two give discordant results, the mean for

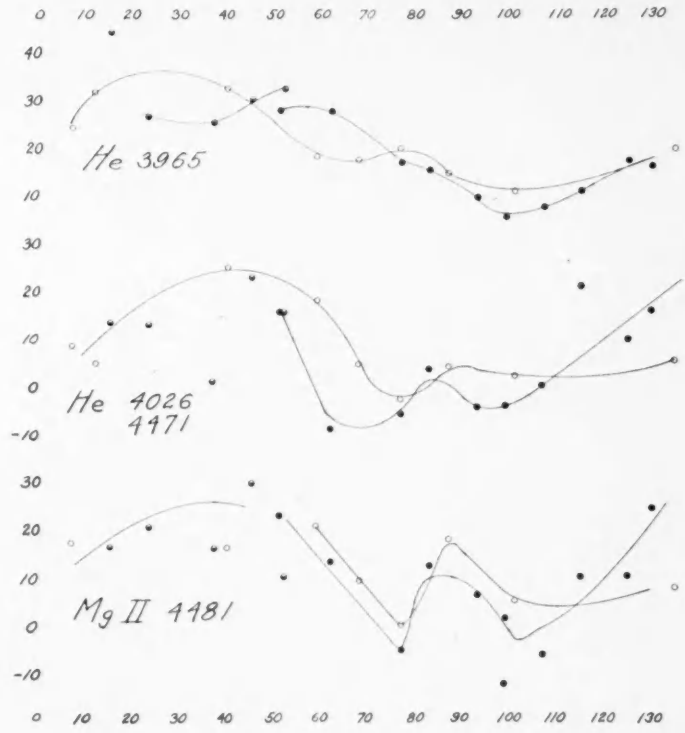

FIG. 3.—Radial velocities of ζ Tauri

the first pair being +15.0 km/sec and for the second pair +29.5 km/sec. The lines are of essentially the same excitation, yet the difference is observationally real. No obvious explanation for it can be found. In the mean the velocity is the same as that of the *H* lines. The velocity-curves of these two pairs of lines are given in Figure 4. The secondary variation is clearly shown in the velocity-curve of the first two but is absent or not so marked in the second two.

The *Ca* II line K gives a velocity-curve which is essentially in agreement with that of *H*, though the former is displaced to the violet by 3 km/sec. In view of the large number of measures—100 for K and more than 400 for the Balmer lines—this difference is probably real. *Ca* II H was not measured because of the blend with the wing of *Hε*. The *Ca* II K velocity-curve is given in Figure 4; the secondary variation at 75^d is apparent.

The *Si* II pair at λ 4128, λ 4130 was measured whenever possible, and despite its weakness and lack of sharpness it gave surprisingly consistent results. The mean velocity for *Si* II is +20.9 km/sec, in very close agreement with the Balmer lines. The velocity-curve for *Si* II is given in Figure 4. The separate curves for cycles G and H in Figure 4 indicate that *Si* II behaves more like the Balmer lines than like *Mg* II or the *He* I triplets. Cycle H shows a more marked secondary variation than cycle G. The gamma axis of *Si* II is also more like that of *H* than of *He* I or *Mg* II.

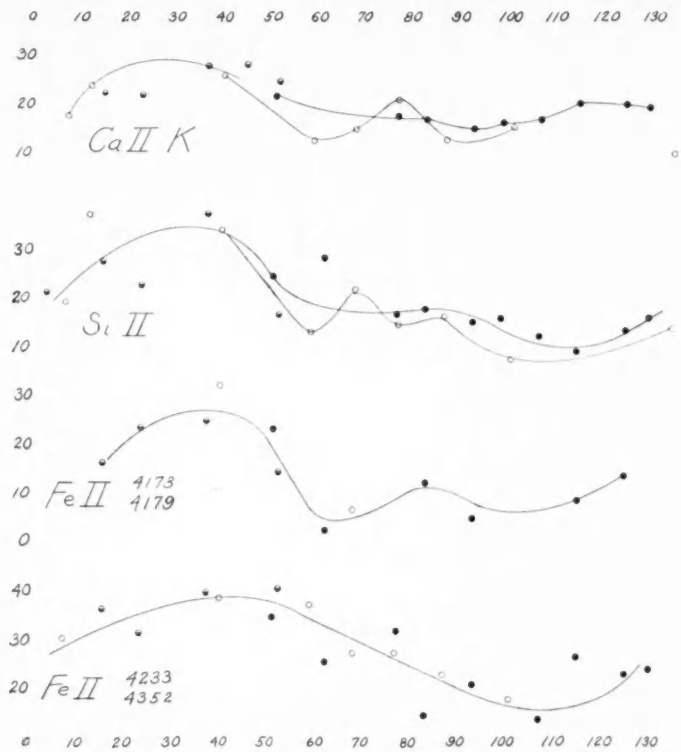

FIG. 4.—Radial velocities of ζ Tauri

Measurements were made whenever possible on the *He* I singlets at λ 4144 and λ 4388. Of the permanent lines in the spectrum these are the most difficult to measure, and, indeed, measures should perhaps not have been attempted. The scatter is too great to obtain a velocity-curve of any significance, but the mean velocity may be significant; for λ 4388 it is −5.1 km/sec, and for λ 4144 it is +27.2 km/sec. The first line is blended with *Fe* II λ 4385, thus accounting for the negative value measured; but λ 4144 is free of any known blend.

THE EMISSION SPECTRUM

The emission spectrum of ζ Tauri is strikingly different from that of φ Persei and is far less interesting. Unlike the latter, it has no relation to the period and does not noticeably extend to higher members of the Balmer series beyond *Hβ*, though many of the metallic lines show emission edges.

The line *Hβ* in the series of plates used by Adams in 1902 and *Hβ* and *Hα* in the pres-

ent series were examined for emission and were found to be practically the same in the two series. The familiar V/R ratio is close to unity, with the violet component appearing slightly stronger on some plates. One plate taken at the Yerkes Observatory in 1929 shows the same condition at $H\beta$. Lockyer[5] and Losh reported nearly equal components in 1921 and 1923–27, but for most of their plates the red component was reported to be slightly the stronger. No marked variation of V/R from unity has been reported, with one notable exception. Losh,[2] Baldwin,[5] and Lockyer[6] state that in 1914–15 the violet component was definitely the stronger. Baldwin has reproduced one of the plates of that epoch, which should be compared with our Plate XXIII. It is significant that at only one epoch has V/R differed markedly from unity, and this at a time when the star showed an enhanced shell spectrum. It should be remarked also that this was the only time the hydrogen velocity-curve was displaced considerably to the red of the curves at all other epochs. It might be that emission at $H\beta$ and incipient emission at the higher Balmer members may have introduced a systematic shift to the red. The evidence points strongly to a sensibly static Balmer emission with V/R close to unity except at times of unusual shell activity. Miss Losh has interpreted this fragmentary portion of the velocity-curve as evidence of a third body. Except for these 1914 observations, the gamma axes of the Balmer velocity-curves are not greatly different and might be explained by systematic errors. The hypothesis of a third body, however, cannot be dismissed until observations of later cycles have been made.

CIRCUMSTELLAR LINES

Baldwin[5] has given a list of the circumstellar lines found in the spectrum in 1914, at which time the shell was especially prominent, and has compared the shell spectrum of that epoch, October 2–11, 1914, with that on January 8, 1921, and with that on February 16–19, 1926. In the 1914 spectrum he measured 210 lines between λ 3927 and λ 4501, the region under present observation. In 1921 only 38 lines were found in this region, and in 1926 only 34.

In the present series of measures relatively few circumstellar lines of the shell were found—77 in all. More significantly, even though some 100 plates of excellent quality were measured, any one circumstellar line (exclusive of the prominent lines measured for velocity) appears on only a few plates, while nearly all plates yielded a few circumstellar lines. This implies that these lines were at the threshold of visibility and appeared to the eye only when the contrast and density in that particular portion of the spectrum were of optimum value. Much effort was expended in the measurement of these very faint lines to eliminate spurious results. Finally, only those lines were considered which appeared on two or more plates. These lines are given in Table 2, with the measured wave length in the first column, the number of plates on which the line appeared in the second column, and their identification in the third column. Because of the scatter of the measures of these threshold lines, the wave lengths are given only to one decimal. When the line had previously been measured by Baldwin, it is indicated by a B in the third column, and the identification has not always been repeated. Twenty-two lines are new, for the most part unidentifiable. Measures were made on 54 additional lines, between λ 3927 and λ 4501, which appeared on one plate only. Though of threshold intensity, 28 of these lines were tentatively identified with lines previously listed by Baldwin.

A comparison of the 1914 shell spectrum and the present one over the region measured reveals the following: of the 210 lines listed by Baldwin, 42 were attributed to *Fe* II, 32 to *Ti* II and *Cr* II, and 31 to other elements, leaving 105 unidentified. Essentially the same proportions are maintained in the present shell spectrum, even with the new lines; hence, the difference is one of strength and not of composition or of ionization.

[6] *M.N.*, **83**, 326, 1923; **84**, 417, 1924; **88**, 689, 1928; **96**, 230, 1936.

Radial-velocity measures or even intensity measures on the majority of shell lines would be of little value; for those stronger ones for which velocity measures have been made, a series of eye-estimates of intensity were made on some forty Process plates. The estimates were made over a period of several days, and each plate was repeated. Total strength, width, and central intensity were estimated separately. Because of the large probable errors inherent in eye-estimates of weak lines on plates of different

TABLE 2

ADDITIONAL SHELL LINES OF ζ TAURI

λ	No. of Plates	Reference	λ	No. of Plates	Reference
3928.0	2	B?	4225.3	2	?
3930.1	4	B	4228.1	2	?
3935.8	8	B	4238.5	2	*Fe* I 8.82?
3939.5	3	B?	4242.5	2	B
3942.2	2	B	4252.8	2	*Cr* II 2.66?
3947.8	9	B	4261.8	2	B
3961.3	4	B	4276.0	2	B
3963.2	4	B	4296.7	6	B
3966.6	9	*Fe* I 6.1?	4303.3	16	B
3967.4	3	B	4325.5	2	B *Fe* I 5.76?
3973.6	3	?	4337.1	2	B
3982.9	3	?	4347.0	3	B
3987.5	3	?	4354.9	2	B?
3995.9	2	?	4357.9	11	B
4015.6	2	B	4361.6	4	?
4029.0	2	B	4362.9	2	?
4032.8	4	B	4368.7	14	B
4045.7	2	*Fe* I?	4371.1	2	?
4048.8	5	B	4385.2	6	B
4063.8	2	B *Fe* I?	4390.4	3	*Mg* II 90.6?
4067.0	49	B *Ni* II	4395.7	12	B
4083.8	2	?	4402.8	2	?
4086.4	2	B	4405.1	5	*Fe* I 4.75
4089.1	2	B	4414.0	2	B
4105.7	2	B	4416.9	37	B
4110.6	2	?	4419.8	50	B
4135.1	3	B	4428.0	3	B?
4137.6	2	?	4430.9	11	B
4152.4	3	B	4435.9	3	?
4161.8	2	*Ti* II 1.54?	4451.7	6	B
4163.6	2	B	4462.2	3	B
4171.5	5	B	4489.2	3	B
4181.8	2	?	4491.6	2	B

densities, only a few results can be stated with certainty, and the individual measures have not been included in this paper. No periodic variations of any of the lines were detected, but definite secular variations were found. In cycle G, *Fe* II was relatively strong, and *Fe* III was relatively weak. In the succeeding cycle H, however, *Fe* III was strong, while *Fe* II was weakened almost to invisibility. This strongly suggests a change in ionization between the two cycles.

SUMMARY OF OBSERVATIONS AND DISCUSSION

The composite spectrum is of class B4ne, in so far as classification is possible. It is composite in the sense that both broad and sharp lines are present, exhibiting periodic velocity variations which are in phase but of varying range and amplitude.

In order of prominence the absorption features in the photographic region are as follows: sharp Balmer lines; broad *He* I λ 4026 and λ 4471; broad *Mg* II λ 4471; sharp *He* I λ 3888 and λ 3965; sharp *Ca* II, H and K; broad Balmer wings; moderately sharp *Si* II λ 4128, λ 4130, *Fe* II λλ 4173, 4178, 4233, and 4352; very broad lines *He* I λλ 4387, 4144, and 4009; and moderately broad *Ni* II λ 4067. Added to these are the lines of threshold visibility of the ionized metals, principally *Fe* II, *Cr* II, and *Ti* II.

Emission at the present epoch is visible at *Hα* and *Hβ* with V/R near unity. The stronger *Fe* II lines also show emission borders. Periodic and secular variations are present in the radial velocities of the measurable lines, and only secular variations in the line intensities. All periodic variations have the same period, $132^{d}91$, which has been constant for the last forty years, within the accuracy of the measures. The ranges and mean velocities as judged from the present velocity-curves are given in Table 3.

TABLE 3

Line	Mean Vel.	Range
Sharp *H*	+22 km/sec	+12 to +35 km/sec
He I λ 3965	22	+10 +36
Si II λ 4128, λ 4130	21	+10 +36
Fe II λ 4233, λ 4352	29	+21 +39
Fe II λ 4173, λ 4178	15	+ 4 +27
He I λ 4144	27	+15 +40
Ca II K	19	+12 +27
Mg II λ 4481	14	+ 5 +24
He I λ 4026, λ 4471	9	− 6 +23

The order of accuracy can best be judged from the scatter in the diagrams. The difference in the mean velocities between the sharp Balmer lines and *Mg* II λ 4481, for instance, is definitely real. Despite the fact that the difference between the two sets of *Fe* II lines seems unreasonable, it is observationally real, notwithstanding the much lower order of accuracy of the measures for these faint, moderately broadened lines.

The velocity-curves of none of the lines measured can be explained by orbital motion alone. A definite secondary variation occurs at about 75^{d}, the phase at which the velocity-curves cross the axis to negative values. This secondary variation shows a marked secular change in amplitude. Indeed, the hydrogen-curve for cycle G (Fig. 2) shows no variation, while in the succeeding cycle, H, it is present.

There is now a wealth of observational material at hand, and an attempt at a physical interpretation of ζ Tauri can be made. The spectrum of ζ Tauri is of particular interest because it exhibits lines of different widths. This effect has already been interpreted as a consequence of stratification in the shell of the star.[7] If we designate by r and R the effective radius of the shell corresponding to a given line and the radius of the star, respectively, and by v_s and v_0 the rotational broadening of the lines of the shell and of the star, the assumption of conservation of angular momentum would demand:

$$r v_s = R v_0 . \tag{1}$$

The rotational broadening of the absorption lines of the shell derived in the usual manner from their contours gives

$$v_s' = v_s \sin \theta = v_s \frac{R}{r}, \tag{2}$$

[7] Struve and Wurm, *Ap. J.*, **88**, 106, 1938.

where θ is the angle subtended by the radius of the star at the shell. The geometrical dilution factor is

$$W = \frac{R^2}{4r^2}. \tag{3}$$

Hence,

$$W = \frac{1}{4}\frac{v_s'}{v_0}. \tag{4}$$

The quantities v_s' and v_0 are directly observable: the former represents the observed rotational broadening of a shell line, the latter the corresponding broadening of a line produced in the reversing layer.

We have measured a Coudé spectrogram of ζ Tauri obtained at the McDonald Observatory and have derived the rotational velocities shown in Table 4. The last three

TABLE 4

He I (diffuse singlets)	$v_0 = 400$ km/sec
He I (diffuse triplets)	$v_s' = 350$
Mg II	$v_s' = 200$
Si II	$v_s' = 100$
Fe II	$v_s' = 75$
Ca II	$v_s' = 50$
He I λ 3965	$v_s' = 50$
H	$v_s' = 50$

values are affected by turbulence, and it is difficult to decide whether the actual rotational broadening is measurable. We shall assume that for a hypothetical layer in the shell, which roughly corresponds to *H*, *He* I λ 3965, and *Ca* II, the rotational broadening is $v_s' = 50$ km/sec. Formula (4) then gives

$$W = 0.03 .$$

This is in excellent agreement with the independent determination, $W = 0.01$, obtained from the intensities of *He* I lines originating in ordinary and in metastable levels.[7] The corresponding ratio is

$$\frac{R}{r} = 0.34 .$$

The actual rotational velocity of the shell is

$$v_s = v_0 \frac{R}{r} = 140 \text{ km/sec} .$$

This may be compared to a value of $v_s = 200$ km/sec, which results from the over-all width of the $H\beta$ emission line. The agreement is probably satisfactory, in view of the fact that the hydrogen shell is not a thin layer and that the effective height above the star represented by the emission and absorption components may not be the same.

We have no direct information concerning the size of the star. Since the spectrum of the reversing layer is normal and does not suggest excessive luminosity, we may probably adopt a radius of about 3×10^{11} cm. The radius of the shell would then be about 10^{12} cm.

We now turn to the interpretation of the velocity-curves. From Figure 1 we see that the most measurable features of the spectrum—the Balmer lines—relate to ephemeral conditions in the shell. The sporadic changes from cycle to cycle in the shell are in marked contrast to the constancy of the period, making it reasonable to assume that

the latter arises from the orbital motion about a secondary component. There is no indication whatever of the presence of a secondary spectrum, and our assumption of binary motion is at present only a working hypothesis. Only a few measurable lines, if any, can be said to arise from the true reversing layer of the primary. *He* λ 4144 may be the only measurable feature arising solely in the reversing layer. The broad underlying Balmer lines must also arise in the reversing layer, but they are so broadened and weak that measures are impossible.

The rapid changes in the shell strongly suggest "prominence" action rather than a continuous and uniform ejection of material from the star and suggest a physical picture which may explain the major features of the spectrum. If we deal with "prominence" action, the velocity-curve of the sharp Balmer lines must represent the velocity of the primary plus the ephemeral effects of the "prominence." The smoothed Balmer curve should then yield the elements of the orbit. Elements sufficiently good for our purposes have already been determined by Adams[1] and by Losh.[2] In the mean a value of 2×10^{12} cm has been obtained for $a \sin i$ and a value of 0.016 ⊙ for the mass-function. Kepler's third law shows that for the sum of the masses equal to 10 ⊙ the separation of the components would be about 1 astronomical unit, while if their sum were as great as 100 ⊙ they would be separated by slightly more than 2 astronomical units. While, of course, the system of ζ Tauri cannot be considered a normal binary system, it is highly improbable that the sum of the masses would be much less than 10 ⊙, in view of the spectrum of the primary. Indeed, even if the sum of the masses were only 1 ⊙, the centers of the stars must still be separated by 0.5 astronomical units. It is probable that the semimajor axis of the orbit is of the order of $a = 10^{13}$ cm. This is ten times larger than the radius of the largest shell.

It is suggested that the primary is rotating sufficiently rapidly to be near the point of instability; the tidal action of the secondary will then be sufficient to upset the stability of the shell and cause ejection of material at the point which is directed toward the secondary. The rapid rotation will cause a tidal lag, so that the material is ejected at phases 40^d–50^d. This ejected material falls back into the primary, causing the greatest inrush at the "neap-tide" portions of the stellar surface, which would be projected upon the line of sight at approximately phase 80^d. The fact that the secondary variation is itself variable in intensity attests to the idea that tidal action produces optimum conditions for "prominence" action but that the amount of material ejected depends upon other factors.

The observations tend to support this mechanism. The secondary variation occurs at about 75^d. The absence of negative increments at phases 30^d–40^d is interesting but does not vitiate the picture. Moreover, the shape of the velocity-curve of *Mg* II, which probably relates to the lower levels of the shell, and perhaps those of other lines, can be explained by the superposition upon a "normal" curve of a negative displacement at 60^d and a positive displacement at 85^d.

PERKINS OBSERVATORY
DELAWARE, OHIO
AND
YERKES OBSERVATORY,
WILLIAMS BAY, WISCONSIN
June 1942

THE NEGATIVE HYDROGEN ION AND ITS ABSORPTION COEFFICIENT

RALPH E. WILLIAMSON

ABSTRACT

A six-parameter wave-function for the negative hydrogen ion has been derived on the basis of the Ritz principle, similar to the wave-function of Hylleraas for the ground state of helium. This new wave-function predicts for the electron affinity a value of 0.0265 atomic units; this value is appreciably different from 0.0253 atomic units currently adopted.

The atomic absorption coefficient of H^- for radiation of different wave lengths has been computed on the basis of the new wave-function. It is found that the absorption coefficient per H^- ion has the maximum value 3.0×10^{-17} cm^2 at 5000 A (instead of 2.6×10^{-17} cm^2 at 4000 A, according to the earlier calculations of Massey and Bates). Throughout the red and the infrared the new values for the absorption coefficient are substantially larger than those now in general use.

I. INTRODUCTION

Since Wildt's discovery[1] of the negative hydrogen ions as the principal source of opacity in the solar atmosphere, several investigations[2] have been carried out to incorporate this new source of opacity in a theoretical analysis of model stellar atmospheres. Most important of these is undoubtedly that of Strömgren,[3] whose quantitative analysis shows that now for the first time a theory of the solar atmosphere becomes possible in which no principal discrepancy remains. On the other hand, Wildt's investigations[4] on the theoretical relation between the color temperature and the effective temperature of stars shows that in this matter there still remains a discordance between observation and the prediction of the theory. Mainly on the strength of this evidence it has been concluded that there might possibly remain further unexplored sources of opacity. However, Wildt's discussion is based on the continuous absorption coefficient $k_\nu(H^-)$ due to H^- as computed by Massey and Bates.[5] According to their calculations, the absorption coefficient, $k_\nu(H^-)$, attains its maximum at 4000 A and decreases throughout the visual region. And, as Wildt has pointed out, it is precisely this decrease of the absorption coefficient in the region to the red of 4000 A which is responsible for the discrepancy noted. A shift of the maximum of the absorption coefficient to the region 5000–6000 A would remove, or at any rate greatly diminish, the extent of the discordance between theory and observation. Massey and Bates's computation of the absorption coefficient of H^- is based on a "third-order" wave-function for the ground state of H^- due to Bethe[6] and Hylleraas,[7] derived on the basis of the Ritz principle. Massey and Bates point out that this wave-function predicts a value of the energy correct to within a fraction of 1 per cent. More precisely, the Bethe-Hylleraas wave-function yields for the energy E of the ground state the value $E = -0.5253$ in Hartree's atomic units, while an extrapolation from other two-electron systems leads to a value $E = -0.5264$.[8] On the other hand, as Chandrasekhar[9] has pointed out, what is relevant for the problem of the absorption co-

[1] *Ap. J.*, **89**, 295, 1939.

[2] Massey and Bates, *Ap. J.*, **91**, 202, 1940; Wildt, *Ap. J.*, **93**, 47, 1941; Strömgren, *Festschrift für Elis Strömgren*, p. 218, Copenhagen, 1940.

[3] *Op. cit.*

[4] *Ap. J.*, **93**, 47, 1941.

[5] *Loc. cit.*

[6] *Zs. f. Phys.*, **57**, 815, 1929.

[7] *Zs. f. Phys.*, **60**, 624, 1930.

[8] *Ibid.*

[9] In a lecture (unpublished) given at the Yerkes Observatory.

efficient is not so much the accuracy with which the total energy E is predicted as it is the accuracy with which the electron affinity is predicted. Judged by this criterion, the Bethe-Hylleraas wave-function does not appear sufficiently accurate; the electron affinity which it predicts is quite appreciably less: 0.0253 instead of 0.0264. If this is the error in the eigenvalue, the extent of the inaccuracy of the wave-function is probably much more serious. In any case it appears worth while to set up for H^- a more accurate sixth-order wave-function following the methods developed by Hylleraas for the ground state of helium and to re-evaluate the absorption coefficient on this basis. This is the object of the present paper. As we shall see, the calculations justify our suspicion that the Bethe-Hylleraas wave-function does not provide the accuracy necessary for our purposes (see Fig. 1).

II. DETERMINATION OF THE WAVE-FUNCTION

The Ritz method for solving the wave-equation

$$H\Psi = E\Psi \tag{1}$$

for the lowest eigenstate is based on the fact that the corresponding wave-function Ψ makes E a minimum, where E is defined by

$$E = \frac{\int \bar{\Psi} H \Psi \, d\tau}{\int |\Psi|^2 d\tau} . \tag{2}$$

The integrations in equation (2) are to be extended over the entire configuration space. In practice, a form for the wave-function is assumed which involves certain parameters. And the "best" wave-function of the assumed form is obtained by assigning to these parameters values which will make the right-hand side of equation (2) a minimum. The success of this method clearly depends on how well the initial form for the wave-function is chosen. But Hylleraas has found that the observed value of E for the ground state of helium can be predicted within spectroscopic accuracy, if one assumes for Ψ the form

$$\Psi = e^{-ks/2}[\, c_0 + c_1(ku) + c_2(kt)^2 + c_3(ks) + c_4(ks)^2 + c_5(ku)^2] , \tag{3}$$

where s, t, and u are related to the distances r_1, r_2, and r_{12}, of the two electrons from the nucleus and from one another, respectively, according to the relations

$$s = r_1 + r_2 , \qquad t = -r_1 + r_2 , \qquad u = r_{12} . \tag{4}$$

In this sixth-order wave-function, k, c_1, c_2, c_3, c_4, and c_5 are six parameters which are adjusted until E takes the smallest possible value consistent with Ψ being of the form of equation (3). Since this type of wave-function predicts the energy of the ground state of helium with extreme precision,[10] we shall adopt it for H^- also and determine the values of the six parameters which will make E defined by equation (2) a minimum.

A convenient procedure that may be followed in practice is described by Bethe.[11] It involves a considerable amount of tedious numerical work, including the evaluation of several sixth-order determinants and the solving of a number of sets of six simultaneous homogeneous linear equations. However, the method was found feasible.

[10] Bethe, in his article on one- and two-electron systems in the *Handbuch der Physik* (XXIV, Part I, 358, Berlin, 1933) compares Hylleraas' value for E with the experimental value.

[11] "Quantentheorie," *ibid.*, p. 353.

We give below the results of the computation:

$$\left.\begin{aligned} E &= -0.52646\,, \\ k &= +1.40239\,, \qquad c_3 = -0.10259\,, \\ c_1 &= +0.18552\,, \qquad c_4 = +0.00222\,, \\ c_2 &= +0.03673\,, \qquad c_5 = -0.00455\,, \end{aligned}\right\} \tag{5}$$

where the constants are expressed in atomic units. We can now write the wave-function for H^- in the form

$$\Psi = e^{-\alpha s}(1 + \beta u + \gamma t^2 + \delta s + \epsilon s^2 + \zeta u^2)\,, \tag{6}$$

where

$$\left.\begin{aligned} \alpha &= \frac{k}{2} = +0.70120\,, \qquad \delta = c_3 k = -0.14387\,, \\ \beta &= c_1 k = +0.26017\,, \qquad \epsilon = c_4 k^2 = +0.00436\,, \\ \gamma &= c_2 k^2 = +0.07225\,, \qquad \zeta = c_5 k^2 = -0.00896\,. \end{aligned}\right\} \tag{7}$$

The "normalization factor," N, defined by

$$N^2 \int \Psi^2 d\tau = 1\,, \tag{8}$$

is related to certain integrals used in the minimizing of E and has the value

$$N = 0.073965\,. \tag{9}$$

It is of interest to compare the relative accuracy with which the different orders of approximations for the wave-function of H^- predict E and the electron affinity for the negative hydrogen ion. The relevant data are given in Table 1. We see that all wave-

TABLE 1

ELECTRON AFFINITY OF H^- AS PREDICTED BY DIFFERENT WAVE-FUNCTIONS

	Ψ	E	Electron Affinity
1	$e^{-0.688s}$	−0.473	−0.027
2	$e^{-0.825s}(1+0.490u)$	.509	+0.009
3	$e^{-0.769s}(1+0.318u+0.125t^2)$	.5253	+0.0253
4	As in eq. (6)	−.52646	+0.02646
Extrapolation from other two electron systems		−0.52642	+0.02642

functions except the first predict the existence of H^-, as they all lead to positive values for the electron affinity. It will be specially noticed that the wave-function which we have just determined actually *increases* the value for the electron affinity over Hylleraas' value extrapolated from the other two-electron systems. It therefore appears likely that our present sixth-order wave-function predicts the value of the electron affinity to within a fraction of 1 per cent. Thus the criticism of the Bethe-Hylleraas wave-function (No. 3 in Table 1) made in section I is not applicable to the present one. It now remains to use this wave-function in the calculation of the absorption coefficient.

III. THE ABSORPTION COEFFICIENT

If a stream of light quanta of frequency ν strikes a slab of matter containing N atoms/cm^3, the number of quanta absorbed in penetrating a distance ds of the material is $Nk_\nu ds$. Here k_ν is the effective cross-section of one atom for absorbing the radiation of frequency ν. Thus, when the stream of quanta has traversed a thickness s of the material, its intensity will be reduced by a factor $e^{-Nk_\nu s}$. We desire to evaluate the absorption cross-section k_ν for H^- ions, as a function of the frequency ν of the incident quanta. The absorption results from a transition of the ion to one of its continuous energy states. In particular, if the electron affinity is E_0, then the velocity v of the photo-electron is given by Einstein's relation

$$\tfrac{1}{2} m v^2 = h\nu - E_0 . \tag{10}$$

The absorption cross-section for such a process is given by the quantum-mechanical formula

$$k_\nu = \frac{32\pi^4 m^2 e^2}{3h^3 c} \nu v |\mu|^2 , \tag{11}$$

where μ is the matrix element, corresponding to the transition from the initial state of the hydrogen ion to the final state of a hydrogen atom in the ground state, and an outgoing current of electrons with velocity v and unit density

$$\mu = \int \bar{\Psi}_A (r_1 + r_2) \Psi_B d\tau . \tag{12}$$

In evaluating this matrix element we shall use for the wave-function representing the ground state of the hydrogen ion our sixth-order approximation,

$$\Psi_A = N e^{-\alpha s}(1 + \beta u + \gamma t^2 + \delta s + \epsilon s^2 + \zeta u^2) , \tag{13}$$

where the constants N, α, β, γ, δ, ϵ, and ζ have the values given in equations (7) and (9). For the wave-function representing the final state we have

$$\Psi_B = \frac{1}{\sqrt{2\pi}}(e^{-r_2 + i\mathfrak{p}\cdot r_1} + e^{-r_1 + i\mathfrak{p}\cdot r_2}) , \tag{14}$$

where $\mathfrak{p}$ denotes the momentum of the free electron. All quantities in equation (14) are expressed in atomic units. It will be noticed that, as required, Ψ_B has been chosen to correspond to an outgoing current of electrons of unit density and further is symmetrical in the co-ordinates of the two electrons. We can write

$$\Psi_B = \frac{1}{\sqrt{2\pi}}(e^{ikz_1 - r_2} + e^{ikz_2 - r_1}) , \qquad (k = |\mathfrak{p}|) , \tag{15}$$

instead of equation (14), if the z-axis of our co-ordinate system is arranged to be in the direction of $\mathfrak{p}$.

It is seen that, for Ψ_A and Ψ_B of the forms (13) and (15), μ_x and μ_y vanish identically, on account of the symmetry of the integrand in equation (12), and the only nonvanishing component is μ_z:

$$\left.\begin{aligned} \mu_z = \frac{N}{\sqrt{2\pi}} \int_{r_1=0}^{\infty}\int_{\vartheta_1=0}^{\pi}\int_{\varphi_1=0}^{2\pi}\int_{r_2=0}^{\infty}\int_{\vartheta_2=0}^{\pi}\int_{\varphi_2=0}^{2\pi} e^{-\alpha(r_1+r_2)}[\,1 + \beta r_{12} + \gamma(r_2 - r_1)^2 \\ + \delta(r_1 + r_2) + \epsilon(r_1 + r_2)^2 + \zeta r_{12}^2\,](z_1 + z_2)\,(e^{ikz_1 - r_2} + e^{ikz_2 - r_1}) \\ \times r_1^2 r_2^2 d r_1 d r_2 \sin\vartheta_1 \sin\vartheta_2 d\vartheta_1 d\vartheta_2 d\varphi_1 d\varphi_2 . \end{aligned}\right\} \tag{16}$$

The angle integrations indicated in equation (16) are readily carried out when all the functions involving the polar angles ϑ_1 and ϑ_2 are expressed in terms of Legendre polynomials. This can be conveniently done by using the following series expansions.

The expansion for the plane wave in terms of half-integral Bessel functions is well known.[12] We have

$$\left.\begin{aligned} e^{ikz} &= e^{ikr\cos\vartheta} \\ &= \left(\frac{\pi}{2kr}\right)^{1/2} \sum_{n=0}^{\infty} i^n (2n+1) J_{n+1/2}(kr) P_n(\cos\vartheta), \end{aligned}\right\} \tag{17}$$

where $J_{n+1/2}(x)$ denotes the Bessel function of order $n+\frac{1}{2}$, and $P_n(x)$ the Legendre polynomial of order n. A series expansion for r_{12} in terms of Legendre polynomials of the angle Θ between r_1 and r_2 may be derived:[13]

$$\left.\begin{aligned} r_{12} &= \sqrt{r_1^2 + r_2^2 - 2r_1 r_2 \cos\Theta} \\ &= \hat{r} \sum_{\nu=0}^{\infty} \left(\frac{x^2}{2\nu+3} - \frac{1}{2\nu-1}\right) x^\nu P_\nu(\cos\Theta), \end{aligned}\right\} \tag{18}$$

where

$$\cos\Theta = \cos\vartheta_1 \cos\vartheta_2 + \sin\vartheta_1 \sin\vartheta_2 \cos(\varphi_1 - \varphi_2) \tag{19}$$

and

$$\left.\begin{aligned} \hat{r} &= r_1, \qquad x = \frac{r_2}{r_1}, \qquad \text{if } r_1 > r_2; \\ \hat{r} &= r_2, \qquad x = \frac{r_1}{r_2}, \qquad \text{if } r_1 < r_2. \end{aligned}\right\} \tag{20}$$

To make use of the series (18), we must further express $P_n(\cos\Theta)$ in terms of associated Legendre polynomials in $\cos\vartheta_1$ and $\cos\vartheta_2$, by using the addition theorem,[14]

$$P_\nu(\cos\Theta) = \sum_{\mu=-\nu}^{\nu} \frac{(\nu - |\mu|)!}{(\nu + |\mu|)!} P_\nu^\mu(\cos\vartheta_1) P_\nu^\mu(\cos\vartheta_2)\, e^{i\mu(\varphi_1 - \varphi_2)}. \tag{21}$$

We can now express equation (16) in the form

$$\mu_z = \frac{N}{\sqrt{2\pi}} (\Lambda + \mathrm{B}\beta + \Gamma\gamma + \Delta\delta + \mathrm{E}\epsilon + \mathrm{Z}\zeta), \tag{22}$$

[12] See, e.g., Mott and Massey, *The Theory of Atomic Collisions*, p. 20, Oxford, 1933.

[13] Jen (*Phys. Rev.*, **43**, 540, 1933) gives relation (18). It can be readily obtained by assuming a series of the form

$$r_{12} = \hat{r} \sum_{\nu=0}^{\infty} a_\nu x^\nu,$$

differentiating it with respect to $\cos\Theta$, and comparing it with the series

$$\frac{1}{r_{12}} = \hat{r} \sum_{n=0}^{\infty} P_n(\cos\Theta)\, x^n.$$

[14] Macmillan, *Theory of the Potential*, p. 376, New York, 1930.

where we have written

$$\left.\begin{aligned}
A &= \int\int e^{-\alpha(r_1+r_2)}\,(r_1\cos\vartheta_1+r_2\cos\vartheta_2)\,(e^{ikz_1-r_2}+e^{ikz_2-r_1})\,d\tau_1 d\tau_2\,,\\
B &= \int\int e^{-\alpha(r_1+r_2)}\,r_{12}\,(r_1\cos\vartheta_1+r_2\cos\vartheta_2)\,(e^{ikz_1-r_2}+e^{ikz_2-r_1})\,d\tau_1 d\tau_2\,,\\
\Gamma &= \int\int e^{-\alpha(r_1+r_2)}\,(r_2-r_1)^2\,(r_1\cos\vartheta_1+r_2\cos\vartheta_2)\,(e^{ikz_1-r_2}+e^{ikz_2-r_1})\,d\tau_1 d\tau_2\,,\\
\Delta &= \int\int e^{-\alpha(r_1+r_2)}\,(r_1+r_2)\,(r_1\cos\vartheta_1+r_2\cos\vartheta_2)\,(e^{ikz_1-r_2}+e^{ikz_2-r_1})\,d\tau_1 d\tau_2\,,\\
E &= \int\int e^{-\alpha(r_1+r_2)}\,(r_1+r_2)^2\,(r_1\cos\vartheta_1+r_2\cos\vartheta_2)\,(e^{ikz_1-r_2}+e^{ikz_2-r_1})\,d\tau_1 d\tau_2\,,\\
Z &= \int\int e^{-\alpha(r_1+r_2)}\,r_{12}^2\,(r_1\cos\vartheta_1+r_2\cos\vartheta_2)\,(e^{ikz_1-r_2}+e^{ikz_2-r_1})\,d\tau_1 d\tau_2\,.
\end{aligned}\right\} \tag{23}$$

All the foregoing integrals except B and Z are of the same type:

$$\left.\begin{aligned}
I &= \int\int f(r_1,\,r_2)\,(r_1\cos\vartheta_1+r_2\cos\vartheta_2)\,(e^{ikz_1-r_2}+e^{ikz_2-r_1})\,d\tau_1 d\tau_2\,,\\
&\qquad f(r_1,\,r_2)=f(r_2,\,r_1)\,.
\end{aligned}\right\} \tag{24}$$

By using equations (17) and (21) we can readily integrate equation (24) over the angles φ_1, φ_2, ϑ_1, and ϑ_2, making use of the orthogonality properties of the Legendre polynomials. We obtain

$$I = 32\pi^2 i\left(\frac{\pi}{2k}\right)^{1/2}\int_0^\infty\int_0^\infty f(r_1,\,r_2)\,e^{-r_2}\,r_1^{5/2}\,r_2^2\,J_{3/2}(kr_1)\,dr_1 dr_2\,. \tag{25}$$

Accordingly, we have

$$\left.\begin{aligned}
A &= 2q\int_0^\infty\int_0^\infty e^{-(\alpha+1)r_2-\alpha r_1}\,r_1^{5/2}\,r_2^2\,J_{3/2}(kr_1)\,dr_1 dr_2\,,\\
\Gamma &= 2q\int_0^\infty\int_0^\infty e^{-(\alpha+1)r_2-\alpha r_1}\,(r_2-r_1)^2\,r_1^{5/2}\,r_2^2\,J_{3/2}(kr_1)\,dr_1 dr_2\,,\\
\Delta &= 2q\int_0^\infty\int_0^\infty e^{-(\alpha+1)r_2-\alpha r_1}\,(r_1+r_2)\,r_1^{5/2}\,r_2^2\,J_{3/2}(kr_1)\,dr_1 dr_2\,,\\
E &= 2q\int_0^\infty\int_0^\infty e^{-(\alpha+1)r_2-\alpha r_1}\,(r_1+r_2)^2\,r_1^{5/2}\,r_2^2\,J_{3/2}(kr_1)\,dr_1 dr_2\,,
\end{aligned}\right\} \tag{26}$$

where for the sake of brevity we have written

$$q = 16\pi^2 i\left(\frac{\pi}{2k}\right)^{1/2}. \tag{27}$$

To evaluate Z we split it into two parts:

$$Z = Z_1 - 2Z_2 , \tag{28}$$

where

$$\left.\begin{aligned} Z_1 &= \int\int e^{-\alpha(r_1+r_2)} (r_1^2+r_2^2) (r_1\cos\vartheta_1+r_2\cos\vartheta_2) (e^{ikz_1-r_2}+e^{ikz_2-r_1})\, d\boldsymbol{r}_1 d\boldsymbol{r}_2 , \\ Z_2 &= \int\int e^{-\alpha(r_1+r_2)} r_1 r_2 \cos\Theta (r_1\cos\vartheta_1+r_2\cos\vartheta_2) (e^{ikz_1-r_2}+e^{ikz_2-r_1})\, d\boldsymbol{r}_1 d\boldsymbol{r}_2 . \end{aligned}\right\} \tag{29}$$

Z_1 is of the form of equation (24) and hence (cf. eq. [25])

$$Z_1 = 2q\int_0^\infty\int_0^\infty e^{-(\alpha+1)r_2-\alpha r_1} (r_1^2+r_2^2)\, r_1^{5/2} r_2^2 J_{3/2}(k r_1)\, d r_1 d r_2 . \tag{30}$$

Remembering that $\cos\Theta = P_1(\cos\Theta)$ and applying equation (21), we effect the angle integrations in Z_2 as we did in equation (25). We obtain

$$Z_2 = \tfrac{2}{3} q\int_0^\infty\int_0^\infty e^{-(\alpha+1)r_2-\alpha r_1} r_1^{5/2} r_2^4 J_{3/2}(k r_1)\, d r_1 d r_2 . \tag{31}$$

The angle integrations for B are carried out, after using equations (18) and (21), in the same way as equations (25) and (31) were obtained:

$$\left.\begin{aligned} B = {} & 2q\int_0^\infty\int_0^\infty e^{-(\alpha+1)r_2-\alpha r_1} \hat{r} \left(\frac{x^2}{3}+1\right) r_1^{5/2} r_2^2 J_{3/2}(k r_1)\, d r_1 d r_2 \\ & + \tfrac{2}{3} q\int_0^\infty\int_0^\infty e^{-(\alpha+1)r_2-\alpha r_1} \hat{r} \left(\frac{x^3}{5}-x\right) r_1^{3/2} r_2^3 J_{3/2}(k r_1)\, d r_1 d r_2 . \end{aligned}\right\} \tag{32}$$

This completes the angle integrations involved in obtaining the matrix element.

The integrals to be evaluated in A, Γ, Δ, E, and Z are seen to be

$$A = 2q\int_0^\infty e^{-\alpha r_1} r_1^{5/2} J_{3/2}(k r_1)\, d r_1 \int_0^\infty e^{-(\alpha+1)r_2} r_2^2 d r_2 , \tag{33}$$

and

$$\Gamma = 2q(\Gamma_1 - 2\Gamma_2 + \Gamma_3) , \tag{34}$$

where

$$\left.\begin{aligned} \Gamma_1 &= \int_0^\infty e^{-\alpha r_1} r_1^{9/2} J_{3/2}(k r_1)\, d r_1 \int_0^\infty e^{-(\alpha+1)r_2} r_2^2 d r_2 , \\ \Gamma_2 &= \int_0^\infty e^{-\alpha r_1} r_1^{7/2} J_{3/2}(k r_1)\, d r_1 \int_0^\infty e^{-(\alpha+1)r_2} r_2^3 d r_2 , \\ \Gamma_3 &= \int_0^\infty e^{-\alpha r_1} r_1^{5/2} J_{3/2}(k r_1)\, d r_1 \int_0^\infty e^{-(\alpha+1)r_2} r_2^4 d r_2 , \end{aligned}\right\} \tag{35}$$

and

$$\Delta = 2q(\Delta_1 + \Delta_2) , \tag{36}$$

where

$$\left.\begin{aligned} \Delta_1 &= \int_0^\infty e^{-\alpha r_1} r_1^{7/2} J_{3/2}(k r_1)\, d r_1 \int_0^\infty e^{-(\alpha+1)r_2} r_2^2 d r_2 , \\ \Delta_2 &= \int_0^\infty e^{-\alpha r_1} r_1^{5/2} J_{3/2}(k r_1)\, d r_1 \int_0^\infty e^{-(\alpha+1)r_2} r_2^3 d r_2 . \end{aligned}\right\} \tag{37}$$

Further

$$E = 2q(\Gamma_1 + 2\Gamma_2 + \Gamma_3), \qquad Z_1 = 2q(\Gamma_1 + \Gamma_3), \qquad Z_2 = \tfrac{2}{3}q\Gamma_3 . \tag{38}$$

In order to express the integrals for B in terms of r_1 and r_2, we note that

$$\left.\begin{aligned}&\int_{r_1=0}^{\infty}\int_{r_2=0}^{\infty} f(r_1, r_2, x, \hat{r})\, dr_2 dr_1 \\ &= \int_{r_1=0}^{\infty}\int_{r_2=0}^{r_1} f\left(r_1, r_2, \frac{r_2}{r_1}, r_1\right) dr_2 dr_1 + \int_{r_1=0}^{\infty}\int_{r_2=r_1}^{\infty} f\left(r_1, r_2, \frac{r_1}{r_2}, r_2\right) dr_2 dr_1 ,\end{aligned}\right\} \tag{39}$$

in accordance with equations (20). It is seen that we can write

$$B = 2q(\tfrac{1}{3}B_1 + B_2 + {}^{1}_{5}B_3 - \tfrac{1}{3}B_4) , \tag{40}$$

where

$$\left.\begin{aligned}B_1 &= \int_{r_1=0}^{\infty} e^{-ar_1} r_1^{3/2} J_{3/2}(kr_1) \int_{r_2=0}^{r_1} e^{-(a+1)r_2} r_2^4 dr_2 dr_1 \\ &\qquad + \int_{r_1=0}^{\infty} e^{-ar_1} r_1^{9/2} J_{3/2}(kr_1) \int_{r_2=r_1}^{\infty} e^{-(a+1)r_2} r_2 dr_2 dr_1 , \\ B_2 &= \int_{r_1=0}^{\infty} e^{-ar_1} r_1^{7/2} J_{3/2}(kr_1) \int_{r_2=0}^{r_1} e^{-(a+1)r_2} r_2^2 dr_2 dr_1 \\ &\qquad + \int_{r_1=0}^{\infty} e^{-ar_1} r_1^{5/2} J_{3/2}(kr_1) \int_{r_2=r_1}^{\infty} e^{-(a+1)r_2} r_2^3 dr_2 dr_1 , \\ B_3 &= \int_{r_1=0}^{\infty} e^{-ar_1} r_1^{-1/2} J_{3/2}(kr_1) \int_{r_2=0}^{r_1} e^{-(a+1)r_2} r_2^6 dr_2 dr_1 \\ &\qquad + \int_{r_1=0}^{\infty} e^{-ar_1} r_1^{9/2} J_{3/2}(kr_1) \int_{r_2=r_1}^{\infty} e^{-(a+1)r_2} r_2 dr_2 dr_1 , \\ B_4 &= \int_{r_1=0}^{\infty} e^{-ar_1} r_1^{3/2} J_{3/2}(kr_1) \int_{r_2=0}^{r_1} e^{-(a+1)r_2} r_2^4 dr_2 dr_1 \\ &\qquad + \int_{r_1=0}^{\infty} e^{-ar_1} r_1^{5/2} J_{3/2}(kr_1) \int_{r_2=r_1}^{\infty} e^{-(a+1)r_2} r_2^3 dr_2 dr_1 .\end{aligned}\right\} \tag{41}$$

The integrations over r_2 are readily performed, using the elementary recursion formula

$$\left.\begin{aligned}K_j &= \int e^{-qr} r^j dr \\ &= -\frac{1}{q}\{e^{-qr} r^j - jK_{j-1}\} .\end{aligned}\right\} \tag{42}$$

After the integrations over r_2 have been carried out, we see that the remaining integrals are of the general type

$$\mathcal{J}_m(q) = \int_0^{\infty} e^{-qr} r^{m+1/2} J_{3/2}(kr)\, dr . \tag{43}$$

Thus,

$$\left.\begin{aligned}
&A=\frac{4q}{(a+1)^3}\mathcal{J}_2(a)\,,\qquad \Delta_1=\frac{2}{(a+1)^3}\mathcal{J}_3(a)\,,\qquad \Delta_2=\frac{6}{(a+1)^4}\mathcal{J}_2(a)\,,\\
&\Gamma_1=\frac{2}{(a+1)^3}\mathcal{J}_4(a)\,,\qquad \Gamma_2=\frac{6}{(a+1)^4}\mathcal{J}_3(a)\,,\qquad \Gamma_3=\frac{24}{(a+1)^5}\mathcal{J}_2(a)\,,\\
&B_1=\frac{24}{(a+1)^5}\mathcal{J}_1(a)-\frac{24}{(a+1)^5}\mathcal{J}_1(2a+1)-\frac{24}{(a+1)^4}\mathcal{J}_2(2a+1)\\
&\qquad\qquad -\frac{12}{(a+1)^3}\mathcal{J}_3(2a+1)-\frac{3}{(a+1)^2}\mathcal{J}_4(2a+1)\,,\\
&B_2=\frac{2}{(a+1)^3}\mathcal{J}_3(a)+\frac{6}{(a+1)^4}\mathcal{J}_2(2a+1)+\frac{4}{(a+1)^3}\mathcal{J}_3(2a+1)\\
&\qquad\qquad +\frac{1}{(a+1)^2}\mathcal{J}_4(2a+1)\,,\\
&B_3=\frac{720}{(a+1)^7}\mathcal{J}_{-1}(a)-\frac{720}{(a+1)^7}\mathcal{J}_{-1}(2a+1)-\frac{720}{(a+1)^6}\mathcal{J}_0(2a+1)\\
&\quad -\frac{360}{(a+1)^5}\mathcal{J}_1(2a+1)-\frac{120}{(a+1)^4}\mathcal{J}_2(2a+1)-\frac{30}{(a+1)^3}\mathcal{J}_3(2a+1)\\
&\qquad\qquad -\frac{5}{(a+1)^2}\mathcal{J}_4(2a+1)\,,\\
&B_4=\frac{24}{(a+1)^5}\mathcal{J}_1(a)-\frac{24}{(a+1)^5}\mathcal{J}_1(2a+1)-\frac{18}{(a+1)^4}\mathcal{J}_2(2a+1)\\
&\qquad\qquad -\frac{6}{(a+1)^3}\mathcal{J}_3(2a+1)-\frac{1}{(a+1)^2}\mathcal{J}_4(2a+1)\,.
\end{aligned}\right\}\tag{44}$$

Since

$$J_{3/2}(x)=\left(\frac{2}{\pi x}\right)^{1/2}\left(\frac{\sin x}{x}-\cos x\right),\tag{45}$$

we have

$$\mathcal{J}_m(q)=\left(\frac{2}{\pi k}\right)^{1/2}\left(\frac{1}{k}\int_0^\infty e^{-qr}r^{m-1}\sin(kr)\,dr-\int_0^\infty e^{-qr}r^m\cos(kr)\,dr\right).\tag{46}$$

The two integrals in equation (46) are elementary and involve Γ-functions. We readily find that, when $m>0$,

$$\mathcal{J}_m(q)=-\left(\frac{2}{\pi k}\right)^{1/2}(m-1)!\,\rho^m k^{-1}\{m\rho k\cos[(m+1)\xi_0]-\sin(m\xi_0)\},\tag{47}$$

where

$$\xi_0=\tan^{-1}\frac{k}{q},\qquad \rho=(q^2+k^2)^{-1/2}.\tag{48}$$

The cases $m=-1, m=0$, occur in the evaluation of B_3 (eq. [44]). They can be treated separately to give

$$\mathcal{J}_{-1}(q)=\left(\frac{2}{\pi k}\right)^{1/2}\left(1-\frac{q}{k}\xi_0\right);\qquad \mathcal{J}_0(q)=\left(\frac{2}{\pi k}\right)^{1/2}\left(\frac{1}{k}\xi_0-\rho\cos\xi_0\right).\tag{49}$$

It is now necessary only to use formulae (47), (48), and (49) to obtain the explicit forms of A, Γ_1, Γ_2, Γ_3, Δ_1, Δ_2, B_1, B_2, B_3, and B_4. Combining these according to formulae (22), (28), (34), (36), (38), and (40) and rearranging the terms, we finally obtain

$$\left.\begin{aligned}\mu_z = &-(2048\pi^3)^{1/2}N\sigma^3k^{-2}i\{6(\gamma+\epsilon+\zeta)\rho_3^4(4\rho_3k\cos 5\xi_1\\ &-\sin 4\xi_1)+2(\beta-6\sigma\gamma+\delta+6\sigma\epsilon)\rho_3^3(3\rho_3k\cos 4\xi_1-\sin 3\xi_1)\\ &+(1+12\sigma^2\gamma+3\sigma\delta+12\sigma^2\epsilon+4\sigma^2\zeta)\rho_3^2(2\rho_3k\cos 3\xi_1-\sin 2\xi_1)\\ &-2\beta[\sigma\rho_4^2(2\rho_4k\cos 3\xi_2-\sin 2\xi_2)+6\sigma^2\rho_4(\rho_4k\cos 2\xi_2-\sin\xi_2)\\ &+12\sigma^3k\rho_4\cos\xi_2-12\sigma^4a(\xi_1-\xi_2)]\},\end{aligned}\right\} \quad (50)$$

where for brevity we have written

$$\left.\begin{aligned}&\rho_3=(a^2+k^2)^{-1/2}, \qquad \xi_1=\tan^{-1}\frac{k}{a},\\ &\rho_4=[(2a+1)^2+k^2]^{-1/2}, \quad \xi_2=\tan^{-1}\frac{k}{2a+1}, \qquad \sigma=(a+1)^{-1}.\end{aligned}\right\} \quad (51)$$

Finally the atomic absorption coefficient k_ν is given by equation (11), setting $|\mu|=|\mu_z|$.

If we put $\delta=\epsilon=\zeta=0$ in equation (50), we recover Massey and Bates's formula[15] for the matrix element obtained by using the third-order wave-function for the ground state of H^-.

It may be of interest to see the numerical form which equation (11) for k_ν takes when the values of the constants from equation (7) are substituted in expressions (50) and (51):

$$\left.\begin{aligned}k_\nu = 10^{-17}\times\frac{\nu_{at}}{k^3}[&1.7984\,\rho_3^5k\cos 5\xi_1-0.44961\,\rho_3^4\sin 4\xi_1\\ &-0.81823\,\rho_3^4k\cos 4\xi_1+0.27274\,\rho_3^3\sin 3\xi_1+2.3295\,\rho_3^3k\cos 3\xi_1\\ &-1.1648\,\rho_3^2\sin 2\xi_1-0.67760\,\rho_4^3k\cos 3\xi_2+0.33880\,\rho_4^2\sin 2\xi_2\\ &-1.1949\,\rho_4^2k\cos 2\xi_2+1.1949\,\rho_4\sin\xi_2-1.4048\,\rho_4k\cos\xi_2\\ &+0.0101060(\xi_1^\circ-\xi_2^\circ)]^2\mathrm{cm}^2,\end{aligned}\right\} \quad (52)$$

where

$$\left.\begin{aligned}&\nu_{at}=\nu\times 2.4190\times 10^{-17}; \quad k=\sqrt{12.566\,\nu_{at}-0.052928}; \quad \tan\xi_1=1.4261\,k;\\ &\tan\xi_2=0.41625\,k; \quad \rho_3=(0.49168+k^2)^{-1/2}; \quad \rho_4=(5.7715+k^2)^{-1/2}.\end{aligned}\right\} \quad (53)$$

The values for k_λ, as computed from equations (52) and (53), are given in Table 2. In Figure 1 we have illustrated the variation of the absorption coefficient with wave length and have compared it with the older absorption-coefficient-curve of Massey and Bates.

It will be seen that at the maximum the new absorption coefficient has a value about 15 per cent greater than the old and that, further, the position of maximum has been shifted by about 1000 A to the red. A consequence of this is that the absorption coefficient now shows a smaller variation in the astronomical region of wave lengths than before; throughout the red and infrared regions the magnitude of the absorption is increased, and near the Paschen limit the increase is as much as 50 per cent.

[15] *Op. cit.*, p. 206.

The changes of the form of the absorption coefficient are qualitatively such as would be expected to remove or diminish the discrepancy between the theoretical and observed

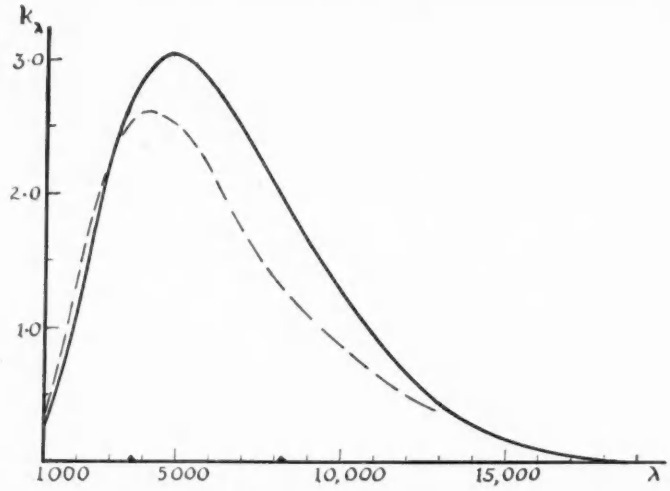

FIG. 1.—Absorption coefficient k_λ per negative hydrogen ion in units of 10^{-17} cm², as a function of wave length in angstroms. The full-line curve is that obtained in the present paper; the broken line represents the previous calculation of Massey and Bates. The positions of the Paschen and the Balmer discontinuities are marked on the wave-length scale.

TABLE 2

CALCULATED ABSORPTION COEFFICIENT FOR H^-

λA	$k_\lambda \times 10^{17}$ cm²	λA	$k_\lambda \times 10^{17}$ cm²	λA	$k_\lambda \times 10^{17}$ cm²	λA	$k_\lambda \times 10^{17}$ cm²
1000	0.2733	4000	2.898	5750	2.899	9000	1.629
1500	0.6546	4250	2.973	6000	2.824	9500	1.436
2000	1.188	4500	3.017	6500	2.657	10,000	1.255
2500	1.761	4750	3.035	7000	2.461	12,000	0.6628
3000	2.268	5000	3.029	7500	2.253	14,000	0.2729
3250	2.477	5250	3.003	8000	2.042	16,000	0.07937
3500	2.653	5500	2.955	8500	1.832	17,217	0.00000
3750	2.792						

effective temperature–color-temperature relations. Calculations along these lines are now being undertaken to determine the extent to which the new absorption coefficient will modify current astrophysical theories.

The writer is deeply indebted to Dr. S. Chandrasekhar for his constant encouragement and friendly advice, without which this work would have been impossible.

YERKES OBSERVATORY
August 27, 1942

APPENDIX

THE CHARGE DISTRIBUTION OF THE H^- ION

The wave-function $\Psi(r_1, r_2; \vartheta_1, \vartheta_2; \varphi_1, \varphi_2)$ for any two-electron system implies a charge distribution about the nucleus given by

$$\left.\begin{aligned} -\frac{dZ}{dr} = N^2 \int_{\vartheta_1=0}^{\pi} \int_{\varphi_1=0}^{2\pi} \int_{r_2=0}^{\infty} \int_{\vartheta_2=0}^{\pi} \int_{\varphi_2=0}^{2\pi} \Psi^2(r, r_2; \vartheta_1, \vartheta_2; \varphi_1, \varphi_2)\, r^2 r_2^2 dr_2 \sin\vartheta_1 \\ \times \sin\vartheta_2 d\vartheta_1 d\vartheta_2 d\varphi_1 d\varphi_2 + N^2 \int_{r_1=0}^{\infty} \int_{\vartheta_1=0}^{\pi} \int_{\varphi_1=0}^{2\pi} \int_{\vartheta_2=0}^{\pi} \int_{\varphi_2=0}^{2\pi} \Psi^2(r_1, r; \vartheta_1, \vartheta_2; \varphi_1\ \varphi_2) \\ \times r_1^2 r^2 dr_1 \sin\vartheta_1 \sin\vartheta_2 d\vartheta_1 d\vartheta_2 d\varphi_1 d\varphi_2\,, \end{aligned}\right\} \quad (1')$$

where N is the normalizing factor for Ψ. For a wave-function Ψ, which is symmetrical in the co-ordinates of the two electrons (such as the sixth-order function [6]), this becomes

$$\left.\begin{aligned} -\frac{dZ}{dr} = 2N^2 \int_{\vartheta_1=0}^{\pi} \int_{\varphi_1=0}^{2\pi} \int_{r_2=0}^{\infty} \int_{\vartheta_2=0}^{\pi} \int_{\varphi_2=0}^{2\pi} \Psi^2(r, r_2; \vartheta_1, \vartheta_2; \varphi_1, \varphi_2)\, r^2 r_2^2 dr_2 \sin\vartheta_1 \\ \times \sin\vartheta_2 d\vartheta_1 d\vartheta_2 d\varphi_1 d\varphi_2\,. \end{aligned}\right\} \quad (2')$$

The charge distribution for the H^- ion can be obtained by substituting the wave-function (6) in equation (2′). The integrations may be performed by using the general methods of section III. This gives the expression

$$\left.\begin{aligned} -\frac{dZ}{dr} = 32\pi^2 N^2 e^{-2ar} \Big\{ r \cdot 2\beta \left[\frac{15(\epsilon+\gamma)+9\zeta}{8a^7} + \frac{5\delta}{8a^6} + \frac{1}{4a^5}\right](1 - e^{-2ar}) \\ + r^2 \left(\frac{1}{4a^3} + \frac{3\delta}{4a^4} + \frac{3}{4a^5}\left[\beta^2 + \delta^2 + 2(\gamma+\epsilon+\zeta)\right] + \frac{15\delta}{4a^6}(\gamma+\epsilon+\zeta) \right. \\ + \frac{45}{8a^7}(\gamma+\epsilon+\zeta)^2 + 2\beta\left[\frac{5(\epsilon-\gamma)}{4a^6} + \frac{\delta}{4a^5} - e^{2ar}\left(\frac{25\epsilon+5\gamma+3\zeta}{8a^6}\right.\right. \\ \left.\left. + \frac{3\delta}{4a^5} + \frac{1}{8a^4}\right)\right]\Big) + r^3\left(\frac{\delta}{2a^3} + \frac{3}{4a^4}(\delta^2 + 2[\epsilon-\gamma]) + \frac{3\delta}{2a^5}(3\epsilon-\gamma+\zeta)\right. \\ + \frac{15}{2a^6}(\gamma+\epsilon+\zeta)(\epsilon-\gamma) + 2\beta\left[\frac{2\epsilon+2\gamma+3\zeta}{2a^5} + \frac{3\delta}{8a^4} + \frac{1}{4a^3}\right. \\ \left.\left. - e^{-2ar}\left(\frac{2\epsilon}{a^5} + \frac{\delta}{4a^4}\right)\right]\right) + r^4\left(\frac{1}{4a^3}\left[\beta^2 + \delta^2 + 2(\gamma+\epsilon+\zeta)\right]\right. \\ + \frac{3\delta}{4a^4}(3\epsilon+\zeta-\gamma) + \frac{3}{2a^5}(3\gamma^2 + 3\epsilon^2 + \zeta^2 - 2\epsilon\gamma + 2\gamma\zeta + 2\epsilon\zeta) \\ + \frac{\zeta^2}{a^5} + 2\beta\left[\frac{3(\epsilon-\gamma)}{4a^4} + \frac{\delta}{4a^3} - \frac{\epsilon}{2a^4}\,e^{-2ar}\right]\Big) + r^5\left[\frac{\delta}{2a^3}(\gamma+\epsilon+\zeta)\right. \\ \left. + \frac{3}{2a^4}(\gamma+\epsilon+\zeta)(\epsilon-\gamma) + 2\beta\left(\frac{\gamma+\epsilon+\zeta}{4a^3}\right)\right] + r^6\left[\frac{1}{4a^3}(\gamma+\epsilon+\zeta)^2\right]\Big\}. \end{aligned}\right\} \quad (3')$$

Numerically, this is equivalent to (using the values of the constants for H^- from equations [7] and [9])

$$-\frac{dZ}{dr} = e^{-2ar}(2.087r + 1.362r^2 - 0.5418r^3 + 0.2614r^4 - 0.02952r^5 + 0.005734r^6) - e^{-4ar}(2.087r + 0.3118r^2 - 0.08749r^3 + 0.008112r^4). \quad (4')$$

TABLE 3

r	$-dZ/dr$	r	$-dZ/dr$	r	$-dZ/dr$	r	$-dZ/dr$
0.00	0.000	0.75	0.553	1.50	0.622	4.00	0.204
0.25	0.154	1.00	0.633	2.00	0.520	5.00	0.124
0.50	0.387	1.25	0.648	3.00	0.327	6.00	0.071

The charge distribution computed from expression (4′) is shown in Table 3. Comparison with Bethe's calculation of the charge distribution,[16] using his third-order wave-function, shows that the difference between his and the present one is for most purposes negligible.

[16] *Zs. f. Phys.*, **57**, 815, 1929.

SPECTROPHOTOMETRIC OBSERVATIONS OF THE LIGHT OF THE NIGHT SKY*

C. T. Elvey and Alice H. Farnsworth

ABSTRACT

Spectrophotometric observations of the light of the night sky have been made for the stronger lines of the visual region of the spectrum to determine (1) the variation of intensity with zenith distance to obtain a measure of the height of the auroral layer and (2) the curves of nocturnal variation of intensity.

The variation of intensity with zenith distance indicates a height of 500 km for the auroral layer producing the red and green auroral lines, as well as the line of uncertain origin at λ 6560. This is greater than the height obtained for the infrared radiations, 125 km.

Curves of nocturnal variations of intensity were obtained at Bosque Alegre, Argentina; at Potrerillos, Chile; in the southern New England states; and at the McDonald Observatory. There were no marked differences with geographical position; however, the observations were not simultaneous, and the terrestrial magnetic activity was generally low at the times the observations were made. The sodium line is relatively constant through the night, but the enhancement at both evening and morning twilights—a resonance effect from the sun illuminating sodium atoms in the upper atmosphere—indicates that the distribution of sodium between levels of 70 and 115 km is exponential with height and in agreement with that of the total number of molecules. The green auroral line is found to be relatively constant throughout the night and through both twilights. The reported maximum near midnight has not been confirmed. The red auroral line, also a radiation of the oxygen atom, has remarkable twilight effects, the one in the evening lasting for three or four hours after the end of twilight and the morning effect beginning two hours before dawn. The morning twilight effect is probably due to the illumination by the sun of the atoms in the upper atmosphere; but the evening effect is composite, there being, in addition, an excess intensity which decreases exponentially with time and which comes from the atoms that are already in the shadow of the earth. That portion of the twilight effect which is related to the direct illumination of the sun indicates a much larger proportion of oxygen atoms in the upper atmosphere than theoretical considerations require.

That part of the light of the night sky which originates in the upper atmosphere has an emission spectrum. V. M. Slipher[1] has shown that the green auroral line is always present in the night sky; and this light has become known as either the "permanent" or the "nonpolar" aurora, to distinguish it from the usual form of polar aurora, or northern lights. The strongest lines of the spectrum are identified with radiations from the atoms of oxygen and sodium, and most of the remaining spectrum is of molecular origin, the nitrogen molecule being the principal contributor. Observations show that the various emissions exist throughout the night, and consequently this requires a source of energy which can supply the excitation. S. Chapman[2] has proposed a theory which is capable of supplying the energy of excitation during the night; and, although it is somewhat uncertain whether his theory can explain the variations that exist in the light of the night sky, it very probably accounts for a part of the excitation. Briefly, the theory assumes that the energy comes from sunlight which dissociates oxygen molecules during the daytime and that during the night the atoms recombine to form molecules with the liberation of the energy of dissociation. The recombination requires the participation of a third particle which will be, in general, another oxygen atom or a molecule of nitrogen. The energy of dissociation, 5.1 volts, is transferred to the third particle in the case it is an oxygen atom, exciting it to produce the green auroral line. He has shown that through these collisions it is possible to excite the various atoms and molecules that produce the spectrum of the night sky. Since there are several features about the light of the night sky which such a theory will have difficulty in explaining—for example, the irregular variations during the night, the reported

* *Contributions from the McDonald Observatory, University of Texas*, No. 59.

[1] *Ap. J.*, **49**, 266, 1919.

[2] *Phil. Mag.*, **23**, 567, 1937.

maximum of intensity of the green auroral line near midnight, and the increase in amplitude of the seasonal variation with distance from the equator—it seemed to us that additional observational material is required.

If such a mechanism as that suggested by Chapman is responsible for the light of the night sky, then we might expect the nocturnal variations of intensity to be an important factor in discussing the theory. Further, his mechanism requires three-body collisions for the transfer of energy through the night; and, since the density of the atmosphere decreases exponentially, there will come very rapidly, with increasing height, a region where the collisions are so infrequent that little or no energy will be supplied above that level. There will also be a lower limit, since at low altitudes the density will be sufficiently high for recombinations to occur at a fast rate, with the result that all atoms will be re-formed into molecules within a short time after sunset. This would then indicate that the light of the night sky should come from a rather definite layer.

Relatively little is known about the diurnal variations of intensity and of the height of the layer from which the light comes. It is our aim to add more observational data on these two points.

The spectrograph used in this investigation was made in the shop of the Yerkes Observatory by Mr. Charles Ridell. The instrument was assembled in a box made of plywood, $6 \times 11 \times 34$ inches, which served as its packing case and also for the support of the instrument. Access doors permitted the exposures to be made, the plates to be changed, and the necessary adjustments to be made with a minimum of trouble. The collimator is 20 inches long, with a slit 2 inches long. The dispersing system is one of the Mantois prisms of the Bruce spectrograph of the Yerkes Observatory. The camera is of the solid Schmidt type and was built by D. O. Hendrix. It is 2 inches in diameter and has an aperture ratio of f/0.66. The resulting linear dispersion is nearly 1500 A/mm at the sodium D line.

Two deckers have been made to fit over the slit head, one containing a set of windows, so that a series of exposures can be made on one film, the other having been provided with a set of right-angle prisms. The prisms are so placed that simultaneous exposures can be made for the following zenith distances: 0°, 40°, 60°, 70°, 80°, and 85°.

Near the end of the slit a small right-angle prism was mounted, so that light from a standard lamp could be photographed at the same time as the spectrum of the night sky. The lamp was not calibrated, since we were interested only in the changes that took place rather than in the absolute intensities. The lamp was burned below normal brightness, and the current through it was regulated by a rheostat and milliammeter. As a further check on the constancy of the light-source, a barrier-layer photocell was mounted on the opposite side of the lamp, and the photoelectric current was read with a microammeter.

The photometric scale was obtained by exposures through photographic step-wedges and Wratten gelatine filters. The sensitometric device was built as a part of the spectrograph, and the standard lamp was used as the source of light. The transmissions of the wedges were obtained with the aid of an Eastman densitometer and checked with the microphotometer which we used to measure the film.

Owing to the long slit and particularly to the set of prisms to pick up light from different parts of the sky, we had to investigate the effects of vignetting. To obtain the calibrating spectra for windows it is merely necessary to make simultaneous exposures; but with the prisms it is more difficult, since the set covers an angle of 85°. The spectrograph was set on a rotating table, so that the prisms would pass in front of a light-source consisting of a lamp behind a flashed opal screen. The intensity of the light-source was controlled so that a large number of rotations was necessary for a proper exposure. A high-contrast film was used in the spectrograph in order to obtain better accuracy for the calibration than was used for the exposures on the night sky. The mean of several determinations gave the following correction factors to be applied to the observed in-

tensities: 1.055, 1.009, 1.000, 1.060, 1.102, and 1.197, respectively, for the zenith distances 0°, 40°, 60°, 70°, 80°, and 85°.

The measurement and reduction of the spectrograms followed the standard practices. The microphotometer, however, is one recently designed by one of us and built by Mr. John Vosatka in the shop of the McDonald Observatory. It has one or two features which make it a satisfactory nonrecording microphotometer and one that can be built at a very reasonable cost. The optical system is of the simple projection type with the axis vertical and is mounted in the center of a small tower constructed of channel iron. The tower is erected on a sturdy table of iron-pipe construction. At the base of the tower and in the table top is the analyzing slit and at the top of the tower, 24 inches from the slit, is the light-source. The light is a low-wattage bulb—a 3-candle-power, tail-light lamp for automobiles. The condensing lens system projects an out-of-focus image on the plate to be measured, which is mounted on a horizontal table and has motions in two co-ordinates. An objective directly below the plate forms an image of the spectrogram on the analyzing slit in the table top. The spectrogram is enlarged roughly twenty fold, but it is possible to reduce this considerably by changing the position of the table carrying the plate. The analyzing slit is mounted on a supporting ring, so that it can be rotated to make the slit parallel with the spectrum line. The slit head also carries the photocell and amplifier tubes in a box below it. The photoelectric current is measured with a micro-microammeter similar to the one described by Roberts.[3] This is a two-stage direct-current, negative feedback amplifier, and the output is read on a microammeter of range 0–100 microamperes. The stability of the amplifier is very good, and the sensitivity is excellent.

A taper potentiometer is used as a shunt in the meter circuit, and the sensitivity of the amplifier is adjusted so that the deflection for the background of the spectrogram is somewhat greater than 100 microamperes. By an adjustment of the potentiometer it is possible to bring the deflections of the background of each plate to the same value—say 100 microamperes—thus eliminating the variation of the background fog.

We have used batteries for the source of power for the light and the amplifier, since our power lines are 110 volts d.c. However, if a source of alternating current is available, a power supply can be built which will adequately serve and thus eliminate the undesirable feature of replacements of batteries and charging of storage batteries.

We have mentioned that one of the probable results of Chapman's theory for the production of the light of the night sky is that the illumination will be produced in a relatively thin layer of the upper atmosphere. If the layer producing the light is uniform over large geographical areas, then one can compute the variation of intensity with zenith distance, by assuming that the intensity is proportional to the thickness as viewed by the observer. P. J. van Rhijn[4] has derived a simple formula, making the assumption that the thickness of the layer is small. Adapting his formula to our notation, we have

$$I_m = \frac{I_m^0}{\varphi(z)} = \frac{I_m^0}{\sqrt{1 - \dfrac{\sin^2 z}{(1+h)^2}}}, \qquad (1)$$

where I_m is the intensity at any zenith distance expressed in magnitudes, I_m^0 is the intensity at the zenith, z is the zenith distance, and h is the height to the bottom of the layer expressed in terms of the earth's radius. It will be seen that this reduces to the secant law when the height is zero. The above formula holds for a thin layer; to investigate the size of the error if the layer were thick, we have made the computations for the variation of intensity with zenith distance, using a rigorous formula with thickness of the layers up to several hundred kilometers, and find that the accuracy of van Rhijn's

[3] *Rev. Sci. Inst.*, **10**, 181, 1939.

[4] *Pub. Astr. Lab. Groningen*, No. 21, 1921.

simplified formula is such that our observational methods could not detect the difference. The resultant height is that of the middle of the thick layer. Thus the thickness of the auroral layer is indeterminate, but we should be able to tell something of its mean height.

We had planned to determine the variation of intensity with zenith distance for the stronger lines in the visual part of the spectrum under various conditions and at various localities. However, we found after the reduction of the observations that the erratic behavior within a set of observations was such that we could not hope to search for any of the detailed variations that might be expected and had to be content with averaging all the observations, thereby hoping to reduce the accidental variations. No doubt the accidental variations are a result of the nonuniform distribution of intensity through the auroral layer. Some of our spectrophotometric observations have indicated such variations, and observations[5] made at the McDonald Observatory with two photoelectric

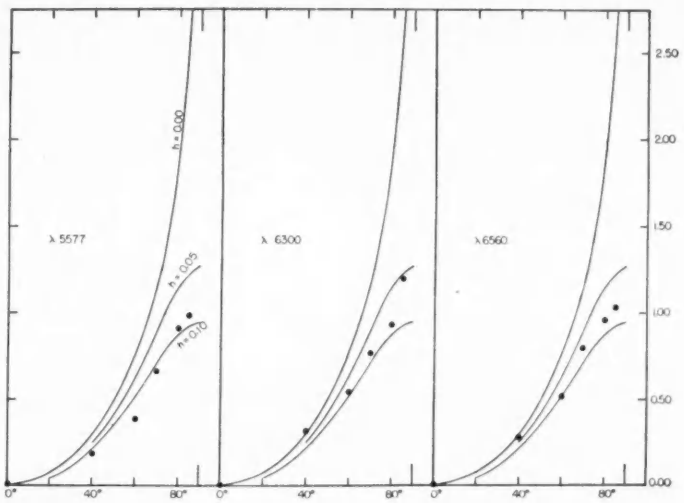

FIG. 1.—Mean variations of intensity with zenith distance. The curves are theoretical variations for heights of the auroral layer, $h=0.00$, 0.05, and 0.10, in terms of the radius of the earth.

photometers show that quite large variations exist in the light of the night sky as seen in different directions from one point. This nonuniform distribution will invalidate the method of arriving at the height from a set of observations of the variation of intensity with zenith distance. However, the irregularities will probably average out when a sufficient number of observations have been used.

The greatest uncertainty in the reduction of our observations is the correction for extinction. The usual value of the extinction determined from astronomical observations gives the loss suffered by the pencil of light from the star; but in the case of the light from the night sky the source covers a hemisphere, and, although the light from a given direction suffers the same loss as in the star, there is light scattered into the line of sight from many other directions, thus reducing the effect of extinction. It was impracticable to determine the extinction for each night of observing from each of the localities; and we have adopted the average value of the extinction for the altitude of the station, and as an approximation we have assumed that the effective value of the extinction was one-half of that of the stellar extinction for the particular wave length. This is certainly of the right order of magnitude, since the corrected observations for elevations near sea-

[5] Paper presented at the dedication of the National Astrophysical Observatory at Tonanzintla, Puebla, Mexico, February 17, 1942.

level and those at elevations of 2000 or more meters give accordant results for the large zenith distances. As a trial the normal astronomical extinction was used, and this gave markedly different variations with zenith distance for the observations taken at sea-level and those from mountains.

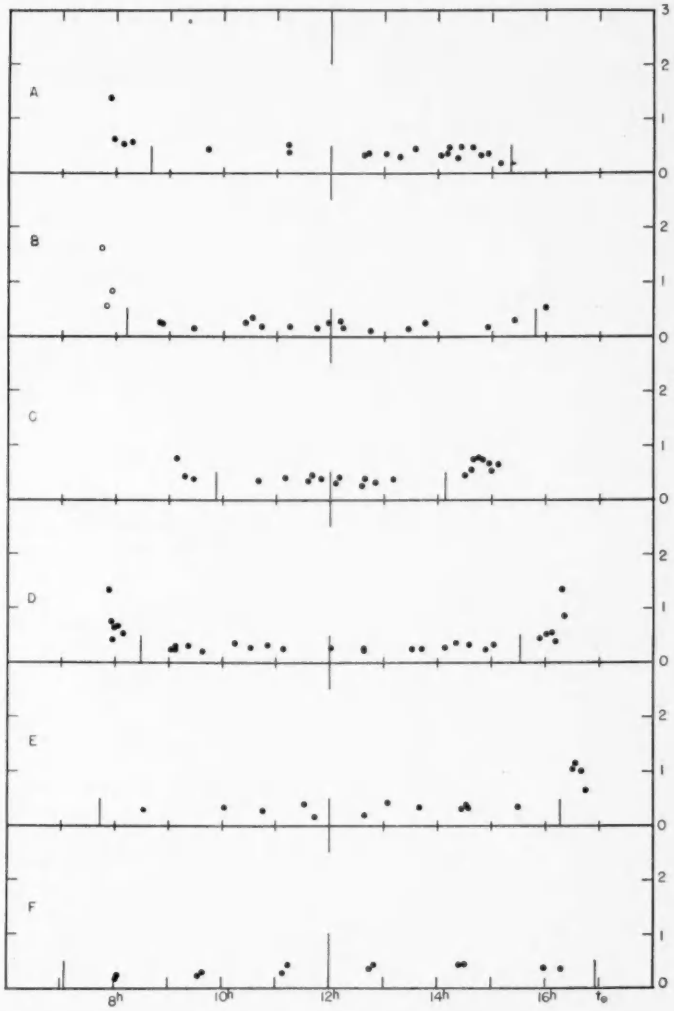

FIG. 2.—The nocturnal variations of intensity of the green auroral line, λ 5577, for *A*, Bosque Alegre, Argentina; *B*, Potrerillos, Chile; and for the southern New England states in *C*, June; *D*, April; *E*, March; and *F*, February.

In all, there were twenty-five determinations of the variation of intensity with zenith distance which were of suitable quality and which were not influenced by twilight effects. These are distributed as follows: Williams Bay, Wisconsin, 3; southern New England states, 4; Mount Locke, Texas, 4; Potrerillos, Chile, 3; and Bosque Alegre, Argentina, 11. Most of the observations were taken during the local summer season. The mean values were taken for each of the lines, λλ 5577, 6300, and 6560; and the result is shown in Figure 1, in which the zenith distances are plotted as abscissas and the intensities in

magnitudes as ordinates. Theoretical curves based on the formula (1) are shown for values of h equal to 0.00, 0.05, and 0.10. The observed curves were forced to agreement with the theoretical curves at the zenith. The data might have been adjusted by ob-

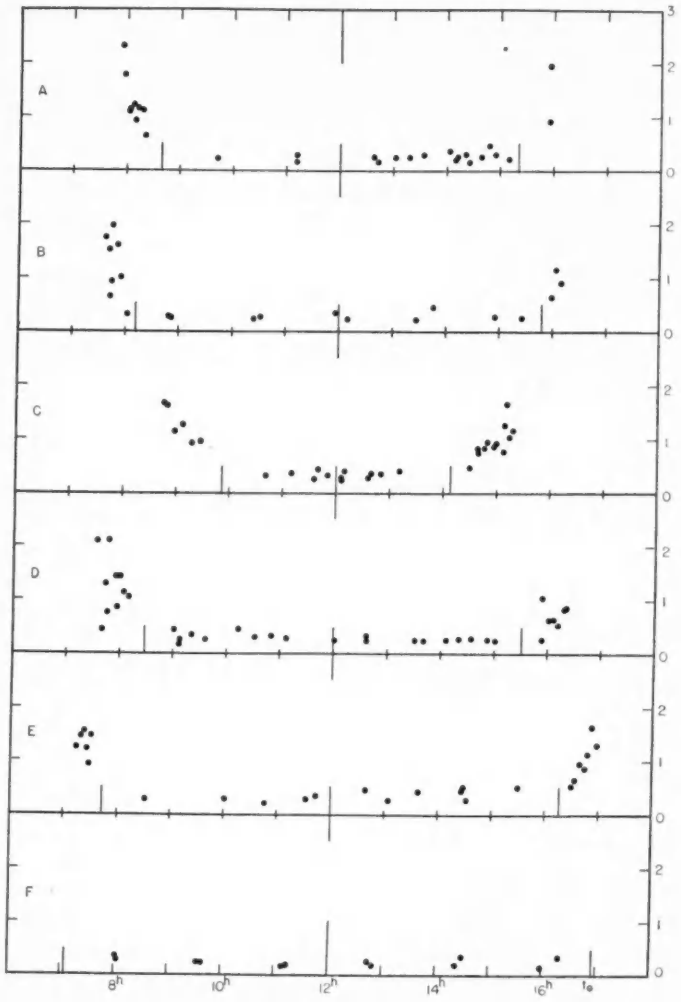

FIG. 3.—The nocturnal variations of intensity of the red auroral line, λ 6300, for *A*, Bosque Alegre, Argentina; *B*, Potrerillos, Chile; and for the southern New England states in *C*, June; *D*, April; *E*, March; and *F*, February.

taining the best fit of all the points rather than the one for the zenith. Since the ordinates are magnitudes, it is necessary only to move the points along that axis.

The mean variations of intensity with zenith distance for the two oxygen lines and the line at λ 6560 of uncertain origin are rather similar and fall between the theoretical curves computed for $h = 0.05$ and $h = 0.10$, at about 0.08. This would correspond to a height of about 500 km for the center of the layer.

This result is in disagreement with that found by one of us[5] for the integrated radia-

tions of the infrared region of the spectrum by using a photoelectric photometer. The value for the layer in that case was around 125 km; but, since there is some uncertainty as to the origin of the radiations of this region which were effective in the determination,

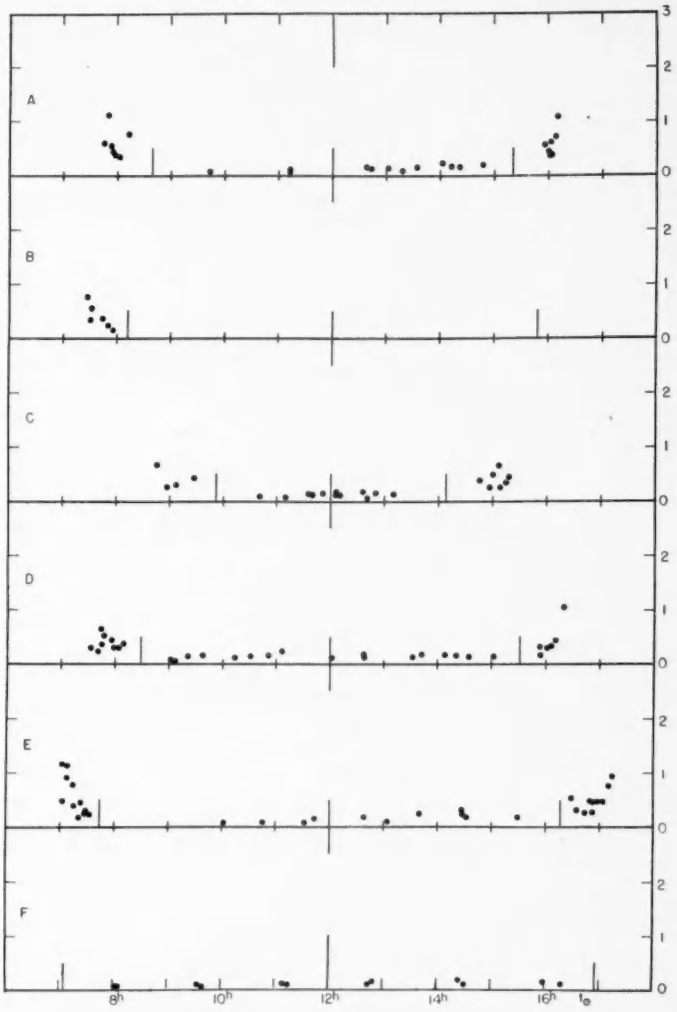

FIG. 4.—The nocturnal variations of intensity of the sodium line, λ 5893, for A, Bosque Alegre, Argentina; *B*, Potrerillos, Chile; and for the southern New England states in *C*, June; *D*, April; *E*, March; and *F*, February.

we have no a priori reason for assuming that they might come from the same region of the atmosphere.

Cabannes and Dufay[6] have observed the ratio of the intensity of the emission spectrum of the night sky at the horizon to that at the zenith and find that the height to the luminous layer must be distinctly greater than 100 km. Garrigue,[7] observing at

[6] *C.R.*, **198**, 306, 1934.

[7] *C.R.*, **202**, 1807, 1936.

Pic du Midi, has measured the ratio of the intensity near the horizon to that at the zenith for several of the stronger lines; and, although considerable variation was found, the average is of the same order of magnitude as the value found by us, thus confirming that the origin of the light is high in the atmosphere.

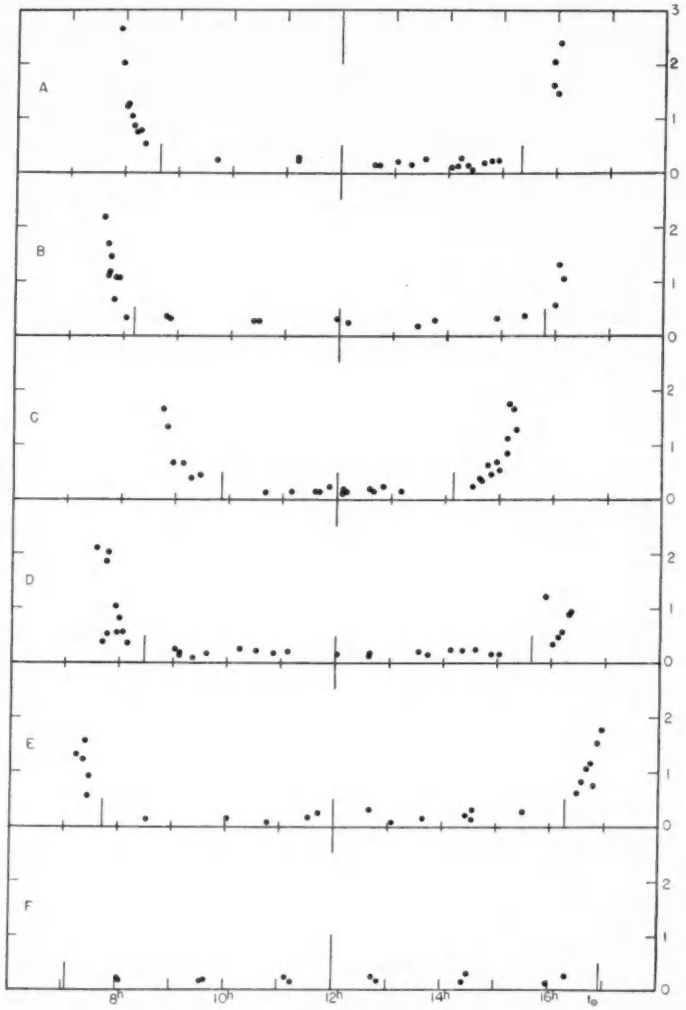

FIG. 5.—The nocturnal variations of intensity of the line of uncertain origin, λ 6560, for *A*, Bosque Alegre, Argentina; *B:* Potrerillos, Chile; and for the southern New England states in *C*, June; *D*, April; *E*, March; and *F*, February.

The studies of the nocturnal variations of intensity of the stronger lines in the visual region of the spectrum of the night sky were accomplished by using the decker containing a number of windows, which could be controlled independently. This made it possible to obtain as many as six exposures on the same spectrogram, in addition to the exposure for the standard lamp. During the twilight periods an exposure of 10 minutes is required to obtain a measurable density of the spectrogram; and, in order that more ex-

posures could be obtained during any one twilight, simultaneous exposures were made, beginning a new one every 5 minutes. In this manner it was possible to follow satisfactorily the variations through twilight. During the dark hours of the night the standard exposure for a zenith distance of 70° was 90 minutes. However, one of the windows was left open for 3–5 hours, and this has been used as a check. In general, the long exposure agreed with the mean of the shorter ones within a few per cent for the stronger lines. For the sodium line, λ 5893, which is the faintest, the percentage variation is often large.

The lines for which measures of the nocturnal variation of intensity were determined are the oxygen lines, λ 5577 and λ 6300; the sodium line, λ 5893; and the line of uncertain origin at λ 6560. The observations made at Bosque Alegre, Argentina; Potrerillos, Chile; and in the southern New England states were obtained at a zenith distance

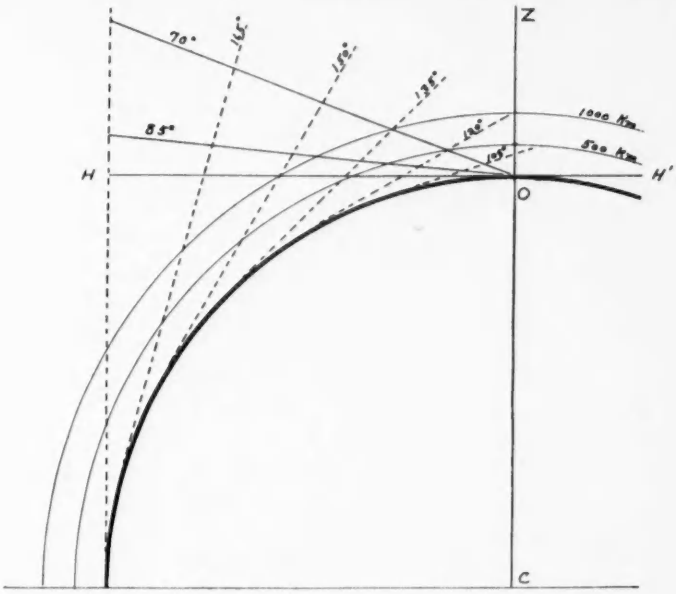

FIG. 6.—A diagram illustrating the amount of the upper atmosphere illuminated by the sun for the two zenith distances employed in this work. The dotted lines represent the limit of the earth's shadow for various zenith distances of the sun.

of 70°, whereas those obtained on Mount Locke, Texas, were at a zenith distance of 85°. Since those taken at 85° give additional information, we will discuss them separately.

The results obtained for zenith distance 70° are shown graphically in Figures 2, 3, 4, and 5. It should be remarked that the accuracy of all observations during the twilight hours is considerably less than those taken during the night, particularly when the continuous spectrum has become quite bright. In the four diagrams the intensities are proportional to the intensity of the continuous spectrum of the standard lamp at the same wave length. However, since the standard lamp has not been calibrated, the intensity of one wave length cannot be compared with another. The hour angle of the sun at the mid-exposure has been used as abscissa. The times of midnight and astronomical twilight have been marked by the longer stub lines. The data for the New England states have been divided into four parts, since there is a large variation in the length of the dark part of the night.

In general, the observations during the evening were with the spectrograph pointed

west and the morning ones with the instrument pointed toward the east. The twilight effects for the various lines which are so prominent for the observations taken at Mount Locke and which will be discussed in another part of the paper are not very evident. This, of course, is due to the fact that the sun at a given time is illuminating a much lower layer of the atmosphere for the observations at zenith distance 85° than for those at 70°. At astronomical twilight the heights are 119 and 190 km, respectively. Figure 6 illustrates the heights of the atmosphere which are being illuminated at various zenith distances of the sun and for the two zenith distances for which observations were made.

Comparing Figures 2, 3, 4, and 5, it is seen that there is less evidence for a twilight effect for the green auroral line than for the red oxygen line, λ 6300. This is confirmed by other observations. The lack of observations for the green auroral line during twilight is due to the line's being so faint that a measurement was impossible, whereas usually the red oxygen line could be measured easily.

There is very little enhancement of the sodium line at twilight, as shown in Figure 4, but this is to be expected, since Bernard[8] has shown that the enhancement of its intensity

TABLE 1

Location	λ 6560	λ 6300	λ 5893	λ 5577
Bosque Alegre, Argentina	0.20	0.29	0.15	0.42
Potrerillos, Chile	.31	.29	.....	.23
New England states (June)	.19	.40	.15	.46
New England states (April)	.22	.34	.18	.36
New England states (March)	.21	.42	.20	.40
New England states (February)	0.24	0.28	0.14	0.43

TABLE 2

Location	λ 6560	λ 6300	λ 5893	λ 5577
Bosque Alegre, Argentina	0.21	0.28	0.13	0.45
Potrerillos, Chile	.23	.25	.09	.18
New England states	.21	.33	.10	.29
Williams Bay, Wisconsin	0.12	0.34	0.14	0.39

is a resonance phenomenon and occurs when the sun illuminates the layers of the atmosphere from 60 to 80 km above the surface. For none of our observations at zenith distance 70° is the above condition fulfilled.

One object in securing observations from widely different geographical positions is to see whether differences in intensities can be detected. The program was not prepared for precise photometry, since it was known that the irregular variations which exist in the light of the night sky would mask the smaller variations, and hence we were looking only for large variations between different geographical positions. We show in Table 1 the mean value of the intensity for each location for the four lines. The data have been corrected for extinction, as was done in the preceding section. The results obtained from the data on the variation of intensity with zenith distance have been placed in Table 2, with the appropriate wave lengths. Our conclusion is that the systematic variations from station to station are smaller than the irregular variations and could therefore not be detected without a large amount of observational material, preferably taken with a photoelectric photometer. There seems to be one possible exception in Tables 1 and 2, namely, the intensity of the green auroral line as observed at Potrerillos, Chile, seems to be faint,

[8] *Zs. f. Phys.*, **110**, 291, 1938.

particularly when one considers it with respect to the other lines. The majority of the observations were taken on days when the magnetic activity was below the average.

We shall next discuss the observations obtained at Mount Locke for the nocturnal variation of intensity. These observations were not calibrated with the aid of a standard lamp and consequently cannot be compared directly with the data of the preceding section. However, we can adjust the scale of intensities so that they are of the same order by making use of the average intensities during the night. This has been done for the following diagrams, and the intensity scales on them are thus similar to those of Figures 2–5.

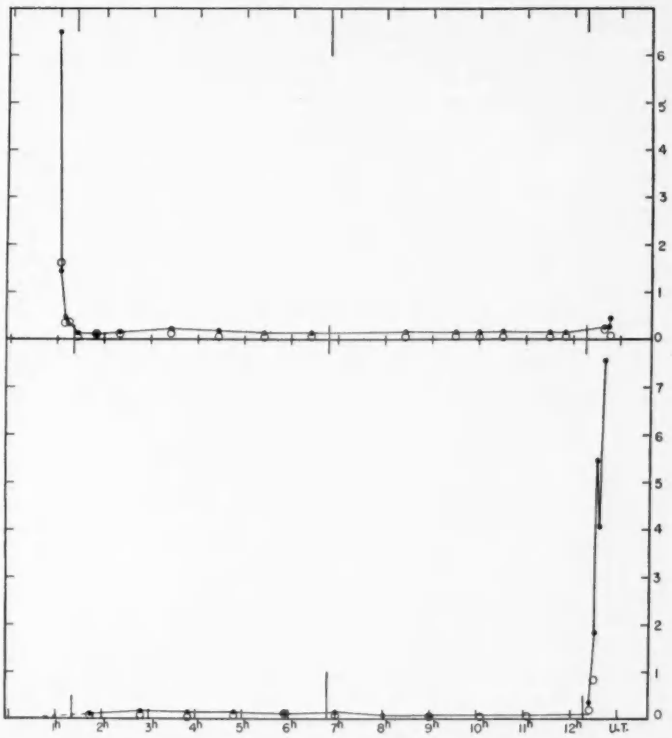

FIG. 7.—Nocturnal variations of intensity of the sodium line (*dots*) and of λ 6560 (*circles*) for the instrument pointed toward the setting sun at zenith distance of 85° (*upper*) and for the instrument pointed toward the rising sun at zenith distance of 85° (*lower*).

We shall discuss, first, the results for the sodium line, λ 5893, and the line of uncertain origin, λ 6560, and then the two oxygen lines, λ 5577 and λ 6300. All the following observations have been taken with the instrument pointed in the direction either of the setting or of the rising sun and at a zenith distance of 85°.

In Figure 7 are shown the curves of nocturnal variations of intensity for the two lines, λ 5893 of sodium and λ 6560. The dots and continuous curve represent the observations of the sodium line. In the upper part of the diagram the observations are for the spectrograph pointed westward and show the great enhancement of the sodium line in the evening twilight. The lower diagram shows similar observations for the morning twilight. This great enhancement of λ 5893 is a resonance effect and led Bernard[9] to the

[9] *C.R.*, **206**, 448, 1938.

identification of the line with the blended sodium D lines. Since the effect at both evening and morning twilights seems to be quite similar but in reverse order, we have collected all observations during December, 1939, to obtain a mean curve showing the variation at twilight. This is shown in Figure 8, in which the intensities have been plotted relative to the beginning of dawn. Since there is considerable scatter in the observations, a mean curve is drawn to represent the variation. By subtracting the background intensity of the sodium line during the night, we obtain the effect which can be attributed to the illumination of the sodium atoms in the upper atmosphere by sunlight. Since the twilight effect is most likely a resonance effect, the intensity of the sodium line will be proportional to the number of atoms illuminated by the sun. We can readily compute the height to the illuminated portion of the atmosphere for, say, each minute after the beginning of dawn and compare this with the intensity observed at that time,

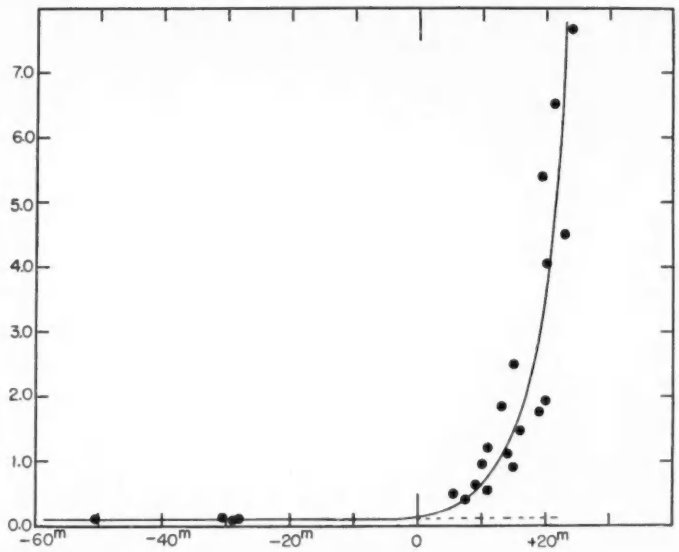

FIG. 8.—The mean variation of intensity of the sodium line at twilight. The zero is the beginning of astronomical dawn.

since the latter will be a function of the number of atoms above that level. Instead of the observed points, we have taken the intensity as indicated by the mean curve of Figure 8. Since we might expect an exponential relationship, we have plotted in Figure 9 the heights as the abscissas and the logarithms of the mean intensity curve as ordinates. Within the errors of observation the solid line can be adequately represented by a straight line, thus showing that the number of atoms above a given level decreases as an exponential function of the height. For a comparison, the theoretical number of molecules above a given level has been represented by the dotted line. We thus see that the distribution of the sodium atoms in the atmosphere between the heights of 70 and 115 km is very similar to that of the total number of molecules. Bernard[8] had interpreted the sudden appearance of the sodium line at dawn or its disappearance at evening twilight as evidence that the sodium atoms occupied a layer in the region from 60 to 80 km, but our observational material confirms the suggestion of S. Chapman[10] that it indicates only the exponential decrease of density of the sodium atoms.

[10] *Ap. J.*, **90**, 309, 1939.

The band, λ 6560, seems to behave in a manner similar to the sodium line; but, owing to the great intensity of the continuous spectrum in this region, it is not possible to measure the intensity of the line equally far into the twilight. If the resonance effect is real, then this information will be useful in the identification of this radiation.

The two oxygen lines, λ 5577 and λ 6300, are both transitions from metastable states of the oxygen atom; the transition which produces the green auroral line leaves the atom in the excited state, which is the origin of the red auroral line. In Figure 10 are shown the curves of nocturnal variation of intensity for the two oxygen lines; the upper diagrams are for the instrument pointed toward the setting sun and the lower diagram for the instrument pointed toward the rising sun. The circles and the dashed line represent the observed intensities of the green auroral line, while the dots and solid line represent the red auroral line. It is noticed that there is a striking effect of twilight on the red line,

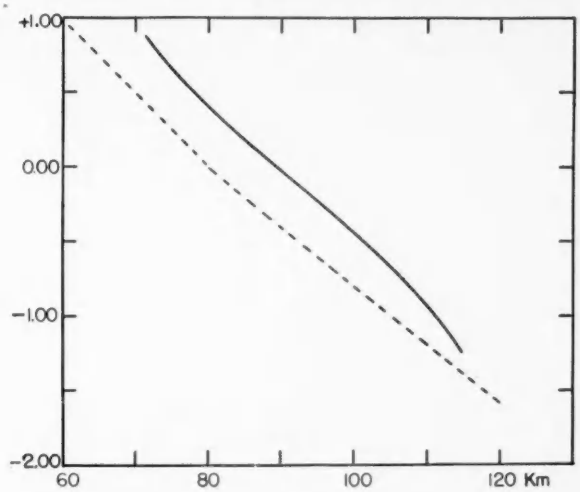

FIG. 9.—The logarithm of the mean intensity of the sodium line at twilight plotted against the height of the illuminated portion of the atmosphere in the line of sight. The broken line is proportional to the total number of atoms above the corresponding levels.

λ 6300, whereas for the green auroral line the intensity remains about the same through the twilight and through the night.

It appears from a study of several curves that the twilight effect for the line λ 6300 is due in large part to the illumination of the sun; but, as has been suggested by Cabannes and Garrigue,[11] the direct sunlight cannot account for all of it, since the red line is distinctly stronger than the green line in the earth's shadow shortly after sunset. This is illustrated by the second set of curves in Figure 10, in which the instrument was pointed toward the eastern horizon, and it is seen that the red line remains stronger than the green one for a period of nearly 4 hours. At no time during these exposures could the sun have been shining on any portion of the atmosphere. The suggestion has been made that resonance might be responsible for the twilight effect of λ 6300, but this seems rather unlikely because the line represents a forbidden transition.

In order to study the remarkable behavior of the oxygen lines in detail we have taken the mean values of the intensities obtained during the month of December, 1939, to obtain the mean curve of nocturnal variation of intensity, and the results are shown in

[11] *C.R.*, **203**, 484, 1936.

Figure 11 (upper part). The values for the first part of the night are for the instrument pointed westward and for the last part toward the east, both at a zenith distance of 85°. The dots and continuous line represent the mean curve for the red oxygen line, while the large open circles represent the green line. The green auroral line, thus, is seen to be relatively constant throughout the night and through both evening and morning twilight. There is a slight variation, but it is not large enough to be considered real. The evening twilight effect for the red oxygen line is distinctly larger than the

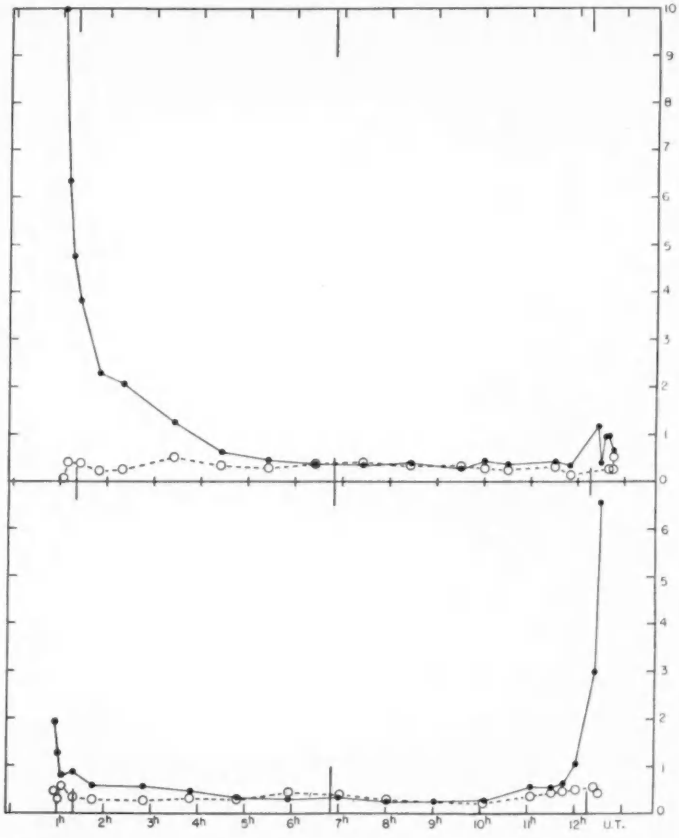

FIG. 10.—Nocturnal variations of intensity for the green auroral line (*circles*) and the red auroral line (*dots*) for the instrument pointed toward the setting sun at a zenith distance of 85° (*upper*) and toward the rising sun at zenith distance 85° (*lower*).

morning twilight or dawn effect. This may be due, no doubt, to the fact that the upper atmosphere has been in the sunshine throughout the day, whereas there has been no such influence preceding the morning twilight effect. From the course of the curve through the middle part of the night it appears that one might easily sketch the probable intensity through the dawn as indicated by the dashed line. By subtraction we have a measure of the dawn effect. For a trial we might assume that the influence of the sunlight on the upper atmosphere which is producing the twilight effects is the same in both cases, and we can then subtract this effect from the evening observations. We have done this, and the results are shown in the lower diagram of Figure 11. The correspond-

ing parts of this curve agree quite well with observations such as those in the lower part of Figure 10. This residual effect is not similar to the variation of the green auroral line, and thus we must assume that after sunset there is a larger number of oxygen atoms in the ^1D state than can be accounted for by transitions downward from the ^1S state, which produces the green auroral line. Since the green auroral line is relatively constant throughout the night, we might expect a relatively constant intensity of the red oxygen line from this cause and hence subtract it in order to get the true residual difference between the morning and the evening twilight effects. After the constant intensity has been subtracted, the remainder is similar to an exponential curve; hence, we have plotted

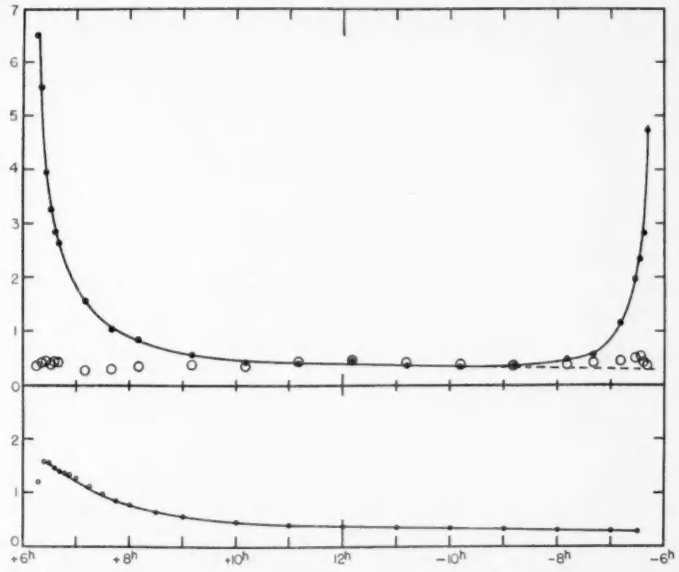

FIG. 11.—Mean curve (*upper diagram*) of nocturnal variations of intensity for the green auroral line (*circles*) and the red auroral line (*dots*). The portions of the curve before midnight were made with the instrument pointing toward the setting sun and after midnight toward the rising sun. The zenith distance is 85°. The residual intensity of the red auroral line is shown in the lower diagram, after the twilight effect as indicated by the morning observations has been subtracted from both evening and morning.

the logarithm of the intensity against time. Figure 12 shows that the decrease in intensity is exponential, and we may thus conclude that in all probability the difference between the evening and the morning twilight effects is due to some phenomenon in the atmosphere independent of the direct illumination of the sun on the upper atmosphere. The measurable effect lasts until about midnight.

Since the morning twilight effect begins as soon as the sun illuminates the upper atmosphere and increases as more of the atmosphere is affected, we might expect that the intensity would be in some manner related to the number of oxygen atoms above the level where the earth's shadow is cutting the line of sight. The height to the shadow can be readily computed, as was done for the discussion of the sodium line, and again we can plot the logarithm of the intensity against this height. This has been done in Figure 13. A line has been drawn which is proportional to the theoretical number of oxygen atoms above a given level, assuming that all oxygen molecules above 80–100 km are dissociated. We see that only at the lower levels does the observed curve approach parallelism with the theoretical line. If we assume that the intensity at 100 km agrees with the theoretical number of oxygen atoms, then at a height of 200 km we find that

the intensity is some 2000 times that to be expected for the theoretical distribution of the number of atoms. Further, if one considers higher levels, the discrepancy is even relatively worse. We may thus conclude that, if the twilight effect is a direct result of the illumination of the upper atmosphere by the sun, the observations indicate a much slower decrease in the number of oxygen atoms with height than previous theoretical considerations had indicated.

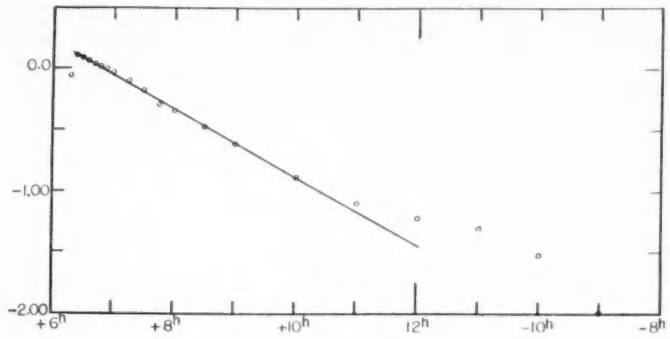

FIG. 12.—A plot of the logarithm of the residual intensity, showing that the residual intensity decreases exponentially with time.

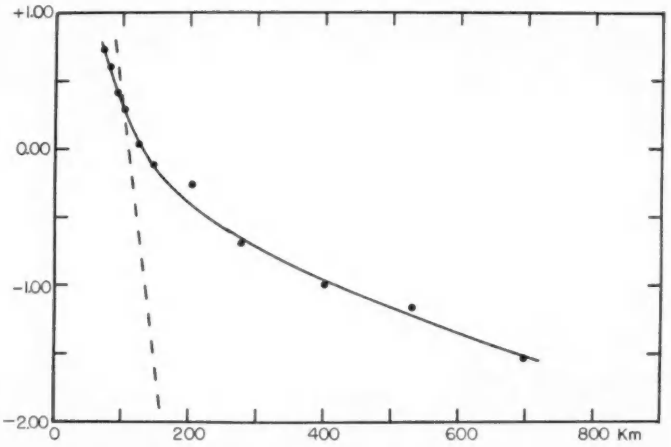

FIG. 13.—A plot of the logarithm of the intensities of the twilight effect against the height to the illuminated portion of the atmosphere. If the intensities were proportional to the theoretical number of atoms, the curve should be a straight line having the slope of the broken line.

We may summarize the results of our observational work as follows: The height of the auroral layer producing the green and red auroral lines and the line of uncertain origin, λ 6560, is about 500 km. The curves of nocturnal variation of intensity show the sodium line to be relatively constant throughout the night, but with a great enhancement in both the evening and the morning twilights. The enhancement is a resonance effect and shows that the sodium atoms are decreasing exponentially between heights of 70 and 115 km, which is similar to the decrease in the total theoretical number of molecules. During the period for which the observations were made there were no marked differences in the intensities between stations of the United States and of Argentina and Chile:

however, these observations were not simultaneous, and, furthermore, the magnetic activity at the time of the observations was low. The nocturnal variations of intensity for the green auroral line throughout both twilights and the night are relatively constant, and we do not find evidence of a maximum near midnight. The curves of nocturnal variation of intensity for the red oxygen line, λ 6300, show remarkable twilight effects; the one for the evening is larger than the one for the morning. The evening twilight effect for the red oxygen line is a result of direct sunlight, as is the morning effect; but in addition there is a residual intensity which decreases exponentially with time, lasting for about 4 or 5 hours after the sun has ceased illuminating the atmosphere. The twilight effects from direct sunlight show that the number of oxygen atoms in the upper atmosphere is much higher than theoretical considerations would lead one to expect.

In conclusion we wish to express our gratitude for a grant from the Permanent Science Fund of the American Academy of Arts and Sciences, which assisted one of us (A. H. F.) to obtain spectroscopic observations in South America, and to Director Enrique Gaviola for his cordial welcome to the Argentine National Observatory at Córdoba, and for his generous provision for work and living arrangements at the mountain station, Bosque Alegre. We are also indebted to Mr. Walter Linke, who assisted in making many of the observations at Mount Locke, and to Mr. Joseph Ross Brown, who assisted with some of the reductions of the observations and with the calibration of the spectrograph for vignetting.

McDonald Observatory
Fort Davis, Texas
and
Mount Holyoke College
South Hadley, Massachusetts
August 1942

SPECTROGRAPHIC OBSERVATIONS OF NOVA HERCULIS (1934) AND NOVA SERPENTIS (1909) WITH IDENTIFICATIONS OF [*Fe* v] AND [*Fe* III] IN NOVA PICTORIS (1925)*

P. SWINGS AND O. STRUVE

ABSTRACT

I. The velocities of expansion of Nova Herculis show a range of from 338 km/sec for [*O* II] to 256 km/sec for [*O* III]. This suggests stratification. The lines show curved outer components, with a faint indication of a central line in the case of $H\gamma$. Considerable change has taken place in the relative intensities of the emission lines since 1940. The continuous spectrum of the central star has decreased in brightness.

II. The forbidden spectra of [*Fe* v] and [*Fe* VI] are well developed in the present spectrum of Nova Serpentis. Although thirty-three years have elapsed since the outburst, the electron density in the nebulosity is still high, compared with most planetary nebulae.

III. Several unidentified lines measured by H. Spencer Jones in Nova Pictoris (1925) can now be attributed to [*Fe* v] and [*Fe* III].

I. THE SPECTRUM OF NOVA DQ HERCULIS (1934)

When the spectrum of Nova Herculis was last described two years ago,[1] its most interesting feature was the structure of the emission lines: each line consisted essentially of two components, with an approximate separation of 600 km/sec, which in terms of nebular expansion corresponded to a velocity of the order of 300 km/sec. The space between the two main components of each line was filled with fainter emission, which reached a maximum intensity in a third central component. The intensity distribution within the complex spectral lines was not exactly the same when the slit was located in different parts of the elongated image of the nebula. Under good seeing conditions, when the guiding was accurate, the two outer components were curved at the ends. Such a line structure must be due to the geometrical and kinematical characteristics of the nebular envelope; and it is interesting to examine how the effect appears now, after two additional years of evolution. The continuous nuclear spectrum, as observed at the McDonald Observatory in 1940, corresponded to a photographic magnitude estimated between 13 and 14; an accurate estimate of the brightness of the nucleus by Baade[2] gave $m_p = 13.35$. Hence, in 1940, the nucleus was still appreciably brighter than in the prenova stage ($m_p = 14.6$, according to Harvard observations). Finally, it is interesting to examine the variations in the physical conditions in the nebulosity brought about by the continued expansion of the excited gas and by the evolution of the exciting nucleus.

Spectrograms of Nova Herculis were obtained in July, 1942, at the McDonald Observatory, using the quartz prisms and the f/5 (dispersion 40 A/mm at λ 3930) and f/2 (dispersion 100 A/mm at λ 3930) cameras. During one f/5 exposure, the seeing was fairly good, and the guiding was made as accurately as possible. The object appeared definitely elongated, and the slit was placed east-west, hence at an angle of 45° with the major axis of the elliptical image. The average length of the lines on the spectrogram is 0.282 mm, corresponding to a length of 4″.17; taking into account the spreading due to inaccurate guiding, the dimension of the nebula in position angle 45° was between 3″ and 4″.

* *Contributions from the McDonald Observatory, University of Texas*, No. 60.

[1] Swings and Struve, *Ap. J.*, **92**, 295, 1940, and **94**, 296, 1941; Humason, *Pub. A.S.P.*, **52**, 369, 1940.

[2] *Pub. A.S.P.*, **52**, 386, 1940. Baade has recently given a new interpretation of the Mount Wilson observations of Nova Herculis (*Harvard Ann. Card*, No. 629).

The continuous spectrum is concentrated in a central strip; the corresponding photographic brightness of the nucleus is lower than in 1940, probably fainter than 14.0; the nucleus is slowly declining toward its prenova brightness.

As in 1940, each line consists of two outer components spaced at mid-length by about 600 km/sec, the corresponding interval being filled in with fainter emission; in $H\gamma$, a faint maximum appears in the center. The two outer components curve strongly at their ends. The complexity of several emissions, especially $H\delta$, *N* III 4640, and [*O* II] 3727 is due to blending. The outer components are not perfectly sharp, the spread in velocity which corresponds to their width being of the order of 100 km/sec. As in 1940, the violet component is slightly more intense than the red component. The separations between the intensity maxima of the outer components have been measured for several lines, and the results are given in Table 1; the images of N_1 and N_2 were too dense to be measured.

TABLE 1

SEPARATIONS OF THE OUTER COMPONENTS OF VARIOUS LINES IN NOVA HERCULIS

λ	Intensity	Identification	Separation (in Km/Sec)	Expansion Velocity (in Km/Sec)	λ	Intensity	Identification	Separation (in Km/Sec)	Expansion Velocity (in Km/Sec)
3726.2	5	[*O* II]	676	338	4685.8	7	*He* II	537	268
4340.5	8	$H\gamma$	629	314	4363.2	4	[*O* III]	511	256
4861.3	12	$H\beta$	628	314					
4379.1	4	*N* III	590	295	Mean				297

For comparison, the following expansion velocities have been measured: by Merrill[3] in 1935: 290 km/sec (from emission lines of *Fe* II and *O* I); by Stratton[4] in 1939: 260 km/sec (from N_1); by Swings and Struve[1] in 1940: 269 km/sec (from eight lines, excluding N_1); and by Humason[1] in 1940: 300 km/sec (from $H\gamma$, $H\beta$, N_1 and N_2).

Table 1 shows a considerable range in the separations. While part of this is undoubtedly due to errors of measurement, it does not seem possible to account in this manner for the difference between the separation of $H\beta$ and $H\gamma$, on the one hand, and of [*O* III] 4363, on the other. Several sets of measures have given essentially the same result. A difference in the same sense appeared in our 1940 measurements. The range in expansion velocities suggests a stratified ring or shell structure for the outer nebulosity, each element moving outward with its own velocity. Stratification effects have been invoked for the interpretation of the wide range of ejection velocities in the Wolf-Rayet and P Cygni stars and in the early stages of novae; stratification, of course, is also well known in the case of planetary nebulae.

The curved outer components of the lines are not of uniform intensity. The curved tips are weak, and the middle sections of the lines are strong. In fact, our plates do not very clearly show that the outer components merge to form complete elliptical rings, like the ones described by Baade[2] from spectrograms obtained by Humason. But it is possible that our guiding was not good enough. A slight trailing along the slit will weaken the tips of the elliptical ring-images of the lines and tend to fill the inner parts of the ring with weak emission, while the central parts of the lines, being parallel to the slit, would not be affected. Hence, it is quite possible that the apparent faintness of the elliptical rings at their tips is not real.

The elements observed in the spectrum are essentially the same as in 1940: *H* (Balmer

[3] *Ap. J.*, **82**, 413, 1935.

[4] *Observatory*, **62**, 236, 1939.

series to H_{15}), *He* I, *He* II, *C* II, *C* III, [*O* II], *O* III, [*O* III], *N* II, *N* III (not excited by Bowen's fluorescence mechanism), [*Ne* III], [*Ne* V], and [*S* II]. But the relative intensities of the different emission lines have changed appreciably. These changes are summarized in Table 2. It is evident at once that the observed variations cannot be interpreted simply on the basis of a change in density and dilution in the expanding nebulosity. Some observations at first sight even appear to be contradictory. For example, the considerable decrease in intensity of [*Ne* III] and [*Ne* V] compared to *H* and [*O* II] suggests that the ionization of neon has decreased in the nebulosity; the ionization potentials of Ne^{+} and Ne^{+++} are 40.9 and 96.7 volts, respectively. Similarly, the intensity increase of the [*O* II] lines—which have an extremely low transition probability—is not solely due to a decrease in density, since the intensity ratio of the auroral (λ 4363) and nebular (N_1, N_2) transitions of [*O* III] has not decreased very much; the intensity increase of [*O* II] is probably due partly to a reduction in the ionization of O^{+}. Yet the *N* III lines have increased

TABLE 2

ESTIMATED LINE INTENSITIES IN NOVA HERCULIS IN 1940 AND IN 1942

λ	Element	Intensity		λ	Element	Intensity	
		1942	1940			1942	1940
3426	[*Ne* V]	0–1	3	4267	*C* II	2–3	3
3444	*O* III	1–0	3	4340	$H\gamma$	8	6
3587	[*Fe* VII]	0	1	4363	[*O* III]	4	4
3726	[*O* II]	5	6	4379	*N* III	4	3
3759	*O* III+[*Fe* VII]	3	6	4471	*He* I	1–0	2
3798	H_{10}	1	2	4515	*N* III	1–2	2
3835	H_9	1–2	3	4542	*He* II	1–0	2
3869	[*Ne* III]	1–2	6	4607	*N* II	1–0	2
3889	H_8+*He* I	3	6	4640	*N* III	10	6
3970	$H\epsilon$+[*Ne* III]	4	7	4650	*C* III	2	2 bl.
4026	*He* I	1–0	1	4686	*He* II	7	5
4068	[*S* II]	2	4	4861	$H\beta$	12	8
4102	$H\delta$+*N* III	10	7	4959	[*O* III]	20	15
4200	*He* II	1–0	2	5007	[*O* III]	30	25

in intensity. A recombination spectrum of *N* III requires the photo-ionization of N^{++}, whose ionization potential is 47.20 volts; hence, an increase of ionization of N^{++} is incompatible with a decrease in ionization of Ne^{+}, if we assume that the nucleus has not changed or even if we assume that the nucleus radiates like a black body of varying temperature. It is more likely that the *N* III lines are due to a fluorescence mechanism excited by the underlying radiation. Such a mechanism is very sensitive to a variation in the far ultraviolet absorption or emission lines of the underlying star. These spectral features of the underlying star may affect the fluorescence considerably, without affecting to a comparable extent the photo-ionization.

II. THE SPECTRUM OF NOVA RT SERPENTIS (1909)

The evolution of Nova Serpentis is very slow, and no very striking spectral changes were found in comparing our spectrograms of 1940[5] and 1942. But the forbidden spectra of [*Fe* V] and [*Fe* VI] have developed more completely and constitute now the main characteristics of the nebular spectrum of Nova Serpentis. Nova Serpentis is well worth investigating at regular intervals, since the forbidden spectra of [*Fe* III, V, VI, and VII] are

[5] Swings and Struve, *Ap. J.*, **92**, 295, 1940.

becoming more and more important for the discussion of high-excitation atmospheres and of novae. For [*Fe* VI], Nova Serpentis is at present an ideal object. Unlike AX Persei and CI Cygni, which also show, at times, the [*Fe* VI] spectrum,[6] Nova Serpentis is not compli-

TABLE 3

LINES IN NOVA SERPENTIS (JULY 26, 1942)

NOVA		IDENTIFICATION		NOTE	NOVA		IDENTIFICATION		NOTE
λ	Int.	Element	λ		λ	Int.	Element	λ	
3346	2	[*Ne* V]	3345.8		4340.8	7	*Hγ*	4340.5	
3425.8	6	[*Ne* V]	3425.8		4363.0	6	[*O* III]	4363.2	
3588	0	[*Fe* VII]	3586.3	1	4471.1	1	*He* I	4471.5	
3663	1	[*Fe* VI]	3662.6	1	4541	0–1	*He* II	4541.6	
3751	0n	[*Fe* V]	3754.8	1	4639.6	1–2	*N* III	4640.6	
		[*Fe* V]	3744.	2	4657	0	[*Fe* III]	4658.2	1
3759.4	2	[*Fe* VII]	3759.4	1	4685.9	8	*He* II	4685.8	
3770	1	[*Fe* V]	3765.	2	4715.6	2	[*Ne* IV]	4714.1	2, 5, 6
		H_{11}	3770.6				*He* I	4713.1	
3783	1	[*Fe* V]	3784.2	1	4725.6	2	[*Ne* IV]	4719.7	2, 5, 6
3834.9	1	H_9	3835.4		4861.6	10	*Hβ*	4861.3	
3839.6	1–0	[*Fe* V]	3839.3	1, 3	4959.2	3–4	[*O* III]	4958.9	
3846.2	0–1	([*Fe* V]	3851)	2	4971.5	3n	[*Fe* VI]	4970.	1
3868.7	8	[*Ne* III]	3868.7				[*Fe* VI]	4974.	1
3890.2	4	[*Fe* V]	3891.4	1, 4	5006.1	7	[*O* III]	5006.8	
		He I	3888.6		5145.4	3	[*Fe* VI]	5147.	2
		H_8	3889.0		5161.0	1	[*Fe* VII]	5158.4	1
		[*Fe* VI]	3891.4	1	5175.3	5	[*Fe* VI]	5177.	1
3894.2	1	[*Fe* V]	3895.4	1	5276.3	0	[*Fe* VI]	5279.	2
3968.3	6	[*Ne* III]	3967.5				[*Fe* VII]	5274.1	1
		He	3970.1		5309.6	3n	[*Ca* V]	5309.2	1
4024.9	0	[*Fe* V]	4027.	2	5335.3	1–0	[*Fe* VI]	5336.	2
		He I	4026.2		5411.8	2–3	*He* II	5411.6	
4070.0	1	[*Fe* V]	4071.4	1	5426.0	2	[*Fe* VI]	5430.	1
		Hδ	4101.7				[*Fe* VI]	5424.	1
4100.8	5	*N* III	4097.3		5490.2	0–1	[*Fe* VI]	5486.	2
		N III	4103.4		5574.0	0–1	[*O* I]	5577.3	7

NOTES

1. These wave lengths were obtained from measurements of AX Persei and CI Cygni.
2. Predicted wave lengths.
3. Blend of two [*Fe* V] lines
4. [*Fe* V] is the main contributor.
5. Separation difficult.
6. The forbidden $^2D-{}^2P$ transition of [*Ne* IV] consists essentially of two lines predicted at λ 4714.1 (transition probability, 0.78) and λ 4719.7 (transition probability, 1.07). These predicted wave lengths may be in error by several Angstrom units. The excitation potential of ^2P is unusually high for forbidden lines (7.7 volts). No other satisfactory identification could be found for the observed lines. On our 1940 spectrograms of lower dispersion the measured wave lengths were 4717.0 and 4728.1. See also J. C. Boyce, *M.N.*, **96**, 690, 1936.
7. Probably night-sky radiation.

cated by late-type features in the visual region and has only an extremely weak continuous spectrum. On the other hand, Nova Serpentis possesses sharper lines than the nebular spectrum of Nova Pictoris which, in its latest stages, was also rich in [*Fe* VII] and [*Fe* VI].[7] Finally, the spectrum of Nova Serpentis is less complex than the spectra of

[6] Swings and Struve, *Ap. J.*, **96**, 254, 1942. [7] Bowen and Edlén, *Nature*, **143**, 374, 1939.

planetary nebulae of high excitation showing *Fe* VI.[8] The only drawback is the faintness of Nova Serpentis, which, at the time of our last observation (July 26, 1942) was approximately of the fourteenth magnitude. Table 3 gives the wave lengths measured on a spectrogram having a dispersion of 100 A/mm at λ 3930.

Besides the lines of *H* and *He* II, the strongest emissions are the forbidden transitions of [*Ne* III], [*Ne* V], [*O* III], [*Fe* VI], [*Ca* V], [*Fe* V], and [*Fe* VII]. It is interesting to notice that, thirty-three years after the nova outburst, the auroral transition of [*O* III] 4363 is still stronger than N_2 and nearly as intense as N_1. Hence the density in the nebular envelope of Nova Serpentis must still be high, compared with most planetary nebulae; it must be similar to the density in other [*Fe* III, V, VI, or VII] nebulosities, such as AX Persei, CI Cygni, and similar objects. It is higher than in the planetary nebula IC 4997, which is characterized by strong λ 4363.

Table 3 shows several [*Fe* VI] lines which could not be detected in AX Persei or CI Cygni because of the presence of late-type features in these latter stars. The [*Fe* VI] spectrum is also better represented in Nova Serpentis than in Nova Pictoris and slightly better than in the planetary nebulae of high excitation.

III. IDENTIFICATION OF FORBIDDEN [*Fe* V] AND [*Fe* III] LINES IN THE SPECTRUM OF NOVA RR PICTORIS (1925)

Nova Pictoris is a remarkable representative of the slow nova type, and the evolution of its spectrum has been studied thoroughly by H. Spencer Jones.[9] When the spectrum was last described in 1934, the emission consisted mainly of lines which were attributed to [*Fe* VII] and [*Fe* VI] by Bowen and Edlén.[10] It may be expected that, at some earlier time, between the [*Fe* II] and the [*Fe* VI and VII] stages, the [*Fe* V] and [*Fe* III] spectra were also present. The attribution to [*Fe* III] of the line λ 4658 observed in various novae, including Nova Pictoris, was made by Edlén and Swings in 1939;[11] additional identifications will be given here. Moreover, the leading transitions of [*Fe* V] will also be identified. The importance of the spectra of [*Fe* III, V, VI, and VII] in the interpretation of nova spectra was emphasized by Edlén at the 1939 Paris Conference on novae and white dwarfs.[12]

[*Fe* V] LINES

As was mentioned by Edlén,[12] the identification of [*Fe* V] is difficult, because several of the predicted lines, which would be expected to be the most probable, fall very close to *H* or *He* I lines. Quite recently, Wyse[13] reached the conclusion that no identification of [*Fe* V] in nebulae could be considered as satisfactory. The situation was improved considerably when it was found last winter[14] that the high-excitation object AX Persei, which has very sharp lines, had reached a stage in which the [*Fe* V] spectrum was outstanding; it was possible to separate most of the [*Fe* V] lines from the *H* or the *He* I transitions and to estimate their relative intensities. It is on the basis of the results obtained in this way that the identifications of [*Fe* V] have been made possible in Nova Pictoris.

Transition $^5D - {}^3F$.—The strongest line is $^5D_4 - {}^3F_4$, whose predicted wave length is λ 3892 and whose wave length in AX Persei is λ 3891.4 (int. 4). An unidentified line was

[8] A. B. Wyse, *Lick Obs. Contr.*, Ser. II, No. 4; *Ap. J.*, **95**, 35, 1942.

[9] For the nebular stages of Nova Pictoris see *M.N.*, **91**, 777, 1931; **92**, 728, 1932; **94**, 35, 1933; and **94**, 816, 1934.

[10] *Loc. cit.*

[11] *Observatory*, **62**, 234, 1939.

[12] "Les novae et naines blanches," *Compt. rend. du colloque internat. d'ap. de 1939*, Paris: Hermann & Co., 1940. A copy of the proof of these *Proceedings* may be borrowed from the authors.

[13] *Loc. cit.*

[14] Swings and Struve, *Ap. J.*, **96**, 254, 1942.

found by Spencer Jones in the 1926 spectra at λ 3893.4 (int. 3); it was described as follows: "The λ 3893.4 line overlaps the $H\zeta$ band, appearing as a well-defined wing on its long wave-length side. It was first seen on the plate of 1926 March 20, but may have been present at an earlier date as the earlier plates of 1926 are too weak at $H\zeta$ to show it." The strongest transition, $^5D_3 - {}^3P_2$ of the second [*Fe* v] multiplet, has the predicted wave length λ 3896 and was observed in AX Persei at λ 3895.4 (int. 3). The line observed by Spencer Jones is a blend of these two [*Fe* v] lines. At later stages the line probably became lost in $H\zeta$.

The second strongest line of the $^5D - {}^3F$ multiplet is $^5D_3 - {}^3F_3$, with predicted wave length λ 3839 and wave length in AX Persei λ 3839.3 (int. 2). Again, another [*Fe* v] line, $^5D_2 - {}^3P_2$, is practically coincident (predicted wave length λ 3838). A line was measured in Nova Pictoris at λ 3840.1 (int. 1) in 1926, λ 3839.8 in 1933, and λ 3841.3 in 1934 (blended with $H\eta$, λ 3835.4, in 1934). It was described as follows:

The λ 3840.2 emission appears as a weak wing to the $H\eta$ band. Comparison with other hydrogen bands indicates that it is not a true wing but a weak overlapping band. The measured wave-length is based on the extent of the overlap and agrees closely with the wave-length, measured by Wright, of a line in the spectrum of BD+30°3639. It had probably strengthened in 1928, as the appearance of a wing was not shown, but the measured wave-length of $H\eta$ on both Cape and Johannesburg plates of that year shows the effect of a blend with a line of longer wave-length than $H\eta$. Its origin is not known.

Transition $^5D - {}^3P$.—The (3–2) and (2–2) lines have been considered in the preceding paragraph. The $^5D_2 - {}^3P_1$ line has the predicted wave length of λ 4071 and was found in AX Persei at λ 4071.4 (int. 2). A line was measured in Nova Pictoris at the following wave lengths:

1925.....λ 4068.6 (int. 6)	1928.....λ 4072.3 (int. 5)
1926.....λ 4070.3 (int. 6)	1934.....λ 4071.3 (weak)

It was described as follows:

The emission at λ 4068.6 first appeared about 1925 October, at the same time as the forbidden iron bands. It is present in the spectra of η Carinae and of "iron" stars, such as BD−12°1500. The measured wave-length shows a general increase, and it appears probable that in the later stages another emission of greater wave-length emerges and blends with it.

The line measured in 1925 at λ 4068.6 is undoubtedly due to [*S* II]. The blending by [*Fe* v] appeared later and increased, hence giving rise to a gradual increase in wave length. Such a gradual shift in wave length cannot be due to the blending by the second, weak [*S* II] line at λ 4076.

Next comes $^5D_1 - {}^3P_0$, whose predicted wave length is λ 4181 and whose wave length in AX Persei is λ 4180.6 (int. 1). In 1926 a line was measured in Nova Pictoris at λ 4178.9 (int. 3) and was attributed to *Fe* II; in 1928 the measured wave lengths were λ 4181.0 (int. 3), and λ 4180.2 (int. 2). The line is described as follows:

The Fe^+, λ 4179, emission is weak in 1926 March and April, but subsequently strengthens. An emission of approximately the same wave-length is present in the spectrum in 1928, when metallic emissions have almost entirely disappeared. It would seem that another emission, at about λ 4180, appears about 1926 May; its origin is unknown.

The line λ 4180 is undoubtedly the $^5D_1 - {}^3P_0$ transition of [*Fe* v].

Finally, the last line of [*Fe* v], which is not hopelessly masked by *H* or *He* I and which is observed in AX Persei, is $^5D_0 - {}^3P_1$, predicted wave length, λ 4003, observed wave length in AX Persei, λ 4003.7 (int. 1–0). A line was measured in Nova Pictoris at λ 4004.9 (int. 0) in 1926 and λ 4005.1 (int. 3) in 1928. Its description is: "The emission at λ 4004.9 is weak and was suspected on several plates and measured only on that of October 4. The wave-length is very uncertain." This line is, at least partly, due to [*Fe* v]. Some doubt

remains in this case, because the line measured at λ 4003.7 in AX Persei may not be entirely due to [*Fe* v]; a line is also present at the same wave length in CI Cygni, although [*Fe* v] is very faint in this latter star.

[*Fe* III] LINES

Transition $^5D - {}^3F$.—The strongest transition, $^5D_4 - {}^3F_4$, λ 4658, is identical with the line measured in Nova Pictoris at λ 4656.3 (int. 3 in 1926); this line was first detected in December, 1925. The transition $^5D_4 - {}^3F_3$, λ 4607, is partly responsible for the line measured at λ 4606.8 (int. 1 in 1926), described as follows: "λ 4606.8 is a weak and ill-defined emission which in 1928 was still present in the spectrum of the nova, with somewhat increased intensity." The fact that the line was still present in 1928, when λ 4658 had disappeared, means that some additional contributor must have existed. $^5D_4 - {}^3F_2$, λ 4573, may contribute to the line measured at λ 4570.1 (int. 1 in 1926), which was described as follows: "The emission at λ 4570 is a weak emission measured only on the plate of 1926 September 7 (a particularly good plate). The origin may be identical with that of a weak line at λ 4571.5 measured by Wright in the spectra of certain nebulae. It was not detected in 1928." Some other agent, such as *Mg* I or some as yet unidentified line, probably contributes, in addition to [*Fe* III]. Finally, $^5D_2 - {}^3F_3$, λ 4769.3, is probably identical with the line measured at λ 4771.2 (int. 0 in 1926) and described as follows: "The λ 4771.2 emission was measured on a few plates only. It is weak and ill-defined and the wave-length is somewhat uncertain. It was not detected in the 1928 spectrum."

Transition $^5D - {}^3P$.—The strongest transition $^5D_3 - {}^3P_2$ is predicted at λ 5270.3. A line was measured at λ 5271.4 (int. 2 in 1926) and attributed to [*Fe* II] with probably a blend with a line of unknown origin: "The [Fe^+] emission at λ 5273 also appears to be involved with another emission; a fairly strong line, at approximately the same wave-length, is present in 1931." The blend in the later stages (e.g., in 1931) was due to [*Fe* VI] and [*Fe* VII].

HYPOTHETICAL [*Fe* IV] LINE

An unidentified emission was measured at λ 5041.2 in 1926 and described as follows: "It is of moderate strength and is present on all the 1926 plates, but does not show on those of 1928 or 1931." This line is also present in the [Fe III] star RY Scuti[15] [λ 5040.1, int. 1), in AX Persei[15] (λ 5041.3, int. 1), in NGC 6572[13] (λ 5040.6, int. 0.7), in NGC 7027[13] (int. 1), and possibly in IC 418[13] and in the Orion Nebula.[13] It is possible that this line belongs to the forbidden $^4G - {}^4F$ transition of [*Fe* IV].[12]

McDONALD OBSERVATORY
August 9, 1942

[15] Swings and Struve, *Ap. J.*, **91**, 546, 1940.

THE INTERPRETATION OF THE SPECTRUM OF HD 190073*

OTTO STRUVE AND P. SWINGS

ABSTRACT

The hypothesis proposed by Beals for the interpretation of the complex contours of lines of *H* and *Ca* II in HD 190073 is discussed in the light of recent observations made at the McDonald Observatory. The absorption lines designated by Beals as A_2 and A_3 and the emission of *Ca* II and *H* probably originate in a shell whose radius is several times larger than the radius of the star. The absence of A_1 near the center of the emission in *Ca* II H suggests that this sharp line is produced at a lower level, where the velocity of expansion is negligible. The central reversals of the *H* lines, on the other hand, may come from an upper layer of the shell where the atoms have become decelerated. In this case the absorbing layer must lie immediately above an optically thick emitting shell, so that it will act somewhat like a reversing layer and not like a detached shell at great distances from the emitting regions.

In a recent paper C. S. Beals[1] has made an attempt to explain the unusual contours of the *H* lines and of the line *Ca* II K in the spectrum of HD 190073. The observational features of this remarkable object have been described by Merrill,[2] Beals,[3] and the present writers.[4] The *H* lines show broad underlying absorption lines corresponding roughly to type A. Superposed over these normal lines are bright lines, which sometimes are accompanied by strong violet absorption borders of the P Cygni type. The emission lines frequently show reversals, which are not quite central. The *Ca* II line K shows a relatively weak, but fairly broad, emission in the normal position of the line. A fairly strong central absorption is designated by Beals as A_1. On the violet side of the emission line is a strong double absorption line, the two components of which are designated as A_2 and A_3. There are numerous other emission lines, especially in the region of confluence of the strong higher members of the normal, Stark-broadened *H* lines and on the violet side of the Balmer limit. The spectrum undergoes slow changes. Most conspicuous is the disappearance of the P Cygni absorption of the *H* lines, which was first observed by Merrill. Our observations at the McDonald Observatory showed conspicuous P Cygni-type absorption lines in 1939 and less conspicuous ones in November, 1941. A plate taken July 8, 1942, shows ordinary Be-type bright lines, which are visible to $H\delta$ but cannot be seen clearly at $H\zeta$. There are no conspicuous changes in the rest of the spectrum, except that the narrow space of continuous spectrum (or of emission) between A_2 and A_3 undergoes slight oscillations in position. In 1939 it was displaced toward the violet side of the center between the outer edges of A_2 and A_3. In 1941 it was displaced toward the red. In 1942 it was still slightly displaced toward the red. The star is particularly interesting because, according to Merrill, the *Na* I lines are bright. They do not show conspicuous absorption components like the lines of *Ca* II.

The stellar lines of *Mg* II and *Si* II are fairly sharp, and the star does not show appreciable rotational broadening. The star is clearly not related to the ordinary Be stars, in which axial rotation has an important bearing upon the origin of the nebulous shell. Nor is the star a supergiant, like α Cygni, where expanding shells are frequently observed. HD 190073 belongs to the small group of stars of the main sequence which possess absorbing and emitting shells. The interpretation proposed by Beals is therefore of great

* *Contributions from the McDonald Observatory, University of Texas*, No. 61.

[1] *J.R.A.S. Canada*, **36**, 145 and 201, 1942; *Pub. A.A.S.*, **10**, 222, 1942.

[2] *Ap. J.*, **77**, 51, 1933.

[3] *Pub. A.S.P.*, **51**, 219, 1939.

[4] *Ap. J.*, **91**, 594, 1940; *Pub. A.S.P.*, **54**, 11, 1942; *Pub. A.A.S.*, **10**, 238, 1942.

interest, and we shall discuss it in the light of our observations made at the McDonald Observatory.

In a convincing manner Beals has demonstrated that the P Cygni structure of the *H* lines arises in an expanding shell above a nonexpanding reversing layer. This agrees with our conclusions from the ultraviolet emission lines, which are not weakened by the strong Balmer continuous absorption or by the wings of the broad Balmer lines.

By a procedure which differs materially from that which we have used in other similar cases, Beals concludes that the P Cygni absorption lines and the emission lines of *H* originate at a height of about $r = 10\ R_*$, while the *Ca* II emission originates at $r = 3.4\ R_*$ and the most displaced *Ca* II absorption component at $r = 5.6\ R_*$. These values are derived upon the assumption that the velocity of A_3, namely, -320 km/sec, corresponds to the velocity of escape at that distance r where A_3 is formed. As to order of magnitude, these values given by Beals agree with those which we have derived for other P Cygni-type stars. The spectrum of HD 190073 shows undisplaced absorption lines of *Mg* II 4481 and *Si* II 4128, 4131, which probably originate in the A-type reversing layer. There are no emission lines of *Mg* II and *Si* II or any violet-displaced absorption components which would correspond to A_2 and A_3. If we had observed in a normal stellar spectrum a *Ca* II line of the intensity of A_2 or A_3, we should certainly have expected to observe fairly strong lines of *Mg* II and *Si* II. The conclusion is therefore justified that the dilution of radiation in the shell is appreciable, though its amount cannot be ascertained. We conclude that our interpretation of the spectrum is consistent with that of Beals.

Perhaps of even greater interest is the origin of the undisplaced absorption line A_1 of *Ca* II. From his discussion of the *H* lines Beals has concluded that the approximately central reversals of these lines can best be explained as absorption by atoms which after "leaving the stellar surface are subjected to a positive outward acceleration which subsequently changes sign and becomes negative, reducing the velocity to relatively small values at great distances from the star." By assuming that the velocity of A_3 (-320 km/sec) corresponds to the velocity of escape at a point where the accelerating force, not otherwise specified, is suddenly cut off, Beals estimates for A_1 a height $r = 1000\ R_*$. He does not give a numerical estimate for the reversals of the *H* lines but suggests that the height is of the same order.[5] Incidentally, he agrees with Merrill that the line A_1 cannot be of interstellar origin. The absence of similar lines of *Na* I is a convincing argument.

It must be emphasized that the estimate of $r = 1000\ R_*$, which Beals gives for the reversals of the emission lines, rests upon the assumption that the accelerating force is cut off in the vicinity of $r = 10\ R_*$. It is therefore desirable to test the estimate $r = 1000\ R_*$ by other methods. If we understand the hypothesis of Beals correctly, we must suppose that for calcium, as well as for hydrogen, all observable emission is produced within about $r = 10\ R_*$. Between this distance and the much larger distance $r = 1000\ R_*$ the atoms are rapidly decelerated by the gravitational field of the star. In this region they are not believed to contribute materially to the observed features of the spectrum. Only at very great distances the atoms have become sufficiently decelerated to produce the absorption line A_1, near the normal wave length of the line. Evidently this picture involves the consideration of a more or less detached absorbing shell at $r = 1000\ R_*$, whose optical thickness within the line is small. It should also be noted that the observed emission at *Ca* II K is fairly weak. Hence the optical thickness of the emitting shell, which Beals estimates at $r = 3.4\ R_*$, is small.

If we can disregard all cyclical processes and assume that the entire absorbed energy is re-emitted in the same frequency, then, on general grounds, the measured energy emitted in the shell is exactly equal to the energy absorbed in the line. Hence, if there is no expansion or rotation, the emission line will be just sufficient to fill in the absorption line. This picture should hold in the case of *Ca* II, where the lower level is the ground

[5] *J.R.A.S. Canada*, **36**, 211, 1942.

state and the upper level is connected with it by a very strong transition. If cycles are present, they must, in the case of *Ca* II, tend to increase the emission relative to the absorption. It is, therefore, difficult to see how the absorption line A_1 can be formed at great distances from the photosphere without a corresponding amount of emission. We can verify this conclusion by computation.

Since the volume of the shell projected upon the apparent disk of the star, or eclipsed by it, is very small, the total energy, in ergs, radiated by the shell in all directions is approximately

$$4\pi r^2 H N_2 h\nu_{12} A_{21} , \tag{1}$$

where H is the thickness of the shell, and N_2 is the number of atoms in the upper level of the particular transition which we are considering. According to Beals, the radius of the star is

$$R_* = 2.1\odot \approx 10^{11} \text{ cm} ,$$

and its distance is

$$D_* = 280 \text{ parsecs} \approx 10^{21} \text{ cm} .$$

The radius of the shell is $r = 1000\, R_* = 10^{14}$ cm, and its angular diameter is therefore of the order of 0".01. All the light given by equation (1) will enter the slit of the spectrograph, and the source can be treated as a point.

In practice the emission of a shell is measured in terms of the radiation of the continuous spectrum of the star. This is

$$\pi R_*^2 c\, \rho_\nu d\nu , \tag{2}$$

where

$$\rho_\nu = \frac{8\pi h}{c^3} \frac{\nu^3}{e^{h\nu/kT} - 1} ; \qquad T = 10{,}000^0 .$$

We choose for $d\nu$ the frequency interval $\delta\nu$, which corresponds to 1 A at the wave length considered. The measured quantity is, therefore,

$$x = \frac{4\pi r^2 N_2 H h\nu_{12} A_{21}}{\pi R_*^2 c\, \rho_\nu \delta\nu} .$$

Recalling that, approximately,

$$W = \frac{R_*^2}{4 r^2} ,$$

we have

$$x = \frac{1}{W} \frac{N_2 H h\nu_{12} A_{21}}{c\, \rho_\nu \delta\nu} = \frac{1}{W} N_2 H \frac{h}{\lambda} A_{21} \frac{1}{\rho_\nu \delta\nu} . \tag{3}$$

The quantity N_2H is not directly known. But we observe the central reversal which we presume to be produced by the shell. For *Ca* II K this gives, in the case of Doppler broadening,

$$\text{E. W.} \approx 10^{-13} N_1 H . \tag{4}$$

For the line A_1 a reasonable estimate is E.W. = 1 A. Hence,

$$N_1 H = 10^{13} . \tag{5}$$

The corresponding value of N_2 is obtained from the Boltzmann relation modified by dilution,

$$N_2 H = N_1 H \frac{g_2}{g_1} W e^{-h\nu/kT} = 0.1\, W N_1 H = 10^{12} W . \tag{6}$$

Introducing into equation (3) this and the numerical values

$$h = 6.6 \times 10^{-27}, \qquad \lambda = 4 \times 10^{-5}, \qquad A_{21} = 10^{8}, \qquad \rho_\nu \delta\nu = 10^{-2},$$

we find

$$x \approx 1 . \tag{7}$$

This is precisely the amount of energy absorbed in the line by equation (4). Hence, if the atoms are at rest, the emission will fill in the absorption line and no central reversal will be observed. In order to maintain Beals's hypothesis we must assume that cycles are operating in the direction contrary to that in which they are set going by the dilution of radiation. Such cycles are not known at the present time.

The case is entirely different for *H*. Here we cannot assume, without further specification, that only two levels are concerned in the line production. If the second Balmer level is not metastable, then the population of it, as well as the population of the third, and higher, levels, is proportional to *W*. Hence, the factor $1/W$ in equation (3) does not cancel out, and *x* becomes roughly 10^6.

Without collisions the lifetime of the 2*s* level of *H* is 1/7 second. When collisions are present, the lifetime becomes shorter, so that for an electron density, $n_e = 10^{10}$ cm^{-3}, the lifetime becomes 10^{-8} sec. If $W \ll \tau_3/\tau_2$, we can write, instead of equation (6),

$$N_3 H = N_2 H \frac{g_3}{g_2} \frac{\tau_3}{\tau_2} e^{-h\nu_{23}/KT} .$$

If, on the other hand, $W \geq \tau_3/\tau_2$, then expressions (6) and (7) remain essentially unaltered. In order that we may obtain, for *H*, $x = 10$, we must have for $W = 10^{-6}$,

$$\frac{\tau_3}{\tau_2} = 10^{-5} .$$

Since, approximately $\tau_3 = 10^{-8}$ sec, this requires that τ_2 must be of the order of 10^{-3} sec. The corresponding electron density[6] would be about $n_e = 10^6$ cm^{-3}. There is no way to test this value. Observations give us only $N_2 H = 10^{13}$. Remembering that in interstellar space $n_e = 3$ cm^{-3}, it is quite plausible that the shell should have an electron density of 10^6. However, we are unable to prove this. We conclude that in the case of *Ca* II physical theory does not favor the hypothesis of an absorbing shell at great distances from the star which does not at the same time give rise to a strong emission line.[7]

The analysis by Beals is concerned for *Ca* II only with the line K. The line H is blended with $H\epsilon$ and is, therefore, more difficult to disentangle. However, our recent plate shows the Balmer lines free of P Cygni-type complications and is therefore useful for making a comparison between K and H. If the undisplaced line A_1 is produced much higher than any other spectroscopic feature of the star, it must superimpose itself with its normal intensity of $\frac{1}{2}$, as compared to K, upon the background produced by the sum of the intensities of the $H\epsilon$ wing and the *Ca* II emission. The central emission of $H\epsilon$ is presumably very weak, since it is not seen at $H\zeta$; but, even if it were present, the argument would still hold. In actual fact only an excessively weak indentation in the *Ca* II emission of *H* can be identified with the central reversal (Fig. 1). This is also confirmed by tracings from other plates and by the tracing published by Merrill. This faint feature has an area of probably not more than 0.1 of the area of the central reversal at K. It is presumably cut down by the very strong $H\epsilon$ line from the reversing layer or from the inner

[6] See eq. 10, *Proc. Natl. Acad.*, **25**, 72, 1939.

[7] The case of interstellar gas is, of course, different. The crucial point in the present discussion is that the shell appears as a point source.

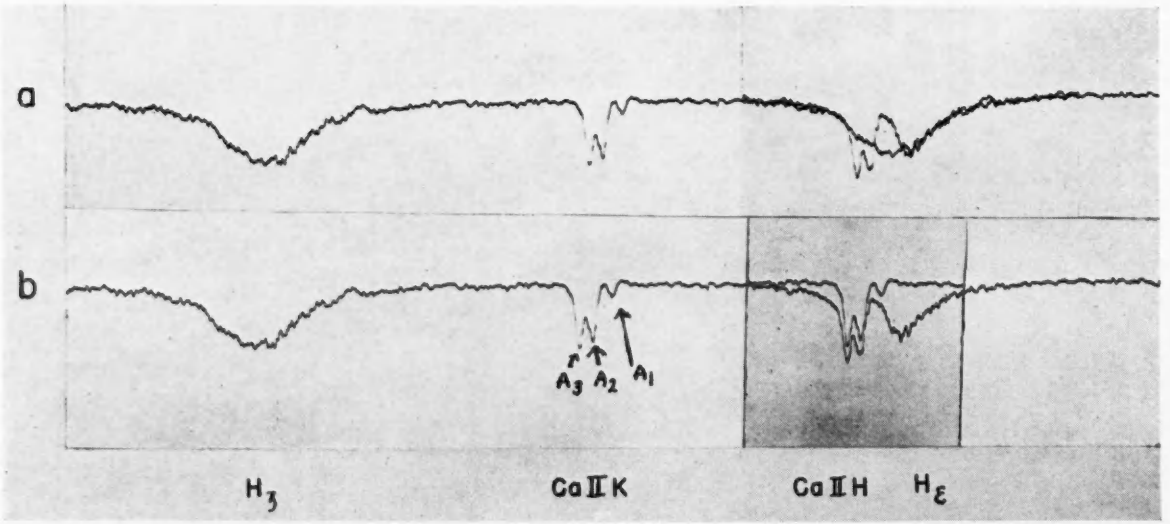

FIG. 1.—Tracing of spectrogram of HD 190073 obtained on July 8, 1942. (*a*) The tracing of H_ζ is superposed over that of H_ϵ. The red wings coincide. The emission and absorption of *Ca* II H show as departures from the curve representing H_ζ. (*b*) The tracing of *Ca* II K is superposed over that of *Ca* II H. The absorptions A_2 and A_3 coincide, but A_1 is very weak or absent in *Ca* II H, although it is strong in *Ca* II K.

shell. We are, therefore, inclined to attribute the line A_1 to a relatively low level, in spite of the difficulties mentioned by Beals.

This result does not invalidate the rest of Beals's discussion and in particular does not disprove his assumption that the accelerating force is reduced to zero (or to a small value) within the expanding shell. The central reversals of the *H* lines can, of course, not be attributed to the reversing layer. Hence the hypothesis proposed by Beals, namely, that they originate in a decelerated shell, merits careful consideration. For the *H* lines the emission is fairly strong, and we approach the case of a shell of considerable optical thickness. To make the hypothesis work, somewhat along the lines suggested by Rosseland,[8] it is only necessary to modify Beals's picture by supposing that the layers which are largely responsible for the broad emission line lie quite close—in fact, immediately below—the layer which is essentially responsible for the reversal. In that case the emission from the outer layer will not fill in the absorption (it acts like a reversing layer). According to this view, emission and absorption are thought to take place within the entire space occupied by the decelerated shell. To achieve this it is perhaps best to abandon the idea that the P Cygni absorption A_3 corresponds to the escape velocity at the appropriate distance r. There is no trouble in explaining the existence of decelerated expansion; and, by dropping the assumption, we can obtain a self-reversal at a much smaller distance from the star.

McDonald Observatory
August 1942

[8] *Theoretical Astrophysics*, p. 294, Oxford, 1936.

NOTES

NOTE ON THE SPECTRUM OF 67 OPHIUCHI

Four spectra taken by the authors on July 28 and 29 and August 6 and 7, 1942, with the ultraviolet four-prism spectrograph attached to the 83-cm reflector, giving a dispersion of 20 A/mm at $H\gamma$, and one spectrogram taken on August 10, 1942, with the violet four-prism spectrograph, giving 13 A/mm at $H\gamma$, show not only that 67 Oph[1] is a Be star, in agreement with O. Mohler's[2] observations, but also that the star is now of the P Cygni type, the emission lines being displaced to the red of the corresponding absorption lines.

The spectrum has been studied between λ 4100 and λ 4520 only, owing to the faintness of the spectrograms; and only the best ultraviolet plate, that of August 6, has been measured. The plate of August 10 has been partly measured for the longer wave lengths. The results obtained from all five plates are:

$H\gamma$	Narrow emission in the broad absorption line displaced 50 km/sec to the red with respect to the center of the latter.
$H\delta$	Shows emission on the red side of the absorption.
He I λλ 4169, 4472	Show narrow emission on the red sides of the narrow absorption lines. The displacements are 47 and 47 km/sec.
λ 4388	Probably emission on the red side.
Mg II λ 4481	Emission line on the red side of absorption. The displacement is 46 km/sec on August 10.
Si II λλ 4174, 4268	Narrow absorptions with emissions on the red sides. The displacements are 35 and 33 km/sec.
Al III λ 4513	Emission on the red side of absorption. The displacement is 55 km/sec on August 10.
Fe II λλ 4508, 4515	Probably emissions on the red sides of the absorption lines.
Si II λλ 4128, 4131	Only absorptions are visible.
C II λ 4267	Absent in absorption, as well as in emission.
O II	Neither emission nor absorption.

The faintness of the spectrograms may contribute to the absence of the last two elements, but cannot fully account for it. The emission component of *He* I λ 4472 is fainter on the spectrogram of August 10 than on the one of August 6, and the measurement of this line gives a displacement of 110 km/sec, while the spectrogram of August 6 gives 47 km/sec. There can be no doubt as to the reality of the disagreement of these two values. This suggests that the P Cygni character of 67 Oph, which evidently did not always exist,[3] is rapidly variable, as is the case with P Cyg itself[4]. The star 67 Oph, being of magnitude 3.92, is the brightest star of its class.

P. LACROUTE
W. H. DIRKS

OBSERVATORY OF TOULOUSE
ASTROPHYSICAL DEPARTMENT
August 13, 1942

[1] 67 Oph = BD + 2°3458 = HD 164353; $\alpha = 17^h55^m38^s$, $\delta = +2°56'$ (1900); mag., 3m92; Sp. B5p.

[2] *Harvard Ann. Card*, No. 507, 1939; *Ap. J.*, **92**, 315, 1940.

[3] O. Struve, *Ap. J.*, **74**, 225, 1931.

[4] P. Lacroute, *C.R.*, **206**, 1091, 1938.

THE SPECTRUM OF 67 OPHIUCHI

As the authors of the foregoing note have stated, 67 Ophiuchi = HD 164353 did not possess P Cygni characteristics when I observed[1] it in 1929–30. Nor do earlier Yerkes spectrograms[2] give any indication of such characteristics. I have no Yerkes plates of 67 Ophiuchi since 1930. However, in collaboration with A. Unsöld, I observed this star several times with the 82-inch reflector of the McDonald Observatory,[3] in May, 1939. Some of these spectrograms were on Process emulsion, while others extended to *Hα*. There is no emission in any of the lines, and no P Cygni structure in the lines listed by Lacroute and Dirks. At my request Dr. P. Swings and Mr. W. P. Bidelman took a spectrogram of 67 Ophiuchi on September 22, 1942, using the glass prisms and the 500-mm camera. The dispersion is 20 A/mm at λ 3933. This spectrogram is of excellent quality and clearly shows the slight Stark broadening of *H* and *He* I, in spite of the fact that the star is a well-known supergiant of luminosity class I–II, according to Morgan. But the lines are entirely in absorption and show no P Cygni structure. In fact, the spectrum resembles very closely that of 1939. The new plate does not show *Hα*, but *Hβ* is normal. Dr. P. W. Merrill has permitted me to say that the spectrum appeared to be normal on plates taken at Mount Wilson on May 30 and September 22, 1942.

Since we have no observations at the precise time of the Toulouse observations and since Lacroute and Dirks point out that the spectrum may change rapidly, the evidence from the Mount Wilson and McDonald plates does not disprove the Toulouse observations. In times of peace it would have been easy to compare our respective observations before publication. At present it seems best to record the results of the three observatories. The possibility of short-lived eruptions in a normal B-type supergiant is not excluded, but more observations will be required to confirm and elucidate them.

O. STRUVE

September 25, 1942

ON THE ORIGIN OF THE SOLAR SYSTEM

In a recent number of this *Journal*[1] Lyttleton once more returns to his theory for the formation of the planets. He states that Spitzer's analysis of the condensation of a planetary filament is vitiated because the gravitational field of the parent-stars has not been considered. How the gravitational attractions, operating in opposite directions, upon a filament situated between two such stars which are only a few stellar radii apart could aid the condensation of such a hot filament is not explained by Lyttleton.

With regard to his remarks relating to my previous criticisms, the following will suffice. In his first paper[2] Lyttleton wrote: ". . . . if the velocities of the condensations in the filament were distributed more or less uniformly between the velocities of the two stars. . . . ." He now writes: "It [i.e., Luyten's paper] assumes a linear distribution of velocities in the filament" and ". . . . the filament is assumed to condense [by internal or other forces, not considered in Luyten's analysis]." Lyttleton seems to imply that the assumption that the filament condenses was not made by him but by me and that the linear distribution of velocities is in a similar situation, whereas it is perfectly clear from his own original paper that these assumptions formed an integral part of his theory, while I have always vigorously objected to the correctness of the assumption concerning condensation.

[1] *Ap. J.*, **74**, 227, 1931 (also Pl. XII).

[2] *Ap. J.*, **64**, 62, 1926 (star 264).

[3] *Ap. J.*, **90**, 699, 1939 (Pl. X).

[1] *Ap. J.*, **96**, 155, 1942.

[2] *M.N.*, **96**, 562, 1936.

Considering another statement by Lyttleton,[3] viz.: "The fact that the theory discussed in the present paper is not open to any objection need not therefore be regarded as in any way precluding the possibility that other explanations may be invented," I believe that any further discussion would be a waste of valuable publication space. I repeat again that when a theory "proves to be astrophysically objectionable, as well as dynamically untenable, and is, in addition, superlatively improbable, then I believe we are justified in concluding that it has been removed from the realm of scientific discussion."[4]

W. J. LUYTEN

[3] *M.N.*, **100**, 553, 1940.

[4] [Until fundamentally new information becomes available, this discussion of the origin of the solar system will be closed herewith.—EDITOR.]

REVIEWS

Annals of the Astrophysical Observatory of the Smithsonian Institution, Vol. 6. By C. G. ABBOT, L. B. ALDRICH, and W. B. HOOVER. Published by the Smithsonian Institution, Washington, D.C., 1942. Pp. viii+207.

The volume opens with extracts, from the annual reports of Dr. Abbot from 1931 to 1940, which explain the work of the observatory. Chapters ii, iii, and iv describe the instruments, procedures, and methods of reduction by which the solar constant has been measured. In 1936 it was realized that an amendment, employed since 1923, to the "short" method of reduction was unsound. All solar-constant values since 1923 have been recomputed, and the revised results are now published in chapter v, which contains day-to-day values of the solar constant from 1923 to 1939. The observations were made at Montezuma in Chile, at Table Mountain in California, and at Mount St. Katherine in Egypt. Ten-day-mean, monthly-mean, and annual-mean values are published in chapter vi, which also contains a discussion of the accuracy of the measurements, and tables and graphs of the "long period" periodic components that the authors believe the solar constant to contain. In chapter vi curves are published, which are believed by the authors to demonstrate that there is a 27-day periodicity in the solar radiation, related to the solar rotation and to the areas of solar faculae.

In chapter vi, also, a plot of the solar constant against sunspot number indicates no relation between those two quantities; and it is concluded that the main weather effect of the sunspot cycle is to alter the cloudiness of the earth and possibly the amount of ozone in the high atmosphere, without altering the solar constant. The reviewer agrees with the authors' conclusion that the plot shows no dependence of solar constant on sunspot number. If there is any dependence, it must be small—too small to be revealed by even the highly accurate measures on which the plot is based. The authors' conclusion, strikingly at variance with their earlier beliefs, tends to weaken the case for variation of the solar constant by destroying the argument based on similar periodicities in the sunspot and solar-constant values. Further, if sunspots alone, without concomitant changes in the solar constant, can account for changes in the weather, then one would expect the authors' belief to be weakened that changes in the solar constant are causes of changes in the weather. Paradoxically, the concluding paragraph on page 201 reiterates their belief that variation of the sun is a major cause of weather changes; but possibly the authors are there referring to sunspots rather than to variation of the solar constant.

The reviewer thinks that observational data which are as accurate as the revised solar-constant values and which have been obtained so skilfully and through such careful labor deserve more careful and accurate discussions than the authors have given them. The reviewer thinks that the lack of rigor in the discussions has resulted in needlessly weak arguments for one certain and for one doubtful conclusion and that in one place it has led the authors into error. The dependence of solar constant on sunspot number could have been tested for significance with the t-test, or χ^2-test. The result of such a test would have compelled the reader to agree with the authors that there was no demonstrable relationship, instead of leaving the question of agreement or disagreement entirely to the reader's judgment.

The lack of a more careful discussion has prevented the authors from exhibiting in its most favorable light the existing evidence for real changes in the solar constant. The crucial test of whether or not there is evidence for such changes is to see whether independently obtained measures, at different stations, show significant correlation. The best series for this purpose are perhaps the Table Mountain and the Montezuma series, from 1926 to 1939. The Harqua Hala–Montezuma comparison has been weakened by the appreciable corrections that were applied to the former values to make them agree with Montezuma, and the comparison is of short duration. The Mount St. Katherine series is of short duration. The reviewer has plotted the Montezuma values (monthly means) against the Table Mountain values, as shown in Figure 1 of this review. The plotted variates show a small but significant correlation. The coefficient is 0.27, with a degree of significance corresponding to 3.6 standard deviations. Chance alone, therefore, is not at all likely to have given rise to the observed degree of correlation. Whether

the statistically significant correlation proves that there has been a real variation of the solar constant can be debated, for some will contend that the correlation has arisen from adjustments of the Table Mountain series to conform to Montezuma, these adjustments destroying the independence. Without entering the debate, one can find an upper limit to the amount of the solar variation during the interval from 1926 to 1939.

If the corrections to the Table Mountain values should have been applied for instrumental reasons, then the errors at the two stations are independent; the covariance of the two series is the variance of the solar constant itself; and the difference variance (at either station) less the variance of the solar constant is the variance of the instrumental errors (at that station). The observations yield for the standard deviation of the solar constant the value 0.0025 calories per square centimeter per minute, and for the standard errors at Table Mountain and Montezuma the values 0.0054 and 0.0030, respectively, in the same units, for monthly means. Comparison of the two best series thus shows that from 1926 until 1939 the solar constant differed, month by month, from constancy by amounts whose root mean square value was only 0.0025 if one concedes the independence of the measures, and less than 0.0025 if part or all of the correlation arises from the adjustment of the Table Mountain values. The mean solar constant is 1.945.

So small a variation as 0.0025 is not consistent with the large amplitudes of the "periodicities" listed in chapter vi, probably because those periodicities have been produced in part by a rather loose method of analysis. Nonsinusoidal periodicities (determined by simple processes

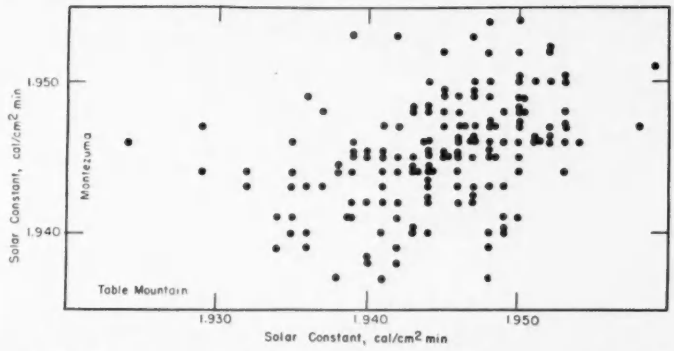

FIG. 1.—Correlation between measures of the solar constant at Montezuma and at Table Mountain

of averaging) have been removed one by one from the observed data. Each time that such a periodicity is removed, its higher Fourier components are actually added with reversed signs to the original data. After repetitions, many higher-order periodic components that may have arisen merely as fluctuations of sampling have thus been added artificially to the data. Such artificially added components contribute to the periodicities later to be discovered and removed, for the series are finite and terms with different periods are thus not truly orthogonal.

The discussion of a 27-day periodicity in the solar constant appears to the reviewer to be erroneous, and the discussion of the relationship of the solar constant to faculae areas appears to the reviewer to be unsound. Daily values of the solar constant have been classified into groups according to the phases of a 27-day period. In Figure 16 the mean solar constant within each group is plotted against the phase of the group. Each of the curves, in which the consecutive points have been joined by straight lines, corresponds to observations over an interval of four consecutive periods of 27 days. To show that a 27-day periodicity is present, if it is not sinusoidal, one must compare the standard deviation within phase groups with the standard deviation between phase groups. This has not been done, and in curves *A* through *E* the phases and solar constant values appear to be unrelated. In the caption of Figure 16 the reader is asked to note the rise of radiation at the nineteenth day, curves *A*–*E*. Among the five curves in question, at that phase, there are two instances of maxima, one instance of minimum, and only two instances of a rising solar constant. Figure 16, contrary to what the authors say, shows, if anything, that there is no evidence for a 27-day periodicity in the solar constant. In Figure 17 an attempt has been made to correlate the solar constant with the areas of faculae. In each of nine diagrams both solar-constant and faculae areas have been plotted against the date. Each dia-

gram covers 27 days of observation only; thus in no case can the diagrams be evidence for a 27-day periodicity. The authors state that they believe the correlations to be so clear as to require no further argument. In Figure 2 of this revew the reviewer shows a correlation diagram of faculae areas against solar constant, corresponding to a rather typical diagram in Figure 17, that of 1925-11-18. The coefficient of correlation is 0.25 and does not differ significantly from zero, t being 1.05 with 17 degrees of freedom. The probability that the coefficient will exceed 0.25, in a sample of 19 pairs drawn at random from a population of uncorrelated pairs, is 0.31. Similar results are obtained when one correlates the solar constant with the faculae areas that follow it by $1\frac{1}{2}$ days. To show that the solar constant and faculae areas were correlated, it would be necessary to make similar studies of the other diagrams and show that the coefficients of correlation were too large on the whole to be reasonably attributable to sampling fluctuations. This has not been done. Actually, it appears to be doubtful whether there is, on the whole, any greater degree of connection between the two variates—solar constant and area of faculae—than there would be between the faculae areas and numbers that had been drawn at random from any collection of solar-constant values. To infer that two variates are

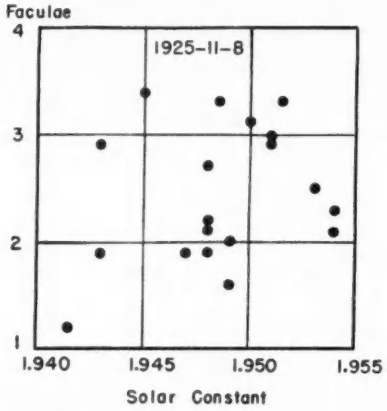

FIG. 2—Areas of faculae plotted against the solar constant

related, on the basis of a casual inspection of separate plots of the variates against some third parameter like the time, is not only not rigorous but has frequently been misleading.

The high accuracy of the solar-constant values constitutes a testimonial to the great instrumental skill and insight of Dr. Abbot and his co-workers. The goodness of the observations causes one to hope that they will be continued long into the future and that those already completed and published will yet be discussed with the care that their excellence deserves.

THEODORE E. STERNE

Molecular Films, the Cyclotron, and the New Biology. By HUGH STOTT TAYLOR, ERNEST O. LAWRENCE, and IRVING LANGMUIR. New Brunswick: Rutgers University Press, 1942. Pp. 95. $1.25.

This book consists of three lectures presented at a symposium in connection with the celebration of the one hundred and seventy-fifth anniversary of Rutgers University. The titles of the lectures are "Fundamental Science from Phlogiston to Cyclotron," by Taylor; "Molecular Films in Chemistry and Biology," by Langmuir; and "Nuclear Physics and Biology" by Lawrence. The book concludes with brief commentaries by Leslie A. Chambers and J. R. Dunning. There are numerous illustrations, including an "Artist's Conception from Early Plans of the Giant Cyclotron" (Fig. 23) and "A Recent View from Above of the Giant Cyclotron Magnet Now under Construction on the University of California Campus."

INDEX TO VOLUME 96

INDEX TO SUBJECTS

INDEX OF AUTHORS